BEILSTEIN JOURNAL OF ORGANIC CHEMISTRY

5th International Symposium on Synthesis and Catalysis (ISySyCat 2023)

Edited by Elisabete P. Carreiro and Anthony J. Burke

Imprint

Beilstein Journal of Organic Chemistry
www.bjoc.org
ISSN 1860-5397
Email: journals-support@beilstein-institut.de

The *Beilstein Journal of Organic Chemistry* is published by the Beilstein-Institut zur Förderung der Chemischen Wissenschaften.

Beilstein-Institut zur Förderung der Chemischen Wissenschaften
Trakehner Straße 7–9
60487 Frankfurt am Main
Germany
www.beilstein-institut.de

BEILSTEIN JOURNAL OF ORGANIC CHEMISTRY

5th International Symposium on Synthesis and Catalysis (ISySyCat2023)

Anthony J. Burke*[1,2] and Elisabete P. Carreiro*[3]

Editorial

Open Access

Address:
[1]Faculty of Pharmacy, University of Coimbra, Pólo das Ciências da Saúde, Azinhaga de Santa Coimbra, 3000-548 Coimbra, Portugal, [2]Coimbra Chemistry Centre, Institute of Molecular Sciences, Chemistry Department, Faculty of Science and Technology, University of Coimbra, 3004-535 Coimbra, Portugal and [3]LAQV-REQUIMTE, Institute for Research and Advanced Training (IIFA), University of Évora, Rua Romão Ramalho, 59, 7000-671 Évora, Portugal

Email:
Anthony J. Burke* - ajburke@ff.uc.pt;
Elisabete P. Carreiro* - betepc@uevora.pt

* Corresponding author

Beilstein J. Org. Chem. **2024,** *20,* 2704–2707.
https://doi.org/10.3762/bjoc.20.227

Received: 06 October 2024
Accepted: 15 October 2024
Published: 28 October 2024

This article is part of the thematic issue "5th International Symposium on Synthesis and Catalysis (ISySyCat 2023)".

Guest Editors: A. J. Burke and E. P. Carreiro

Organic synthesis and catalysis are two of the main stalwarts of the chemical sciences, and they have undergone extraordinary advances over the past 150 years. They are a crucial tool for the development of new molecules across a wide range of fields, including drug discovery, energy, materials science, and many more. The ability to design and create novel compounds through organic synthesis, aided by catalysis, is fundamental to advancing technologies that address global challenges in health, sustainability, and beyond. By enabling the production of complex molecules with specific functions, chemical synthesis and catalysis play a key role in innovation across the above-mentioned fields and thus improve our quality of life [1-10].

For almost 10 years, the International Symposium on Synthesis and Catalysis (ISySyCat) has brought together the biggest names in the fields of synthesis and catalysis, along with cohorts of dedicated practitioners, researchers, and students from these fields, presenting, discussing, and learning about the latest developments and cutting-edge innovations in the fields of synthesis and catalysis.

In this thematic issue dedicated to the 5th International Symposium on Synthesis and Catalysis (ISySyCat2023), which took place in Evora, Portugal from September 5–8, 2023, a diverse selection of contributions from a cross section of these participants is presented. The variety of material from different fields showcased in this thematic issue truly reflects the range and breath of this conference.

In the contribution by Dargó et al. [11], "A novel recyclable organocatalyst for the gram-scale enantioselective synthesis of (*S*)-baclofen", an interesting approach to recycling the very useful cinchona squaramide organocatalysts was described. This approach involved functionalization of the organocatalyst with a lipophilic linker (octadecyl side chains), resulting in a novel lipophilic cinchona squaramide organocatalyst. This organocatalyst was evaluated in a benchmark Michael addition of acetylacetone to *trans*-β-nitrostyrene, yielding the Michael adduct with high yield and enantioselectivity. The hydrophobic chain of the catalyst allowed the organocatalyst to be easily recovered by precipitation using polar solvents. This catalyst proved

to be excellent for the preparation of (*S*)-baclofen on a gram scale, furnishing the main chiral intermediate in high yield and enantioselectivity. Furthermore, the catalyst was recycled over five cycles while maintaining its performance.

In their contribution "Metal-catalyzed coupling/carbonylative cyclizations for accessing dibenzodiazepinones: an expedient route to clozapine and other drugs", Moutayakine and Burke described a new synthetic route for the synthesis of 10,11-dihydro-5*H*-dibenzo[*b*,*e*][1,4]diazepinone (DBDAP) derivatives, which possess recognized pharmacological properties [12]. They used sequential reactions catalyzed by palladium and copper. The process involves an initial amination, which can be carried out via either the Buchwald–Hartwig or the Chan–Lam reaction, followed by a palladium-catalyzed intramolecular aminocarbonylation using $Mo(CO)_6$. Both catalytic approaches successfully produced the desired DBDAPs.

As previously mentioned, organic synthesis is a crucial tool for preparing complex molecules of high value to industry. Frackenpohl et al. [13] designed and synthesized a new library of 2,3-dihydro[1,3]thiazolo[4,5-*b*]pyridine derivatives that exhibited strong herbicidal activity against commercially significant grass weeds in preemergence greenhouse tests. The synthetic route for this new family of compounds was developed and optimized, involving several reaction steps, included Pd-catalyzed Suzuki couplings and the reduction of the thiazole moiety to 2,3-dihydro[1,3]thiazolo[4,5-*b*]pyridines, a crucial intermediate, using $BH_3{\cdot}NH_3$ and tris(pentafluorophenyl)borane as a Lewis acid, followed by treatment with formic acid.

Gillie et al. reported the synthesis of a laterally fused N-heterocyclic carbene (NHC) framework from polysubstituted aminoimidazo[5,1-*b*]oxazol-6-ium salts, which demonstrated strong catalytic activity in gold-catalyzed alkyne hydration and arylative cyclization reactions [14]. The synthesis of this new carbene involved the use of a novel nitrenoid reagent that was successfully synthesized on a gram scale through a three-step reaction sequence. The process began with 2,6-diisopropylphenylamine, which underwent alkylation, formylation, and substitution reactions. The carbene synthesis was then achieved via a two-step process involving ynamide annulation, followed by imidazolium ring formation. The resulting carbene was metalated at the C2 position with Au(I), Cu(I), and Ir(I), obtaining an L-shaped NHC ligand scaffold.

Līpiņš et al. introduced a new method for synthesizing 4-azido-6,7-dimethoxy-2-alkyl/arylsulfonylquinazolines, which are key intermediates in the preparation of biologically active compounds [15]. The synthesis was achieved via a sulfonyl group rearrangement driven by the azide–tetrazole equilibrium in quinazolines. The researchers utilized two synthetic pathways to prepare the target compounds. The first pathway involved a nucleophilic aromatic substitution (S_NAr) reaction between 2-chloro-6,7-dimethoxy-4-sulfonylquinazoline derivatives and NaN_3, while the second involved an S_NAr reaction between 2,4-dichloro-6,7-dimethoxyquinazoline and alkyl/arylsulfinates, followed by substitution with NaN_3. Using this developed methodology, the adrenoblockers terazosin and prazosin were successfully synthesized.

Oliveira Jr. et al. developed a new methodology for the asymmetric synthesis of β-aryl-γ-lactam derivatives with very good yield and enantioselectivity [16]. This was achieved through a palladium-catalyzed Heck–Matsuda desymmetrization of N-protected 2,5-dihydro-1*H*-pyrroles using aryldiazonium salts and (*S*)-PyraBox, followed by sequential Jones oxidation. They showcased their methodology by preparing both (*R*)-rolipram and (*R*)-baclofen hydrochloride.

Tóth et al. reported the design and synthesis of new analogues of HeE1-2Tyr, a nonnucleoside SARS-CoV-2 RdRp inhibitor, and their evaluation in an in vitro polymerase assay, targeting SARS-CoV-2 [17]. The synthesis of the new molecules involved three modifications of the HeE1-2Tyr inhibitor, which included changing the core structure from a benzothiazole to a benzoxazole unit and simplifying it to pyridone and thiazolopyridone derivatives. This work is interesting from the point of view that it involved the emerging technique of "chemical editing". The pyridone and thiazolopyridone derivatives were the most promising inhibitors, with IC_{50} values below 90 μM.

Marques et al. described the synthesis of a new family of isatin-based α-acetamide carboxamide oxindole hybrids using the versatile Ugi four-component reaction [18]. Sixteen hybrids were prepared by reacting 5-amino-1-benzyl-3,3-dimethoxyindolin-2-one, benzyl isocyanide, carboxylic acids, and aldehyde/ketone derivatives, catalyzed by ZnF_2 in MeOH at room temperature with a short reaction time. Some of them were further functionalized with a 1,2,3-triazole ring via copper-catalyzed azide–alkyne cycloaddition (CuAAC) and deprotected with trifluoroacetic acid. Several hybrids were evaluated against six cancer cell lines, displaying GI_{50} values in the range of 1–10 μM.

Teixeira et al. reported the preparation of new triazinephosphonate-based dopants and their application in the production of Nafion proton exchange membranes, which exhibited higher conductivity with only 1 wt % loading [19]. These new triazinephosphonate dopants could significantly impact the production of enhanced Nafion membranes, contributing to the development of more efficient decarbonized energy systems based

on hydrogen technologies. The six triazinephosphonate derivatives bearing 4-aminophenyl or 4-hydroxyphenyl groups were obtained in very good yields through a nucleophilic substitution reaction between cyanuric chloride and 4-aminophenylphosphonate or 4-hydroxyphenylphosphonate derivatives. These synthesized dopants were used to prepare the modified Nafion membranes using a casting methodology.

Almodovar and Tomé reported the synthesis and characterization of nine novel diketopyrrolopyrrole derivatives through versatile S_NAr reactions between *N*,*N*'-bis(pentafluorobenzyl)-substituted diketopyrrolopyrrole and thiols and phenols under smooth conditions, resulting in the final compounds with satisfactory yields [20]. These newly synthesized compounds exhibited a high fluorescence quantum yield, which is an important property for their potential application in the field of optoelectronics (particularly for energy and biological chemistry applications).

In this thematic issue, Nieto et al. contributed a timely Review article on the chemical space of 2-phenethylamines, focusing on heteroaromatic structures with known pharmacological profiles [21]. They highlighted that changes in the phenyl and heteroaryl ring systems often stemmed from structure–activity relationship (SAR) exploration, where bioisosteric modifications of the original phenyl hits were prevalent. They reported that imidazole analogs behaved differently due to the L-histidine unit representing a nonphenyl scaffold. Some important data on the bioisosteric modifications of 2-phenethylamine derivatives, focusing on their affinity and core aromatic diversity, were included.

In another Review article contributed to this thematic issue, Fehér et al. [22] carried out a critical assessment of the factors that affect the activity of immobilized organocatalysts. As mentioned earlier, organocatalysis has proven to be a powerful tool in the preparation of enantiopure compounds. However, their preparation can be time-consuming, complex, and expensive. Consequently, it is of utmost interest to immobilize them for reuse but without affecting their catalytic activity. The main factors discussed were the type of support, immobilization, and interaction between the support and the organocatalyst. The particular challenges were presented for each support, which are unique for different reaction substrates. Furthermore, the solutions to these problems as well as the limitations presented by these supports were discussed as well.

To conclude, you as a reader are encouraged to take a closer look at the contributions mentioned above, spanning diverse areas of modern synthesis and catalysis. We hope that you will find them beneficial, enlightening, and stimulating.

The 6th International Symposium on Synthesis and Catalysis (ISySyCat2025) will take place at the University of Coimbra from September 2–5, 2025 (https://isysycat2025.events.chemistry.pt/), and we hope that it will attract the attention of colleagues and practitioners from all corners of the world, who will share in the rich chemistry to be discussed during those four days.

As a final remark, we are very grateful to the *Beilstein Journal of Organic Chemistry* for the opportunity to publish a thematic issue dedicated to ISySyCat2023.

Anthony J. Burke and Elisabete P. Carreiro

Coimbra and Évora, October 2024

Data Availability Statement

Data sharing is not applicable as no new data was generated or analyzed in this study.

References

1. Sun, A. W.; Lackner, S.; Stoltz, B. M. *Trends Chem.* **2019,** *1,* 630–643. doi:10.1016/j.trechm.2019.05.008
2. Hopkinson, M. N.; Sahoo, B.; Li, J.-L.; Glorius, F. *Chem. – Eur. J.* **2014,** *20,* 3874–3886. doi:10.1002/chem.201304823
3. Burke, A. J.; Marques, C. S.; Turner, N. J.; Hermann, G. J., Eds. *Active Pharmaceutical Ingredients in Synthesis: Catalytic Processes in Research and Development;* Wiley-VCH: Weinheim, Germany, 2018. doi:10.1002/9783527807253
4. O'Connell, A.; Barry, A.; Burke, A. J.; Hutton, A. E.; Bell, E. L.; Green, A. P.; O'Reilly, E. *Chem. Soc. Rev.* **2024,** *53,* 2828–2850. doi:10.1039/d3cs00689a
5. Kinner, A.; Nerke, P.; Siedentop, R.; Steinmetz, T.; Classen, T.; Rosenthal, K.; Nett, M.; Pietruszka, J.; Lütz, S. *Biomedicines* **2022,** *10,* 964. doi:10.3390/biomedicines10050964
6. Wetzel, S.; Bon, R. S.; Kumar, K.; Waldmann, H. *Angew. Chem., Int. Ed.* **2011,** *50,* 10800–10826. doi:10.1002/anie.201007004
7. Kakuchi, R. *Angew. Chem., Int. Ed.* **2014,** *53,* 46–48. doi:10.1002/anie.201305538
8. Peng, F.; Qi, J.; Zhang, J.; Wang, E.; Cao, X.; Chen, L.; Fan, C.; Fan, W.; Feng, C.; Lin, M.; Liu, M.; Nawrat, C. C.; Schultz, D. M.; Song, C.; Wang, F.; Yin, J.; Zhang, Y. *Org. Process Res. Dev.* **2024,** *28,* 2150–2156. doi:10.1021/acs.oprd.4c00003
9. Olivieri, E.; Gallagher, J. M.; Betts, A.; Mrad, T. W.; Leigh, D. A. *Nat. Synth.* **2024,** *3,* 707–714. doi:10.1038/s44160-024-00493-w
10. Tu, Z.; Stuyver, T.; Coley, C. W. *Chem. Sci.* **2023,** *14,* 226–244. doi:10.1039/d2sc05089g
11. Dargó, G.; Erdélyi, D.; Molnár, B.; Kisszékelyi, P.; Garádi, Z.; Kupai, J. *Beilstein J. Org. Chem.* **2023,** *19,* 1811–1824. doi:10.3762/bjoc.19.133
12. Moutayakine, A.; Burke, A. J. *Beilstein J. Org. Chem.* **2024,** *20,* 193–204. doi:10.3762/bjoc.20.19

13. Frackenpohl, J.; Barber, D. M.; Bojack, G.; Bollenbach-Wahl, B.; Braun, R.; Getachew, R.; Hohmann, S.; Ko, K.-Y.; Kurowski, K.; Laber, B.; Mattison, R. L.; Müller, T.; Reingruber, A. M.; Schmutzler, D.; Svejda, A. *Beilstein J. Org. Chem.* **2024,** *20,* 540–551. doi:10.3762/bjoc.20.46
14. Gillie, A. D.; Wakeling, M. G.; Greene, B. L.; Male, L.; Davies, P. W. *Beilstein J. Org. Chem.* **2024,** *20,* 621–627. doi:10.3762/bjoc.20.54
15. Līpiņš, D. D.; Jeminejs, A.; Ušacka, U.; Mishnev, A.; Turks, M.; Novosjolova, I. *Beilstein J. Org. Chem.* **2024,** *20,* 675–683. doi:10.3762/bjoc.20.61
16. de Oliveira, A. G., Jr.; Wang, M. F.; Carmona, R. C.; Lustosa, D. M.; Gorbatov, S. A.; Correia, C. R. D. *Beilstein J. Org. Chem.* **2024,** *20,* 940–949. doi:10.3762/bjoc.20.84
17. Tóth, L. J.; Krejčová, K.; Dejmek, M.; Žilecká, E.; Klepetářová, B.; Poštová Slavětínská, L.; Bouřa, E.; Nencka, R. *Beilstein J. Org. Chem.* **2024,** *20,* 1029–1036. doi:10.3762/bjoc.20.91
18. Marques, C. S.; González-Bakker, A.; Padrón, J. M. *Beilstein J. Org. Chem.* **2024,** *20,* 1213–1220. doi:10.3762/bjoc.20.104
19. Teixeira, F. C.; Teixeira, A. P. S.; Rangel, C. M. *Beilstein J. Org. Chem.* **2024,** *20,* 1623–1634. doi:10.3762/bjoc.20.145
20. Almodovar, V. A. S.; Tomé, A. C. *Beilstein J. Org. Chem.* **2024,** *20,* 1933–1939. doi:10.3762/bjoc.20.169
21. Nieto, C.; Manchado, A.; García-González, Á.; Díez, D.; Garrido, N. M. *Beilstein J. Org. Chem.* **2024,** *20,* 1880–1893. doi:10.3762/bjoc.20.163
22. Fehér, Z.; Richter, D.; Dargó, G.; Kupai, J. *Beilstein J. Org. Chem.* **2024,** *20,* 2129–2142. doi:10.3762/bjoc.20.183

License and Terms

BEILSTEIN JOURNAL OF ORGANIC CHEMISTRY

A novel recyclable organocatalyst for the gram-scale enantioselective synthesis of (*S*)-baclofen

Gyula Dargó[1], Dóra Erdélyi[1], Balázs Molnár[1], Péter Kisszékelyi[1], Zsófia Garádi[2] and József Kupai[*1]

Full Research Paper

Open Access

Address:
[1]Department of Organic Chemistry and Technology, Budapest University of Technology and Economics, Műegyetem rkp. 3., H-1111 Budapest, Hungary and [2]Department of Pharmacognosy, Semmelweis University, Üllői út. 26, H-1085 Budapest, Hungary

Email:
József Kupai[*] - kupai.jozsef@vbk.bme.hu

* Corresponding author

Keywords:
baclofen; catalyst recovery; lipophilic cinchona squaramide; organocatalysis; stereoselective catalysis

Beilstein J. Org. Chem. **2023,** *19,* 1811–1824.
https://doi.org/10.3762/bjoc.19.133

Received: 28 August 2023
Accepted: 06 November 2023
Published: 24 November 2023

This article is part of the thematic issue "5th International Symposium on Synthesis and Catalysis (ISySyCat 2023)".

Guest Editor: A. Burke

Abstract

Synthesizing organocatalysts is often a long and cost-intensive process, therefore, the recovery and reuse of the catalysts are particularly important to establish sustainable organocatalytic transformations. In this work, we demonstrate the synthesis, application, and recycling of a new lipophilic cinchona squaramide organocatalyst. The synthesized lipophilic organocatalyst was applied in Michael additions. The catalyst was utilized to promote the Michael addition of cyclohexyl Meldrum's acid to 4-chloro-*trans*-β-nitrostyrene (quantitative yield, up to 96% ee). Moreover, 1 mol % of the catalyst was feasible to conduct the gram-scale preparation of baclofen precursor (89% yield, 96% ee). Finally, thanks to the lipophilic character of the catalyst, it was easily recycled after the reaction by replacing the non-polar reaction solvent with a polar solvent, acetonitrile, with 91–100% efficiency, and the catalyst was reused in five reaction cycles without the loss of activity and selectivity.

Introduction

In today's chemical industry, catalytic processes are of paramount importance. In particular, the application of asymmetric organocatalysts is receiving increased attention [1-4]. This is illustrated by the fact that in 2021 the Nobel Prize in Chemistry was awarded for the discovery of asymmetric organocatalysis [5]. The use of organocatalysts has been a major breakthrough in the realization of enantioselective transformations. Stereoselective synthesis is essential in the pharmaceutical industry, as the development of drugs often requires the production of enantiomerically pure chiral compounds [6-8].

The application of organocatalysts is well-established in several organic reactions, including but not limited to aldol reactions [6], Michael additions [9], Mannich reactions [10], aza-Henry reactions [11], and Diels–Alder cycloadditions [12,13]. Although the benefits of organocatalysts are undoubted, their syn-

thesis is often a long and expensive process. Therefore, for sustainable application, the cost-efficient recovery and reuse of organocatalysts are critical issues. Fortunately, a wide range of recycling options are known in the literature, often based on liquid–solid phase separation [14].

Catalyst recycling can be achieved, for example, by immobilizing the catalysts to a solid support [15], e.g., silica gel [16-18], organic polymers [19-21], magnetic nanoparticles [22,23], or by membrane separation, e.g., using organic solvent nanofiltration (OSN) [24-26], which methods can be easily implemented in flow systems. Accordingly, the main recycling methods rely on the immobilization of catalysts on heterogeneous supports, however, this could often lead to the deterioration of activity and/or selectivity [27]. A possible solution to avoid these drawbacks is the heterogenization of the catalyst after a homogeneous reaction.

For example, by incorporating a lipophilic side chain [28] on the organocatalyst that does not interfere with its catalytic activity thanks to a linker between the catalyst and lipophilic units. In this way, a significant difference in polarity can be achieved between the catalyst and the other components of the reaction mixture. The lipophilic *O*-alkylated gallic acid unit increases the solubility of the organocatalyst in less polar solvents, such as DCM or toluene but leads to the precipitation of the organocatalyst in polar solvents, including MeOH or MeCN. As a result, the recycling of the organocatalysts can be achieved in a simple step by centrifugation or filtration.

Previously, we have demonstrated the homogeneous and heterogeneous recycling of cinchona-based organocatalysts [20,25,26,29]. Continuing our work, we aimed to synthesize a novel, recyclable lipophilic cinchona squaramide organocatalyst. Its catalytic activity and recyclability were examined in a new stereoselective synthesis of baclofen, which is used to treat muscle spasms [30]. Finally, the catalyst was easily recycled by centrifugation over five reaction cycles without significant loss of activity (Figure 1).

Results and Discussion

Synthesis of the lipophilic cinchona squaramide organocatalyst

Previously, we successfully applied quinine-derived squaramide (SQ) organocatalyst **1** in stereoselective Michael and aza-Michael additions with excellent enantiomeric excess values [26]. Our aim was to recycle this catalyst easily by incorporating a lipophilic unit, which leads to a drastic increase (5.78 to 28.8) in the log*P* value of the organocatalyst **2**. The recyclable organocatalyst can be divided into three units: the catalytic unit, the linker, and the lipophilic tag with octadecyl chains (Figure 1).

The cinchona amine **3** was prepared starting from the naturally occurring quinine [31]. The gained catalyst was demethylated using BBr_3 to give alcohol **4**. The demethylated cinchona amine was reacted with half-squaramide [9] **5**, resulting in demethylated squaramide **6**. A short and flexible linker was applied between the catalytic and lipophilic units to avoid a decrease in the catalytic activity. The demethylated cinchona squaramide **6** was reacted with *O*-*p*-toluenesulfonyl-*N*-Boc-ethanolamine. The protecting group was removed using trifluoroacetic acid, followed by a neutralization step, gaining the cinchona squaramide organocatalyst **7** with a linker (Scheme 1).

The lipophilic unit from methyl gallate (**8**) was gained by following a literature procedure [32] with minor modifications. The octadecyl groups were attached to the hydroxy groups using Williamson-type ether synthesis. The octadecylated gallic acid ester **9** was hydrolyzed under basic conditions in an ethanol/water mixture. After the reaction, the pH of the mixture was adjusted to 4 with hydrochloric acid, which resulted in the precipitation of the product **10** in excellent yield (95%). Next, carboxylic acid **10** was converted into the corresponding acyl chloride **11** with thionyl chloride. Finally, the cinchona squaramide with linker **7** and the octadecylated gallic acid chloride **11** were coupled to form an amide using triethylamine as a base. The crude product was purified by chromatography and precipitated from acetonitrile to gain the lipophilic organocatalyst **2** (Scheme 2).

Application and recycling of the lipophilic cinchona-squaramide organocatalyst in the stereoselective Michael addition

To prove that the previously applied catalytic unit kept its activity, the lipophilic organocatalyst **2** was applied in the stereoselective Michael addition of *trans*-β-nitrostyrene (**12**) and acetylacetone (**13**). Choosing the best solvent for the reaction is crucial, thus, solubility tests were carried out (Table 1). Since homogeneous catalysts usually exhibit higher activity and selectivity than their heterogeneous counterparts [27], our aim was to carry out the catalytic reaction homogeneously. The solubility of the lipophilic catalyst **2** was investigated in ten solvents with low polarity, including a new, bio-based polar aprotic solvent, MeSesamol [33]. The catalyst's precipitation – which is necessary for its recycling – was tested by adding a polar solvent, i.e., methanol, to its solution.

The main requirement for the polar solvent is that it should not dissolve the catalyst while it should completely dissolve the product. Therefore, we investigated the solubility of the

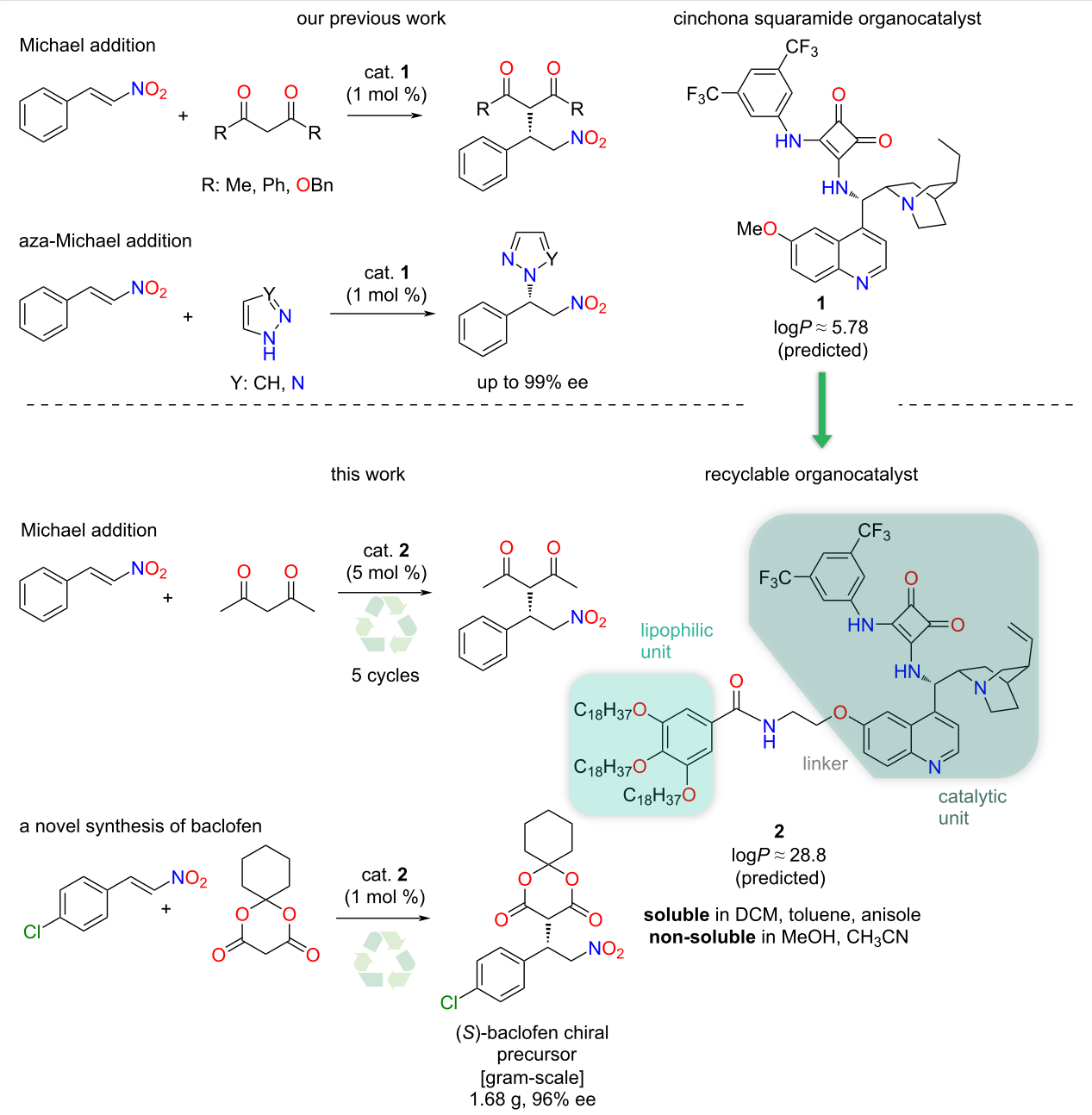

Figure 1: Application of cinchona squaramide **1** and recyclable, lipophilic cinchona squaramide organocatalysts **2** in a new, gram-scale stereoselective synthesis of baclofen precursor.

Michael adduct **14** in methanol, ethanol, propan-2-ol, Patosolv® (a mixture of 85% of ethanol and 15% of propan-2-ol), and acetonitrile. The highest solubility of **14** was found in acetonitrile (63 mg mL^{-1}) and methanol (17 mg mL^{-1}). In both of these solvents, a low solubility of the lipophilic catalyst **2** was measured (<0.5 mg mL^{-1}). Based on these results, acetonitrile was chosen as a precipitating solvent for the catalyst recycling.

To investigate the solvent effect, the stereoselective Michael addition reaction was carried out in those solvents that dissolved the catalyst and from which the catalyst was successfully precipitated by adding methanol. Furthermore, a reaction in which acetylacetone (**13**) did not only act as a reactant but also as a solvent was examined (Table 2).

The highest yields and enantiomeric excess values were reached in CPME, toluene, and dichloromethane (Table 2, entries 1–3). When acetylacetone was used as solvent, the enantiomeric excess was slightly lower because the catalyst was not completely dissolved in acetylacetone, which resulted in a hetero-

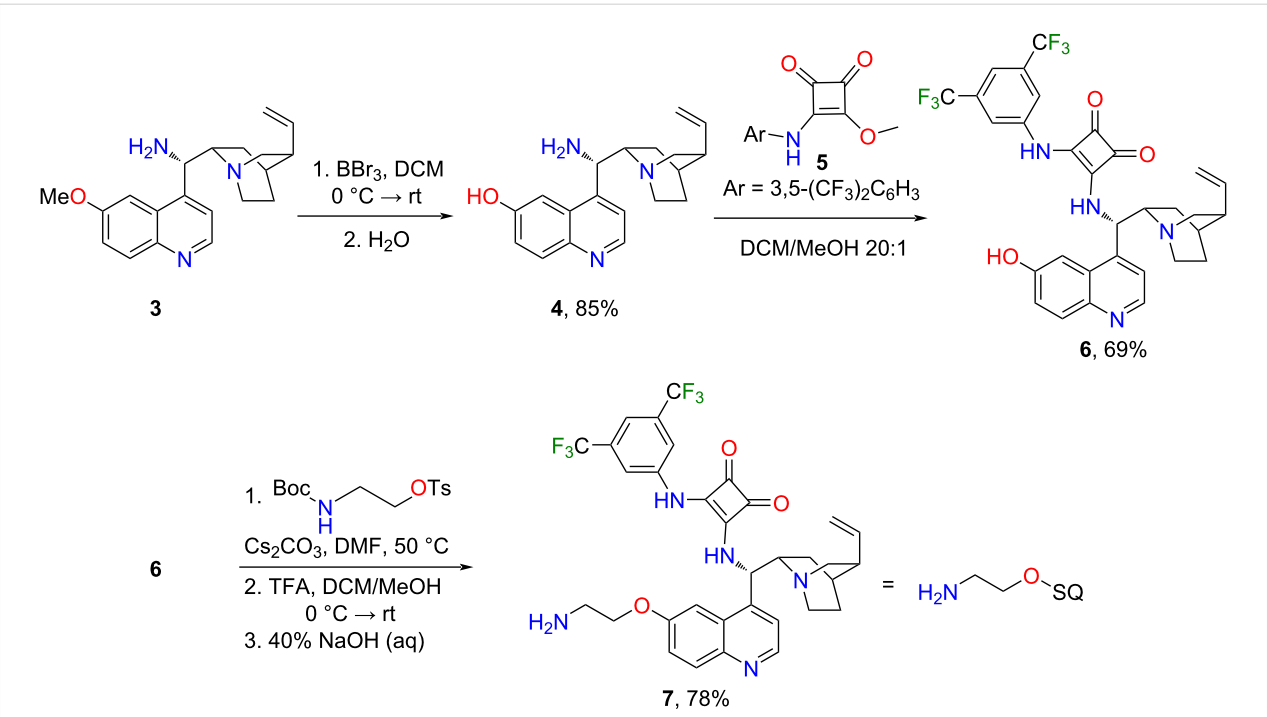

Scheme 1: Synthesis of demethylated cinchona squaramide organocatalyst and the incorporation of the flexible 2-aminoethylene linker.

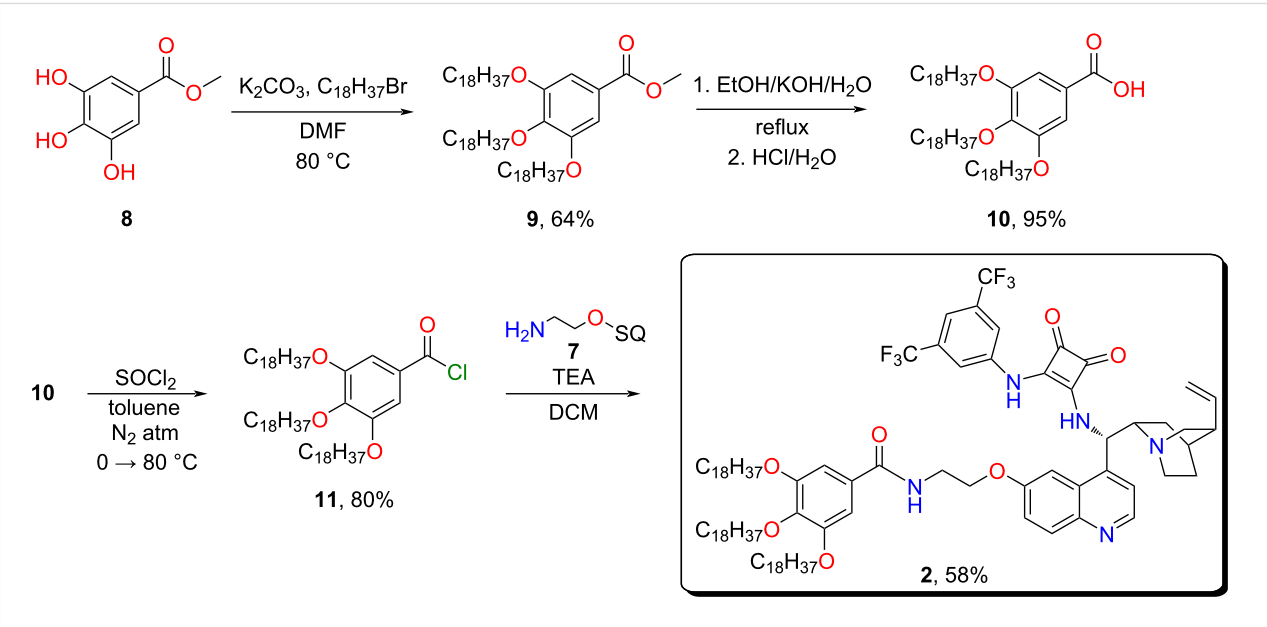

Scheme 2: Synthesis of the lipophilic tag from methyl gallate (**8**) and attachment to the cinchona squaramide.

geneous reaction mixture (Table 2, entry 4). The importance of correct solvent selection is illustrated by the case of butyl acetate, in which only a low yield was observed (Table 2, entry 5). During solvent selection, both the catalytic performance and green chemistry aspects were addressed. For this purpose, we followed GSK's solvent sustainability guide [34], which ranks solvents according to their properties, such as waste generation, environmental and health impacts, and boiling point (Figure 2).

Considering the three factors mentioned above (yield, enantiomeric excess, and green chemistry), toluene was chosen as a

Table 1: Catalyst **2** solubility in solvents with low polarity.[a]

Solvent	Dissolved?	Precipitated by MeOH?
anisole	✓	✓
butyl acetate	✓	✓
cyclohexane[b]	✓	✓
cyclopentyl methyl ether (CPME)	✓	✓
dichloromethane (DCM)	✓	✓
dimethyl carbonate (DMC)	✗	–
heptane	✗	–
MeSesamol [33]	✗	–
2-methyltetrahydrofuran (2-MeTHF)	✓	✓
toluene	✓	✓

[a]To the lipophilic catalyst (2 mg) in a vial the appropriate solvent (200 µL) was added. Then, to check the precipitability of the catalyst, MeOH (800 µL) was added. [b]Larger amounts of cyclohexane (1 mL) was needed to dissolve the catalyst.

Table 2: Solvent screening in the Michael addition of acetylacetone (**13**) to *trans*-β-nitrostyrene (**12**).[a]

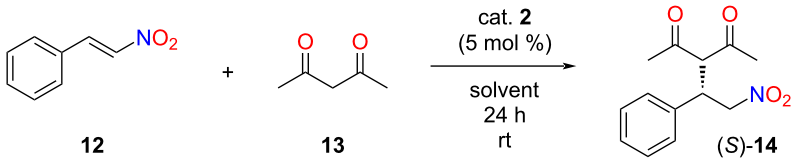

12 + **13** → (*S*)-**14**

Entry	Solvent	Yield[b] [%]	ee[c] [%]
1	CPME	85	91
2	toluene	88	93
3	DCM	91	93
4	acetylacetone	89	88
5	butyl acetate	22	94
6	2-MeTHF	94	87
7	anisole	84	89

[a]Reaction conditions: acetylacetone (**13**, 0.21 mmol) was added to the solution of *trans*-β-nitrostyrene (**12**, 0.08 mmol) and 5 mol % of catalyst **2** in 0.5 mL of solvent, then, the resulting mixture was stirred at room temperature for 24 hours. [b]Isolated yields. [c]Determined by chiral HPLC ((*S*)-enantiomer).

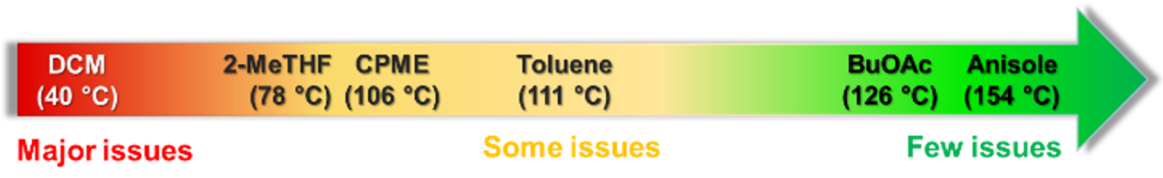

Figure 2: Classification of the tested non-polar solvents according to the GSK's solvent sustainability guide [34].

solvent for the recycling reactions. The schematic for the recycling by solvent replacement is shown in Figure 3.

After the stereoselective Michael addition was completed in non-polar toluene, toluene was evaporated in vacuo and then a polar solvent, acetonitrile was added, leading to the precipitation of the lipophilic catalyst but dissolution of the other reaction components. The reaction mixture was then transferred to Eppendorf vials and centrifuged (8 min, 13500 rpm). After phase separation, the product was isolated from the supernatant by preparative thin-layer chromatography, while the catalyst was reused in subsequent reaction cycles. The precipitated catalyst was further washed twice with acetonitrile, and dried in vacuo. The results are collected in Table 3.

Application and recycling of the lipophilic cinchona-squaramide organocatalyst in the synthesis of a baclofen precursor

After the successful application of the lipophilic catalyst, its catalytic activity was also investigated in another industrially relevant stereoselective Michael addition. This type of reaction could be used in the synthesis of several drugs to form a

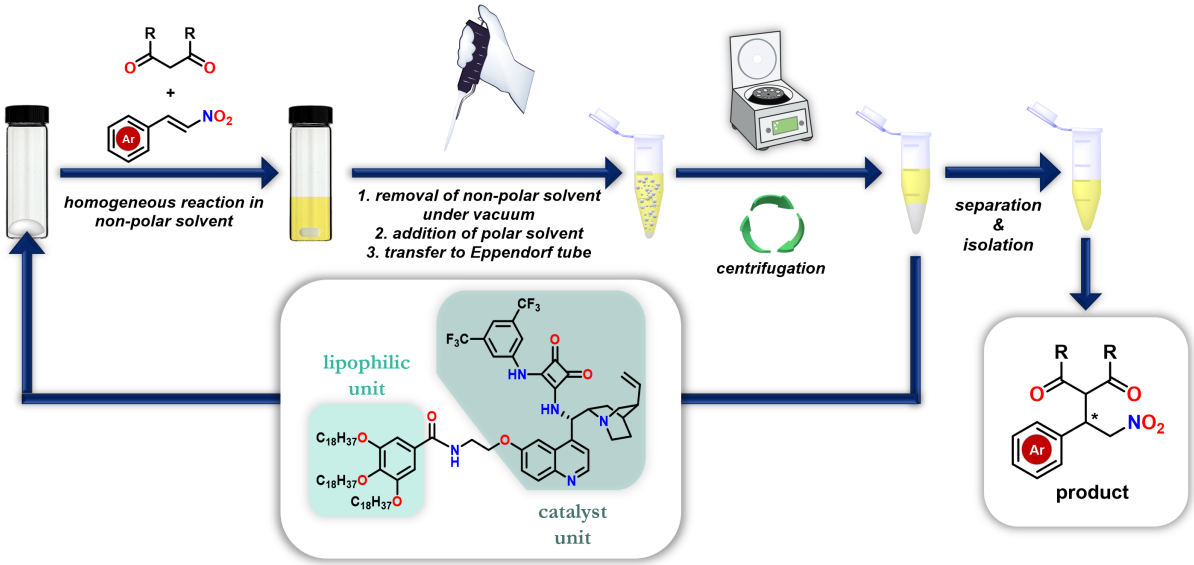

Figure 3: Recycling of the lipophilic organocatalyst in the stereoselective Michael addition by replacing the solvent.

Table 3: Recycling of lipophilic organocatalyst **2** in the Michael addition of acetylacetone (**13**) to *trans*-β-nitrostyrene (**12**).[a]

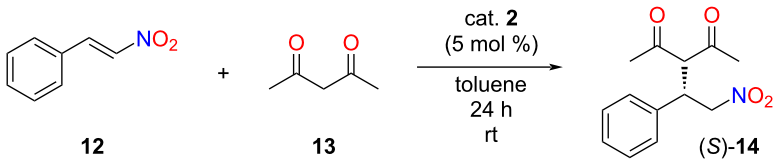

12 **13** (*S*)-**14**

Round	Yield[b] [%]	ee[c] [%]	Catalyst recycling efficiency [%]
1	84	91	91
2	89	90	99
3	94	91	92
4	93	91	99
5	96	92	97

[a]Reaction conditions: acetylacetone (**13**, 0.96 mmol) was added to the solution of *trans*-β-nitrostyrene (**12**, 0.38 mmol) and 5 mol % of catalyst **2** in 2 mL of toluene, then, the resulting mixture was stirred at room temperature for 24 hours. After the reaction was completed, the volatile components were evaporated, and acetonitrile was added for the recycling of the catalyst **2**. [b]Isolated yields. [c]Determined by chiral HPLC ((*S*)-enantiomer).

carbon–carbon bond in a stereoselective manner [6,35]. Our goal was to synthesize the chiral precursor **17** of baclofen (Scheme 3).

To achieve this objective, we first planned to use Meldrum's acid and 4-chloro-*trans*-β-nitrostyrene (**16**). Based on the literature [36], Meldrum's acid has a low solubility in non-polar solvents, resulting in diminished enantioselectivity. Furthermore, in our case, the application of polar solvents would not be favorable due to the low solubility of the lipophilic organocatalyst in these solvents. Consequently, we applied the cyclohexyl derivative of Meldrum's acid **15**, which exhibits enhanced solubility in non-polar solvents [36]. The Meldrum's acid derivative **15** was synthesized from malonic acid and cyclohexanone using acetic anhydride and sulfuric acid as a catalyst (see Supporting Information File 1) [37].

In a similar manner as the former Michael addition, a solvent screening was carried out in the previously well-established four solvents: CPME, 2-MeTHF, anisole, and toluene (Table 4, entries 1–4).

Based on the solvent screening, high yields and good enantioselectivity can be achieved in anisole and toluene, while using 2-MeTHF drastically decreased the enantioselectivity. From the perspective of green chemistry, anisole would be more favorable, but toluene is also a distinctly better alternative to the other solvents (e.g., DCM) commonly used in Michael addi-

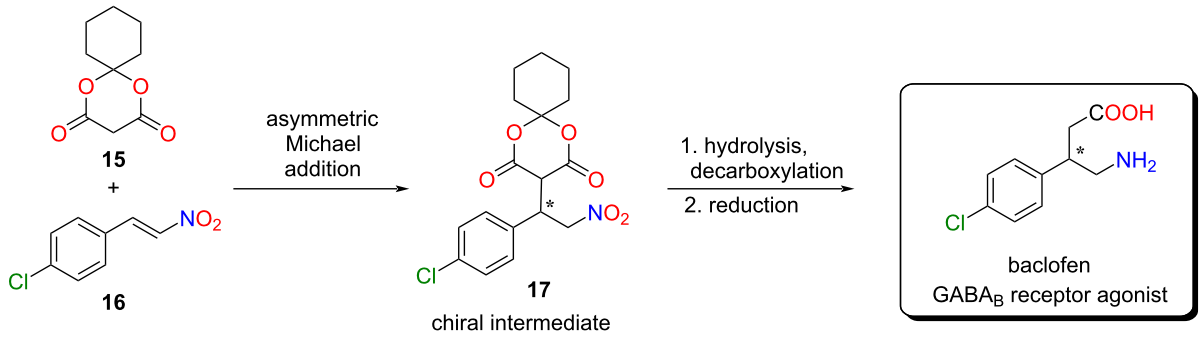

Scheme 3: A new, stereoselective synthetic route for baclofen.

Table 4: Solvent and catalyst amount screening in the Michael addition of the cyclohexyl derivative of Meldrum's acid **15** to 4-chloro-*trans*-β-nitrostyrene (**16**).[a]

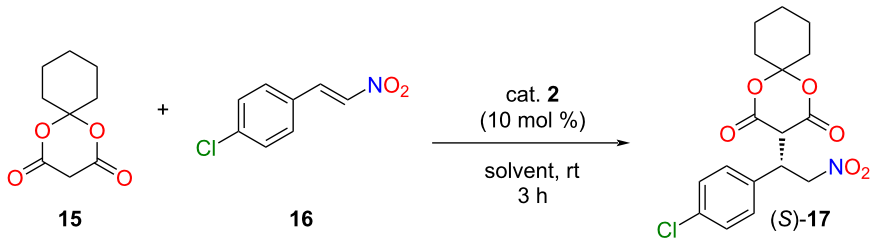

Entry	Solvent	Catalyst amount [mol%]	Yield[b] [%]	ee[c] [%]
1	CPME	10	93	82
2	2-MeTHF	10	93	29
3	anisole	10	>99	93
4	toluene	10	>99	92
5	toluene	5	97	93
6[d]	toluene	1	94	96

[a]Reaction conditions: Meldrum's acid derivative **15** (0.064 mmol) was added to the solution of 4-chloro-*trans*-β-nitrostyrene (**16**, 0.096 mmol) and 1, 5 or 10 mol % of catalyst **2** in 470 µL of solvent, then, the resulting mixture was stirred at room temperature for 3 hours. [b]Isolated yields. [c]Determined by chiral HPLC ((*S*)-enantiomer). [d]Reaction time was 5 hours to achieve full conversion.

tions. Another critical aspect that needs to be considered is how difficult the removal of the solvent is. In this respect, the boiling point of toluene (111 °C) is preferable to that of anisole, which has a boiling point of 154 °C. The results of catalyst recycling in anisole and toluene are shown in Table 5.

The lipophilic organocatalyst maintained its activity in both solvents over the five reaction cycles while the catalyst loss was marginal (<10%). It is important to note that in an industrial-scale process, the catalyst loss could be further diminished, and the centrifugation could be replaced by a simple filtration. Furthermore, for large-scale applications, the effect of catalyst amount was also investigated (Table 4, entries 4–6). Yields and enantiomeric excess values did not change significantly when the catalyst amount was reduced from 10 mol % to 1 mol %, however, a longer reaction time (5 hours) was required for the 1 mol % catalyst loading.

Gram-scale synthesis of baclofen

Finally, we planned to demonstrate the recyclability of our lipophilic organocatalyst **2** in the gram-scale synthesis of baclofen precursor (*S*)-**17**. The catalyst loading was set to 1 mol % to reduce the needed catalyst amount and the reaction time was increased to 5 hours to achieve full conversion. After the organocatalytic reaction in toluene, the volatile components were evaporated, and acetonitrile was added to precipitate the catalyst. In contrast to the small-scale recycling, in this case, we used filtration instead of centrifugation to recover the catalyst without significant loss (<5%). This demonstrates that we developed an organocatalytic reaction that can be easily scaled-up and the novel lipophilic catalyst can be recovered not only by centrifugation but also by filtration.

From the baclofen precursor (*S*)-**17**, baclofen can be synthesized in two steps. The nitro acid (*S*)-**18** was obtained using HCl in THF in good yield (70%), which could be reduced to (*S*)-baclofen hydrochloride using Raney nickel as catalyst (Scheme 4) [38].

Conclusion

In conclusion, we have prepared a new lipophilic cinchona squaramide organocatalyst **2** modified with octadecyl side chains. Thanks to the lipophilic unit, the catalyst can be easily precipitated by exchanging the non-polar solvent with a more polar one, and then its separation can be achieved by centrifugation. The lipophilic catalyst **2** demonstrated its excellent catalytic activity in two stereoselective Michael addition reactions. Homogeneous catalysis was carried out in non-polar solvents (i.e., toluene), which allows the high performance of the lipophilic organocatalyst in terms of yield and stereoselectivity.

Table 5: Recycling of lipophilic organocatalyst **2** in the Michael addition of the cyclohexyl derivative of Meldrum's acid **15** to 4-chloro-*trans*-β-nitrostyrene (**16**).[a]

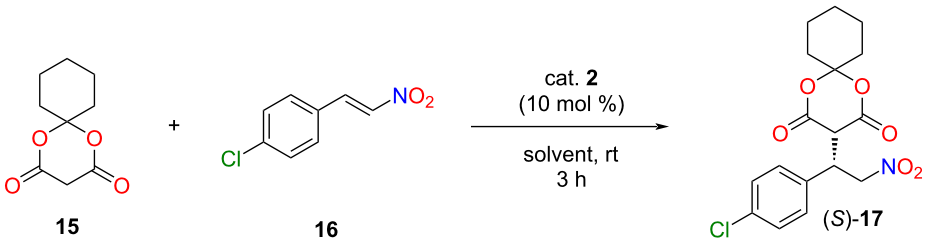

15 + **16** → (*S*)-**17**

Round	Solvent	Yield[b] [%]	ee[c] [%]
1	anisole	95	92
2		>99	95
3		>99	94
4		>99	93
5		>99	93
1	toluene	94	93
2		>99	94
3		>99	94
4		>99	94
5		97	92

[a]Reaction conditions: Meldrum's acid derivative **15** (0.19 mmol) was added to the solution of 4-chloro-*trans*-β-nitrostyrene (**16**, 0.29 mmol) and 10 mol % of catalyst **2** in 1.4 mL of solvent, then, the resulting mixture was stirred at room temperature for 3 hours. After the reaction was completed, the volatile components were evaporated, and acetonitrile was added for the recycling of the catalyst **2**. [b]Isolated yields. [c]Determined by chiral HPLC ((*S*)-enantiomer).

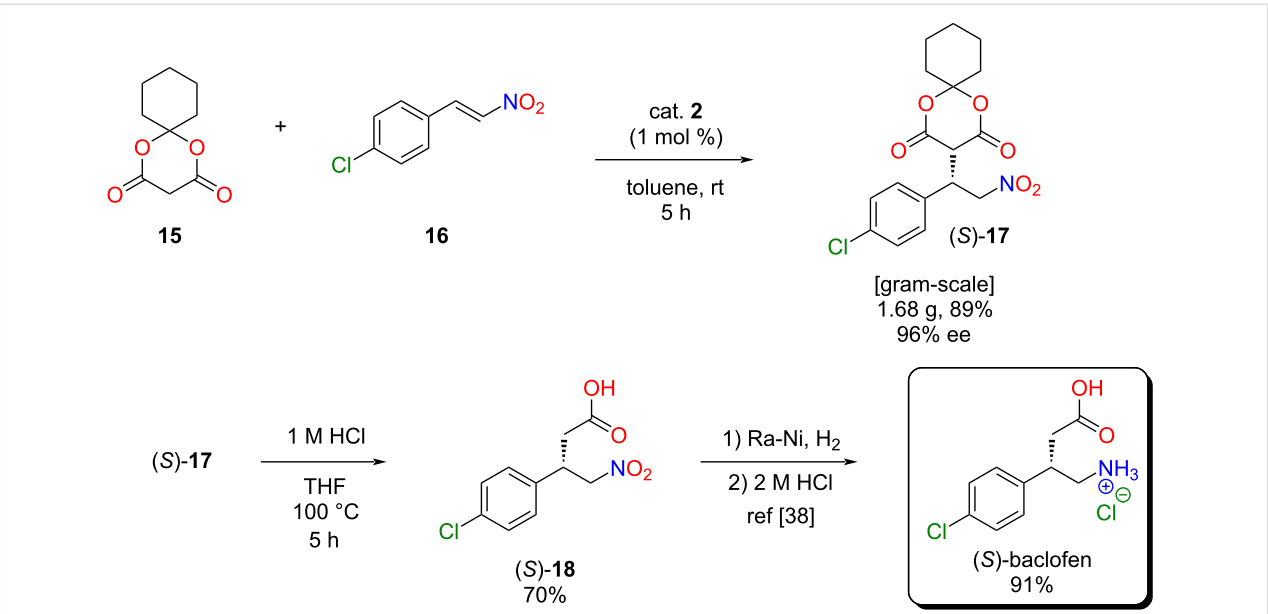

Scheme 4: Gram-scale synthesis of (*S*)-baclofen hydrochloride.

To facilitate the pharmaceutical use of the lipophilic organocatalyst, we investigated a new, industry-relevant synthesis route of baclofen in the gram-scale. The chiral precursor **17** of baclofen was obtained with quantitative yield and excellent enantiomeric excess (up to 96%). The catalyst was applied in five consecutive runs without a decrease in catalytic activity, moreover, the catalyst loss was also negligible (<10%). Overall, it can be concluded that the incorporation of the lipophilic unit does not affect the catalytic activity and selectivity but enables the facile recycling of the catalyst.

Experimental

General information

The starting materials and reagents were purchased from commercially available sources (Merck, TCI Europe, and VWR). Infrared (IR) spectra were recorded on a Bruker Alpha-T Fourier-transform IR (FTIR) spectrometer. Optical rotations were measured on a Perkin Elmer 241 polarimeter calibrated by measuring the optical rotations of both enantiomers of menthol. The reactions under pressure were carried out in a 150 mL pressure flask (Synthware Glass). Thin-layer chromatography (TLC) was performed using silica gel 60 F_{254} (Merck) plates. The spots of the materials on TLC plates were visualized by UV light at 254 nm. The reactions were monitored by TLC and high-performance liquid chromatography–mass spectrometry (HPLC–MS). The solvent ratios of the eluents are given in volume units (mL mL^{-1}). Nuclear magnetic resonance (NMR) spectra were recorded on a Bruker DRX-500 Avance spectrometer (at 500 and 126 MHz for the ^1H and ^{13}C spectra, respectively) or on a Bruker 300 Avance spectrometer (at 300 and 75.5 MHz for the ^1H and ^{13}C spectra, respectively) or on a Bruker Avance III HD (at 600 MHz for ^1H and at 150 MHz for ^{13}C spectra) at specified temperatures. High-resolution MS was measured on a Bruker MicroTOF II instrument using positive electrospray ionization. HPLC–MS was performed on an HPLC system using a Shimadzu LCMS-2020 (Shimadzu Corp., Japan) device equipped with a Reprospher (Altmann Analytik Corp., Germany) 100 Å C18 (5 µm; 100 × 3 mm) column and a positive/negative double ion source with a quadrupole MS analyzer in the range of 50–1000 *m*/*z*. Further details are available in Supporting Information File 1. The enantiomeric ratios of the samples were determined by chiral high-performance liquid chromatography (HPLC) measurements. The exact conditions of chiral HPLC are indicated in the experimental section of the corresponding compound. MarvinSketch was used for log*P* prediction, MarvinSketch 20.11, ChemAxon (https://www.chemaxon.com).

Demethylated cinchona squaramide **6**

The demethylated cinchona squaramide was prepared according to the literature procedure [39]. To the best of our knowledge, the NMR assignment has not been reported yet. ^1H NMR (methanol-d_4, 600 MHz, 295 K) δ 8.68 (d, $^3J_{H,H}$ = 4.7 Hz, 1H), 8.01 (bs, 2H), 7.94 (d, $^3J_{H,H}$ = 9.1 Hz, 1H), 7.72 (bs, 1H), 7.55 (m, 2H), 7.40 (dd, $^3J_{H,H}$ = 9.1 Hz, $^4J_{H,H}$ = 2.5 Hz, 1H), 6.15 (bs, 1H), 5.91 (m, 1H), 5.07 (bd, $^2J_{H,H}$ = 17.2 Hz, 1H), 5.02 (bd, $^2J_{H,H}$ = 10.4 Hz, 1H), 3.49 (m, 1H), 3.48 (m, 1H), 3.33 (m, 1H), 2.86 (m, 1H), 2.82 (m, 1H), 2.41 (bs, 1H), 1.69 (m, 1H), 1.68 (m, 2H), 1.54 (m, 1H), 0.85 (m, 1H); ^{13}C NMR (methanol-d_4, 150 MHz, 295 K) δ 185.7, 182.1, 170.4, 164.8, 158.3, 147.6,

145.3, 144.6, 142.5, 142.3, 133.9 (q, $^2J_{C,F}$ = 33.4 Hz), 131.7, 129.7, 124.5 (q, $^1J_{C,F}$ = 272.0 Hz), 123.9, 120.0, 119.3 (q, $^3J_{C,F}$ = 3.0 Hz), 116.7 (m), 115.2, 105.4, 61.9, 56.9, 54.7, 41.8, 40.7, 28.8, 28.3, 26.9; for the full ^{1}H and ^{13}C assignment of demethylated cinchona squaramide structure, see Supporting Information File 1.

Cinchona squaramide organocatalyst with linker, **7**

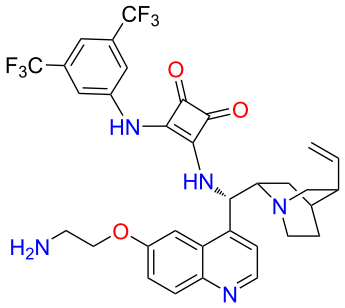

7

The demethylated cinchona squaramide **6** (732 mg, 1.19 mmol) was dissolved in DMF (15 mL), and caesium carbonate (1.75 g, 5.37 mmol, 4.5 equiv) was added to the solution at 0 °C. The reaction mixture was stirred for 20 min at this temperature. Then, the DMF (10 mL) solution of tosylated *N*-Boc-protected ethanolamine (955 mg, 3.03 mmol, 2.5 equiv, Scheme 2) was added dropwise. The reaction mixture was stirred at 50 °C for 8 hours. The volatile components were removed under reduced pressure. To the resulting orange oil, water (60 mL) was added, and the product was extracted with dichloromethane (3 × 60 mL). The combined organic phase was washed with water (2 × 60 mL), dried over $MgSO_4$, and concentrated in vacuo. The intermediate (1.24 g) was used in the next reaction without purification. The crude, *N*-Boc-protected intermediate was dissolved in dichloromethane (25 mL) and the solution cooled to 0 °C with an ice bath. Next, trifluoroacetic acid (5.74 mL, 75 mmol, 63 equiv) was added dropwise. The reaction mixture was stirred at room temperature for 1 h. Then, it was cooled to 0 °C, and a 40% NaOH(aq) solution was added to set the pH to 13. To this mixture, water (60 mL) was added, and it was extracted with DCM/MeOH 20:1 (60 mL). After the separation of the phases, the aqueous phase was extracted again with DCM/MeOH 20:1 (3 × 40 mL). The combined organic phase was dried over $MgSO_4$ and concentrated in vacuo. The obtained residue (609 mg, 78% for 2 steps) was a dark orange solid, and we used this product in the next step without further purifications. TLC (SiO_2; DCM/MeOH/25% NH_4OH(aq) 10:1:0.01, R_f 0.22); mp 158–160 °C; $[\alpha]_D^{25}$ −51.8 (*c* 1.00, DMSO); IR (cm^{-1}) ν_{max}: 2957, 2923, 2853, 1664, 1620, 1609, 1560, 1508, 1437, 1378, 1331, 1277, 1201, 1175, 1126, 1021, 930, 884, 832, 799, 719, 700, 679, 620, 550, 521, 414; ^{1}H NMR (500 MHz, MeOH-d_4, 298 K) δ 8.77 (d, *J* = 4.7 Hz, 1H), 8.03–7.96 (m, 3H), 7.94 (bs, 1H), 7.69 (d, *J* = 4.7 Hz, 1H), 7.51 (dd, *J* = 2.57 Hz, 9.27 Hz, overlapped, 1H) 7.49 (bs, overlapped, 1H), 6.28 (d, *J* = 8.9 Hz, 1H), 5.95 (ddd, *J* = 17.5, 10.3, 7.7 Hz, 1H), 5.08 (bd, *J* = 17.5 Hz, 1H), 5.03 (bd, *J* = 10.3 Hz, 1H), 4.37 (m, 2H), 3.69–3.59 (m, 1H), 3.56–3.47 (m, 1H), 3.30–3.27 (m, overlapped, 1H), 2.99 (s, 1H), 2.93–2.86 (m, 1H), 2.86 (s, 1H), 2.84–2.76 (m, 1H), 2.43–2.37 (m, 1H), 1.70–1.61 (m, overlapped, 4H), 1.27 (m, 1H), 0.73–0.66 (m, 1H) ppm; ^{13}C NMR (126 MHz, MeOH-d_4, 298 K) δ 186.4, 182.8, 170.9, 165.9, 159.7, 149.3, 146.1, 146.0, 143.5, 143.0, 134.2 (q, *J* = 33.1 Hz), 132.4, 129.9, 125.1 (q, *J* = 272.1 Hz), 124.9, 120.3, 117.0, 115.8, 103.7, 69.6, 61.4, 57.5, 55.4, 42.2, 41.5, 41.2, 37.4, 32.1, 29.4, 29.0, 28.0 ppm.; HRESI(+)-MS (*m*/*z*): [M + H$^+$] calcd for $C_{33}H_{32}F_6N_5O_3$, 660.2409; found, 660.2424.

Methyl 3,4,5-tris(octadecyloxy)benzoate (**9**)

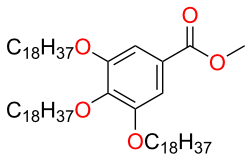

9

Methyl gallate (**8**, 15 g, 0.082 mol) was dissolved in DMF (150 mL), and 1-bromooctadecane (87.3 g, 0.262 mol) and potassium carbonate (67.5 g, 0.489 mol) were added. To the resulting reaction mixture, further DMF (150 mL) was added. After stirring for 16 hours at 80 °C, the reaction mixture was cooled, and diluted with toluene, water, and chloroform to precipitate the product. The crude product was filtered and recrystallized using chloroform/methanol mixed solvents. For a typical recrystallization of 1 gram crude product, 30 mL chloroform and 90 mL methanol were applied. The recrystallized solid was filtered to obtain product **9** as a white solid (49.2 g, 64%). The products had the same spectroscopic data than those reported in the literature [32].

Lipophilic organocatalyst **2**

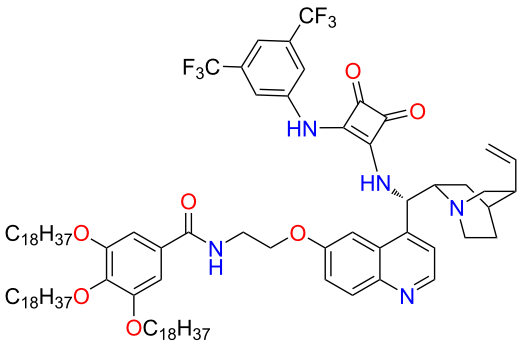

2

The cinchona squaramide with the aminoethylene linker **7** (534 mg, 0.81 mmol, 1.05 equiv) and triethylamine (1.09 mL, 8.26 mmol, 10.2 equiv) were dissolved in dichloromethane (8.8 mL). Then, a solution of 3,4,5-tris(octadecyloxy)benzoyl chloride (**11**, 729.3 mg, 0.77 mmol) in dichloromethane (22 mL) was added. To the resulting yellow solution further dichloromethane (12.6 mL) was added, and the mixture was stirred for 24 hours. Next, the reaction mixture was washed with water (2 × 30 mL), and the organic phase was dried over $MgSO_4$, and concentrated in vacuo. The crude product was purified by column chromatography (SiO_2, DCM/MeOH/NH_3(aq) 20:1:0.01 → DCM/MeOH/NH_3 10:1:0.01). The product was dissolved in a small amount of dichloromethane (1 mL) and added dropwise to acetonitrile (100 mL) to precipitate the product as an off-white solid (698 mg, 58%). TLC (SiO_2, DCM/MeOH 20:1, R_f 0.35); mp 68–69 °C; $[\alpha]_D^{25}$ +14.1 (*c* 1.00, $CHCl_3$); IR (cm^{-1}) ν_{max}: 3267, 2916, 2850, 1792, 1689, 1622, 1604, 1587, 1551, 1466, 1437, 1378, 1335, 1277, 1226, 1181, 1133, 1117, 1047, 1000, 930, 879, 851, 821, 764, 721, 701, 680, 619, 526; ^{1}H NMR (500 MHz, $CDCl_3$, 318 K) δ 8.73 (d, *J* = 3.6 Hz, 1H), 8.03 (m, 1H), 7.90–7.62 (m, 2H), 7.57–7.42 (m, overlapped, 1H), 7.40–7.33 (m, overlapped, 3H), 7.28 (m, 1H), 7.08 (br s, 2H), 6.30 (br s, 1H), 5.70 (m, 1H), 5.21–4.90 (m, 2H), 4.45 (m, 2H), 4.06–3.88 (m, overlapped, 10H), 3.76–3.69 (m, 2H), 3.61–3.19 (m, 2H), 3.09–2.65 (m, 2H), 1.93–1.61 (m, overlapped, 7H), 1.52–1.11 (m, overlapped, 94H), 0.88 (t, *J* = 7.0 Hz, 9H,) ppm; ^{13}C NMR (75 MHz, $CDCl_3$, 318 K) δ 185.4, 180.3, 175.4, 168.3, 165.1, 157.8, 153.3, 153.0, 147.9, 145.1, 141.6, 141.4, 140.3, 132.7 (q, $^2J_{C,F}$ = 34.2 Hz), 132.3, 130.3, 129.0, 127.6, 122,9 (q, $^1J_{C,F}$ = 272.0 Hz), 118.4, 116.5, 116.1, 108.0, 105.9, 101.3, 73.7, 73.6, 69.5, 69.2, 66.7, 60.4, 53.5, 41.2, 39.1, 32.1, 30.5, 29.9, 29.8, 29.6, 29.5, 26.3, 26,2 22.8, 14.2 ppm; ^{19}F NMR −63.1 ppm; HRESI(+)-MS (*m*/*z*): [M + H^+] calcd for $C_{94}H_{144}F_6N_5O_7$, 1569.0970; found, 1569.957.

General procedure for the solvent screening of stereoselective Michael addition of acetylacetone to *trans*-β-nitrostyrene

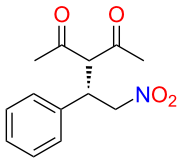

(*S*)-**14**

First, *trans*-β-nitrostyrene (**12**, 11.9 mg, 0.08 mmol) and the lipophilic organocatalyst **2** (6.3 mg, 0.004 mmol, 5 mol %) were dissolved in the appropriate solvent (500 µL). Then, acetylacetone (**13**, 21.1 µL, 0.205 mmol) was added. The reaction mixture was stirred for 24 hours at room temperature. After the reaction was completed, the solvent was evaporated, and the crude product was purified by preparative thin-layer chromatography (SiO_2, hexane/ethyl acetate 2:1, R_f 0.36) to obtain the product (*S*)-**14** as pale-yellow crystals. The products had the same spectroscopic data than those of reported (the absolute configuration was determined by the optical rotation of the products) [26]. HPLC: Phenomenex Lux Cellulose-3 column (3 mm, 250 × 4.6 mm), eluent CH_3CN/H_2O (0.1% formic acid) 40:60, isocratic mode; 0.6 mL min^{-1}; UV detector 222 nm, 30 °C. The retention time for the (*S*)-enantiomer was 12.3 min, for the (*R*)-enantiomer 14.7 min.

General procedure for recycling of the lipophilic organocatalyst in the stereoselective Michael addition of acetylacetone to *trans*-β-nitrostyrene

trans-β-Nitrostyrene (**12**, 57 mg, 0.382 mmol) and the lipophilic organocatalyst **2** (30 mg, 0.0191 mmol, 5 mol %) were dissolved in toluene (2.0 mL), and acetylacetone (**13**, 99 µL, 0.962 mmol) was added. The reaction mixture was stirred for 24 hours at room temperature. Then, the volatile components were evaporated, and acetonitrile (2 mL) was added. The dissolution of the product and the suspension of the catalyst were aided by using an ultrasonic bath. The reaction mixture was transferred to Eppendorf tubes, and the insoluble components were separated by centrifugation (8 min, 13500 rpm). After the separation, the precipitated catalyst was similarly washed twice with acetonitrile (2 × 2 mL). The combined acetonitrile phase was evaporated, and the crude product was purified by using preparative thin-layer chromatography (SiO_2, hexane/ethyl acetate 2:1, R_f 0.36) to obtain the product (*S*)-**14**. The catalyst was dried in vacuo and reused in the following reaction cycle.

General procedure for the solvent screening of stereoselective Michael addition of the cyclohexyl derivative of Meldrum's acid to 4-chloro-*trans*-β-nitrostyrene

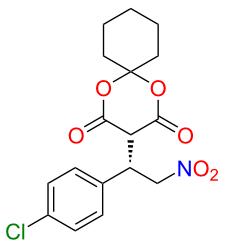

(*S*)-**17**

Cyclohexyl derivative of Meldrum's acid **15** (11.7 mg, 0.064 mmol), 4-chloro-*trans*-β-nitrostyrene (**16**, 17.5 mg, 0.096 mmol), and the lipophilic organocatalyst **2** (1, 5, or 10 mol %) were dissolved in the appropriate solvent (470 μL), and stirred for 3 hours at room temperature. Then, the solvent was evaporated, and the crude product was purified by preparative thin-layer chromatography (SiO_2, hexane/ethyl acetate/AcOH 2:1:0.01, R_f 0.34) to obtain the product as a pale-yellow foam. To the best of our knowledge, the synthesis of (*S*)-**17** has not been reported so far. TLC (SiO_2, hexane/acetone 1:3, R_f 0.85); mp 61–69 °C; $[\alpha]_D^{25}$ −5.7 (*c* 1.00, $CHCl_3$); IR (cm^{-1}) ν_{max} 2941, 2860, 1780, 1744, 1709, 1637, 1553, 1493, 1448, 1433, 1416, 1367, 1339, 1299, 1272, 1223, 1184, 1133, 1091, 1068, 1036, 1014, 998, 976, 956, 912, 49, 825, 783, 743, 718, 679, 654, 530, 425; ^{1}H NMR (500 MHz, $CDCl_3$, 298 K) δ 7.33–7.28 (m, 4H), 5.35 (dd, *J* = 13.9, 8.7 Hz, 1H), 5.00 (dd, *J* = 13.9, 6.7 Hz, 1H), 4.63 (ddd, *J* = 8.8, 6.7, 3.1 Hz, 1H), 4.02 (d, *J* = 3.2 Hz, 1H), 1.91 (t, *J* = 6.2 Hz, 2H), 1.67 (m, overlapped, 2H), 1.48–1.42 (m, 2H), 1.30–1.26 (m, overlapped, 4H) ppm; ^{13}C NMR (75 MHz, $CDCl_3$, 298 K) δ 164.4, 163.9, 135.1, 133.7, 130.7, 129.5, 106.9, 76.1, 49.0, 41.4, 36.8, 36.7, 29.8, 21.8 ppm; HRESI(+)-MS (*m*/*z*): [M + Na^+] calcd for $C_{17}H_{18}ClNO_6Na$, 390.0720; found, 390.0682; HPLC: Phenomenex Lux Cellulose-3 column (3 mm, 250 × 4.6 mm), eluent CH_3CN/H_2O (0.2% formic acid) 40:60, isocratic mode; 1 mL min^{-1}; UV detector 265 nm, 35 °C. The retention time for the (*S*)-enantiomer was 27.2 min, for the (*R*)-enantiomer 29.1 min.

General procedure for recycling of the lipophilic organocatalyst in the stereoselective Michael addition of the cyclohexyl derivative of Meldrum's acid to 4-chloro-*trans*-β-nitrostyrene

Cyclohexyl derivative of Meldrum's acid **15** (35.2 mg, 0.19 mmol), 4-chloro-*trans*-β-nitrostyrene (**16**, 52.7 mg, 0.29 mmol), and the lipophilic organocatalyst **2** (30 mg, 0.0019 mmol, 10 mol %) were dissolved in toluene or anisole (1.4 mL), and stirred for 3 hours at room temperature. After the reaction was completed, the solvent was evaporated, and acetonitrile (1.5 mL) was added. The dissolution of the product and the suspension of the catalyst were aided by using an ultrasonic bath. The reaction mixture was transferred to Eppendorf tubes, and the insoluble components were separated by centrifugation (8 min, 13500 rpm). After the separation, the precipitated catalyst was similarly washed twice with acetonitrile (2 × 1.5 mL). The combined acetonitrile phase was evaporated, and the crude product was purified by using preparative thin-layer chromatography (SiO_2, hexane/ethyl acetate/AcOH 2:1:0.01, R_f 0.34) to obtain the product (*S*)-**17**. The catalyst was dried in vacuo and reused in the following reaction cycle.

Gram-scale synthesis of baclofen precursor 17

Cyclohexyl derivative of Meldrum's acid **15** (938.4 mg, 5.1 mmol), 4-chloro-*trans*-β-nitrostyrene (**16**, 1404.2 mg, 7.6 mmol), and the lipophilic organocatalyst **2** (80 mg, 0.05 mmol, 1 mol %) were dissolved in toluene or anisole (37.6 mL), and stirred for 5 hours at room temperature. After the reaction was completed, the solvent was evaporated, and acetonitrile (30 mL) was added. The dissolution of the product and the suspension of the catalyst were aided by using an ultrasonic bath. The resulting solid was filtrated, and washed with acetonitrile (3 × 10 mL). The combined acetonitrile phase was evaporated, and the crude product was purified by using column chromatography (SiO_2, heptane/ethyl acetate/AcOH 4:1:0.01) to obtain the product ((*S*)-**17**, 1.675 g, 89%).

Synthesis of nitro acid (*S*)-18

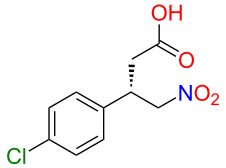

(*S*)-**18**

In a 150 mL pressure flask (Synthware), the baclofen precursor (*S*)-**17** (0.5 g, 1.36 mmol) was dissolved in THF (71 mL), and 1 M HCl (aq. solution, 36 mL) was added. The reaction mixture was heated in a 100 °C oil bath for 5 hours. Then, the volatile components were evaporated, and the aqueous phase was extracted with EtOAc (3 × 10 mL). The combined organic phase was dried over $MgSO_4$ and concentrated in vacuo. The crude product was purified by column chromatography (SiO_2, heptane/ethyl acetate/AcOH 4:1:0.01 → heptane/ethyl acetate/AcOH 1:1:0.01) to gain the product (*S*)-**18** as a white solid (232 mg, 70%). TLC (SiO_2, heptane/ethyl acetate/AcOH 1:1:0.01, R_f 0.52, visualized by bromocresol green); mp 82–84 °C (lit. [40] 78–80 °C); $[\alpha]_D^{25}$ −10.5 (*c* 2.00, MeOH), (lit. [38]: $[\alpha]_D^{25}$ −10.1 (*c* 2.00, MeOH)). The products had the same spectroscopic data than those reported in the literature [41].

Supporting Information

Supporting Information File 1

Experimental part, NMR, IR, and chiral HPLC spectra.
[https://www.beilstein-journals.org/bjoc/content/supplementary/1860-5397-19-133-S1.pdf]

Acknowledgements

The authors are grateful to Péter Bagi for his help with the chiral HPLC measurements.

Funding

This research was funded by the National Research, Development, and Innovation Office (grant number FK138037), the Richter Gedeon Excellence PhD Scholarship of the Richter Gedeon Talentum Foundation, Richter Gedeon Plc. (G. D.). Further support was provided by the UNKP-22-3-I-BME-125 New National Excellence Program of the Ministry for Culture and Innovation sourced from the National Research, Development and Innovation Fund. Project no. RRF-2.3.1-21-2022-00015 has been implemented with the support provided by the European Union.

ORCID® iDs

Gyula Dargó - https://orcid.org/0000-0003-4997-5151
Péter Kisszékelyi - https://orcid.org/0000-0002-9529-0674
József Kupai - https://orcid.org/0000-0002-4212-4517

References

1. García Mancheño, O.; Waser, M. *Eur. J. Org. Chem.* **2023,** *26,* e202200950. doi:10.1002/ejoc.202200950
2. Xiang, S.-H.; Tan, B. *Nat. Commun.* **2020,** *11,* 3786. doi:10.1038/s41467-020-17580-z
3. da Gama Oliveira, V.; do Carmo Cardoso, M. F.; da Silva Magalhães Forezi, L. *Catalysts* **2018,** *8,* 605. doi:10.3390/catal8120605
4. Krištofíková, D.; Modrocká, V.; Mečiarová, M.; Šebesta, R. *ChemSusChem* **2020,** *13,* 2828–2858. doi:10.1002/cssc.202000137
5. Castelvecchi, D.; Stoye, E. *Nature* **2021,** *598,* 247–248. doi:10.1038/d41586-021-02704-2
6. Han, B.; He, X.-H.; Liu, Y.-Q.; He, G.; Peng, C.; Li, J.-L. *Chem. Soc. Rev.* **2021,** *50,* 1522–1586. doi:10.1039/d0cs00196a
7. Burke, A. J. *Expert Opin. Drug Discovery* **2023,** *18,* 37–46. doi:10.1080/17460441.2023.2160437
8. Reyes, E.; Prieto, L.; Milelli, A. *Molecules* **2022,** *28,* 271. doi:10.3390/molecules28010271
9. Yang, W.; Du, D.-M. *Org. Lett.* **2010,** *12,* 5450–5453. doi:10.1021/ol102294g
10. Bagheri, I.; Mohammadi, L.; Zadsirjan, V.; Heravi, M. M. *ChemistrySelect* **2021,** *6,* 1008–1066. doi:10.1002/slct.202003034
11. Marqués-López, E.; Merino, P.; Tejero, T.; Herrera, R. P. *Eur. J. Org. Chem.* **2009,** 2401–2420. doi:10.1002/ejoc.200801097
12. Merino, P.; Marqués-López, E.; Tejero, T.; Herrera, R. P. *Synthesis* **2010,** 1–26. doi:10.1055/s-0029-1217130
13. Dargó, G.; Nagy, S.; Kis, D.; Bagi, P.; Mátravölgyi, B.; Tóth, B.; Huszthy, P.; Drahos, L.; Kupai, J. *Synthesis* **2022,** *54,* 3823–3830. doi:10.1055/s-0040-1719886
14. Fulgheri, T.; Della Penna, F.; Baschieri, A.; Carlone, A. *Curr. Opin. Green Sustainable Chem.* **2020,** *25,* 100387. doi:10.1016/j.cogsc.2020.100387
15. Rodríguez-Escrich, C.; Pericàs, M. A. *Chem. Rec.* **2019,** *19,* 1872–1890. doi:10.1002/tcr.201800097
16. Corma, A.; Garcia, H. *Adv. Synth. Catal.* **2006,** *348,* 1391–1412. doi:10.1002/adsc.200606192
17. Rostamnia, S.; Doustkhah, E. *RSC Adv.* **2014,** *4,* 28238–28248. doi:10.1039/c4ra03773a
18. Ferré, M.; Pleixats, R.; Wong Chi Man, M.; Cattoën, X. *Green Chem.* **2016,** *18,* 881–922. doi:10.1039/c5gc02579f
19. Benaglia, M.; Puglisi, A.; Cozzi, F. *Chem. Rev.* **2003,** *103,* 3401–3430. doi:10.1021/cr010440o
20. Nagy, S.; Fehér, Z.; Kárpáti, L.; Bagi, P.; Kisszékelyi, P.; Koczka, B.; Huszthy, P.; Pukánszky, B.; Kupai, J. *Chem. – Eur. J.* **2020,** *26,* 13513–13522. doi:10.1002/chem.202001993
21. Rodríguez-Rodríguez, M.; Maestro, A.; Andrés, J. M.; Pedrosa, R. *Adv. Synth. Catal.* **2020,** *362,* 2744–2754. doi:10.1002/adsc.202000238
22. Gawande, M. B.; Branco, P. S.; Varma, R. S. *Chem. Soc. Rev.* **2013,** *42,* 3371–3393. doi:10.1039/c3cs35480f
23. Dalpozzo, R. *Green Chem.* **2015,** *17,* 3671–3686. doi:10.1039/c5gc00386e
24. O'Neal, E. J.; Lee, C. H.; Brathwaite, J.; Jensen, K. F. *ACS Catal.* **2015,** *5,* 2615–2622. doi:10.1021/acscatal.5b00149
25. Kisszékelyi, P.; Fehér, Z.; Nagy, S.; Bagi, P.; Kozma, P.; Garádi, Z.; Dékány, M.; Huszthy, P.; Mátravölgyi, B.; Kupai, J. *Symmetry* **2021,** *13,* 521. doi:10.3390/sym13030521
26. Didaskalou, C.; Kupai, J.; Cseri, L.; Barabas, J.; Vass, E.; Holtzl, T.; Szekely, G. *ACS Catal.* **2018,** *8,* 7430–7438. doi:10.1021/acscatal.8b01706
27. Benaglia, M., Ed. *Recoverable and Recyclable Catalysts;* John Wiley & Sons: New York, NY, USA, 2009. doi:10.1002/9780470682005
28. Jichu, T.; Inokuma, T.; Aihara, K.; Kohiki, T.; Nishida, K.; Shigenaga, A.; Yamada, K.-i.; Otaka, A. *ChemCatChem* **2018,** *10,* 3402–3405. doi:10.1002/cctc.201800714
29. Kisszekelyi, P.; Alammar, A.; Kupai, J.; Huszthy, P.; Barabas, J.; Holtzl, T.; Szente, L.; Bawn, C.; Adams, R.; Szekely, G. *J. Catal.* **2019,** *371,* 255–261. doi:10.1016/j.jcat.2019.01.041
30. Olpe, H.-R.; Demiéville, H.; Baltzer, V.; Bencze, W. L.; Koella, W. P.; Wolf, P.; Haas, H. L. *Eur. J. Pharmacol.* **1978,** *52,* 133–136. doi:10.1016/0014-2999(78)90032-8
31. Vakulya, B.; Varga, S.; Csámpai, A.; Soós, T. *Org. Lett.* **2005,** *7,* 1967–1969. doi:10.1021/ol050431s
32. Kim, S.; Matsumoto, M.; Chiba, K. *Chem. – Eur. J.* **2013,** *19,* 8615–8620. doi:10.1002/chem.201300655
33. Dargo, G.; Kis, D.; Gede, M.; Kumar, S.; Kupai, J.; Szekely, G. *Chem. Eng. J.* **2023,** *471,* 144365. doi:10.1016/j.cej.2023.144365
34. Alder, C. M.; Hayler, J. D.; Henderson, R. K.; Redman, A. M.; Shukla, L.; Shuster, L. E.; Sneddon, H. F. *Green Chem.* **2016,** *18,* 3879–3890. doi:10.1039/c6gc00611f
35. Hayashi, Y. *Chem. Sci.* **2016,** *7,* 866–880. doi:10.1039/c5sc02913a
36. Kimmel, K. L.; Weaver, J. D.; Ellman, J. A. *Chem. Sci.* **2012,** *3,* 121–125. doi:10.1039/c1sc00441g
37. Jiang, H.; Zhang, J.-M.; Du, W.-Q.; Zhu, S.-Z. *Chin. J. Chem.* **2007,** *25,* 86–89. doi:10.1002/cjoc.200790023
38. Camps, P.; Muñoz-Torrero, D.; Sánchez, L. *Tetrahedron: Asymmetry* **2004,** *15,* 2039–2044. doi:10.1016/j.tetasy.2004.05.021
39. Hajra, S.; Jana, B. *Org. Lett.* **2017,** *19,* 4778–4781. doi:10.1021/acs.orglett.7b02150
40. Felluga, F.; Gombac, V.; Pitacco, G.; Valentin, E. *Tetrahedron: Asymmetry* **2005,** *16,* 1341–1345. doi:10.1016/j.tetasy.2005.02.019
41. Zu, L.; Xie, H.; Li, H.; Wang, J.; Wang, W. *Adv. Synth. Catal.* **2007,** *349,* 2660–2664. doi:10.1002/adsc.200700353

BEILSTEIN JOURNAL OF ORGANIC CHEMISTRY

Metal-catalyzed coupling/carbonylative cyclizations for accessing dibenzodiazepinones: an expedient route to clozapine and other drugs

Amina Moutayakine[1,2] and Anthony J. Burke*[2,3,4]

Full Research Paper

Open Access

Address:
[1]Instituto Universitario de Bio-Orgánica “Antonio González” (IUBO-AG), University of la Laguna, 38206 San Cristóbal de La Laguna, Santa Cruz de Tenerife, Spain, [2]LAQV-REQUIMTE, University of Évora, Rua Romão Ramalho, 59, 7000 Évora, Portugal, [3]University of Évora, Department of Chemistry Rua Romão Ramalho, 59, 7000 Évora, Portugal, and [4]Faculty of Pharmacy, University of Coimbra, Pólo das Ciências da Saúde, Azinhaga de Santa Coimbra, 3000-548 Coimbra, Portugal

Email:
Anthony J. Burke* - ajburke@ff.uc.pt

* Corresponding author

Keywords:
Buchwald–Hartwig; carbonylative cyclization; Chan–Lam; nitrogen heterocycle; one-pot

Beilstein J. Org. Chem. **2024,** *20,* 193–204.
https://doi.org/10.3762/bjoc.20.19

Received: 18 November 2023
Accepted: 17 January 2024
Published: 31 January 2024

This article is part of the thematic issue "5th International Symposium on Synthesis and Catalysis (ISySyCat 2023)".

Associate Editor: T. J. J. Müller

Abstract

A sequential strategy to access 10,11-dihydro-5*H*-dibenzo[*b*,*e*][1,4]diazepinones (DBDAPs) is disclosed in this article through a palladium and copper-catalyzed amination (Buchwald–Hartwig (B–H) or Chan–Lam (C–L)) followed by a palladium-catalyzed intramolecular aminocarbonylation with $Mo(CO)_6$ as CO surrogate (to avoid toxic CO handling) of readily available *o*-phenylenediamines and either 1,2-dibromobenzene or 2-bromophenylboronic acid. The 10,11-dihydro-5*H*-dibenzo[*b*,*e*][1,4]diazepinone could be synthesized in good yield using a sequential catalytic procedure, using both C–L and B–H approaches. Gratifingly, the use of the C–L reaction was more impressive, and afforded the dibenzodiazepinones in good yields (up to 45%; 2 steps) and much milder conditions using copper as the catalyst. The synthetic utility of this novel strategy was showcased by demonstrating a formal synthesis for the antipsychotic drug clozapine and to an anticancer triazole–DBDAP hybrid.

Introduction

Dibenzodiazepine units are without doubt highly privileged structures, endowed with numerous medicinally relevant properties, and notably include anti-anxiolytic and antidepressant activities. These scaffolds have received much interest from the medicinal chemist community, which led to the development of several antidepressant agents such as dibenzepin, sintamil, as well as the well-known medication, clozapine, an FDA-approved atypical antipsychotic drug, that has been adopted as a treatment of schizophrenia and schizoaffective disorders (Figure 1) [1,2]. Dibenzodiazepinones were also found to exhib-

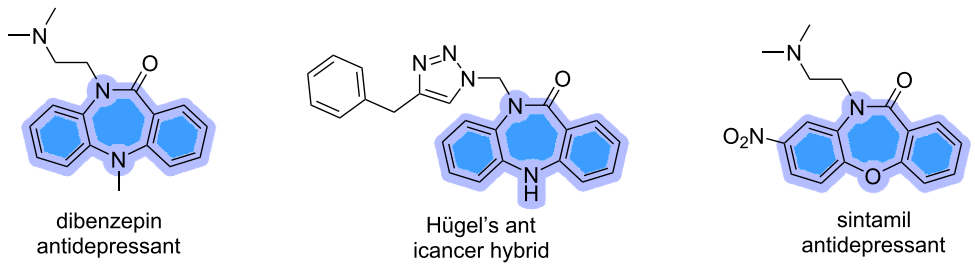

Figure 1: Biologically active dibenzodiazepinones.

it significant anticancer properties [3], as they were found to effectively inhibit tumor invasion in vitro [4], and induce apoptosis among several cancer cell lines [5]. Additionally, several dibenzodiazepinone-based structures were proven to act as p21-activated kinase (PAK) inhibitors [6], and Chk1 inhibitors [7]. The abovementioned pharmaceutical properties of the dibenzodiazepinone class have driven the development of novel synthetic strategies leading to these scaffolds in a step-economical and greener manner. Our previous review in 2018 focused on a variety of routes to these compounds [8].

The well-known Buchwald–Hartwig (B–H) and Chan–Lam (C–L) reactions have proven to be highly useful procedures that allow the step-economical synthesis of diverse biologically relevant heterocycles through C–N bond formation [9]. These approaches resulted in shortening the synthetic routes that were widely employed to access these heterocyclic scaffolds. Over the last decades, the Chan–Lam coupling reaction has drawn great attention among the synthetic chemistry community which contributed to the development of various synthetic routes to relevant heterocycles in high efficiency [10]. The Chan–Lam coupling is considered a greener alternative to traditional C–N coupling reactions, as it can be carried out under mild reaction conditions (room temperature and short reaction times, etc.), plus it does not require expensive metals like Pd, being carried out with Cu.

The aminocarbonylation reaction which was introduced by Schoenberg and Heck in 1974 is an efficient catalytic route to carboxamides [11]. It was a major step forward and has been amply applied in a number of carbonylation reactions over the years [12].

In 2011, Buchwald and Tsvelikhovsky introduced an efficient synthetic strategy to construct diverse dibenzodiazepinones through a sequential methodology consisting of a B–H coupling between *o*-carbonylanilines and 1,2-dihaloarene derivatives providing access to key precursors that undergo a tandem amination–intramolecular cyclization via a cross-coupling reaction with NH_3 [13]. The reaction was undertaken in the presence of a catalytic amount of a palladium catalyst and afforded a library of dibenzodiazepinones in good to excellent yields (Scheme 1a).

In 2013, Zhang et al. developed a synthetic route leading to structurally diverse dibenzodiazepinones via a copper-catalyzed C–N bond coupling between 2-halobenzoates and *o*-phenylenediamines leading to a key intermediate that undergoes an intramolecular *N*-acylation to afford the corresponding dibenzodiazepinone structure in high yields (Scheme 1b) [14]. Another innovative strategy was reported by Laha et al., aiming to access dibenzodiazepinone structures via a double *N*-arylation of 2-aminobenzamides with 1,2-dihaloarenes using a palladium-based catalytic system [15].

Mechanistic investigations supported the fact that the regioselective *N*-arylation of the 2-aminobenzamide occurs first at the amide position. This approach enabled the successful synthesis of a broad spectrum of dibenzodiazepinone units in a one-pot fashion. The synthetic utility of Laha's approach was highlighted by preparing the corresponding dibenzodiazepinone which was further reacted with *N*-methylpiperazine in the presence of $TiCl_4$ to afford clozapine, an antipsychotic drug.

We now disclose a different, but facile approach to access several 10,11-dihydro-5*H*-dibenzo[*b*,*e*][1,4]diazepinones, using a sequential Chan–Lam and Buchwald–Hartwig intramolecular aminocarbonylation (Scheme 1d). This approach has not been reported previously (the methods a–c indicated in Scheme 1 have a different route, and none involve either a Chan–Lam or carbonylative cyclization). For the sake of health and safety, and given that our infrastructures did not permit the use of molecular CO, we felt more secure with a suitable surrogate. Not only that, the use of safer to use surrogates, is important for use in enabling technologies, like continuous flow and microwave-heated reactions. In fact, CO-free aminocarbonylation reactions are well known, and molybdenum hexacarbonyl ($Mo(CO)_6$) is a very useful surrogate having been used in a multitude of reactions [16,17].

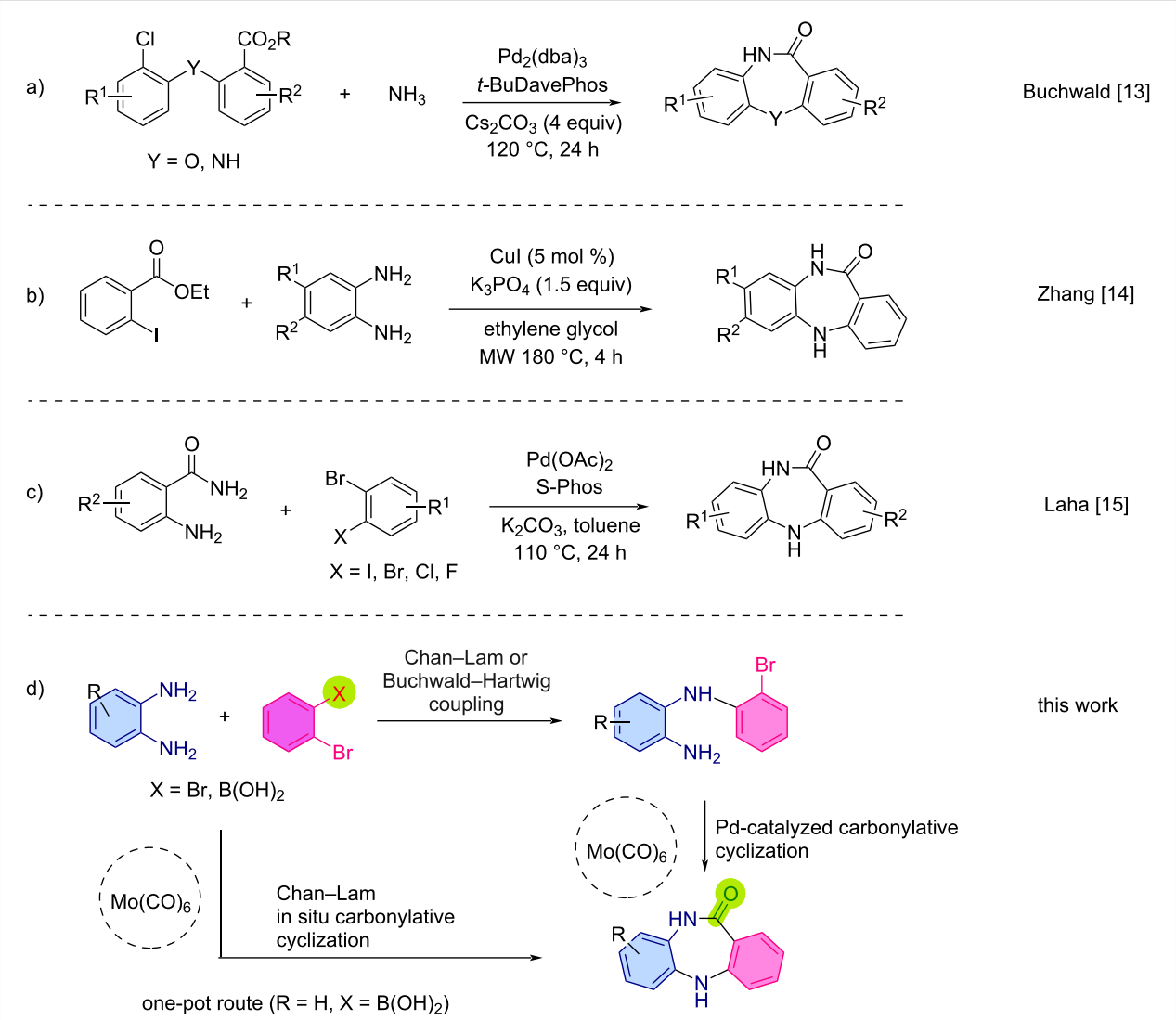

Scheme 1: Different synthetic routes to DBDAPs (a–c), including our novel approach (d).

The present approach enables the formation of two C–N bonds along with a C–C bond and provides a good alternative to previously reported strategies, as it enables the formation of these structures in a multicomponent fashion in the presence of a CO surrogate through the in situ formation of an *o*-(2-bromophenyl)aminoaniline intermediate (Scheme 1d). It should be noted these target compounds have been of great interest to our group and in 2015 we reported a proposed novel methodology for the synthesis of dibenzodiazepines [18], however, upon later careful review of the product structure it was revealed that the purported dibenzodiazepine products were, in fact, diarylimines, which resulted from a nucleophilic addition of the aniline reagents to the aldimine substrates, followed by elimination of an tosylamine product. This was one of the principle driving forces for the development of the work discussed in this report.

Results and Discussion

Synthesis of *o*-(2-bromophenyl)aminoaniline via Buchwald–Hartwig C–N coupling

One-pot synthesis of dibenzodiazepinones

Our preliminary attempt to synthesize DBDAPs via B–H amination and carbonylation was carried out in the presence of *o*-phenylenediamine (**1a**) and 1,2-dibromobenzene (**2**) as model reactants using $Pd(OAc)_2$ in combination with *t*-BuXPhos (2-di-*tert*-butylphosphino-2',4',6'-triisopropyl-1,1'-biphenyl) (5 mol %), and Et_3N (2.5 equiv) as base in DMF. In this case, DMF served as the CO surrogate, as it was disclosed that DMF, the reaction solvent, could act as a potential carbon monoxide surrogate under certain circumstances, notably, in metal-catalyzed aminocarbonylation procedures [19,20]. Unfortunately, no DBDAP was obtained and we only observed the formation

of intermediate **3a** in 25% yield (entry 1, Table 1). Next, the same procedure was carried out in the presence of molybdenum hexacarbonyl ($Mo(CO)_6$, 2 equiv) as CO surrogate, under the previous conditions, but again we only observed the formation of intermediate **3a** in 21% yield (entry 2, Table 1). Changing the ligand to triphenylphosphine, did not provide any improvement of the reaction outcome as only traces of the intermediate **3a** were obtained (entry 3, Table 1). Switching to DBU as the base under these conditions, gave intermediate **3a** in 35% yield (entry 4, Table 1). In fact, DBU was previously shown by Wannberg and Larhed to be an effective ligand in a variety of highly efficient aminocarbonylation reactions with $Mo(CO)_6$ due to its strong basicity and accelerated release of CO from this reagent [21]. The reaction was then screened using two different bidentate ligands, XPhos and XantPhos, and using the previous reaction conditions. However, we only obtained traces of intermediate **3a** (entries 5 and 6, Table 1). A slight improvement of the yield of the intermediate **3** was obtained when using DBU in dioxane, which gave **3a** in 42%, but only traces of the target DBDAP were observed (entry 7, Table 1). The difficulty encountered in the formation of DBDAP, prompted us to test alternative CO surrogates. When the reaction was performed using $Co_2(CO)_8$ (0.3 equiv) in the presence of DBU, the intermediate **3a** was isolated in 35% yield, but again no DBDAP **4** was obtained (entry 8, Table 1). Formic acid, an effective CO surrogate [20,22], was also screened. The reaction was carried out in the presence of acetic anhydride (Ac_2O) as an activator, but unfortunately, no DBDAP was obtained (entry 9, Table 1). The use of triphosgene as the CO transfer agent failed to give any product.

When we undertook the B–H amination/carbonylative cyclization of *o*-phenylenediamine (**1a**) with 1,2-dibromobenzene (**2**) in the presence of 5 mol % of $PdCl_2(CH_3CN)_2$ and 5 mol % of *t*-BuXPhos, with Et_3N (2.5 equiv) and $Mo(CO)_6$ in DMF at 150 °C, surprisingly this afforded the 5*H*-dibenzo[*b*,*e*][1,4]diazepin-11-ol (**5**), the tautomer of DBDAP (**4a**) in 53% (Scheme 2). We attempted to convert compound **5** into the keto

Table 1: Explorative study of the sequential Buchwald–Hartwig amination/Pd-catalyzed carbonylative cyclization leading to DBDAPs.[a]

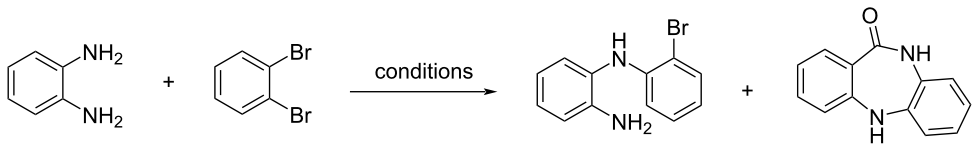

1a **2** **3a** **4a**

Entry	Cat (mol %)	Ligand (5 mol %)	CO	Base	Solvent	**3a**[b]	**4a**[b]
1	$Pd(OAc)_2$ (5)	*t*-BuXPhos	–	Et_3N	DMF	25%	0
2	$Pd(OAc)_2$ (5)	*t*-BuXPhos	$Mo(CO)_6$	Et_3N	DMF	21%	0
3	$Pd(OAc)_2$ (5)	PPh_3	$Mo(CO)_6$	Et_3N	DMF	traces	0
4	$Pd(OAc)_2$ (5)	*t*-BuXPhos	$Mo(CO)_6$	DBU	DMF	35%	0
5	$Pd(OAc)_2$ (5)	XPhos	$Mo(CO)_6$	Et_3N	DMF	traces	0
6	$Pd(OAc)_2$ (5)	XantPhos	$Mo(CO)_6$	Et_3N	DMF	traces	0
7[c]	$Pd(OAc)_2$ (5)	*t*-BuXPhos	$Mo(CO)_6$	DBU	dioxane	42%	traces
8[c]	$Pd(OAc)_2$ (5)	*t*-BuXPhos	$Co_2(CO)_8$	DBU	DMF	35%	–
9[c]	$Pd(OAc)_2$ (5)	*t*-BuXPhos	$HCOOH/Ac_2O$	Et_3N	DMF	–	–

[a]Reaction conditions: *o*-phenylenediamine (**1a**, 0.46 mmol), dibromobenzene (**2**, 0.46 mmol), $Pd(OAc)_2$, base (2.5 equiv), CO surrogate ($Mo(CO)_6$ and other CO surrogate (2 equiv) or $Co_2(CO)_8$ (0.3 equiv)), solvent (5 mL), 130 °C, 20 h. [b]Isolated yields. [c]The reaction was carried out during 24 h.

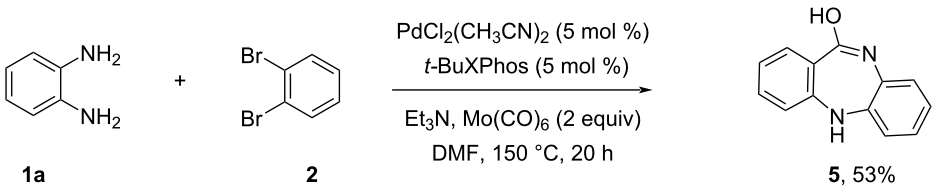

1a **2** **5**, 53%

Scheme 2: One-pot synthesis of 5*H*-dibenzo[*b*,*e*][1,4]diazepin-11-ol (**5**).

form **4a** by using TFA to shift the equilibrium towards the desired product, but this proved to be futile under these conditions, as only the iminol **5** structure was observed.

Attempt at accessing dibenzodiazepinone via step-wise synthesis

Due to the difficulty encountered in the one-step synthesis of DBDAPs, we embarked on an in-depth study of the B–H coupling/carbonylative cyclization in a step-wise fashion. Our first attempt was conducted using the previous conditions, which led to the desired compound **3a** in 15% yield (entry 1, Table 2). Changing the ligand to PPh_3 under the same conditions (entry 2, Table 2) resulted in poorer results, as only traces of the desired compound **3a** were observed. Then, we considered XPhos (entry 3, Table 2), and the bidendate ligands XantPhos and DPEPhos (entries 4 and 5, Table 2), but no improvements were observed. Then, we tested an alternative palladium source, namely Pd_2dba_3, but again only traces of the compound **3a** were observed (entry 6, Table 2). Next, we increased the $Pd(OAc)_2$ catalyst loading to 10 mol % and the amount of the *t*-BuXphos ligand to 15 mol % in the presence of DBU and DMF. Under these conditions, the intermediate **3a** was obtained in 15% yield along with the undesired dihydrophenazine **6** side product in 5% yield, produced by a further C–N bond coupling (entry 7, Table 2). We decided to decrease the amount of base and time, but little improvement was observed (entry 8, Table 2). Given the well-established role of the base on the B–H coupling, we considered exploring alternative bases. We conducted the reaction in the presence of the previously disclosed catalytic system but using *t*-BuOK as the base and obtained compound **3a** in 22% yield (entry 9, Table 2). Conducting the reaction in the presence of Cs_2CO_3 in DMF, failed to provide any improvement (entry 10, Table 2). However, replacing DMF by dioxane as the solvent in the presence of DBU led to a significant improvement in the yield of the reaction, as the intermediate **3a** could be obtained in 40% yield, along with the phenazine **6** in 48% (entry 11, Table 2). Next, we screened other ligands such as XPhos and DPEPhos in the presence of Cs_2CO_3 as base in dioxane, however, the undesired phenazine product **6** was still obtained in moderate yield under these conditions (entries 12 and 13, Table 2). In the presence of SPhos as ligand, Cs_2CO_3, and toluene as solvent, the desired intermediate **3a** was obtained in 20% yield along with 55% of the phenazine **6** (entry 14, Table 2). Although toluene was shown to be a good solvent for this B–H coupling reaction, we were unable to prevent the double B–H reaction from occurring leading to the phenazine **6**, even when shortening the reaction time to 1 h.

Table 2: Influence of the catalytic system, base, and solvent combination on the outcome of the Buchwald–Hartwig reaction.[a]

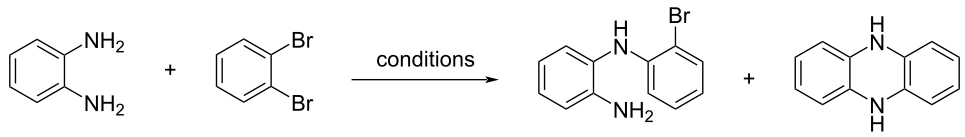

1a **2** **3a** **6**

Entry	Cat (mol %)	Ligand	Base	Solvent	Time	**3a**[b]	**6**[b]
1	$Pd(OAc)_2$ (5)	*t*-BuXPhos	Et_3N	DMF	10 h	15	–
2	$Pd(OAc)_2$ (5)	PPh_3	Et_3N	DMF	10 h	–	–
3	$Pd(OAc)_2$ (5)	XPhos	Et_3N	DMF	10 h	–	–
4	$Pd(OAc)_2$ (5)	XantPhos	Et_3N	DMF	10 h	–	–
5	$Pd(OAc)_2$ (5)	DPEPhos	Et_3N	DMF	10 h	–	–
6	Pd_2dba_3 (5)	*t*-BuXPhos	DBU	DMF	24 h	traces	–
7	$Pd(OAc)_2$ (10)	*t*-BuXPhos	DBU	DMF	24 h	15	5
8[c]	$Pd(OAc)_2$ (10)	*t*-BuXPhos	DBU	DMF	10 h	10	–
9[c]	$Pd(OAc)_2$ (10)	*t*-BuXPhos	*t*-BuOK	DMF	24 h	22	–
10[c]	$Pd(OAc)_2$ (10)	*t*-BuXPhos	Cs_2CO_3	DMF	24 h	traces	–
11[c]	$Pd(OAc)_2$ (10)	*t*-BuXPhos	DBU	dioxane	24 h	40	48
12[c]	$Pd(OAc)_2$ (10)	XPhos	Cs_2CO_3	dioxane	10 h	45	39
13[d]	$Pd(OAc)_2$ (10)	DPEPhos	Cs_2CO_3	dioxane	10 h	35	30
14[d]	$Pd(OAc)_2$ (10)	SPhos	Cs_2CO_3	toluene	10 h	20	55

[a]Reaction conditions: *o*-phenylenediamine (**1a**, 0.46 mmol), dibromobenzene (**2**, 0.46 mmol), Pd catalytic system, base (2.5 equiv), DMF (5 mL), 110 °C, 24 h; *o*-(2-bromophenyl)aminoaniline (**3a**) and 5,10-dihydrophenazine (**6**) products were detected by TLC and ^{1}H NMR, and yields determined after product isolation. [b]Isolated yields. [c]1.5 Equivalents of base were used. [d]1.2 Equivalents of base were used.

Interestingly, we noticed that in the initial one-pot reactions indicated in Table 1, the yields of the diarylamine **3a** were better when $Mo(CO)_6$ was present (compare entry 4, Table 1 to entry 7, Table 2). This might be due to (a) the fact that the temperature used for the reactions described in Table 1, involving $Mo(CO)_6$ were 20 °C higher than the reactions described in Table 2 and/or (b) $Mo(CO)_6$ acts as a co-catalyst. An investigative study was thus undertaken to elucidate the effect of the molybdenum reagent on the reaction using a simple model system consisting of aniline and bromobenzene (see Figure S1 and Table S1 in Supporting Information File 1). The experimental design was limited, in that we only monitored the reaction over a 90 min period. Contrary to what was originally believed the reaction without the Mo reagent gave better results during the first 90 min, but without additional data it is impossible to draw firm conclusions about this reaction, and thus further studies will be carried out in the near future.

After uncovering the optimum conditions to access *o*-(2-bromophenyl)aminoaniline via the B–H coupling reaction, it was decided to explore the carbonylative intramolecular cyclization of the intermediate **3a** using different catalytic systems. To elucidate the role of the palladium catalyst in this process, we carried out the initial attempt under metal free-conditions using molybdenum hexacarbonyl ($Mo(CO)_6$) as CO surrogate, in the presence of Et_3N in DMF. The reaction was performed at 130 °C, as we believed that high temperature will promote the cyclization of the sterically hindered intermediate **3a**, but no DBDAP was achieved under these conditions (entry 1, Table 3). Next, $Pd(OAc)_2$ was employed under ligand-free conditions, but again the desired DBDAP product **4a** could not be attained (entry 2, Table 3). Then, we performed the reaction in the presence of *t*-BuXPhos as ligand and in this case, only traces of the DBDAP **4a** were obtained (entry 3, Table 3). When the reaction was carried out in the presence of DPEPhos (entry 4, Table 3), we were delighted to obtain the final dibenzodiazepine in 80% yield. Next, we tested another bidentate ligand, XantPhos, which led to the obtention of the desired product **4a** in an excellent yield of 90% (entry 5, Table 3). This result implied that diphosphine ligands were essential for the success of this reaction. The reactivity of Co_2CO_8 as CO surrogate was also explored, in this case the reaction afforded the DBDAP product **4a** in 55% yield (entry 6, Table 3). Molybdenum hexacarbonyl ($Mo(CO)_6$), was shown to be a powerful CO surrogate in this carbonylative intramolecular cyclization. The efficacy of $Mo(CO)_6$ is due to the energetically favorable dissociation of $Mo(CO)_n$ into $Mo(CO)_{n-1}$ which was proven to be a highly exothermic reaction in the presence of metal catalysts especially after the dissociation of the first CO group [23].

Table 3: The intramolecular catalytic carbonylative cyclization conditions for *o*-(2-bromophenyl)aminoaniline.[a]

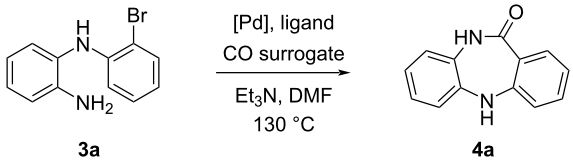

3a **4a**

Entry	Catalytic system	CO surrogate	Yield **4a**[b] (over 2 steps)
1	None	$Mo(CO)_6$	–
2	$Pd(OAc)_2$	$Mo(CO)_6$	–
3	$Pd(OAc)_2$/*t*-BuXPhos	$Mo(CO)_6$	traces
4	$Pd(OAc)_2$/DPEPhos	$Mo(CO)_6$	80% (44%)
5	$Pd(OAc)_2$/XantPhos	$Mo(CO)_6$	90% (50%)
6	$Pd(OAc)_2$/XantPhos	$Co_2(CO)_8$	55% (30%)

[a]Reaction conditions: *o*-(2-bromophenyl)aminoaniline (**3a**, 0.46 mmol), $Pd(OAc)_2$ (10 mol %), ligand (30 mol %, $Mo(CO)_6$ (1 equiv), Et_3N (1 equiv) DMF (5 mL), 130 °C, 20 h. The reaction was monitored by TLC. [b]Isolated yields.

It should be noted that the best overall yield for the synthesis of **4a** using the step-wise approach was 50% (Table 3).

Synthesis of dibenzodiazepinones via Chan–Lam amination/carbonylative coupling

Synthesis of *o*-(2-bromophenyl)aminoaniline via Chan–Lam C–N coupling

Inspired by the previously independently reported work by Chan [24] and Lam [25] and co-workers, we considered performing the reaction of *o*-phenylenediamine (**1a**) with 2-bromophenylboronic acid (**7**) in the presence of $Cu(OAc)_2$, Et_3N as base in DCM at 50 °C (entry 1, Table 4), and gratifingly under these conditions, the reaction afforded compound **3a** in 48% yield. The Chan–Lam couplings were undertaken under an aerobic atmosphere which is an environmentally benign oxidant. Further screening using dioxane as solvent resulted in an increase in the yield to 55%, whilst DMF gave access to **3a** in a lower yield (30%) (entries 2 and 3, Table 4). Next, we considered testing the performance of copper iodide (CuI, 20 mol %) as catalyst, in the presence of Et_3N both in dioxane and DMF. These conditions resulted in the obtainment of the desired compound **3a** in 59% and 35% yield, respectively (entries 4 and 5, Table 4). Increasing the reaction temperature to 100 °C resulted in a reduction of the reaction yield due to purported catalyst degradation (entry 6, Table 4). Then, we considered decreasing the amount of CuI to 10 mol % which led to a decrease of the reaction yield to 31% (entry 7, Table 4). Other bases such as dimethylaminopyridine (DMAP) and diisopropylethylamine (DIPEA) were tested under the previous reac-

Table 4: Optimization of the Chan–Lam coupling conditions between *o*-phenylenediamine (**1a**) and 2-bromophenylboronic acid (**7**).[a]

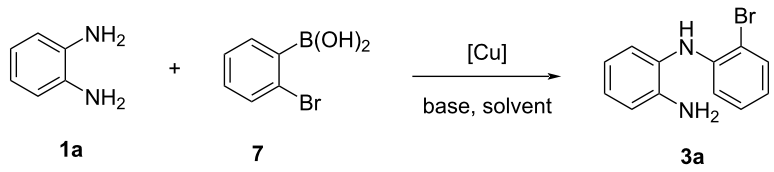

1a **7** **3a**

Entry	Copper source	Base	Solvent	Yield **3a**[b]
1	$Cu(OAc)_2$	Et_3N	DCM	48%
2	$Cu(OAc)_2$	Et_3N	dioxane	55%
3	$Cu(OAc)_2$	Et_3N	DMF	30%
4	CuI	Et_3N	dioxane	59%
5	CuI	Et_3N	DMF	35%
6[c]	CuI	Et_3N	DMF	23%
7[d]	CuI	Et_3N	DMF	31%
8	CuI	DMAP	DMF	ND
9	CuI	DIPEA	DMF	19%
10	$CuSO_4{\cdot}5H_2O$	Et_3N	dioxane	60%
11	$CuSO_4{\cdot}5H_2O$	Et_3N	DCM	50%

[a]Reaction conditions: *o*-phenylenediamine (**1a**, 0.46 mmol), 2-bromophenylboronic acid (**7**, 0.46 mmol, 1 equiv), copper catalyst (20 mol %), base (1.5 equiv), solvent (5 mL), 50 °C, 1–2 h. The reaction was monitored by TLC. [b]Isolated yield; ND: not detected [c]Reaction performed at 100 °C. [d]10 mol % CuI were used.

tion conditions but failed to improve the yield. In the presence of DMAP, no sign of the target compound was detected, while with DIPEA, **3a** was obtained in 19% yield (entries 8 and 9, Table 4). Then, we tested $CuSO_4{\cdot}5H_2O$ in the presence of Et_3N as the base in two different solvents DCM and dioxane, and both gave the desired compound in good yields of 60% and 50%, respectively (entries 10 and 11, Table 4).

Accessing the scope of the one-pot Chan–Lam/Pd-catalyzed carbonylative cyclization

Once the abovementioned conditions were obtained, we undertook a screening of the Chan–Lam/carbonylative synthesis of the DBDA in a one-pot manner. In the first reaction, *o*-phenylenediamine (**1a**) and 2-bromophenylboronic acid (**7**) were reacted in a pressure flask under an inert atmosphere using copper iodide (CuI) as the copper catalyst, Et_3N, and $Mo(CO)_6$ as CO surrogate in the presence of $Pd(OAc)_2$/XantPhos as catalytic system for the carbonylative intramolecular cyclization. These conditions led to the obtainment of the compound **4a** in 45% yield (entry 1, Table 5). Using dioxane as solvent, in the presence of the same catalytic system, afforded the desired structure **4a** in moderate yield (37%, entry 2, Table 5). Changing the ligand to DPEPhos resulted in a slight increase of the yield of **4a**, which was obtained in 40% (entry 3, Table 5). When the catalytic system $PdCl_2(NCCH_3)$/DPEPhos was employed, the product **4a** was accessed in a lower yield of 18% (entry 4, Table 5). Under these reaction conditions, copper bromide was shown to be a good catalyst for this transformation, as it allowed the production of **4a** in 40% yield (entry 5, Table 5). Then, we considered testing the performance of a different copper source $Cu(OAc)_2$ under these reaction conditions using DMF and dioxane as solvents. In these cases, the final compound **4a** was obtained in 38% and 41% yield, respectively (entries 6 and 7, Table 5). Next, we evaluated the performance of $CuSO_4{\cdot}5H_2O$ in dioxane and DMF, but lower yields were obtained (entries 8 and 9, Table 5). With the optimized conditions in hand, we tested the one pot Chan–Lam intramolecular cyclization with several other *o*-phenyldiamine derivatives, however, several impurities were obtained. In the hope of obtaining better yields (best obtained with the one pot method = 41%) we looked at the step-wise synthesis.

Synthesis of 5,10-dihydro-11*H*-dibenzo[*b*,*e*][1,4]diazepin-11-ones via a stepwise Chan–Lam/carbonylative cyclization

After disclosing the optimal conditions for the Chan–Lam coupling, we screened different varieties of *o*-phenylenediamine derivatives. Overall, the *o*-phenylenene substrates bearing electron-donating substituents on the benzene ring proceeded smoothly under these conditions and led to the desired structures in moderate to good yields (Scheme 3). The reactions were generally regioselective, except in the case of 4-methyl-*o*-phenylenediamine (**1b**) and *o*-bromophenylboronic acid (**7**) which gave a mixture of products **3b** and **3c** in 60% yield (the

Table 5: Substrate scope of the one-pot synthesis of dibenzodiazepine using via Chan–Lam coupling/carbonylative intramolecular cyclization.[a]

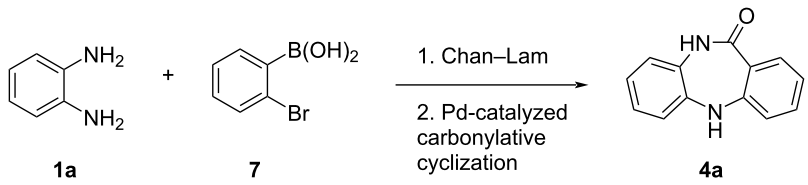

1a **7** **4a**

Entry	Copper source	Base	Solvent	Pd/ligand	Yield **4a**[b]
1	CuI	Et_3N	DMF	$Pd(OAc)_2$/XantPhos	45%
2	CuI	Et_3N	dioxane	$Pd(OAc)_2$/XantPhos	37%
3	CuI	Et_3N	DMF	$Pd(OAc)_2$/DPEPhos	40%
4	CuI	Et_3N	DMF	$PdCl_2(NCCH_3)_2$/XantPhos	18%
5	CuBr	Et_3N	DMF	$Pd(OAc)_2$/Xantphos	40%
6	$Cu(OAc)_2$	Et_3N	DMF	$Pd(OAc)_2$/DPEPhos	38%
7	$Cu(OAc)_2$	Et_3N	dioxane	$Pd(OAc)_2$/DPEPhos	41%
8	$CuSO_4.5H_2O$	Et_3N	dioxane	$Pd(OAc)_2$/DPEPhos	18%
9	$CuSO_4.5H_2O$	Et_3N	DMF	$Pd(OAc)_2$/DPEPhos	traces

[a]Reaction conditions: *o*-phenylenediamine (**1a**, 0.5 mmol), **7** (0.5 mmol), Cu catalyst (20 mol %), base (0.6 mmol), solvent (5 mL), 50 °C, 1 h; Pd catalytic system (5 mol %), $Mo(CO)_6$ (0.5 mmol) and base (0.5 mmol), 130 °C. [b]Isolated yields.

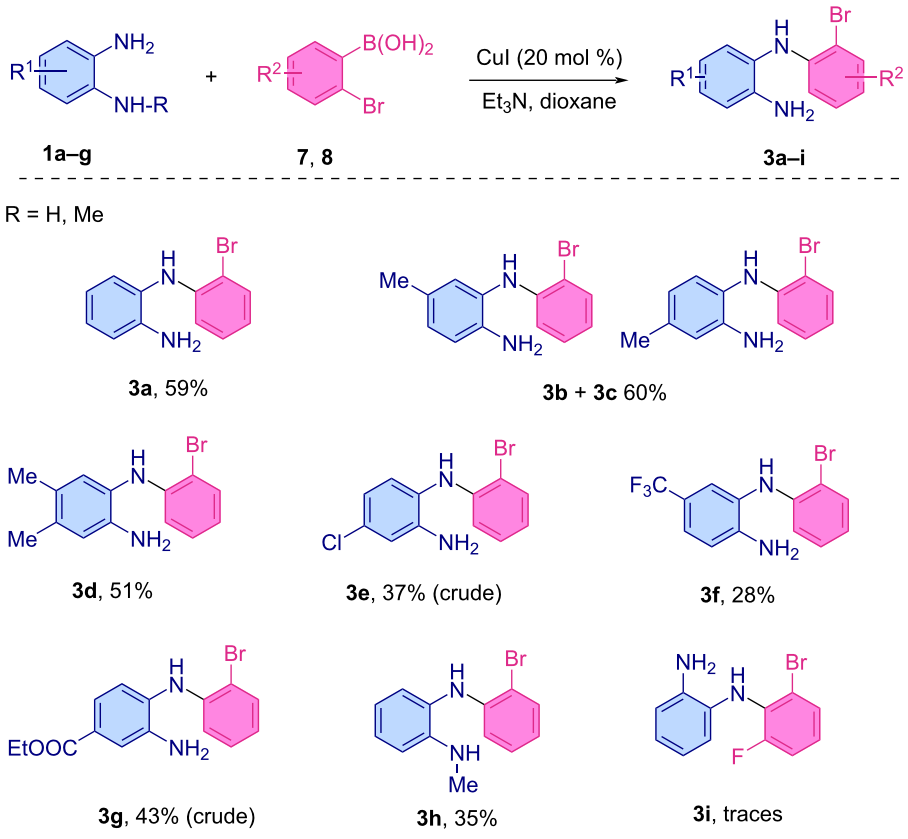

Scheme 3: Scope of the Chan–Lam coupling between *o*-phenylenediamines and 2-bromophenylboronic acids (please note products **3e** and **3g** contained some unidentified impurities that were impossible to remove via chromatography).

ratio could not be determined). These were eventually separated and used in the cyclization step discussed below. The dimethylated *o*-phenylenediamine **1d**, gave the desired compound **3d** in 51% yield. A slight decrease in yield was observed in the presence of an ester (COOEt) substituent, which furnished compound **3g** in 43% yield. Lower yields were observed in the case of electron-withdrawing substituents such as Cl and CF_3 groups, which afforded the compounds **3e** and **3f** in 37% and 28% yields, respectively. The N-methylated precursor **1h** was also tolerated by this system and afforded the desired compound **3h** in 35% yield. Unfortunately, the reaction with 2-bromo-6-fluorophenylboronic acid (**8**) afforded the corresponding product **3i** only in trace amounts.

With the *o*-(2-bromophenyl)aminoaniline derivatives in hand, we conducted the carbonylative intramolecular cyclization according to the previously disclosed conditions, in order to access the desired DBDAP structures. The unsubstituted DBDAP structure **4a** was obtained in 80% under these conditions (Scheme 4). The methyl-substituted *o*-(2-bromophenyl)aminoanilines **3** obtained via Chan–Lam coupling could be efficiently separated and were subjected to the intramolecular carbonylative cyclization to yield the DBDAPs **4b** and **4c** in excellent yields of 95% and 93%, respectively. The dimethyl-DBDAP **4d** could also be efficiently obtained under these conditions in 75% yield. The chloro-substituted DBDAP **4e**, which is the intermediate to the antipsychotic drug clozapine, could also be obtained in good yield (this represented a formal synthesis to clozapine [26], if the procedure of Rao [27] is used, which entails heating **4e** with 1-methylpiperidine and Ti(IV)Cl_4, Scheme 4). Also compound **4a** can be transformed to Hügel's 1,2,3-triazole-DBDAP using the methodology described in their

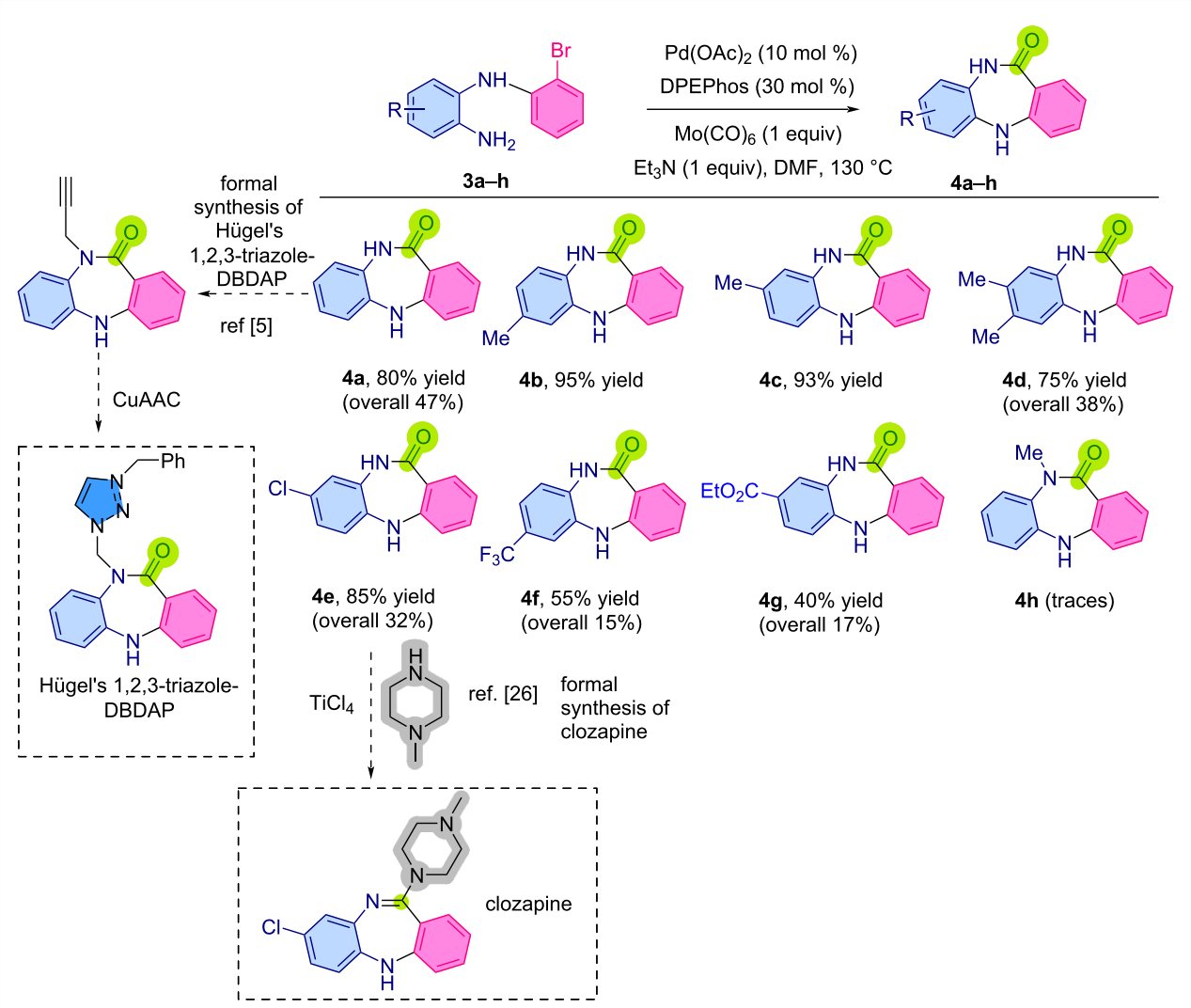

Scheme 4: Scope of the synthesis of DBDAPs. Please note that product **4g** contained some unidentified impurities that were impossible to remove via chromatography.

report (Scheme 4) [5]. The CF_3- and COOEt-substituted DBDAs **4f** and **4g** were obtained with a slightly decreased yield of 55% and 40%, respectively. The *N*-methyldibenzodiazepine **4h** could be accessed, but only in trace quantity. It should be noted that the stepwise approach was slightly better than the one-pot approach in the case of the synthesis **4a** (47% vs 41%).

Our mechanistic proposal is based on the information in previous reports by the groups of Bose [28], Watson [29], and Stahl [30]. Mechanistically, under basic conditions, the reaction is triggered by copper-catalyzed activation of *o*-phenylenediamine (**1a**), followed by the oxygen-promoted insertion of the phenylboronic acid coupling partner **7** to deliver intermediate **II** that undergoes reductive elimination to give diarylamine **3a** along with regeneration of the copper catalyst (Scheme 5). Then, a palladium-promoted oxidative addition of the C–Br bond takes places to deliver palladium species **III**. Then the insertion of CO that is released by $Mo(CO)_6$, should afford intermediate **IV** that undergoes a base-promoted intramolecular cyclization via nucleophilic attack of the amine [31]. Finally, the dibenzodiazepinone **4a** would be obtained through reductive elimination of the palladium catalyst.

Conclusion

In summary, we have reported two one-pot pathways and two step-wise pathways to access dibenzodiazepinone (DBDAP) derivatives via copper-catalyzed Chan–Lam amination/carbonylative cyclization and Buchwald–Hartwig amination/carbonylative cyclization and their step-wise counterparts. Although the one-pot method worked for one example in both cases (but in one case it gave the DBDAP enol form), it failed to work for other substrates, and for that reason we had to rely on the step-wise approach. The more efficient method to access the diamine intermediates **3** was via the Chan–Lam amination (milder conditions, cheaper, earth-abundant catalyst, no expensive ligand requirement) as the Buchwald–Hartwig amination required harsher conditions and an expensive metal catalyst, and also gave an unwanted phenazine side product. The sequential stepwise Chan–Lam amination/carbonylative cyclization afforded a number of DBDAP products, showing good functional group tolerance and giving the final products in good yields. In terms of the overall best efficiency, it also would appear that the step-wise Chan–Lam/Pd-catalyzed carbonylative cyclization was slightly better than the one-pot method. The most important of which was the chloro-containing DBDAP **4e** that can be used to synthesize the antipsychotic drug clozapine (see above), a triazole-hybrid with anticancer properties, and can easily be used as the key part in the synthesis of other drugs like dibenzepine and biologically active natural products such as BU-4664L. We are currently looking at this methodology to access some of these targets, including the agrochemical boscalid.

Experimental

Synthesis of *o*-(2-bromophenyl)aminoaniline (**3a**)

Via Buchwald–Hartwig coupling: *o*-Phenylenediamine (**1a**, 0.05g, 1 equiv, 0.46 mmol) was added to a Radleys reaction tube (a Radleys® 12 position carousel reactor station was used) under N_2 and dissolved in dry dioxane (5 mL). Next, (0.055 mL, 0.46 mmol) of 1,2-dibromobenzene (**2**) was added to the reaction mixture, followed by the addition of $Pd(OAc)_2$ (0.01 g, 0.046 mmol), XPhos (0.032 g, 0.069 mmol), and Cs_2CO_3 (0.18 g, 0. 56 mmol, 1,2 equiv). The resulting reaction mixture was allowed to stir at 100 °C. The reaction was left stirring for several hours, followed by TLC. After consumption of

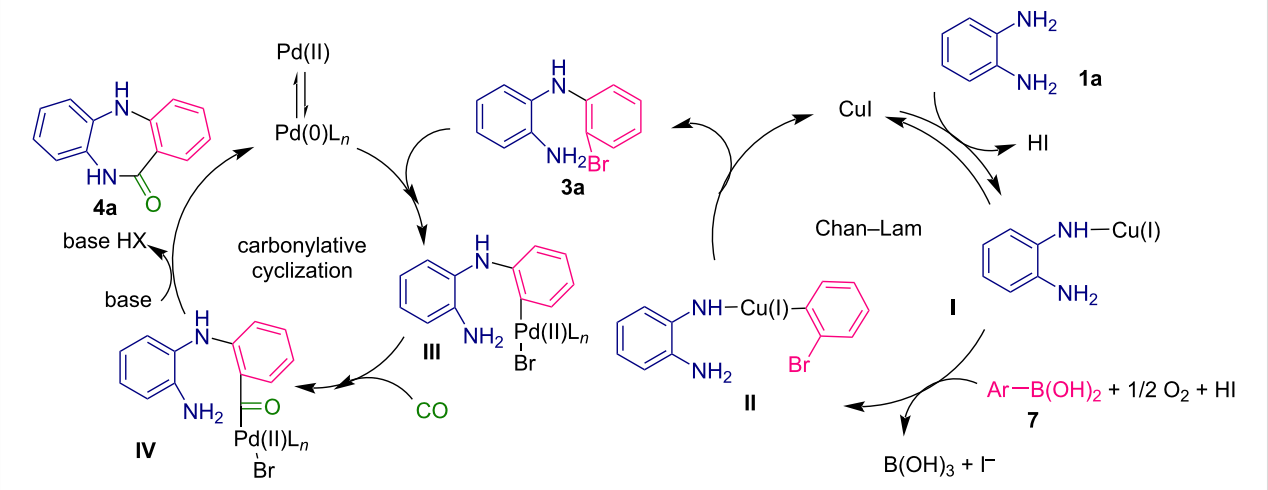

Scheme 5: Proposed mechanism.

the starting material (verified through TLC). The reaction was allowed to cool and filtered through a celite pad to remove the residual catalyst and base. The solvent was then evaportated under reduced pressure and the crude was purified by flash chromatography (hexane/AcOEt 9:1), to yield *o*-(2-bromophenyl)aminoaniline (**3**) compound as a purple oil (0.057 g, 47% yield).

Via Chan–Lam coupling: *o*-Phenylenediamine (**1a**, 0.05 g, 1 equiv, 0.46 mmol) was added to a round-bottomed flask and dissolved in dry dioxane (5 mL). Next, 2-bromophenyl)boronic acid (**7**, 0.092 g, 1 equiv,0.46 mmol) was added, followed by the addition of Et_3N (0.07 mL, 0.055 mmol), CuI (0.018 g, 0.092 mmol, 20 mol %), and molecular sieves 3 Å. The reaction was left stirring at room temperature for several hours, and monitored by TLC. After consumption of the starting material (verified through TLC), the reaction mixture was filtered through a celite pad to remove the residual catalyst and molecular sieves. The volatiles were then evaporated under reduced pressure and the crude was purified by flash chromatography (hexane/AcOEt 9:1), to yield *o*-(2-bromophenyl)aminoaniline (**3a**) as a purple oil (0.07 g, 59% yield).^{1}H NMR ($CDCl_3$, 400 MHz) δ 4.00 (s, NH_2, 2H), 5.76 (s, NH, 1H), 6.59–6.61 (d, *J* = 8 Hz, Ar, 1H), 6.65–6.69 (t, *J* = 8 Hz, Ar, 1H), 6.79–6.83 (t, *J* = 8 Hz, Ar, 1H), 6.85–6.87 (d, *J* = 8 Hz, Ar, 1H), 7.09–7.13 (m, Ar, 3H), 7.49–7.51 (d, *J* = 8 Hz, Ar, 1H); ^{13}C NMR ($CDCl_3$, 100 MHz) δ 110.42, 114.41, 116.47, 119.48, 119.70, 127.00, 127.04, 128.39, 132.62, 142.45, 143.03; HRESIMS (*m*/*z*): [M + H^+] calcd for $C_{12}H_{11}BrN_2$, 263,0184; found, 263.0178.

Synthesis of 5,10-dihydro-11*H*-dibenzo[*b*,*e*][1,4]diazepin-11-one (**4a**)

o-(2-Bromophenyl)aminoaniline (**3a**, 0.05 g, 0.19 mmol) was added to a Radley's® 12 position carousel reactor tube to which DMF, then $Pd(OAc)_2$ (4.26 mg, 0.019 mmol), DPEPhos (30 mg, 0.057 mmol), $Mo(CO)_6$ (50 mg, 1 equiv, 0.19 mmol), and Et_3N (0.026 mL, 0.19 mmol) were added. The reaction mixture was then stirred at 130 °C under a nitrogen atmosphere. After completion of the reaction, as determined by TLC, the reaction mixture was allowed to cool to room temperature. The mixture was filtered through a pad of celite and washed with DCM, then, the solvent was evaporated under reduced pressure to give a crude mixture. Further purification by flash chromatography (hexane/AcOEt 1:1), gave the desired compound 5,10-dihydro-11*H*-dibenzo[*b*,*e*][1,4]diazepin-11-one (**4a**) as a yellow solid yield (0.032 g, 80%). Mp 249–251 °C; ^{1}H NMR (DMSO-d_6, 400 MHz) δ 6.87–7.00 (m, Ar, 6H), 7.31–7.35 (t, *J* = 8 Hz, Ar, 1H), 7.66–7.68 (d, *J* = 8 Hz, Ar,1H), 7.84 (s, Ar, 1H), 9.85 (s, Ar, 1H); ^{13}C NMR ($CDCl_3$, 100 MHz) δ 119.52, 120.23, 121.17, 121.73, 123.24, 123.40, 124.95, 130.29, 132.56, 133.67, 140.43, 150.92, 168.40; ESIMS (*m*/*z*): 221.12 [M + H^+].

Supporting Information

Supporting Information File 1

Experimental procedures and spectral data (NMR, mass spectra) and key kinetic studies.
[https://www.beilstein-journals.org/bjoc/content/supplementary/1860-5397-20-19-S1.pdf]

Funding

This work received financial support from the Fundação para a Ciência e Tecnologia (FCT Portugal) through the project UIDB/50006/2020 | UIDP/50006/2020.

ORCID® iDs

Anthony J. Burke - https://orcid.org/0000-0001-8248-1116

Preprint

A non-peer-reviewed version of this article has been previously published as a preprint: https://doi.org/10.3762/bxiv.2023.51.v1

References

1. Khokhar, J. Y.; Henricks, A. M.; Sullivan, E. D. K.; Green, A. I. *Adv. Pharmacol. (San Diego, CA, U. S.)* **2018,** *82,* 137–162. doi:10.1016/bs.apha.2017.09.009
2. Jafari, S.; Fernandez-Enright, F.; Huang, X.-F. *J. Neurochem.* **2012,** *120,* 371–384. doi:10.1111/j.1471-4159.2011.07590.x
3. Cao, K.; Yan, J.; Yan, F.; Yin, T. *Mol. Diversity* **2021,** *25,* 1111–1122. doi:10.1007/s11030-020-10051-z
4. Miyanaga, S.; Sakurai, H.; Saiki, I.; Onaka, H.; Igarashi, Y. *Bioorg. Med. Chem. Lett.* **2010,** *20,* 963–965. doi:10.1016/j.bmcl.2009.12.055
5. Praveen Kumar, C.; Reddy, T. S.; Mainkar, P. S.; Bansal, V.; Shukla, R.; Chandrasekhar, S.; Hügel, H. M. *Eur. J. Med. Chem.* **2016,** *108,* 674–686. doi:10.1016/j.ejmech.2015.12.007
6. Minucci, S.; Pelicci, P. G. *Nat. Rev. Cancer* **2006,** *6,* 38–51. doi:10.1038/nrc1779
7. De Clercq, D. J. H.; Heppner, D. E.; To, C.; Jang, J.; Park, E.; Yun, C.-H.; Mushajiang, M.; Shin, B. H.; Gero, T. W.; Scott, D. A.; Jänne, P. A.; Eck, M. J.; Gray, N. S. *ACS Med. Chem. Lett.* **2019,** *10,* 1549–1553. doi:10.1021/acsmedchemlett.9b00381
8. Aniban, X.; Mamidala, S.; Burke, A. J. *Eur. J. Org. Chem.* **2018,** 6743–6753. doi:10.1002/ejoc.201801304
9. Guo, W.; Zhao, M.; Tan, W.; Zheng, L.; Tao, K.; Fan, X. *Org. Chem. Front.* **2019,** *6,* 2120–2141. doi:10.1039/c9qo00283a
10. Chen, J.-Q.; Li, J.-H.; Dong, Z.-B. *Adv. Synth. Catal.* **2020,** *362,* 3311–3331. doi:10.1002/adsc.202000495
11. Schoenberg, A.; Heck, R. F. *J. Org. Chem.* **1974,** *39,* 3327–3331. doi:10.1021/jo00937a004
12. Brennführer, A.; Neumann, H.; Beller, M. *Angew. Chem., Int. Ed.* **2009,** *48,* 4114–4133. doi:10.1002/anie.200900013

13. Tsvelikhovsky, D.; Buchwald, S. L. *J. Am. Chem. Soc.* **2011,** *133,* 14228–14231. doi:10.1021/ja206229y
14. Zhang, Q.-Y.; Wang, X.-J.; Tian, Y.-L.; Qi, J.-G.; Li, C.; Yin, D.-L. *Chin. Chem. Lett.* **2013,** *24,* 825–828. doi:10.1016/j.cclet.2013.04.049
15. Laha, J. K.; Manral, N.; Hunjan, M. K. *New J. Chem.* **2019,** *43,* 7339–7343. doi:10.1039/c9nj00539k
16. Åkerbladh, L.; Odell, L. R.; Larhed, M. *Synlett* **2019,** *30,* 141–155. doi:10.1055/s-0037-1610294
17. Odell, L. R.; Russo, F.; Larhed, M. *Synlett* **2012,** *23,* 685–698. doi:10.1055/s-0031-1290350
18. Peixoto, D.; Locati, A.; Marques, C. S.; Goth, A.; Ramalho, J. P. P.; Burke, A. J. *RSC Adv.* **2015,** *5,* 99990–99999. doi:10.1039/c5ra19599c
19. Wan, Y.; Alterman, M.; Larhed, M.; Hallberg, A. *J. Org. Chem.* **2002,** *67,* 6232–6235. doi:10.1021/jo025965a
20. Oseghale, C. O.; Onisuru, O. R.; Fapojuwo, D. P.; Mogudi, B. M.; Molokoane, P. P.; Maqunga, N. P.; Meijboom, R. *RSC Adv.* **2021,** *11,* 26937–26948. doi:10.1039/d1ra05177f
21. Wannberg, J.; Larhed, M. *J. Org. Chem.* **2003,** *68,* 5750–5753. doi:10.1021/jo034382d
22. Hussain, N.; Chhalodia, A. K.; Ahmed, A.; Mukherjee, D. *ChemistrySelect* **2020,** *5,* 11272–11290. doi:10.1002/slct.202003395
23. Dupont, C.; Wan, X.; Petukhov, M.; Krüger, P. *Int. J. Quantum Chem.* **2014,** *114,* 1630–1635. doi:10.1002/qua.24744
24. Chan, D. M. T. *Tetrahedron Lett.* **1996,** *37,* 9013–9016. doi:10.1016/s0040-4039(96)02116-8
25. Lam, P. Y. S.; Clark, C. G.; Saubern, S.; Adams, J.; Winters, M. P.; Chan, D. M. T.; Combs, A. *Tetrahedron Lett.* **1998,** *39,* 2941–2944. doi:10.1016/s0040-4039(98)00504-8
26. Nucifora, F. C., Jr.; Mihaljevic, M.; Lee, B. J.; Sawa, A. *Neurotherapeutics* **2017,** *14,* 750–761. doi:10.1007/s13311-017-0552-9
27. Venkat Rao, S. *Arabian J. Chem.* **2020,** *13,* 6040–6043. doi:10.1016/j.arabjc.2020.05.003
28. Bose, S.; Dutta, S.; Koley, D. *ACS Catal.* **2022,** *12,* 1461–1474. doi:10.1021/acscatal.1c04479
29. Vantourout, J. C.; Miras, H. N.; Isidro-Llobet, A.; Sproules, S.; Watson, A. J. B. *J. Am. Chem. Soc.* **2017,** *139,* 4769–4779. doi:10.1021/jacs.6b12800
30. King, A. E.; Ryland, B. L.; Brunold, T. C.; Stahl, S. S. *Organometallics* **2012,** *31,* 7948–7957. doi:10.1021/om300586p
31. Shen, C.; Neumann, H.; Wu, X.-F. *Green Chem.* **2015,** *17,* 2994–2999. doi:10.1039/c5gc00427f

License and Terms

BEILSTEIN JOURNAL OF ORGANIC CHEMISTRY

Synthesis and biological profile of 2,3-dihydro[1,3]thiazolo[4,5-*b*]pyridines, a novel class of acyl-ACP thioesterase inhibitors

Jens Frackenpohl*, David M. Barber, Guido Bojack, Birgit Bollenbach-Wahl, Ralf Braun, Rahel Getachew, Sabine Hohmann, Kwang-Yoon Ko, Karoline Kurowski, Bernd Laber, Rebecca L. Mattison, Thomas Müller, Anna M. Reingruber, Dirk Schmutzler and Andrea Svejda

Full Research Paper

Open Access

Address:
Research & Development, Weed Control, Crop Science Division, Bayer AG, Industriepark Höchst, 65926 Frankfurt am Main, Germany

Email:
Jens Frackenpohl* - jens.frackenpohl@bayer.com

* Corresponding author

Keywords:
2,3-dihydro[1,3]thiazolo[4,5-*b*]pyridine; acyl-ACP thioesterase; bioisostere; herbicide; heterocycle

Beilstein J. Org. Chem. **2024,** *20,* 540–551.
https://doi.org/10.3762/bjoc.20.46

Received: 15 November 2023
Accepted: 16 February 2024
Published: 01 March 2024

This article is part of the thematic issue "5th International Symposium on Synthesis and Catalysis (ISySyCat 2023)".

Guest Editor: A. Burke

Abstract

The present work covers novel herbicidal lead structures that contain a 2,3-dihydro[1,3]thiazolo[4,5-*b*]pyridine scaffold as structural key feature carrying a substituted phenyl side chain. These new compounds show good acyl-ACP thioesterase inhibition in line with strong herbicidal activity against commercially important weeds in broadacre crops, e.g., wheat and corn. The desired substituted 2,3-dihydro[1,3]thiazolo[4,5-*b*]pyridines were prepared via an optimized BH_3-mediated reduction involving tris(pentafluorophenyl)borane as a strong Lewis acid. Remarkably, greenhouse trials showed that some of the target compounds outlined herein display promising control of grass weed species in preemergence application, combined with a dose response window that enables partial selectivity in certain crops.

Introduction

The presence of weed infestations exerts a high strain on food production around the globe by depleting resources for the crops and facilitating the transmission of diseases [1]. Although herbicides remain the most effective solution for weed control due to the associated efficiency and simplicity, they face multiple challenges, such as the emergence and growth of resistant weed populations. It is therefore essential that crop protection research acts rapidly to provide farmers with new solutions

that enable them to fight back against resistant weed species [2]. Nevertheless, discovering novel and commercially viable modes of action within the timeframe needed to significantly impact the control of resistant weeds is a demanding task. Thus, we analyzed several herbicidal modes of action with emphasis on the structural diversity of small-molecule ligands. In this context, acyl-acyl carrier protein (acyl-ACP) thioesterase inhibitors have shown a remarkable variability. Fatty acid thioesterase (FAT) enzymes represent a family of proteins exclusively found in higher plants. They mediate the release of fatty acids from the plastids to the endoplasmic reticulum, where they are utilized for the synthesis of acyl lipids that are essential components for various physiological and defensive processes [3-6]. As this enzyme target does not exist in other kingdoms, structure–activity relationship (SAR) studies on selective inhibitors reduce the prevalence of undesired effects, such as toxicity in mammals [4]. Despite being employed in the field for over three decades, the mode of action of preemergence herbicide cinmethylin (**1**, Scheme 1) has remained unknown until 2018. At that time, the binding affinity to enzyme targets, e.g., acyl-ACP thioesterases, belonging to the protein family of FATs, was demonstrated by using co-crystallization, fluorescence-based thermal shift assays, and chemoproteomics techniques [3]. Likewise, methiozolin (**2**) is a recently assigned FAT inhibitor that has shown good results in selectively controlling grass weeds in both cool and warm seasons [7-9]. Recently, it has been shown that several herbicides bearing a *gem*-dimethylbenzylamide motif, e.g., cumyluron (**3a**) and oxaziclomefone (**3b**), previously exhibiting an unknown mode of action, control weeds due to the inhibition of FAT [10]. In search for further chemical entities that can control resistant weed species via the inhibition of FAT, we were interested in exploring a compound class containing a 1,8-naphthyridine core that was first reported by BASF, e.g., compound **4** [11].

In contrast to bicyclic cinmethylin (**1**) and methiozolin (**2**), substituted 1,8-naphthyridine **4** does not contain any stereocenters but still displays promising efficacy against grass weeds. Further considering the rather low molecular weight (220 g/mol) and structural simplicity, compound **4** is a highly attractive initial lead structure with ample space for structural variations. By formally replacing one pyridine moiety of 1,8-naphthyridine **4** by a five-membered thiazole unit, we have identified thiazolo[4,5-*b*]pyridine **5** as a strong inhibitor of acyl-ACP thioesterase, which has further been confirmed via an X-ray co-crystal structure [12]. Additionally, greenhouse trials have shown that thiazolopyridine **5** and a large number of closely related analogues display excellent control of grass weed species in preemergence applications [13,14]. Independently, researchers at Syngenta have shown that the pyridine unit in the 1,8-naphthyridine scaffold can also be formally substituted by an isothiazole group, as can be seen in isothiazolo[3,4-*b*]pyridine **6** [15].

Thus, several bicyclic heteroaromatic motifs containing two nitrogen atoms serve as structural surrogates of cinmethylin (**1**),

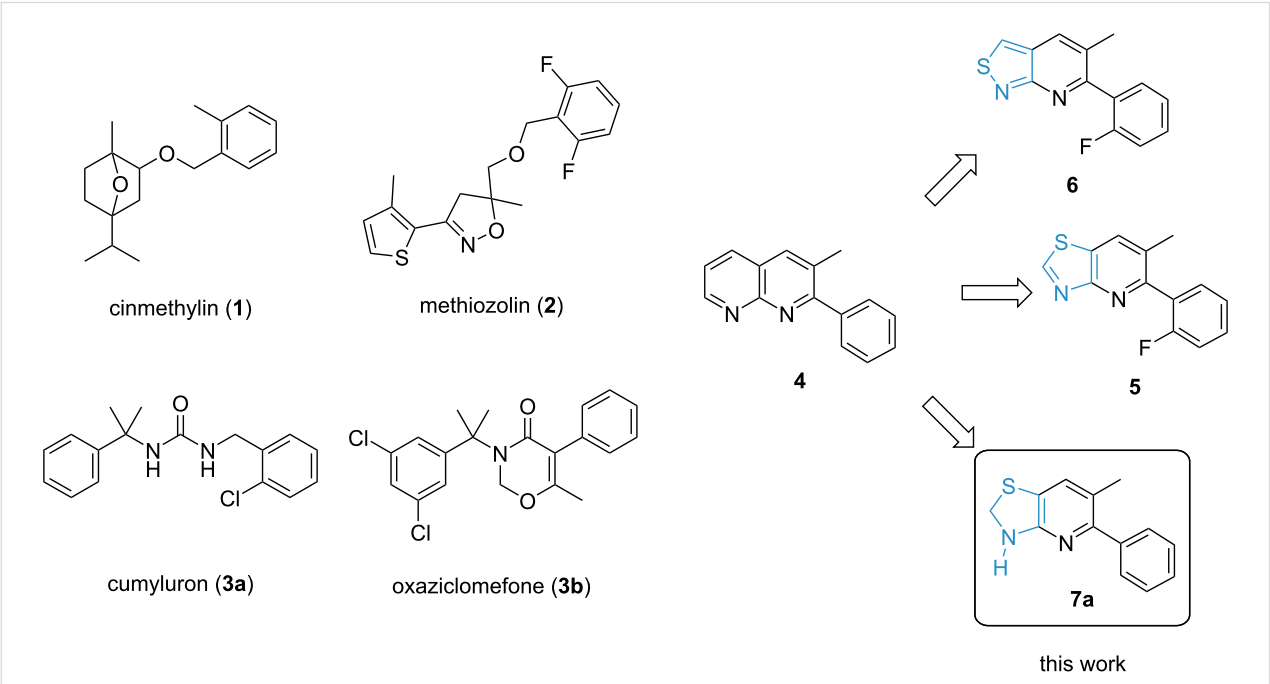

Scheme 1: Selected known inhibitors **1–3** of acyl-ACP thioesterases (belonging to the protein family of FATs) and new lead structures **4–7a**.

bearing a substituted 7-oxabicyclo[2.2.1]heptane scaffold [16]. Based on the findings outlined above and based on other plant-specific modes of action, it is plausible that FAT inhibitors encompass a broader range of structural motifs [16,17]. Herein, we present our approach to complement heteroaromatic lead structures **4**–**6** by introducing a nonaromatic motif via preparation of the novel 2,3-dihydro[1,3]thiazolo[4,5-*b*]pyridines **7**.

Results and Discussion

Although the 2,3-dihydro[1,3]thiazolo[4,5-*b*]pyridine scaffold looks relatively simple at a first glance, it displays a very different reactivity compared to the parent naphthyridine series. Likewise, 1,8-naphthyridines are easily accessed in high yield and on a multigram scale via Friedländer synthesis [18]. This was in clear contrast to the intermediate thiazolo[4,5-*b*]pyridines and the desired 2,3-dihydro[1,3]thiazolo[4,5-*b*]pyridine that we wanted to access, with approaches to prepare the thiazolo[4,5-*b*]pyridines using the Friedländer synthesis often being met with failure or disappointingly low product yield [12]. We thus particularly emphasized on upscaling, facile workup, and a robust yield for each step. This was due to the potential need for the preparation of multigram quantities of the most active compounds for advanced biological testing. Pleasingly, our four-step approach using a potassium *O*-ethyl dithiocarbonate-mediated formation of thio intermediates **11a**–**c** (thiol–thione tautomers) with subsequent sulfur removal using iron powder in acetic acid [19] proceeded smoothly to afford thiazolopyridines **12a**–**c** in good yield. This allowed us to circumvent the previously employed alkylation–oxidation–reduction sequences (Scheme 2) [12]. Thereupon, we recognized that we could introduce two halogen atoms in the halogenation step and carry one through to the end of the synthetic route, which enabled us to

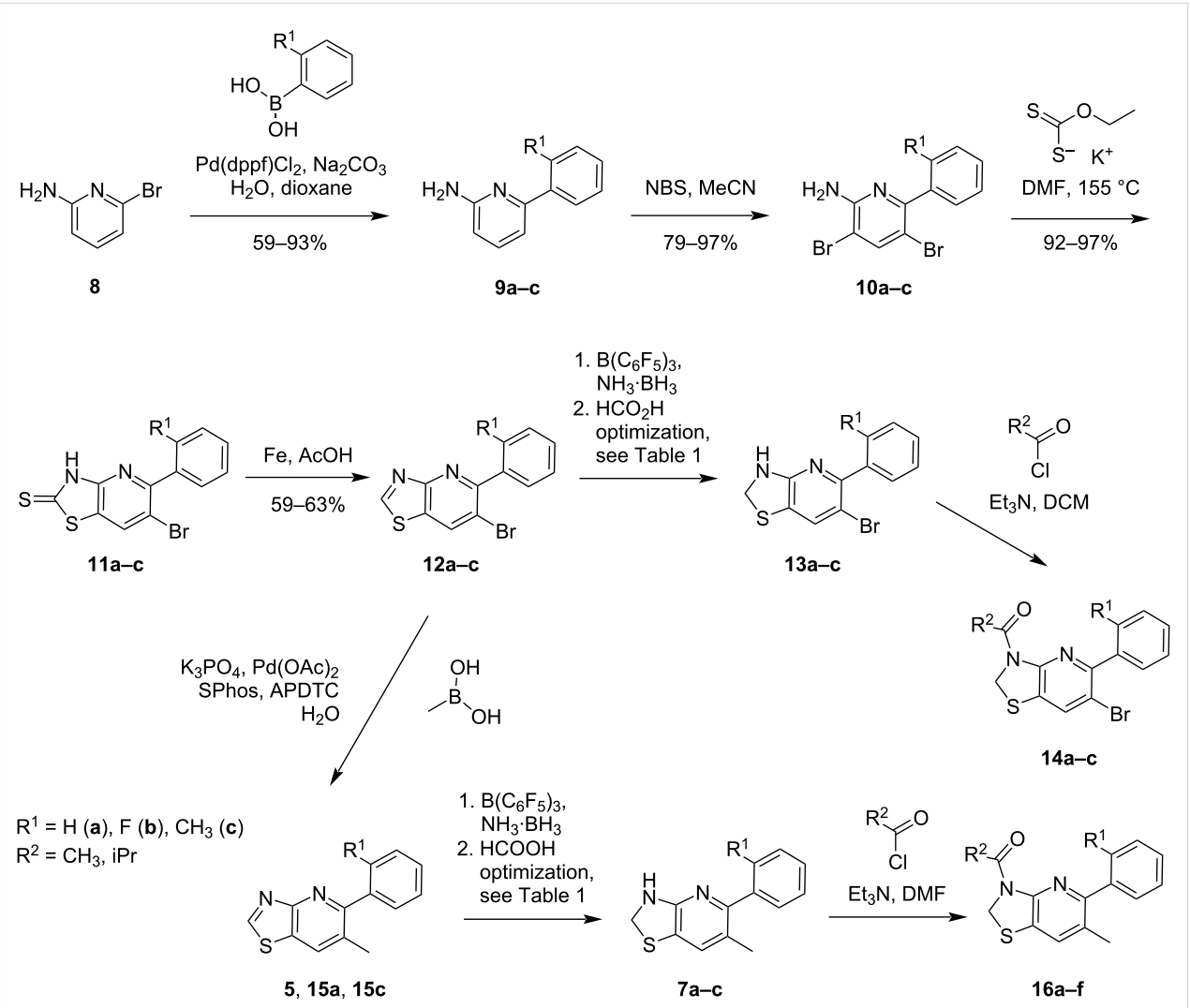

Scheme 2: Preparation of 2,3-dihydro[1,3]thiazolo[4,5-*b*]pyridines **7a–c** and **13a–c** via iron-mediated sulfur removal and subsequent reduction. dppf = 1,1'-bis(diphenylphosphino)ferrocene, SPhos = 2-dicyclohexylphosphino-2',6'-dimethoxybiphenyl, APDTC = ammonium pyrrolidinedithiocarbamate.

introduce a methyl substituent in this position. Likewise, methyl-substituted thiazolo[4,5-*b*]pyridines **5**, **15a**, and **15c** were synthesized using an optimized Suzuki coupling and served together with compounds **12a**–**c** as key intermediates to explore different reagents and conditions to prepare 2,3-dihydro[1,3]thiazolo[4,5-*b*]pyridines **7a**–**c** and **13a**–**c** via a late-stage reduction (Scheme 2 and Table 1).

Whilst several synthetic approaches towards 2,3-dihydro-1,3-benzothiazoles involving the hydrogenation of 1,3-benzothiazoles have been described [20], the corresponding preparation of 2,3-dihydro[1,3]thiazolo[4,5-*b*]pyridines remained unexplored to our great surprise. Thus, we investigated the conversion of [1,3]thiazolo[4,5-*b*]pyridines **5** (R^1 = F), **15a** (R^1 = H), and **15c** (R^1 = CH_3) into 2,3-dihydro[1,3]thiazolo[4,5-*b*]pyridines **7a**–**c** thoroughly, with the aim to establish a practicable and robust synthetic route enabling us to carry out a broad SAR study. Initial attempts to prepare 2,3-dihydro[1,3]thiazolo[4,5-*b*]pyridines **7a** and **7b** using hydrogen and palladium on charcoal under elevated pressure did not show any conversion of the starting material (Table 1, entries 1 and 2). Correspondingly, [1,3]thiazolo[4,5-*b*]pyridine **5** remained unchanged upon application of methods that had been successfully utilized in the hydrogenation of 1,3-benzothiazoles, involving diboronic acid or hydrazine hydrate as key reagents [21] in protic solvents at an elevated temperature (Table 1, entries 3 and 4). Whilst tetrabutylammonium borohydride [22] at room temperature did not lead to a conversion of the starting material **5** either, a trace amount of desired 2,3-dihydro[1,3]thiazolo[4,5-*b*]pyridine **7b** was formed at elevated temperature, accompanied by disulfide **18b** as the main product (Table 1, entries 5 and 6). This result indicated that borohydride reagents were able to

Table 1: Preparation of 2,3-dihydro[1,3]thiazolo[4,5-*b*]pyridines **7a**–**c** via reduction of the thiazole moiety: optimization of the reaction conditions.[a]

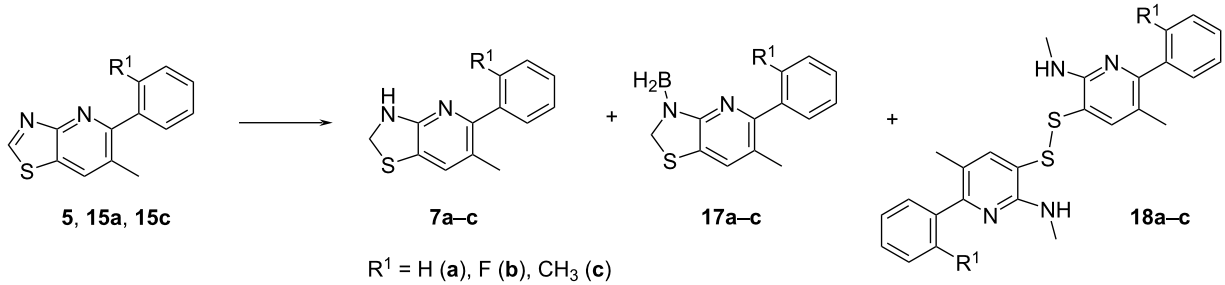

entry	R^1	reagents	solvent	*T*, °C	*T*, h	**7a**–**c**, %[b]	**17a**–**c**, %[b]	**18a**–**c**, %[b]
1	CH_3	H_2, Pd/C, 2–20 bar	MeOH	20	4	—	—	—
2	F	H_2, Pd/C, 4–35 bar	MeOH	20	6	—	—	—
3	F	N_2H_4, Pd/C	EtOH	80	6	—	—	—
4	F	$B_2(OH)_4$	H_2O	80	6	—	—	—
5	F	Bu_4NBH_4	THF	20	5	—	—	—
6	F	Bu_4NBH_4	THF	70	5	5	—	48
7	H	Bu_4NBH_4	dioxane	80	5	8	—	59
8	F	$NaCNBH_3$, AcOH	MeOH	60	5	4	—	15
9	F	$SiCl_3H$	toluene	110	3	—	—	35
10	CH_3	$SiEt_3H$	dioxane	80	3	—	—	43
11	F	NH_3-BH_3	toluene	80	4	5	4	12
12	F	$NH_3{\cdot}BH_3$, $B(C_6F_5)_3$	toluene	80	4	16	33	18
13	CH_3	$NH_3{\cdot}BH_3$, $B(C_6F_5)_3$	toluene	80	7	8	29	30
14	CH_3	$NH_3{\cdot}BH_3$, $B(C_6F_5)_3$	toluene	45	6	4	51	3
15	H	$NH_3{\cdot}BH_3$, $B(C_6F_5)_3$, HCO_2H	toluene	45	7	64[c]	—	2
16	F	$NH_3{\cdot}BH_3$, $B(C_6F_5)_3$, HCO_2H	toluene	45	5	66[c]	—	5
17	CH_3	$NH_3{\cdot}BH_3$, $B(C_6F_5)_3$, HCO_2H	toluene	45	7	59[c]	—	4

[a]All reactions in the optimization phase were carried out using 0.2 mmol of **5**, **15a**, and **15c**, respectively. [b]Determined by analytical HPLC. [c]Isolated yield after silica gel column chromatography.

activate the thiazole moiety in [1,3]thiazolo[4,5-*b*]pyridines, leaving the pyridine unit unchanged. While sodium cyanoborohydride afforded a comparable result, albeit with lower conversion, the use of silane reagents at elevated temperature [23] led to the cleavage of the thiazole ring, furnishing disulfides **18b** and **18c** exclusively (Table 1, entries 7–10). Interestingly, the reaction of **5** with ammonia borane at elevated temperature in toluene [20] furnished three reaction products with a low yield since 2,3-dihydro[1,3]thiazolo[4,5-*b*]pyridine **7b** was formed together with disulfide **18b** and aminoborane **17b** (Table 1, entry 11). We thus evaluated $B(C_6F_5)_3$ as a nonmetallic catalyst to activate ammonia borane in the reductive hydrogenation of the C=N-bond in [1,3]thiazolo[4,5-*b*]pyridines **5** and **15c**. In line with reports on the hydrogenation of quinolines and indoles [24], pyridines [25], and imines [26], the reactions of **5** and **15c** with ammonia borane (3 equiv) in the presence of a catalytic amount of $B(C_6F_5)_3$ in toluene as an aprotic solvent at a temperature of 80 °C afforded aminoboranes **17b** (R^1 = F) and **17c** (R^1 = CH_3) as main products along with desired target compounds **7b** and **7c** (Table 1, entries 12 and 13). However, disulfides were still formed as side products in a significant amount. Pleasingly, the undesired thiazole cleavage could successfully be minimized by reducing the reaction temperature to 45 °C, furnishing aminoborane **17c** in 51% yield (Table 1, entry 14). The borane group could be cleaved off easily by the subsequent treatment of **17c** with formic acid in acetonitrile, affording 2,3-dihydro[1,3]thiazolo[4,5-*b*]pyridine **7c** as the only reaction product. By applying this optimized two-step procedure to [1,3]thiazolo[4,5-*b*]pyridines **5**, **15a**, and **15c**, the desired 2,3-dihydro[1,3]thiazolo[4,5-*b*]pyridines **7a**–**c** were prepared in good yield (Table 1, entries 15–17, 59–66% isolated yield), enabling us to investigate the biological profiles as well as the reactions with acyl chlorides to form amides **16a**–**f** (Scheme 2) [27]. These acylations proceeded cleanly under mild conditions, using the corresponding acyl chloride together with triethylamine as a suitable base in DCM.

Furthermore, we evaluated the tolerance of [1,3]thiazolo[4,5-*b*]pyridines **12a**–**c**, containing a bromine atom, towards the optimized $B(C_6F_5)_3$-mediated reduction. In good accordance with the results obtained for dimethylated [1,3]thiazolo[4,5-*b*]pyridine **15c**, the corresponding aminoboranes **17d** and **17e** were formed when 6-bromo[1,3]thiazolo[4,5-*b*]pyridine **12c** was treated with ammonia borane in toluene at 45 °C in the presence of a catalytic amount of $B(C_6F_5)_3$ (Scheme 3). Whilst diphenyl analogue **17f** was isolated as a side product upon arylation with $B(C_6F_5)_3$, debromination was only observed in traces. Both aminoboranes **17d** and **17e** were then cleaved separately in clean conversions using formic acid to afford the desired substituted 6-bromo-5-(2-tolyl)-2,3-dihydrothiazolo[4,5-b]pyridine (**13c**, 54% combined isolated yield). As shown for N-acylated target compounds **16a**–**f**, the acylation of 6-bromo-2,3-dihydro[1,3]thiazolo[4,5-*b*]pyridines **13a**–**c**, affording target compounds **14a**–**c**, proceeded under mild conditions with a suitable acyl chloride reagent and triethylamine as base in DCM. It was not necessary to add a further base to activate the thiazoline nitrogen atom. Following the aforementioned two-step procedure, more than 15 unprecedented 2,3-dihydro[1,3]thiazolo[4,5-*b*]pyridines bearing different substituents were obtained for biological and biochemical tests.

Converting the thiazole moiety into a thiazoline unit had a measurable impact on several physicochemical parameters,

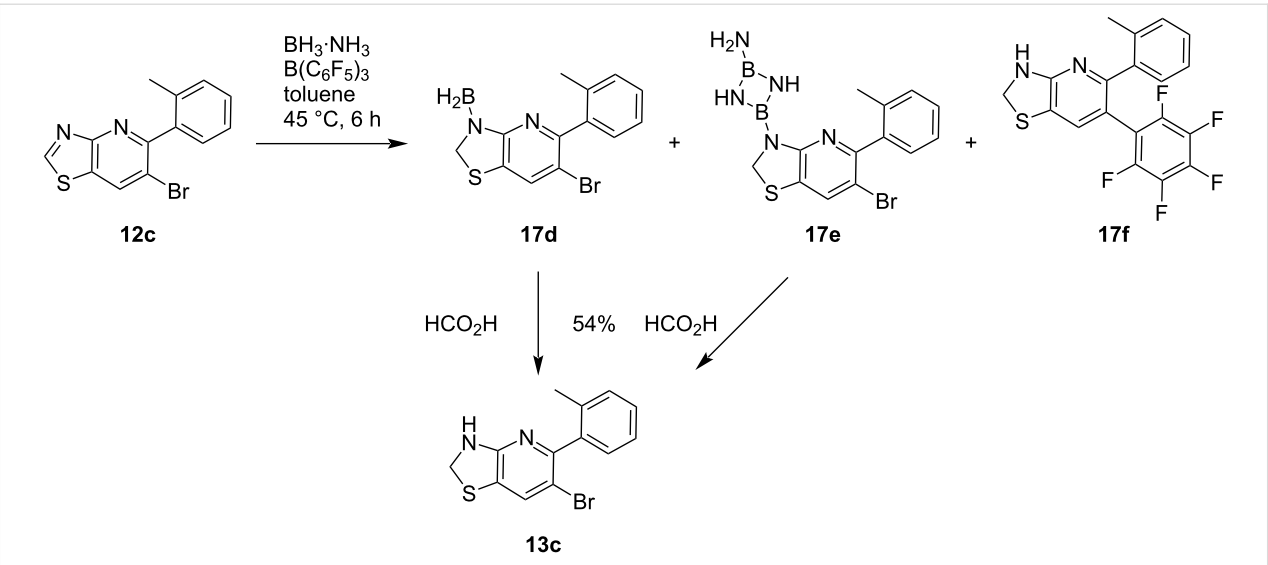

Scheme 3: Evaluation of potential side reactions in the borane-mediated preparation of 2,3-dihydro[1,3]thiazolo[4,5-*b*]pyridine **13c**.

such as LogP and water solubility. Whilst thiazolo[4,5-*b*]pyridine **5** afforded a moderate water solubility of 49 mg/L, paired with a LogP of 2.28 (pH 2.3), the corresponding 2,3-dihydro[1,3]thiazolo[4,5-*b*]pyridine **7b** had a higher water solubility of 173 mg/L and a lower LogP of 1.59 (pH 2.3). However, the lipophilicity of the new 2,3-dihydro[1,3]thiazolo[4,5-*b*]pyridines was highly dependent on the substituents. For example, the brominated analogs **13b** and **13c** showed considerably higher LogP values of 2.88 (i.e., **13b**) and 3.17 (i.e., **13c**). We were thus curious to see how the structural change from a heteroaromatic thiazole unit to a partially saturated thiazoline moiety affected the in vitro and in vivo efficacy of the target compounds.

All compounds that were prepared to explore the SAR of substituted 2,3-dihydro[1,3]thiazolo[4,5-*b*]pyridines, i.e., **13a–c**, and **7a–c**, the acylated analogues **14a–c** and **16a–f**, as well as selected aminoboranes **17d** and **17e**, were tested for target affinity in dedicated in vitro tests, as well as for herbicidal effects in vivo upon preemergence application to plants. Based on our experience with thiazolopyridine-based FAT inhibitors [12,13], five representative grass weeds (ALOMY, ECHCG, LOLRI, POAAN, and SETVI) were chosen as model plants to assess initial preemergence activity using a dose rate of 320 g/ha, whereas in vitro tests were carried out using FAT A, isolated from duckweed (*Lemna paucicostata*, LEMPA, *Lp*). As outlined in Table 2, entries 19 and 20, cinmethylin (**1**) and methiozolin (**2**) proved to be suitable commercial reference compounds. They showed good and broad control of grass weeds in various test systems, albeit with incomplete control of the commercially important grass weed LOLRI, paired with insufficient control of ECHCG by methiozolin (**2**) in our greenhouse tests. Furthermore, we used thiazolo[4,5-*b*]pyridine **5** as a strong internal standard to assess how modification of the thiazole moiety would affected the biological activity. It is worth noting that we emphasized investigating the preemergence efficacy as this application type is still important for cereals.

Firstly, we investigated 6-methyl-2,3-dihydro[1,3]thiazolo[4,5-*b*]pyridines **7a–c** containing a variously substituted phenyl moiety. Moderate receptor affinity towards FAT A isolated from LEMPA could be observed for all three target compounds **7a–c** (pI_{50} 5.9–6.3, Table 2, entries 1–3). However, this was paired with strong in vivo efficacy on the level of internal standard **5** and exceeding the results obtained for cinmethylin (**1**) and methiozolin (**2**). Whilst compounds **7a–c** afforded complete control of all tested weeds at an application rate of 320 g/ha, the corresponding 6-bromo analogues **13a–c** showed higher sensitivity towards changes in the phenyl moiety. 6-Bromo-5-phenyl-2,3-dihydrothiazolo[4,5-*b*]pyridine (**13a**) showed only partial control of ALOMY and LOLRI, combined with moderate target affinity (pI_{50} 5.7), whereas compound **13c**, bearing an *o*-tolyl substituent, provided insufficient control of three weeds, i.e., ALOMY, POAAN, and LOLRI (Table 2, entry 6), in line with a surprisingly weak target affinity (pI_{50} 4.5). Remarkably, 6-bromo-5-(2-fluorophenyl)-2,3-dihydro[1,3]thiazolo[4,5-*b*]pyridine (**13b**) exhibited the highest affinity towards FAT A of all new analogues (pI_{50} 7.3), paired with full control of all tested weeds (Table 2, entry 5). As shown by the results outlined for 2,3-dihydro[1,3]thiazolo[4,5-*b*]pyridines **7a–c** and **13a–c** (Table 2, entries 1–6) our approach to introduce a thiazoline moiety via hydrogenation was well tolerated with respect to in vivo efficacy, albeit paired with reduced target affinity except for **13b**. Likewise, the N-acylated 2,3-dihydro[1,3]thiazolo[4,5-*b*]pyridines **14a–c** and **16a–f** afforded a moderate target affinity in line with moderate to good control of the tested weeds (Table 2, entries 7–15). Interestingly, N-acylated analogues **14a** and **16a**, both bearing an unsubstituted phenyl substituent, delivered the best in vivo results, fully controlling four grass weeds, including commercially important LOLRI, and only showing partial control of ALOMY (Table 2, entries 7 and 10). Thus, both N-acylated compounds afforded nearly the same level of in vivo efficacy as the parent 2,3-dihydro[1,3]thiazolo[4,5-*b*]pyridines **13a** and **7a**. Aminoboranes **17d** and **17e** also showed partial control of the tested grass weeds, albeit on a significantly lower level. Accordingly, the target binding affinities were considerably lower than those measured for the strongest analogues **7b**, **7c**, and **13b**.

To gain further insights into the biological profile, we chose compounds **7b**, **7c**, and **13b** with promising initial in vivo activity as representatives of our new class of FAT inhibitors to assess the activity in advanced greenhouse tests (i.e., more replicates, larger pots, and lower application rate). Emphasis was put on the efficacy against resistant weeds and on crop selectivity profiles. We thus expanded our investigations to resistant monocotyledon weed species, i.e., resistant blackgrass (ALOMY_R, also known as black twitch or slender foxtail) and ryegrass (LOLSS_R), together with nonresistant ALOMY, LOLRI, APESV, and BROTE as commercially relevant target weeds, and wheat (TRZAS) as the crop (Figure 1).

Whilst all three new 2,3-dihydro[1,3]thiazolo[4,5-*b*]pyridine-based FAT inhibitors exceeded the efficacy of commercial standard methiozolin (**2**), target compound **7b** controlled grass weeds on the same level or slightly better than cinmethylin (**1**). Accordingly, application of **7c**, **13b**, and **2** resulted in low crop damage in wheat (in particular at an application rate of 50 g/ha), whereas compounds **7b** and **1** exhibited higher crop damage in the test systems on a comparable level. Methiozolin (**2**) only showed moderate control of nonresistant ALOMY (85% at

Table 2: Preemergence in vivo efficacy screening of 2,3-dihydro[1,3]thiazolo[4,5-*b*]pyridines **7a–c** and **13a–c** as well as of N-acylated analogs **14a–c** and **16a–f** against selected monocotyledon weeds, and binding affinity to FAT A from LEMPA.

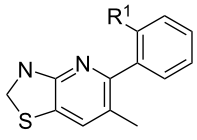

7a–c

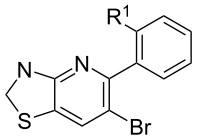

13a–c

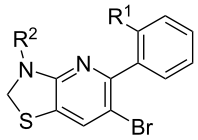

14a–c
17d, **17e**

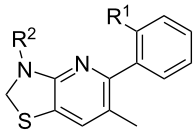

16a–f

entry	compound	R^1	R^2	pI_{50}[a]	ALOMY[b,c]	ECHCG[b,c]	POAAN[b,c]	SETVI[b,c]	LOLRI[b,c]
1	**7a**	H	H	5.9	5	5	5	5	5
2	**7b**	F	H	6.1	5	5	5	5	5
3	**7c**	CH_3	H	6.3	5	5	5	5	5
4	**13a**	H	H	5.7	4	5	5	5	3
5	**13b**	F	H	7.3	5	5	5	5	5
6	**13c**	CH_3	H	4.5	1	5	1	5	1
7	**14a**	H	Ac	5.5	4	5	5	5	5
8	**14b**	F	iBtr[d]	4.7	3	3	3	5	2
9	**14c**	CH_3	Ac	4.3	3	3	3	5	1
10	**16a**	H	Ac	5.5	4	5	5	5	5
11	**16b**	H	iBtr	4.7	3	3	5	5	4
12	**16c**	F	Ac	5.3	4	4	5	5	4
13	**16d**	F	iBtr	4.7	3	5	5	5	4
14	**16e**	CH_3	Ac	4.1	3	3	5	4	3
15	**16f**	CH_3	iBtr	4.8	3	5	5	5	3
16	**17d**	CH_3	BH_2	4.8	2	5	3	5	3
17	**17e**	CH_3	BX_2[e]	<4.0	1	3	3	5	1
18	**5**	F	—	7.2	5	5	5	5	5
19	**1**			6.8	5	5	4	4	1
20	**2**			7.1	4	1	5	5	1

[a]In vitro inhibition of FAT A (from LEMPA). [b]*n* = 10, i.e., 10 monocotyledonous weed seeds were grown per pot. [c]Dose rate 320 g/ha. Efficacy values are given based on a rating scale by final visual experts' assessment of green mass, i.e., 5 ≥ 90% inhibition, 4 = 70–89% inhibition, 3 = 50–69% inhibition, 2 = 40–49% inhibition, 1 = 21–39% inhibition, and — < 20% inhibition. Cinmethylin (**1**), methiozolin (**2**), and thiazolo[4,5-*b*]pyridine **5** were used as comparative internal standards. [d]Isobutyryl. [e]BX_2 = 1,3,2,4-diazadiboretidin-2-amine.

200 g/ha and 20% at 50 g/ha vs more than 90% control at both application rates by **7b**, Figure 1). Likewise, **2** had only marginal effects against ALOMY_R and LOLSS_R. Whilst 2,3-dihydro[1,3]thiazolo[4,5-*b*]pyridines **7c** and **13b** showed weak to moderate efficacy against ALOMY_R (strongly dependent on the application rate), *o*-fluorophenyl analogue **7b** exhibited strong control of this resistant, commercially important grass weed. Remarkably, all three 2,3-dihydro[1,3]thiazolo[4,5-*b*]pyridines **7b**, **7c**, and **13b** afforded very good control of the second resistant monocotyledon weed LOLSS_R, reaching an efficacy level of above 90% at both application rates. Considering the low crop damage of **7c** and **13b**, their strong control of sensitive and resistant lolium species emphasizes their potential as lead structures to identify tailored solutions for sustainable lolium control in relevant countries (e.g., Australia). In line with good control of other grass weeds (APESV and BROTE, Figure 1), target compound **7b** showed the most promising spectrum of efficacy of all new test compounds, being on the same level or slightly better than **1**. Hence, 2,3-dihydro[1,3]thiazolo[4,5-*b*]pyridines represent a propitious class of herbicidal lead structures with the potential to control resistant grass weeds. To complement our investigations that focused on relevant monocotyledon weeds in wheat, including resistant species, we tested the three selected 2,3-dihydro[1,3]thiazolo[4,5-*b*]pyridines **7b**, **7c**, and **13b** against commercially relevant weeds in corn, e.g., crabgrass or red fingergrass (DIGSA) and goosegrass or crowsfoot grass (ELEIN), together with Johnson grass (SORHA) and broad-leaved signal grass (BRAPP). We used **1** and **5** as standards to assess the potential of the new lead structures. Both standards

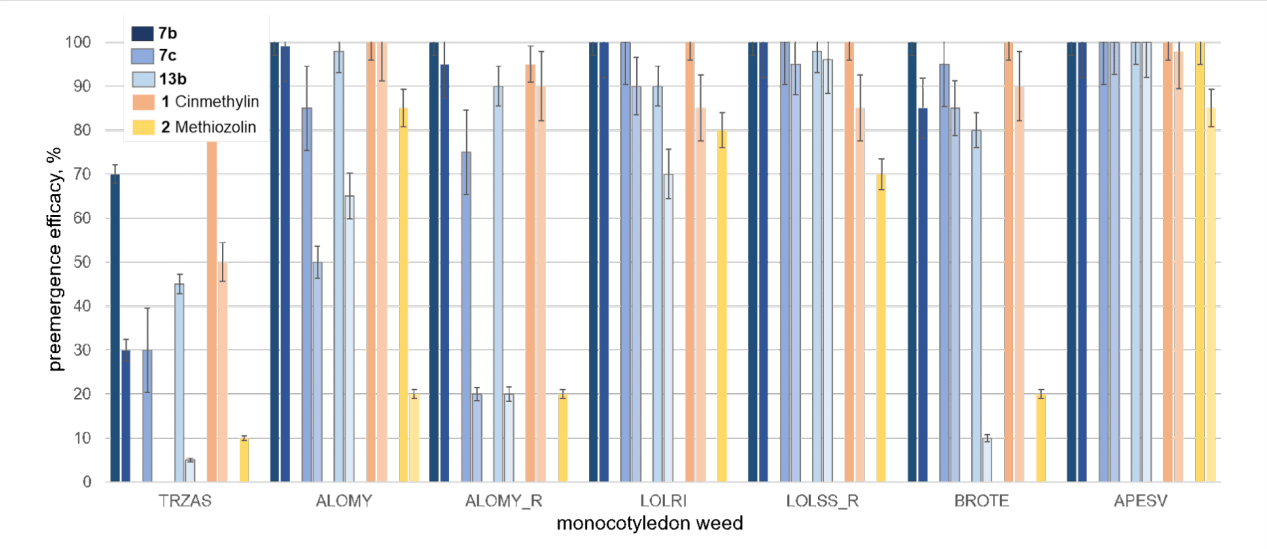

Figure 1: Preemergence efficacy of 2,3-dihydro[1,3]thiazolo[4,5-*b*]pyridine-based FAT inhibitors **7b**, **7c**, and **13b** as well as internal standards cinmethylin (**1**) and methiozolin (**2**) against selected resistant and nonresistant monocotyledon weeds in wheat at application rates of 200 and 50 g/ha in advanced greenhouse trials, e.g., LOLSS_R and ALOMY_R (replicates: 10 plants per pot).

showed sufficient crop selectivity only at the lower application rate of 50 g/ha. [1,3]Thiazolo[4,5-*b*]pyridine **5** showed good control of all tested warm-season weeds, whilst **1** showed only insufficient control of BRAPP, ELEIN, and SORHA at the lower application rate of 50 g/ha. 2,3-Dihydro[1,3]thiazolo[4,5-*b*]pyridines **7b**, **7c**, and **13b** showed good crop selectivity at both application rates in our advanced preemergence greenhouse test, affording low damage in corn and only marginal damage in soy (Figure 2). However, **7c** showed a moderate damage of 20% in both crops at the higher application rate of 150 g/ha. Remarkably, 2,3-dihydro[1,3]thiazolo[4,5-*b*]pyridine **7b** afforded good efficacy at both dose rates against all five monocotyledon weeds, including BRAPP, ELEIN, and SORHA, which were not sufficiently controlled by **1**. Whilst the structurally closely related compounds **7b** and **5** showed comparable efficacy against all tested weeds, **7b** afforded considerably lower crop damage at the higher application rate in corn and at both application rates in soy compared to **5** (Figure 2). Furthermore, **7b**, **7c**, and **13b** provided full control of ELEIN, one of the most difficult turfgrass weeds to control in

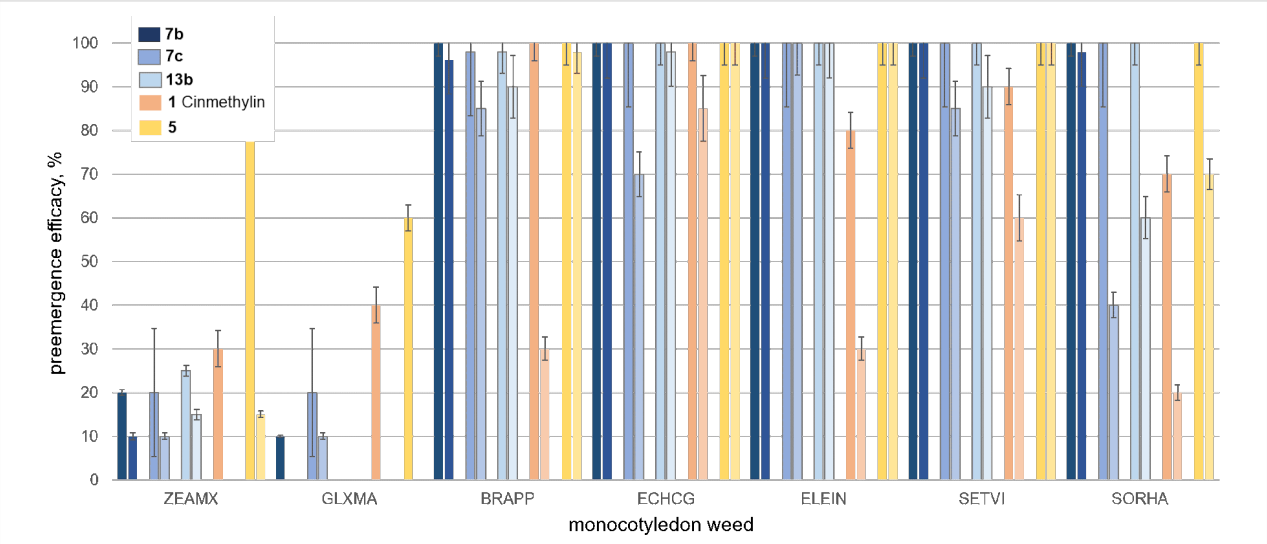

Figure 2: Preemergence efficacy of 2,3-dihydro[1,3]thiazolo[4,5-*b*]pyridine-based FAT inhibitors **7b**, **7c**, and **13b** as well as internal standards cinmethylin (**1**) and [1,3]thiazolo[4,5-*b*]pyridine **5** against selected warm-season monocotyledon weeds in corn and soy at application rates of 150 and 50 g/ha in advanced greenhouse trials, e.g., BRAPP and ELEIN (replicates: 10 plants per pot).

the tropics and warmer temperate zones, emphasizing the potential of novel FAT inhibitors to contribute to integrated weed and resistance management.

Conclusion

The agrochemical work outlined herein covers a series of novel herbicidal lead structures that contain a 2,3-dihydro[1,3]thiazolo[4,5-*b*]pyridine unit as the essential structural feature, with all of them carrying an *o*-substituted phenyl group. Inspired by earlier work in our group focusing on substituted thiazolo[4,5-*b*]pyridines that showed promising inhibition of the plant-specific enzyme FAT, we explored the selective late-stage conversion into the corresponding 2,3-dihydro[1,3]thiazolo[4,5-*b*]pyridines via different reduction methods. Noteworthy, substituted 2,3-dihydro[1,3]thiazolo[4,5-*b*]pyridines had remained almost entirely unexplored prior to our investigations. Likewise, we identified an optimized $BH_3{\cdot}NH_3$-mediated reduction involving tris(pentafluorophenyl)borane as a strong Lewis acid and subsequent treatment with formic acid as the most suitable conditions to prepare the desired 2,3-dihydro[1,3]thiazolo[4,5-*b*]pyridines. It is worth noting that this reduction proved to be thiazole-specific and gave access to a broad range of desired target compounds. Several substituted 2,3-dihydro[1,3]thiazolo[4,5-*b*]pyridines showed promising herbicidal activity against commercially important grass weeds in preemergence greenhouse tests in line with competitive application rates and hints for crop selectivity, particularly in wheat and soy. Furthermore, the new heterocyclic lead structures have the potential to mitigate and affect weeds that have become resistant towards commercial herbicides, such as resistant blackgrass (ALOMY_R, also known as slender foxtail or black twitch) and ryegrass (LOLSS_R). Remarkably, 2,3-dihydro[1,3]thiazolo[4,5-*b*]pyridine **7b** turned out to be superior to market standards (i.e., **1** and **2** in wheat) in terms of overall efficacy and resistance breaking potential. Halogen-free target compound **7c** also showed strong efficacy against commercially important weeds, in particular resistant ryegrass (LOLSS_R), combined with promising crop safety. In our view, these results underline that chemical innovation using isostere concepts and addressing unusual structural features is a useful tool to broaden the structural scope of modern agrochemical research and to address sustainability goals, e.g., overcoming herbicide resistance and meeting demanding environmental safety goals.

Experimental

Synthesis

Representative procedure for the synthesis of 6-bromo-5-(2-fluorophenyl)-2,3-dihydro[1,3]thiazolo[4,5-*b*]pyridine (13b): To a stirred mixture of 6-bromopyridin-2-amine (**8**, 10.00 g, 56.88 mmol, 1.00 equiv), 2-fluorophenylboronic acid (9.52 g, 65.98 mmol, 1.16 equiv), and Na_2CO_3 (12.06 g, 113.8 mmol, 2.00 equiv) in a mixture of 1,4-dioxane (80 mL) and water (80 mL) at room temperature was added $Pd(dppf)Cl_2$ (1.67 g, 2.28 mmol, 0.04 equiv), and the mixture was stirred at 80 °C for 3 h. Thereafter, the reaction mixture was cooled to room temperature, diluted with water, and extracted thoroughly with ethyl acetate. The combined organic layer was washed with brine, dried over Na_2SO_4, filtered, and concentrated under reduced pressure. The remaining residue was purified via column chromatography (gradient ethyl acetate/hexane) to afford 6-(2-fluorophenyl)pyridin-2-ylamine (**9b**, 9.98 g, 93%). ^{1}H NMR (400 MHz, $CDCl_3$, δ) 7.92–7.88 (m, 1H), 7.53–7.49 (m, 1H), 7.36–7.31 (m, 1H), 7.25–7.20 (m, 1H), 7.16–7.10 (m, 1H), 6.50–6.48 (d, 1H), 4.53–4.44 (br s, 2H, NH_2).

6-(2-Fluorophenyl)pyridin-2-ylamine (**9b**, 9.98 g, 52.49 mmol, 1.0 equiv) was dissolved in acetonitrile (140 mL) and cooled to 0 °C. Thereafter, *N*-bromosuccinimide (20.56 g, 115.49 mmol, 2.2 equiv) was added carefully. The reaction mixture was warmed to room temperature and stirred for 4 h. Subsequently, the reaction mixture was diluted with water, and the resulting solid was filtered off. The solid was washed thoroughly with water and dried to afford 3,5-dibromo-6-(2-fluorophenyl)pyridin-2-ylamine (**10b**, 17.62 g, 97%) as an orange solid. ^{1}H NMR (400 MHz, $CDCl_3$, δ) 7.92 (s, 1H), 7.44–7.33 (m, 2H), 7.25–7.20 (m, 1H), 7.17–7.12 (m, 1H), 5.07–4.98 (br s, 2H, NH_2).

To a stirred solution of 3,5-dibromo-6-(2-fluorophenyl)pyridin-2-ylamine (**10b**, 17.62 g, 50.93 mmol, 1.0 equiv) in DMF (120 mL) at room temperature was added potassium *O*-ethyl dithiocarbonate (18.52 g, 112.04 mmol, 2.2 equiv). The resulting mixture was heated at reflux for 7 h. Thereafter, the reaction mixture was cooled to room temperature, poured onto ice water, and acidified with 2 N HCl. The obtained precipitate was filtered, washed with water, collected, and dried under reduced pressure to afford **11b** as thiol–thione tautomer consisting of 6-bromo-5-(2-fluorophenyl)[1,3]thiazolo[4,5-*b*]pyridine-2-thiol and 6-bromo-5-(2-fluorophenyl)[1,3]thiazolo[4,5-*b*]pyridine-2(3*H*)thione (17.20 g, 97%). ^{1}H NMR (400 MHz, $CDCl_3$, δ) 9.96 (br s, 1H), 8.01 (s, 1H), 7.50–7.44 (m, 1H), 7.41–7.38 (m, 1H), 7.29–7.25 (m, 1H), 7.19–7.15 (m, 1H).

The thiol–thione tautomer **11b** (14.55 g, 42.64 mmol, 1.0 equiv) was dissolved in acetic acid (200 mL), and iron powder (35.71 g, 639.61 mmol, 15 equiv) was carefully added in portions. The resulting reaction mixture was stirred at 100 °C for 10 h. After full conversion (indicated by LC–MS), the reaction mixture was cooled to 60 °C, and the iron powder was filtered off. The remaining solution was diluted with water, and the resulting precipitate was filtered, washed with water, and dried under reduced pressure. The remaining crude residue was

redissolved in DCM, then water was added, followed by thorough extraction. The combined organic layer was dried over magnesium sulfate, filtered, and dried under reduced pressure. The remaining residue was purified via column chromatography (gradient ethyl acetate/hexane) to afford 6-bromo-5-(2-fluorophenyl)[1,3]thiazolo[4,5-*b*]pyridine (**12b**, 8.75 g, 63%). ^{1}H NMR (400 MHz, $CDCl_3$, δ) 9.32 (s, 1H), 8.64 (s, 1H), 7.54–7.45 (m, 2H), 7.31–7.27 (m, 1H), 7.21–7.16 (m, 1H).

6-Bromo-5-(2-fluorophenyl)[1,3]thiazolo[4,5-*b*]pyridine (**12b**, 1,000 mg, 3.07 mmol, 1.0 equiv) was dissolved in absolute toluene (10 mL) in an oven-dried round-bottom flask under argon, to which ammonia borane (285 mg, 9.20 mmol, 3.0 equiv) and $B(C_6F_5)_3$ (79 mg, 0.15 mmol, 0.05 equiv) were added. The resulting reaction mixture was stirred at a temperature of 45 °C for 5 h and then concentrated under reduced pressure. The remaining residue was redissolved in acetonitrile, formic acid was added, and the reaction mixture was stirred at room temperature for 2 h. The phases were separated via phase separator, and the organic layer was concentrated under reduced pressure. The remaining crude product was purified via column chromatography (gradient ethyl acetate/hexane) to afford 6-bromo-5-(2-fluorophenyl)-2,3-dihydro[1,3]thiazolo[4,5-*b*]pyridine (**13b**, 596 mg, 59%). ^{1}H NMR (600 MHz, $CDCl_3$, δ) 4.56 (s, 2H), 6.88 (br s, 1H), 7.11–7.16 (m, 1H), 7.21 (td, *J* = 7.5; 1.1 Hz, 1H), 7.31 (s, 1H), 7.34 (td, *J* = 7.4; 1.9 Hz, 1H), 7.36–7.41 (m, 1H); ^{13}C NMR (151 MHz, $CDCl_3$, δ) 49.0 (CH_2), 108.1 (C), 115.7 (CH), 115.9 (CH), 123.5 (C), 124.0 (CH), 127.7 (d, C), 130.4 (CH), 131.1 (CH), 146.2 (C), 158.7 (C), 160.3 (d, C); HRESIMS (*m*/*z*): $[M + H]^+$ calcd for $C_{12}H_9BrFN_2S$, 310.9671; found, 310.9654.

5-(2-Fluorophenyl)-6-methyl-2,3-dihydro[1,3]thiazolo[4,5-*b*]pyridine (7b): 6-Bromo-5-(2-fluorophenyl)[1,3]thiazolo[4,5-*b*]pyridine (**12b**, 1.88 g, 4.56 mmol, 1.0 equiv), methylboronic acid (1.13 g, 18.24 mmol, 4.0 equiv), potassium phosphate (1.94 g, 9.12 mmol, 2.0 equiv), palladium(II) acetate (103 mg, 0.46 mmol, 0.1 equiv), and 2-dicyclohexylphosphino-2',6'-dimethoxybiphenyl (579 mg, 1.37 mmol, 0.3 equiv) were dissolved in absolute toluene (40 mL) in an oven-dried round-bottom flask under argon. The resulting reaction mixture was stirred at reflux for 3.5 h. After cooling to room temperature, water (80 mL) and toluene (20 mL) were added, followed by addition of ammonium pyrrolidinedithiocarbamate (328 mg, 2.00 mmol, 0.44 equiv). The reaction mixture was stirred for 1 h at room temperature, and the organic layer was washed with saturated sodium hydrogencarbonate solution, dried over magnesium sulfate, filtered, and concentrated under reduced pressure. The remaining residue was purified via column chromatography (gradient ethyl acetate/hexane) to afford 5-(2-fluorophenyl)-6-methyl[1,3]thiazolo[4,5-*b*]pyridine (**5**, 900 mg, 81%). ^{1}H NMR (400 MHz, $CDCl_3$, δ) 9.25 (s, 1H), 8.23 (s, 1H), 7.55–7.51 (m, 1H), 7.47–7.41 (m, 1H), 7.30–7.27 (m, 1H), 7.19–7.15 (m, 1H), 2.40 (s, 3H).

5-(2-Fluorophenyl)-6-methyl[1,3]thiazolo[4,5-*b*]pyridine (**5**, 320 mg, 1.23 mmol, 1.0 equiv) was dissolved in absolute toluene (10 mL) in an oven-dried round-bottom flask under argon, to which ammonia borane (114 mg, 3.69 mmol, 3.0 equiv) and $B(C_6F_5)_3$ (32 mg, 0.06 mmol, 0.05 equiv) were added. The resulting reaction mixture was stirred at a temperature of 45 °C for 5 h and then concentrated under reduced pressure. The remaining residue was redissolved in acetonitrile, formic acid was added, and the reaction mixture was stirred at room temperature for further 45 min. The phases were separated via phase separator, and the organic layer was concentrated under reduced pressure. The remaining crude product was purified via column chromatography (gradient ethyl acetate/hexane) to afford 5-(2-fluorophenyl)-6-methyl-2,3-dihydro[1,3]thiazolo[4,5-*b*]pyridine (**7b**, 62%). ^{1}H NMR (600 MHz, $CDCl_3$, δ) 2.00 (s, 3H), 4.55 (s, 2H), 6.61 (br s, 1H), 7.07 (s, 1H), 7.09–7.12 (m, 1H), 7.19–7.21 (m, 1H), 7.32–7.36 (m, 2H); ^{13}C NMR (151 MHz, $CDCl_3$, δ) 17.96 (CH_3), 17.99 (CH_3), 48.8 (CH_2), 115.6 (CH), 115.7 (CH), 121.0 (C), 121.8 (C), 124.15 (CH), 124.18 (CH), 129.59 (CH), 129.64 (CH), 130.2 (CH), 131.40 (CH), 131.43 (CH), 145.6 (C), 158.9 (C), 159.2 (C), 160.5 (C); HRESIMS (*m*/*z*): $[M + H]^+$ calcd for $C_{13}H_{12}FN_2S$, 247.0705; found, 247.0724.

General procedure for the synthesis of N-acylated 6-methyl-2,3-dihydro[1,3]thiazolo[4,5-*b*]pyridines 16a–f: The corresponding acyl chloride (0.31 mmol, 1.1 equiv) and triethylamine (0.09 mL, 0.63 mmol, 2.2 equiv) were added to a stirred solution of the corresponding 6-methyl-5-phenyl-2,3-dihydro[1,3]thiazolo[4,5-*b*]pyridine **7a–c** (0.28 mmol, 1.00 equiv) in absolute DCM (5 mL). The resulting reaction mixture was stirred at room temperature for 30–120 min, followed by dilution with DCM and water, and subsequent extraction and phase separation. The aqueous layer was thoroughly extracted with DCM, and the combined organic layer was dried over anhydrous $MgSO_4$, filtered, and concentrated under reduced pressure. The remaining crude product was purified via column chromatography (gradient ethyl acetate/heptane) to afford the corresponding desired target compound **16a–f**, for example, 1-[5-(2-fluorophenyl)-6-methyl[1,3]thiazolo[4,5-*b*]pyridin-3(2*H*)-yl]ethanone (**16c**, 150 mg, 84%). ^{1}H NMR (600 MHz, $CDCl_3$, δ) 2.16 (d, *J* = 2.2 Hz, 3H), 2.61 (s, 2H), 5.32 (s, 2H), 7.12–7.15 (m, 1H), 7.21–7.24 (m, 1H), 7.34 (s, 1H), 7.37–7.49 (m, 2H); ^{13}C NMR (151 MHz, $CDCl_3$, δ) 18.41 (CH_3), 18.44 (CH_3), 24.7 (CH_3), 49.3 (CH_2), 115.7 (CH), 115.8 (CH), 124.09 (CH), 124.12 (CH), 125.2 (C), 127.8 (C), 129.9 (CH), 130.0 (CH), 131.37 (CH), 131.40 (CH), 132.1 (CH),

147.0 (C), 149.6 (C), 158.9 (C), 160.6 (C), 170.6 (C); HRESIMS (*m*/*z*): $[M + H]^+$ calcd for $C_{15}H_{14}FN_2OS$, 289.0811; found, 289.0806.

Biology and biochemistry

In vivo greenhouse screening: Seeds of mono- and dicotyledonous weed plants and crop plants were sown in plastic or organic planting pots in sandy loam and covered with soil (replicates: n = 10, i.e., 10 monocotyledonous weed seeds were grown per pot or n = 5, i.e., 5 dicotyledonous weed seeds were grown per pot). The 2,3-dihydro[1,3]thiazolo[4,5-*b*]pyridines described above (e.g., **7a–c**, **13a–c**, **14a–c**, **16a–f**, and **17a–b**), formulated in the form of wettable powder (WP) , were applied to the surface of the covering soil as aqueous suspension or emulsion, with the addition of 0.5% of an additive at an application rate of 600 L of water/ha (converted). Following treatment, the pots were placed in a greenhouse and kept under optimum growth conditions for the test plants. The test plants were placed in the greenhouse for ca. three weeks under optimum growth conditions, and then the effect of the preparations was assessed visually in comparison to untreated control plants (herbicidal effect: 100% = plants died off, 0% = as untreated control plants). Efficacy values were given based on a rating scale by final visual experts' assessment of green mass, i.e., 5 = ≥90% inhibition, 4 = 70–89% inhibition, 3 = 50–69% inhibition, 2 = 40–49% inhibition, 1 = 21–39% inhibition, and — = <20% inhibition. Advanced screening was carried out with or as emulsifiable concentrate formulations, three replicate pots, and a standardized number of seeds per pot depending on the plant species (10 seeds for corn and wheat spectrum). The harmful plants and crops used in greenhouse tests were the following species: *Alopecurus myosuroides* (ALOMY), resistant *Alopecurus myosuroides* (ALOMY_R, origin: Germany), *Apera spica-venti* (APESV), *Brachiaria platyphylla* (BRAPP), *Bromus tectorum* (BROTE), *Echinochloa crus-galli* (ECHCG), *Digitaria sanguinalis* (DIGSA), *Eleusine indica* (ELEIN), *Glycine max* (GLXMA), *Lolium rigidum* (LOLRI), *Lolium sp.* (LOLSS), resistant *Lolium sp.* (LOLSS_R, origin: France), *Poa annua* (POAAN), *Setaria viridis* (SETVI), *Sorghum halepense* (SORHA), *Triticum aestivum* (TRZAS), and *Zea mays* (ZEAMX).

***Lp*FAT A expression and purification:** The *fat a03* gene from *Lemna paucicostata*, in which the N-terminal amino acids representing the chloroplast transit peptide were replaced by an N-terminal 6xHis-tag, was cloned into a pET24 vector [3]. The *Lp*FAT A protein was expressed in *E. coli* BL21Star(DE3) cells. 5 mL of an overnight culture of *E. coli* cells grown in LB medium with 100 µg/mL carbenicillin were used to inoculate 0.5 L of autoinduction medium containing 100 µg/mL carbenicillin [28]. The bacteria were grown at 37 °C and 120 rpm for about 4.5 h to reach OD_{600} = 0.6 and then further cultivated at 21 °C overnight. The bacteria were harvested by centrifugation (20 min, 6,000*g*) and stored frozen at −80 °C. *Lp*FAT A protein was purified using the Ni-NTA Fast Start Kit (Qiagen GmbH, Germany) according to the instructions of the manufacturer. Active fractions were pooled together, and the buffer was exchanged into 25 mM potassium phosphate buffer pH 7.3 containing 10% glycerol with PD10 columns (GE Healthcare). Aliquots of the protein solution were frozen in liquid nitrogen and stored at −80 °C.

***Lp*FAT A fluorescence polarization assay:** Fluorescence polarization (FP) competition assays were performed at room temperature in black 96-well microtiter plates (Greiner, Catalog No. 655900). The assay mixture contained 25 mM potassium phosphate buffer pH 7.3, 200 mM NaCl, 0.01% Triton X-100, 2 nM fluorescent tracer, 0.4 µg of purified *Lp*FAT A protein and different amounts of the test compound in a total volume of 100 µL. FP was measured with a BMG CLARIOstar microtiter plate reader using the FP filter set for fluorescein (Ex 482-16, Em 530-40, LP504). FP is the difference between wells containing *Lp*FAT A and wells containing only tracer. The pI_{50} values were calculated from plots of inhibition values vs test compound concentration using Model 205 of the ID Business Solutions Ltd Xlfit software suite. The FAT A binding fluorescent tracer was synthesized from (2*S*,4*S*)-4-[(2,6-difluorophenyl)methoxymethyl]-4-ethyl-2-methyl-*N*-(prop-2-ynylcarbamoyl)-1,3-dioxolane-2-carboxamide [3] and FAM azide, 5-isomer (Broadpharm BP-22544, San Diego, CA) by click chemistry [29] and was purified by flash column chromatography on silica gel.

Supporting Information

Supporting Information File 1

General synthetic procedures, characterization of all target compounds, methods for biological and biochemical testing, and scans of ^1H and ^{13}C NMR spectra of the new 2,3-dihydro[1,3]thiazolo[4,5-b]pyridines.
[https://www.beilstein-journals.org/bjoc/content/supplementary/1860-5397-20-46-S1.pdf]

Acknowledgements

We would like to thank Susanne Ries, Gudrun Fey, Andreas Uhl, Peter Zöllner, and Martin Annau for valuable analytical support. R. L. M. and K.-Y. K. would like to thank the Herbicide Innovation Partnership (HIP) between the Grains Research and Development Corporation (GRDC) and Bayer AG for a Postdoctoral Research Fellowship.

ORCID® iDs

Jens Frackenpohl - https://orcid.org/0000-0003-3457-0290
David M. Barber - https://orcid.org/0000-0001-9906-1695
Bernd Laber - https://orcid.org/0000-0003-2955-0746
Thomas Müller - https://orcid.org/0009-0001-5422-3053

References

1. Busi, R.; Dayan, F. E.; Francis, I.; Goggin, D.; Lerchl, J.; Porri, A.; Powles, S. B.; Sun, C.; Beckie, H. J. *Pest Manage. Sci.* **2020,** *76,* 2601–2608. doi:10.1002/ps.5798
2. Dayan, F. E. *Plants* **2019,** *8,* 341. doi:10.3390/plants8090341
3. Campe, R.; Hollenbach, E.; Kämmerer, L.; Hendriks, J.; Höffken, H. W.; Kraus, H.; Lerchl, J.; Mietzner, T.; Tresch, S.; Witschel, M.; Hutzler, J. *Pestic. Biochem. Physiol.* **2018,** *148,* 116–125. doi:10.1016/j.pestbp.2018.04.006
4. Kalinger, R. S.; Pulsifer, I. P.; Hepworth, S. R.; Rowland, O. *Lipids* **2020,** *55,* 435–455. doi:10.1002/lipd.12226
5. Salas, J. J.; Ohlrogge, J. B. *Arch. Biochem. Biophys.* **2002,** *403,* 25–34. doi:10.1016/s0003-9861(02)00017-6
6. Johnen, P.; Zimmermann, S.; Betz, M.; Hendriks, J.; Zimmermann, A.; Marnet, M.; De, I.; Zimmermann, G.; Kibat, C.; Cornaciu, I.; Mariaule, V.; Pica, A.; Clavel, D.; Márquez, J. A.; Witschel, M. *Pest Manage. Sci.* **2022,** *78,* 3620–3629. doi:10.1002/ps.7004
7. Brabham, C.; Johnen, P.; Hendriks, J.; Betz, M.; Zimmermann, A.; Gollihue, J.; Serson, W.; Kempinski, C.; Barrett, M. *Weed Sci.* **2021,** *69,* 18–30. doi:10.1017/wsc.2020.87
8. Kim, J.-H.; Seo, J.-S.; An, J.-Y.; Kwon, Y.-S.; Hwang, K.-H.; Koo, S.-J.; Kim, J.-H. *Bull. Environ. Contam. Toxicol.* **2020,** *105,* 656–664. doi:10.1007/s00128-020-02976-w
9. Koo, S.-J.; Hwang, K.-H.; Jeon, M.-S.; Kim, S.-H.; Lim, J.; Lee, D.-G.; Cho, N.-G. *Pest Manage. Sci.* **2014,** *70,* 156–162. doi:10.1002/ps.3541
10. Messelhäuser, M. H.; Saile, M.; Sievernich, B.; Gerhards, R. *Plant, Soil Environ.* **2021,** *67,* 46–54. doi:10.17221/586/2020-pse
11. Bratz, M.; Meyer, N.; Koenig, H.; Walter, H.; Gerber, M.; Westphalen, K.-O. Substituierte Naphthyridine und deren Verwendung. German Patent DE4405712A1, Aug 24, 1995.
12. Abel, S. A. G.; Alnafta, N.; Asmus, E.; Bollenbach-Wahl, B.; Braun, R.; Dittgen, J.; Endler, A.; Frackenpohl, J.; Freigang, J.; Gatzweiler, E.; Heinemann, I.; Helmke, H.; Laber, B.; Lange, G.; Machettira, A.; McArthur, G.; Müller, T.; Odaybat, M.; Reingruber, A. M.; Roth, S.; Rosinger, C. H.; Schmutzler, D.; Schulte, W.; Stoppel, R.; Tiebes, J.; Volpin, G.; Barber, D. M. *J. Agric. Food Chem.* **2023,** *71,* 18212–18226. doi:10.1021/acs.jafc.3c02490
13. Barber, D. M.; Helmke, H.; Braun, R.; Tiebes, J.; Machettira, A. B.; Asmus, E.; Rosinger, C. H.; Gatzweiler, E.; Schmutzler, D.; Frackenpohl, J.; Reingruber, A. M.; Bollenbach-Wahl, B.; Dittgen, J. Substituted pyrrolidin-2-ones, salts thereof and their use as herbicidally active substances. WO Patent WO2021/204589, Oct 14, 2021.
14. Barber, D. M.; Braun, R.; Frackenpohl, J.; Heinemann, I.; Schmutzler, D.; Reingruber, A. M.; Bollenbach-Wahl, B.; Dittgen, J.; Roth, S. Substituted thiazolopyridines, salts thereof and their use as herbicidally active substances. WO Patent WO2023/036706, March 16, 2023.
15. Scutt, J. N.; Seden, P. T.; Wailes, J. S. Isothiazolo[3,4-*b*]pyridines as herbicides. WO Patent WO2023/156398, Aug 24, 2023.
16. Barber, D. M. *J. Agric. Food Chem.* **2022,** *70,* 11075–11090. doi:10.1021/acs.jafc.1c07910
17. Frackenpohl, J.; Abel, S. A. G.; Alnafta, N.; Barber, D. M.; Bojack, G.; Brant, N. Z.; Helmke, H.; Mattison, R. L. *J. Agric. Food Chem.* **2023,** *71,* 18141–18168. doi:10.1021/acs.jafc.3c01809
18. Marco-Contelles, J.; Pérez-Mayoral, E.; Samadi, A.; Carreiras, M. d. C.; Soriano, E. *Chem. Rev.* **2009,** *109,* 2652–2671. doi:10.1021/cr800482c
19. Seganish, W. M.; Brumfield, S. N.; Lim, J.; Matasi, J. J.; Mcelroy, W. T.; Tulshian, D. B.; Lavey, B. J.; Altman, M. D.; Gibeau, C. R.; Lampe, J. W.; Methot, J.; Zhu, L. Aminopyrimidinones as interleukin receptor-associated kinase inhibitors. WO Patent WO2013/066729, May 10, 2013.
20. Pang, M.; Chen, J.-Y.; Zhang, S.; Liao, R.-Z.; Tung, C.-H.; Wang, W. *Nat. Commun.* **2020,** *11,* 1249. doi:10.1038/s41467-020-15118-x
21. Xia, Y.-T.; Sun, X.-T.; Zhang, L.; Luo, K.; Wu, L. *Chem. – Eur. J.* **2016,** *22,* 17151–17155. doi:10.1002/chem.201604503
22. Forlani, L.; Ferrara, A.; Lugli, A.; Todesco, P. E. *J. Chem. Soc., Perkin Trans. 2* **1994,** 1703–1707. doi:10.1039/p29940001703
23. Okamoto, H.; Kobutani, T.; Kato, S. *Bull. Chem. Soc. Jpn.* **1992,** *65,* 674–678. doi:10.1246/bcsj.65.674
24. Ding, F.; Zhang, Y.; Zhao, R.; Jiang, Y.; Bao, R. L.-Y.; Lin, K.; Shi, L. *Chem. Commun.* **2017,** *53,* 9262–9264. doi:10.1039/c7cc04709f
25. Liu, Z.-Y.; Wen, Z.-H.; Wang, X.-C. *Angew. Chem., Int. Ed.* **2017,** *56,* 5817–5820. doi:10.1002/anie.201702304
26. He, Y.; Nie, W.; Xue, Y.; Hu, Q. *RSC Adv.* **2021,** *11,* 20961–20969. doi:10.1039/d1ra02399c
27. Frackenpohl, J.; Barber, D. M.; Braun, R.; Brown, R. W.; Heinemann, I.; Kallus, C.; Dittgen, J.; Reingruber, A. M.; Bollenbach-Wahl, B.; Gatzweiler, E. Substituted 2,3-dihydro[1,3]thiazolo[4,5-b]pyridines, salts thereof and their use as herbicidally active substances. WO Patent WO2023/036707, March 16, 2023.
28. Studier, F. W. *Protein Expression Purif.* **2005,** *41,* 207–234. doi:10.1016/j.pep.2005.01.016
29. Punna, S.; Kaltgrad, E.; Finn, M. G. *Bioconjugate Chem.* **2005,** *16,* 1536–1541. doi:10.1021/bc0501496

License and Terms

BEILSTEIN JOURNAL OF ORGANIC CHEMISTRY

A laterally-fused N-heterocyclic carbene framework from polysubstituted aminoimidazo[5,1-*b*]oxazol-6-ium salts

Andrew D. Gillie, Matthew G. Wakeling‡, Bethan L. Greene‡, Louise Male and Paul W. Davies*

Letter

Open Access

Address:
School of Chemistry, University of Birmingham, Birmingham, B15 2TT, UK

Email:
Paul W. Davies* - p.w.davies@bham.ac.uk

* Corresponding author ‡ Equal contributors

Keywords:
annulation; carbene; gold; imidazolium; NHC

Beilstein J. Org. Chem. **2024,** *20,* 621–627.
https://doi.org/10.3762/bjoc.20.54

Received: 15 December 2023
Accepted: 29 February 2024
Published: 18 March 2024

This article is part of the thematic issue "5th International Symposium on Synthesis and Catalysis (ISySyCat 2023)".

Guest Editor: A. Burke

Abstract

A polysubstituted 3-aminoimidazo[5,1-*b*]oxazol-6-ium framework has been accessed from a new nitrenoid reagent by a two-step ynamide annulation and imidazolium ring-formation sequence. Metalation with Au(I), Cu(I) and Ir(I) at the C2 position provides an L-shaped NHC ligand scaffold that has been validated in gold-catalysed alkyne hydration and arylative cyclisation reactions.

Introduction

Imidazolium-derived nucleophilic heterocyclic carbenes (NHCs) have had a sustained impact across the fields of organometallic and main group chemistry, transition-metal catalysis, materials synthesis and organocatalysis [1]. Laterally annellated polycyclic NHCs offer a useful contrast to the most widely used 'umbrella-like' NHCs (Figure 1) [2,3]. An extended π-system influences the donor and acceptor properties of the carbene whilst substitution on the polycycle can position groups adjacent to the active centre.

The imidazo[1,5-*a*]pyridin-3-ylidene motif (**ImPy**), independently introduced by the groups of Lassaletta [4] and Glorius [5], is the most widely explored framework for L-shaped ligands (Figure 1a). Even when only considering gold catalysis [6], the **ImPy** framework has been used to great effect [7]. The motif has been used to introduce sterically demanding NHCs with secondary gold-ligand interactions [8-10], chiral environments [11-13] including those enabling secondary interactions with substrates for asymmetric catalysis [14], cooperative and bimetallic catalysis [7,15], and redox-enabling function for Au(I)/(III) cycles [16,17].

Such L-shaped ligands provide scope to influence the reactivity profile of their resulting metal complexes through steric shielding, direct stabilising interactions with the metal, or by proximal effects to reactive species. Given the sensitivity of

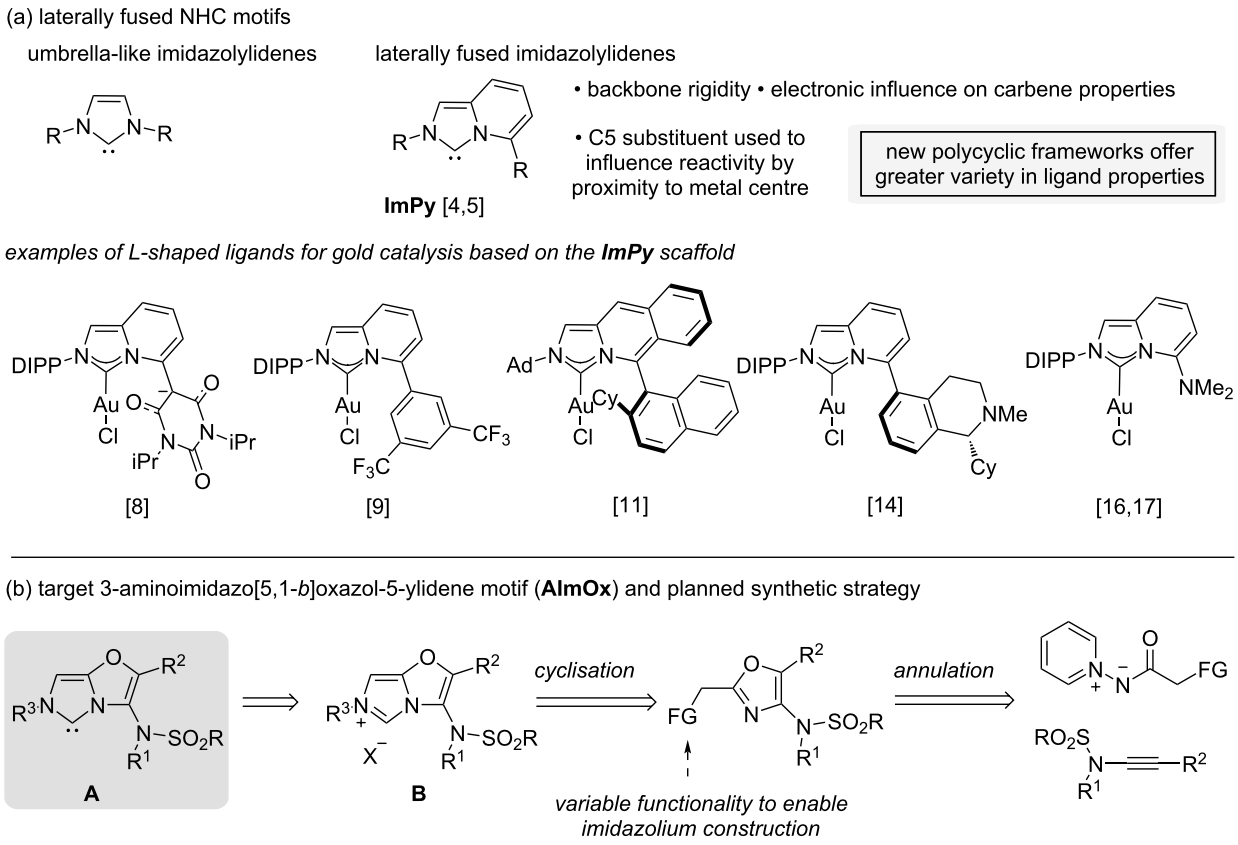

Figure 1: Laterally fused NHC motifs.

metal catalysis to even subtle steric and electronic changes in the ligand sphere, accessing more diverse fused imidazolium frameworks and different peripheral functionality offers significant scope to influence catalytic properties. Few studies into L-shaped imidazolylidines have explored core motifs beyond **ImPy**, with NHCs derived from two π-rich rings fused together particularly underinvestigated [2,18,19].

In this work we report the preparation of a new L-shaped NHC motif, the 3-aminoimidazo[5,1-*b*]oxazol-5-ylidene **A** (shortened hereafter to **AImOx**), which fuses two π-rich rings and positions a sulfonamide group alongside the metal centre (Figure 1b). We envisaged that the potential NHC precursor to **A**, a polysubstituted 3-aminoimidazo[5,1-*b*]oxazol-6-ium motif **B**, might be rapidly accessed from an ynamide by sequential oxazole-forming annulation and imidazolium formation steps. The basis of this approach was a gold-catalysed oxazole formation developed in our group [20,21] that should facilitate access to different groups at the oxazole C-2 position allowing a range of imidazolium-forming cyclisation strategies to be explored. Glorius and co-workers reported the formation of symmetrical NHCs by imidazolium ring formation from bisoxazoline motifs [22] but incorporating the unsaturated oxazole counterparts has not been explored.

Results and Discussion

Reaction of ynamide **1a** with the *N*-acylpyridinium-*N*-aminide reagent **2** proceeded in good yield to afford oxazole **3** bearing a C-2 methyleneamino moiety as the first example of a free secondary amine in this annulation type (Scheme 1a, path a). However, attempts to form the desired imidazolium ring from **3** using triethyl orthoformate and different additives were unsuccessful. Similarly, an imine precursor **6**, prepared in high yields by synthesising the known acetal-bearing oxazole **5** [21] and reacting it with 2,6-diisopropylphenylamine, could not be converted into the desired imidazolium salt (Scheme 1a, path b). Applying a range of conditions, including those successful on other annulated systems, led to unreacted starting material or hydrolysis products after work-up (see Supporting Information File 1) [5,18,19,23-27]. The unique Schiff base **6** can however be stored without precautions for several months without degradation and is prepared with minimal processing in 75% yield by telescoping the annulation and condensation steps.

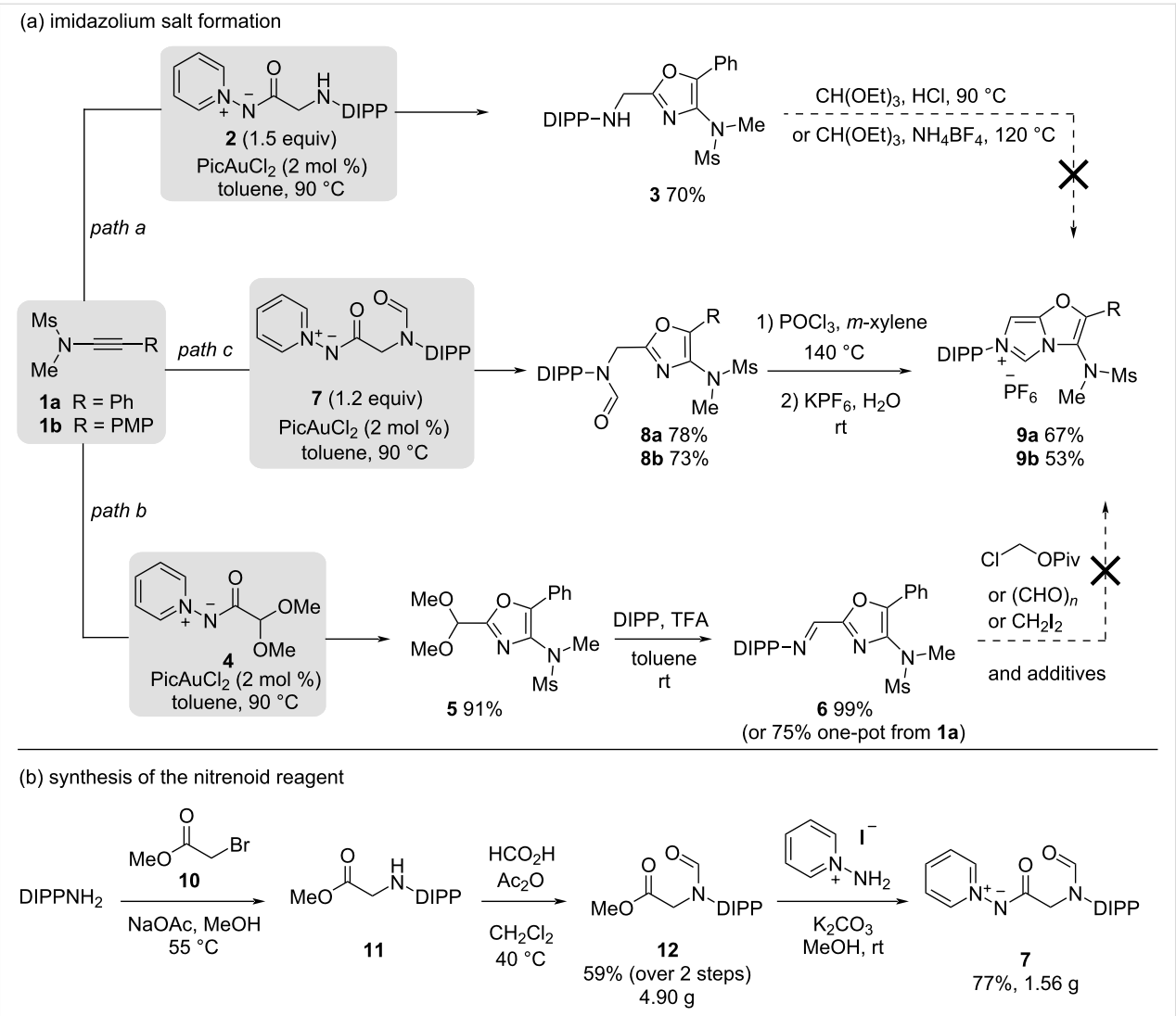

Scheme 1: Synthetic studies into the formation of a 3-aminoimdazo[5,1-*b*]oxazol-6-ium motif based on a gold-catalysed oxazole formation. DIPP = 2,6-diisopropylphenylamine; Pic = picolinate; PMP = *p*-methoxyphenyl.

As the 4-aminooxazole motif appeared to be a poor nucleophile, we sought to introduce a formamide motif in place of the amine or imine to allow the use of more forcing cyclisation conditions (Scheme 1a, path c). Oxazole **8a** was obtained in good yield from **1a** using only a slight excess of nitrenoid **7** and 2 mol % catalyst loading. Heating **8a** in the presence of $POCl_3$ afforded the 3-aminoimidazo[5,1-*b*]oxazol-6-ium motif, followed by salt metathesis using KPF_6 leading to the clean hexafluorophosphate salt **9a** in 67% yield after recrystallisation [4].

This two-step assembly of the 3-aminoimidazo[5,1-*b*]oxazol-6-ium motif was also applied to ynamide **1b** affording the PMP-substituted salt **9b** in good yield.

The new nitrenoid reagent **7** is readily prepared from 2,6-diisopropylphenylamine in three steps. Alkylation with methyl bromoacetate is followed by formylation of **11** and then substitution [21] of **12** with *N*-aminopyridinium iodide to yield the bench-stable and crystalline *N*-acylpyridinium aminide **7** in good yield on a gram scale (Scheme 1b).

With the novel 3-aminoimidazo[5,1-*b*]oxazol-6-ium salt in hand, we examined its use as an NHC precursor for the preparation of late transition metal complexes. Treating compound **9a** with triethylamine and either dimethyl sulfide gold(I) chloride or copper(I) chloride in acetone led to the formation of the desired **AImOx**AuCl and **AImOx**CuCl metal chloride complexes **13** and **14**, respectively (Scheme 2) [7].

The ^{1}H NMR spectra of the resulting **AImOx** metal complexes show a loss of symmetry for the diisopropyl substituents, indicating restricted rotation about the C(oxazole)–N(sulfonamide)

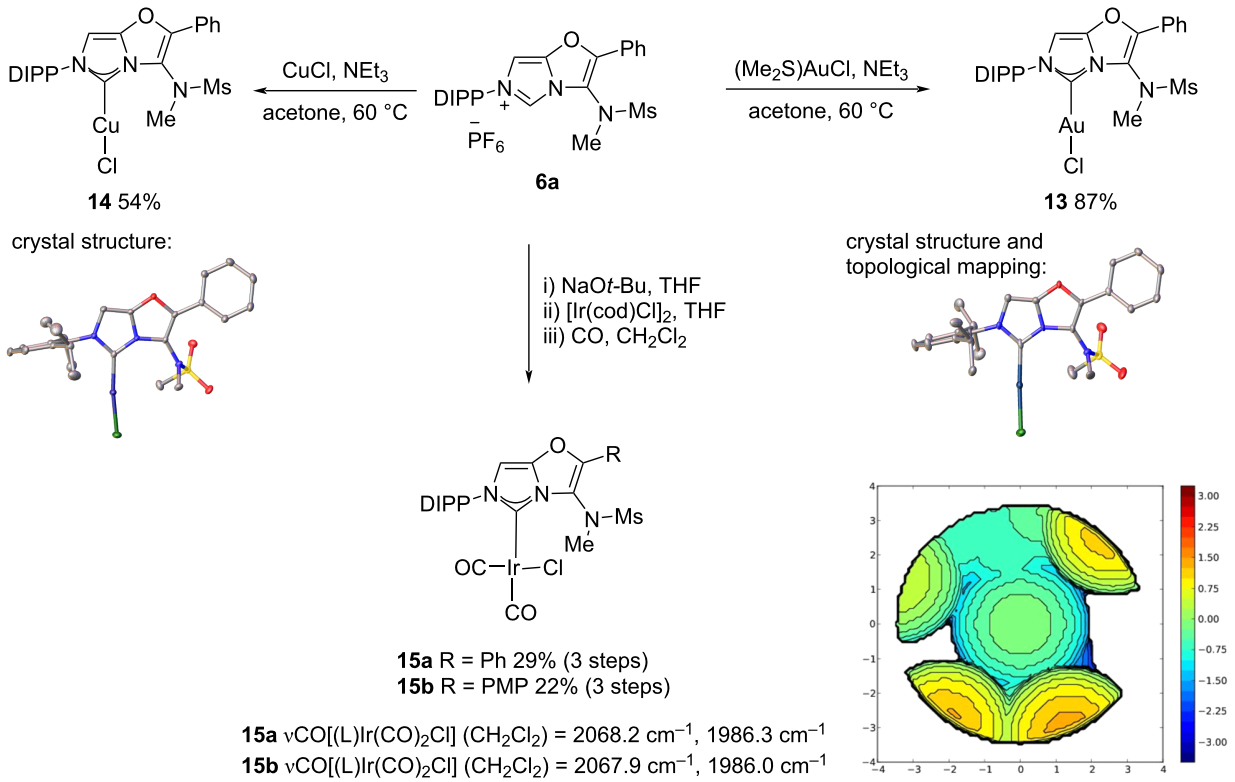

Scheme 2: The synthesis of **AImOx**Au(I)Cl, **AImOx**Cu(I)Cl, and **AImOx**Ir(CO)$_2$Cl complexes from **6a**. The single crystal X-ray diffraction structures of **13** and **14** have ellipsoids drawn at 50% probability, with hydrogens and solvent omitted for clarity. Selected bond angles and distances: **13**: C1–Au: 1.98 Å, Au–Cl: 2.28 Å, N2–Au: 3.65 Å. N1–C1–N3: 102.7°, N3–C1–Au: 129.5°, N1–C1–Au: 127.1°, C1–Au–Cl: 175.8°. **14**: C1–Au: 1.97 Å, Au–Cl: 2.28 Å, N2–Au: 3.66 Å. N1–C1–N3: 102.6°, N3–C1–Au: 129.4°, N1–C1–Au: 127.9°, C1–Au–Cl: 177.7°. Topographic steric maps of AImOxAuCl **13**. Au–carbene bond selected as *z*-axis, nitrogen's flanking carbene define *xz* plane. Bondi radii scaled by 1.17, sphere radius 3.5 Å, mesh spacing 0.10, H atoms removed for calculations. Colour coding represents positioning of steric bulk relative to the centre of the sphere, scale in Å.

bond. No coalescence is observed at up to 110 °C indicating that these motifs might be useful as a robust atropisomeric system. The molecular structure of **13** and **14** have been unambiguously determined by single crystal X-ray diffraction (Scheme 2) [28]. The N–metal interatomic distances are between 3.53 and 3.66 Å leaving insufficient space for bond rotation about the C–N axis with the sulfonamide substituents being approximately perpendicular to the fused aromatic unit. A percentage buried volume of 44.6% was calculated from the crystal structure of **13** using Cavallo's method and Sambvca V.2.0 software (Scheme 2) [29]. Although a similar value to that reported for IPrAuCl (%Vbur = 45.4%) [30] the steric map shows a very different steric environment on either side of the ligand.

The **AImOx**Ir(CO)$_2$Cl complex **15** was targeted in order to assess the electronic effects of the fused imidazolium core (Scheme 2). No reaction was observed between **6a** and [Ir(cod)Cl]$_2$ in the presence of NEt$_3$. A solution of the free carbene was prepared from **6** and reacted with [Ir(cod)Cl]$_2$ and then CO to afford the **AImOx**Ir(CO)Cl complex **15**. A minor side-product with a strong red colour was formed which could not be fully purified or characterised but has a characteristic AQ quartet of two protons replacing the singlet for the *N*-methyl group in the ^{1}H NMR spectra consistent with a cyclometallated complex from C–H insertion [31,32].

Three distinct sets of *N*-methyl and *N*-methylsulfonyl signals, with a major one accounting for approximately 80% of the total, were observed in the ^{1}H NMR spectra of **15** likely due to restricted rotation around the metal carbene bond combining with the locked rotation around the oxazole C4–N bond. Elemental analysis was consistent with the proposed structure and only two sharp CO stretching frequencies were observed in the IR (Scheme 2) and so a value for Tolman's electronic parameter (TEP) could be estimated. [33] At TEP[Ir] = 2053.1 cm^{-1} and 2052.8 cm^{-1} for **15a** and **15b**, respectively, the values for these **AImOx** ligands are towards the electron-deficient end seen with imidazolidines (cf. for IPr TEP[Ir] = 2050.2 cm^{-1}) [34].

A benchmarking exercise was then performed looking at the reactivity of **13** compared against reaction of symmetrical IPrAuCl across a range of known gold-mediated transformations of alkynes featuring intermolecular attack [35], intramolecular cyclisation [36] or a mixture of both [8,37-39]. The new ligand system proved to deliver competent catalysis. Conversion was seen in all cases at 1 mol % catalyst loading (Scheme 3). Use of **13** resulted in a slight increase of the anti-Markovnikov hydration product **17** over **18** when compared to IPrAuCl [35]. In arylative cyclisations incomplete reaction was

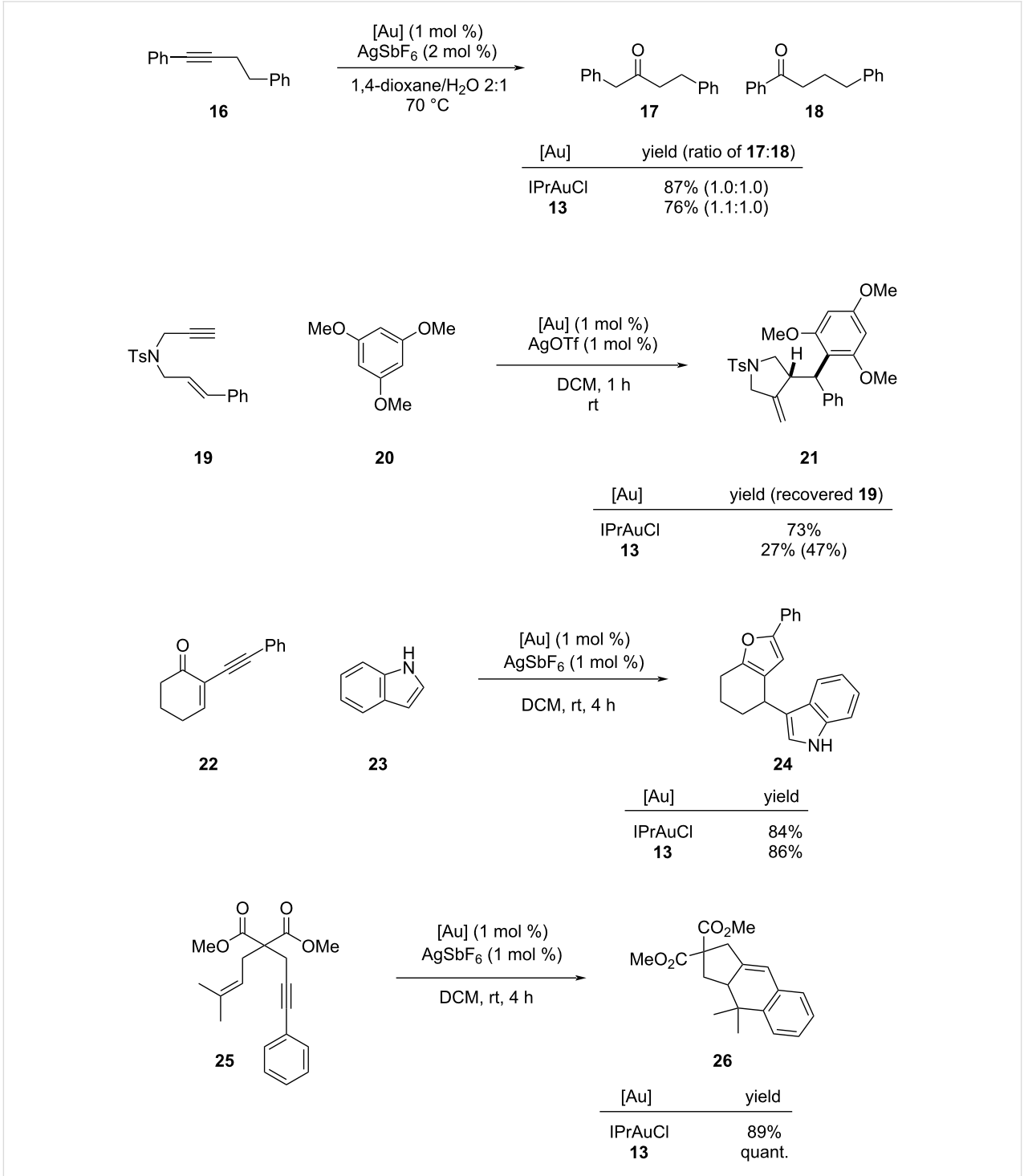

Scheme 3: Use of **AImOx**AuCl **13** in catalysis. [a]Yields are calculated from the ^{1}H NMR spectra against an internal standard unless otherwise stated. Isolated yield of **17**:**18** with ratios determined from the ^{1}H NMR spectra.

seen with enyne **19** [8,37] but ynone **22** [39] afforded high yield of **24**. A quantitative conversion was seen in the intramolecular arylative cyclisation of **25** where **13** outperformed IPrAuCl [36].

Conclusion

An L-shaped NHC ligand motif, **AImOx**, has been developed and used to access monoligated Au(I), Cu(I) and Ir(I) complexes. The NHC precursors, polysubstituted 3-aminoimidazo[5,1-*b*]oxazol-6-ium salts are readily prepared in an efficient two-step sequence from ynamides using a newly developed nitrenoid reagent **4**. The resulting **AImOx**Au(I) complex is catalytically competent across several transformations with excellent conversions at 1 mol % loading and with broadly comparable reactivity to IPrAuCl. Having validated the **AImOx** motif as a viable ligand platform for development, further elaboration and applications will be reported in due course.

Supporting Information

Supporting Information File 1

Experimental procedures and characterisation data, additional cyclisation studies, XRD data and NMR spectra of compounds.
[https://www.beilstein-journals.org/bjoc/content/supplementary/1860-5397-20-54-S1.pdf]

Acknowledgements

The authors gratefully acknowledge support from the Centre for Chemical and Materials Analysis in the School of Chemistry (UoB). We thank the EPSRC UK National Crystallography Service at the University of Southampton for the collection of the crystallographic data for compound **14**. [40] We thank Dr Richard Mudd (UoB) for the preparation of literature substrates for catalysis studies. This work is based on Andrew D. Gillie's doctoral thesis ("Synthesis and Applications of 4N-Substituted Oxazoles", University of Birmingham, 2015).

Funding

We thank EPSRC and the School of Chemistry at the University of Birmingham for studentship support (ADG, MGW, BLG). P.W.D. is grateful to the Royal Society and Leverhulme Trust for the award of a Senior Research Fellowship (SRF\R1\191033).

ORCID® iDs

Andrew D. Gillie - https://orcid.org/0009-0005-3227-9186
Matthew G. Wakeling - https://orcid.org/0000-0002-8802-7667
Bethan L. Greene - https://orcid.org/0009-0008-9222-8876
Louise Male - https://orcid.org/0000-0002-8295-2528
Paul W. Davies - https://orcid.org/0000-0002-0340-2414

Data Availability Statement

The data generated and analyzed during this study is openly available in the University of Birmingham eData Repository (UBIRA) at https://doi.org/10.25500/edata.bham.00001041.

References

1. Hopkinson, M. N.; Richter, C.; Schedler, M.; Glorius, F. *Nature* **2014,** *510,* 485–496. doi:10.1038/nature13384
2. Reshi, N. U. D.; Bera, J. K. *Coord. Chem. Rev.* **2020,** *422,* 213334. doi:10.1016/j.ccr.2020.213334
3. Iglesias-Sigüenza, J.; Izquierdo, C.; Díez, E.; Fernández, R.; Lassaletta, J. M. *Dalton Trans.* **2016,** *45,* 10113–10117. doi:10.1039/c6dt01700b
4. Alcarazo, M.; Roseblade, S. J.; Cowley, A. R.; Fernández, R.; Brown, J. M.; Lassaletta, J. M. *J. Am. Chem. Soc.* **2005,** *127,* 3290–3291. doi:10.1021/ja0423769
5. Burstein, C.; Lehmann, C. W.; Glorius, F. *Tetrahedron* **2005,** *61,* 6207–6217. doi:10.1016/j.tet.2005.03.115
6. Fürstner, A.; Davies, P. W. *Angew. Chem., Int. Ed.* **2007,** *46,* 3410–3449. doi:10.1002/anie.200604335
7. Teixeira, P.; Bastin, S.; César, V. *Isr. J. Chem.* **2023,** *63,* e202200051. doi:10.1002/ijch.202200051
8. Tang, Y.; Benaissa, I.; Huynh, M.; Vendier, L.; Lugan, N.; Bastin, S.; Belmont, P.; César, V.; Michelet, V. *Angew. Chem., Int. Ed.* **2019,** *58,* 7977–7981. doi:10.1002/anie.201901090
9. Pedrazzani, R.; Pintus, A.; De Ventura, R.; Marchini, M.; Ceroni, P.; Silva López, C.; Monari, M.; Bandini, M. *ACS Org. Inorg. Au* **2022,** *2,* 229–235. doi:10.1021/acsorginorgau.1c00052
10. Kim, Y.; Kim, Y.; Hur, M. Y.; Lee, E. *J. Organomet. Chem.* **2016,** *820,* 1–7. doi:10.1016/j.jorganchem.2016.07.023
11. Varela, I.; Faustino, H.; Díez, E.; Iglesias-Sigüenza, J.; Grande-Carmona, F.; Fernández, R.; Lassaletta, J. M.; Mascareñas, J. L.; López, F. *ACS Catal.* **2017,** *7,* 2397–2402. doi:10.1021/acscatal.6b03651
12. Pallova, L.; Abella, L.; Jean, M.; Vanthuyne, N.; Barthes, C.; Vendier, L.; Autschbach, J.; Crassous, J.; Bastin, S.; César, V. *Chem. – Eur. J.* **2022,** *28,* e202200166. doi:10.1002/chem.202200166
13. Francos, J.; Grande-Carmona, F.; Faustino, H.; Iglesias-Sigüenza, J.; Díez, E.; Alonso, I.; Fernández, R.; Lassaletta, J. M.; López, F.; Mascareñas, J. L. *J. Am. Chem. Soc.* **2012,** *134,* 14322–14325. doi:10.1021/ja3065446
14. Zhang, J.-Q.; Liu, Y.; Wang, X.-W.; Zhang, L. *Organometallics* **2019,** *38,* 3931–3938. doi:10.1021/acs.organomet.9b00400
15. Rawat, V. K.; Higashida, K.; Sawamura, M. *ACS Catal.* **2022,** *12,* 8325–8330. doi:10.1021/acscatal.2c01701
16. Gao, P.; Xu, J.; Zhou, T.; Liu, Y.; Bisz, E.; Dziuk, B.; Lalancette, R.; Szostak, R.; Zhang, D.; Szostak, M. *Angew. Chem., Int. Ed.* **2023,** *62,* e202218427. doi:10.1002/anie.202218427
17. Scott, S. C.; Cadge, J. A.; Boden, G. K.; Bower, J. F.; Russell, C. A. *Angew. Chem., Int. Ed.* **2023,** *62,* e202301526. doi:10.1002/anie.202301526
18. Kriechbaum, M.; List, M.; Berger, R. J. F.; Patzschke, M.; Monkowius, U. *Chem. – Eur. J.* **2012,** *18,* 5506–5509. doi:10.1002/chem.201200465

19. Lohre, C.; Fröhlich, R.; Glorius, F. *Synthesis* **2008,** 2221–2228. doi:10.1055/s-2008-1067147
20. Davies, P. W.; Cremonesi, A.; Dumitrescu, L. *Angew. Chem., Int. Ed.* **2011,** *50,* 8931–8935. doi:10.1002/anie.201103563
21. Gillie, A. D.; Jannapu Reddy, R.; Davies, P. W. *Adv. Synth. Catal.* **2016,** *358,* 226–239. doi:10.1002/adsc.201500905
22. Glorius, F.; Altenhoff, G.; Goddard, R.; Lehmann, C. *Chem. Commun.* **2002,** 2704–2705. doi:10.1039/b208045a
23. Hintermann, L. *Beilstein J. Org. Chem.* **2007,** *3,* No. 22. doi:10.1186/1860-5397-3-22
24. Calder, I. C.; Spotswood, T. M.; Sasse, W. H. P. *Tetrahedron Lett.* **1963,** *4,* 95–100. doi:10.1016/s0040-4039(01)90585-4
25. Chien, C.-H.; Fujita, S.; Yamoto, S.; Hara, T.; Yamagata, T.; Watanabe, M.; Mashima, K. *Dalton Trans.* **2008,** 916–923. doi:10.1039/b712901g
26. Samanta, T.; Kumar Rana, B.; Roymahapatra, G.; Giri, S.; Mitra, P.; Pallepogu, R.; Kumar Chattaraj, P.; Dinda, J. *Inorg. Chim. Acta* **2011,** *375,* 271–279. doi:10.1016/j.ica.2011.05.017
27. Zhang, J.-L.; Chen, L.-A.; Xu, R.-B.; Wang, C.-F.; Ruan, Y.-P.; Wang, A.-E.; Huang, P.-Q. *Tetrahedron: Asymmetry* **2013,** *24,* 492–498. doi:10.1016/j.tetasy.2013.03.004
28. CCDC 2310256–2310257 contain the supplementary crystallographic data for this paper. These data can be obtained free of charge from The Cambridge Crystallographic Data Centre via https://www.ccdc.cam.ac.uk/data_request/cif.
29. Falivene, L.; Credendino, R.; Poater, A.; Petta, A.; Serra, L.; Oliva, R.; Scarano, V.; Cavallo, L. *Organometallics* **2016,** *35,* 2286–2293. doi:10.1021/acs.organomet.6b00371
30. Gómez-Suárez, A.; Nelson, D. J.; Nolan, S. P. *Chem. Commun.* **2017,** *53,* 2650–2660. doi:10.1039/c7cc00255f
31. Hanasaka, F.; Tanabe, Y.; Fujita, K.-i.; Yamaguchi, R. *Organometallics* **2006,** *25,* 826–831. doi:10.1021/om050723x
32. Corberán, R.; Sanaú, M.; Peris, E. *Organometallics* **2006,** *25,* 4002–4008. doi:10.1021/om060343r
33. Chianese, A. R.; Li, X.; Janzen, M. C.; Faller, J. W.; Crabtree, R. H. *Organometallics* **2003,** *22,* 1663–1667. doi:10.1021/om021029+
34. Nelson, D. J.; Nolan, S. P. *Chem. Soc. Rev.* **2013,** *42,* 6723–6753. doi:10.1039/c3cs60146c
35. Marion, N.; Ramón, R. S.; Nolan, S. P. *J. Am. Chem. Soc.* **2009,** *131,* 448–449. doi:10.1021/ja809403e
36. Nieto-Oberhuber, C.; López, S.; Echavarren, A. M. *J. Am. Chem. Soc.* **2005,** *127,* 6178–6179. doi:10.1021/ja042257t
37. Toullec, P. Y.; Genin, E.; Leseurre, L.; Genêt, J.-P.; Michelet, V. *Angew. Chem., Int. Ed.* **2006,** *45,* 7427–7430. doi:10.1002/anie.200601980
38. Yao, T.; Zhang, X.; Larock, R. C. *J. Am. Chem. Soc.* **2004,** *126,* 11164–11165. doi:10.1021/ja0466964
39. Martí, À.; Montesinos-Magraner, M.; Echavarren, A. M.; Franchino, A. *Eur. J. Org. Chem.* **2022,** e202200518. doi:10.1002/ejoc.202200518
40. Coles, S. J.; Allan, D. R.; Beavers, C. M.; Teat, S. J.; Holgate, S. J. W.; Tovee, C. A. Leading Edge Chemical Crystallography Service Provision and Its Impact on Crystallographic Data Science in the Twenty-First Century. In *21st Century Challenges in Chemical Crystallography I: History and Technical Developments;* Mingos, D. M. P.; Raithby, P. R., Eds.; Springer International Publishing: Cham, Switzerland, 2020; pp 69–140. doi:10.1007/430_2020_63

License and Terms

BEILSTEIN JOURNAL OF ORGANIC CHEMISTRY

Regioselective quinazoline C2 modifications through the azide–tetrazole tautomeric equilibrium

Dāgs Dāvis Līpiņš[1], Andris Jeminejs[1], Una Ušacka[1,2], Anatoly Mishnev[3], Māris Turks[1] and Irina Novosjolova[*1]

Full Research Paper

Open Access

Address:
[1]Faculty of Natural Sciences and Technology, Riga Technical University, P. Valdena Str. 3, Riga, LV-1048, Latvia, [2]Ķekava Secondary School, Gaismas Str. 9, Ķekava, Ķekava Parish, Ķekava Municipality, LV-2123, Latvia and [3]Latvian Institute of Organic Synthesis, Aizkraukles Str. 21, Riga, LV-1006, Latvia

Email:
Irina Novosjolova[*] - irina.novosjolova@rtu.lv

* Corresponding author

Keywords:
aromatic nucleophilic substitution; azide–tetrazole equilibrium; 4-azido-2-sulfonylquinazolines; quinazolines; sulfonyl group dance

Beilstein J. Org. Chem. **2024,** *20,* 675–683.
https://doi.org/10.3762/bjoc.20.61

Received: 15 December 2023
Accepted: 18 March 2024
Published: 28 March 2024

This article is part of the thematic issue "5th International Symposium on Synthesis and Catalysis (ISySyCat 2023)".

Guest Editor: A. Burke

Abstract

2-Chloro-4-sulfonylquinazolines undergo functional group swap when treated with an azide nucleophile: 1) the azide replaces the sulfonyl group at the C4 position; 2) the intrinsic azide–tetrazole tautomeric equilibrium directs the nucleofugal sulfinate from the first step to replace chloride at the C2 position. This transformation is effective with quinazolines bearing electron-rich substituents. Therefore, the title transformations are demonstrated on the 6,7-dimethoxyquinazoline core, which is present in pharmaceutically active substances. The methodology application is showcased by transforming the obtained 4-azido-6,7-dimethoxy-2-sulfonylquinazolines into the α_1-adrenoceptor blockers terazosin and prazosin by further C2-selective S_NAr reaction and azide reduction.

Introduction

The quinazoline core is a privileged structure with a wide range of applications. Quinazoline derivatives exhibit a broad spectrum of biological activities, finding use as anticancer, antimicrobial, antimalarial, and antiviral agents [1,2]. Furthermore, numerous 2-amino-6,7-dimethoxyquinazoline analogs are extensively employed as α_1-adrenoceptor blockers [3,4]. In recent years quinazoline-based OLED materials have also gained attention showing great quantum efficiencies [5-7]. Consequently, ongoing efforts focus on advancing methodologies for synthesizing established quinazoline-based drugs and acquiring novel modified quinazoline derivatives for pharmaceutical or materials science purposes.

Aromatic nucleophilic substitution [8] or metal-catalyzed reactions [9,10] are commonly employed for quinazoline modification (Scheme 1). Existing literature underscores the reactivity of

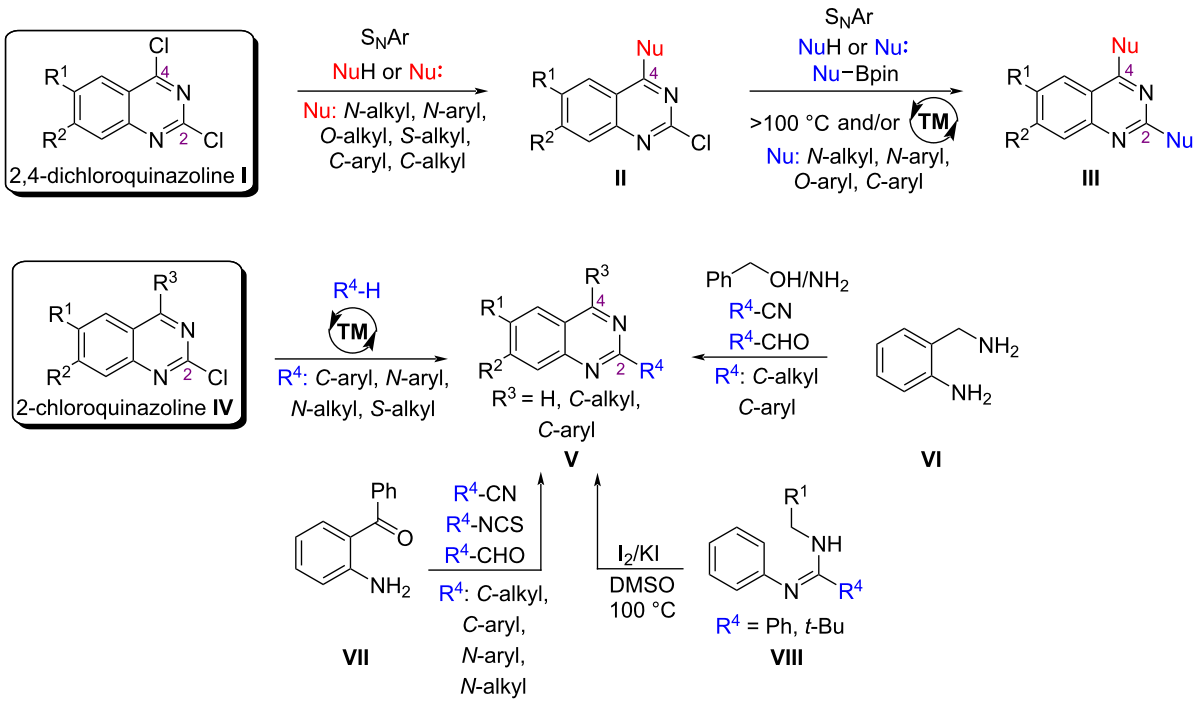

Scheme 1: Approaches for quinazoline modifications at the C2 and C4 positions.

the C4 position in aromatic nucleophilic substitutions of quinazolines **I** while achieving regioselective replacement at the C2 position poses challenges [11]. Modification of the C2 position of quinazolines requires longer time, higher temperatures, and sometimes the use of expensive transition-metal catalysts [12]. A selective C2 modification can be achieved by using 2-chloroquinazolines **IV**, where the C4 position is blocked by an unreactive C–C or C–H bond (Scheme 1). Cyclization reactions of substituted anilines **VI**, **VII** or *N*-arylamidines **VIII** are frequently employed for synthesizing C2-substituted quinazolines (Scheme 1), thereby influencing the spatial arrangement of the desired substituents [13,14]. Moreover, there have been recent advancements in efficient C–H activation techniques employing transition-metal and photocatalysis [15,16]. These methods facilitate C–C bond formation, enabling the introduction of alkyl groups at the C2 position of quinazoline derivatives.

While arylsulfanyl group rearrangement reactions have been documented by us for modifying 2,4-substituted quinazolines [17,18], and sulfonyl group rearrangement has been applied to functionalize purines [19], the literature lacks information on sulfonyl group migration in quinazolines. Notably, this transformation has not been previously reported, despite its potential utility in the synthesis of drugs such as terazosin and prazosin [20].

Herein, we report the use of the sulfonyl group dance to synthesize novel 4-azido-2-sulfonylquinazolines and their C2-selective modification in S_NAr reactions. In addition, we offer an approach for the synthesis of terazosin and prazosin, known medications against hypertension, using sulfonyl group dance products.

Results and Discussion

Synthesis of 4-azido-2-sulfonylquinazolines

We started our experiments with commercially available 2,4-dichloroquinazoline (**1a**). It was treated with sodium 4-methylphenylsulfinate in order to yield 4-sulfonylquinazoline **2a** (Scheme 2), but the first attempts in iPrOH did not provide the starting material conversion. The reaction in THF resulted in the full conversion of the starting material, but the analysis of the crude product revealed the quantitative formation of hydrolysis product **5a**. Assuming the instability of intermediate **2a**, a one-pot reaction was performed by adding sodium 4-methylphenylsulfinate in the first step which was followed by NaN_3. As the result, the formation of hydrolysis product **5a** and 2,4-diazidoquinazoline (**6a**) was observed.

Next, the reaction **1a** → **4a** in DMSO yielded diazidoquinazoline **6a** as a major product and hydrolysis product **5a**. In MeCN the conversion to derivative **2a** was stopped at 50% and was not facilitated by an extra addition of sulfinate. To our delight, in

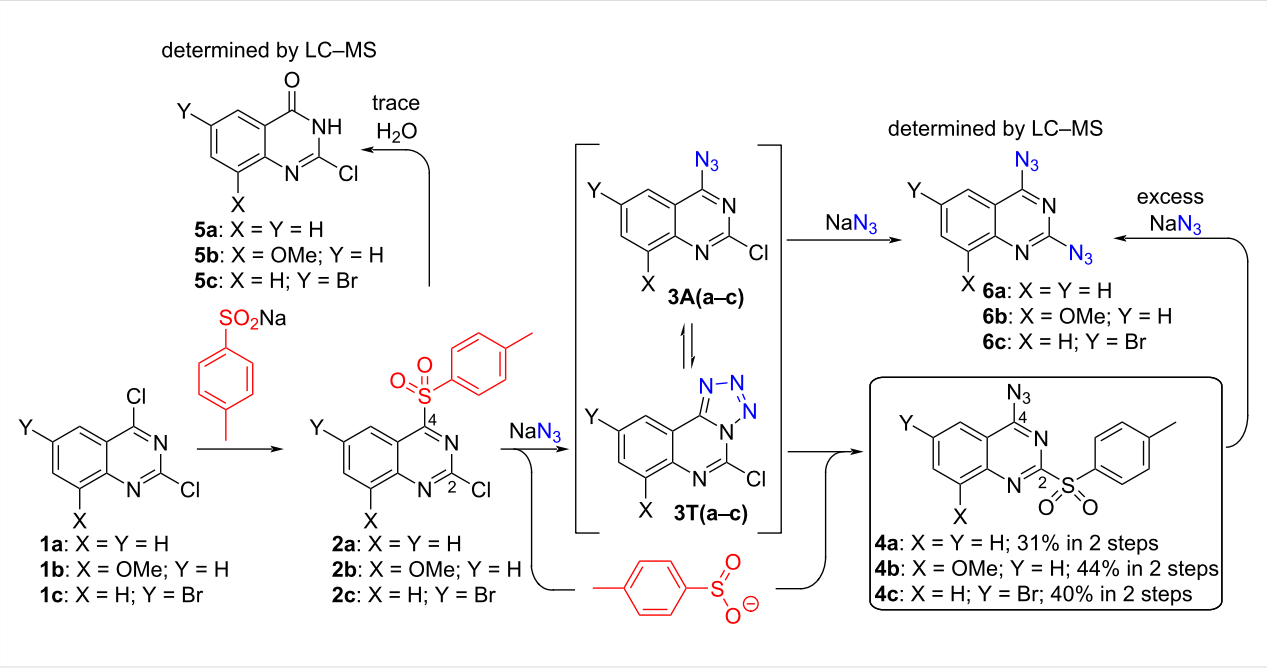

Scheme 2: Attempts toward sulfonyl group dance using 2,4-dichloroquinazolines **1a–c**.

MeOH we observed the formation of intermediate **2a** over 5 hours, and after the subsequent addition of sodium azide product **4a** was isolated in 31% yield over 2 steps. The full conversion was achieved by keeping the reaction mixture at a temperature of 0 °C and by the stepwise additions of the sulfinate and NaN_3. Any deviation from these conditions facilitated the formation of byproducts.

In addition, the sulfonyl group dance reactions were carried out also with quinazoline derivatives **1b** and **1c** (Scheme 2), the structure features of which may slow-down the fast S_NAr processes due to the substituents' character. The desired products **4b** and **4c** were obtained in MeOH and isolated in 44 and 40% yields, respectively. Methanol is known to decrease reactivity in the S_NAr reactions in comparison to polar solvents such as DMSO and DMF. This is explained by solvent hydrogen bond acidity and basicity descriptors α and β, for example, α(DMSO) = 0, β(DMSO) = 0.88, α(MeOH) = 0.43, β(MeOH) = 0.47. The rate constant of the S_NAr process escalates with an increase of β parameters and diminishes with an increase of α parameters [21,22]. Therefore, it was possible to accomplish the sulfonyl group dance reactions of very reactive quinazolines **1a–c** in MeOH.

Synthesis of 4-azido-6,7-dimethoxy-2-sulfonylquinazolines

Next, we aimed to explore the sulfonyl group dance process using a more electron-rich quinazoline. The commercially available 2,4-dichloro-6,7-dimethoxyquinazoline (**7**) was chosen for this purpose (Scheme 3). The common dimethoxy motif is also found in a variety of quinazoline-based pharmaceuticals [2,3,8,23].

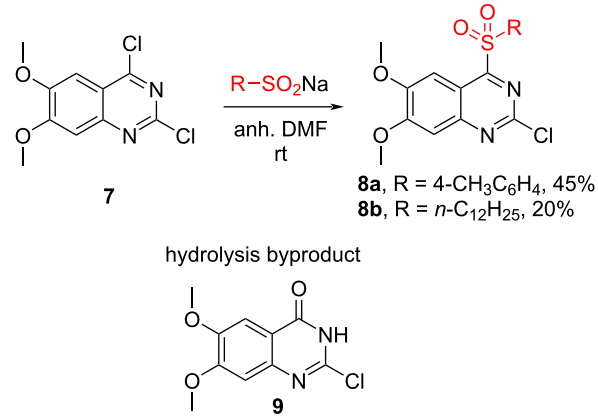

Scheme 3: Synthesis of 2-chloro-6,7-dimethoxy-4-sulfonylquinazoline derivatives **8**.

We commenced our study with the preparation of 2-chloro-4-sulfonylquinazolines **8** (Scheme 3). The starting material **7** underwent S_NAr reactions with sodium sulfinates and the C4-substituted products **8a**,**b** were isolated [24]. The complete conversion was achieved in DMF or DMSO. In the case of sodium dodecylsulfinate, the reaction stopped at 70% conversion when 1 equivalent of sulfinate was used. Products **8** exhibited

instability in the presence of water, leading to the formation of hydrolysis product **9** [25] in the reaction mixture. This instability caused issues during the reaction work-up, and attempts for purification using column chromatography resulted in full degradation of the formed product.

Consequently, an alternative pathway toward product **8** was explored (Scheme 4). 2-Chloro-4-thioquinazolines **10** were prepared from starting material **7** in an S_NAr reaction with thiols in the presence of K_2CO_3 in good 75–93% yields. Next, thioquinazolines **10** were oxidized to the corresponding sulfonylquinazolines **8**. Inspired by our previous work [19] a TFAA/H_2O_2 oxidizing system was tried first but yielded several side-products, such as the hydrolysis product and unwanted oxidation of the quinazoline N3 position. Changing the oxidant to *m*CPBA (with 96% purity) [26] provided a more selective reaction, no water-based work-up was needed and the pure product was obtained by simple recrystallization from ethanol in yields up to 88%. The oxidation step thiol → sulfoxide was fast and full conversion to the intermediate was achieved in one hour for most substrates, but the step sulfoxide → sulfone was entirely slower and required stirring overnight (except for **8d** (R = iC_3H_7)).

With 2-chloro-6,7-dimethoxy-4-sulfonylquinazolines **8** in hand, we started to explore the reactivity in S_NAr reactions (Scheme 5). Sulfonyl group dance reactions did not work in anhydrous THF, MeCN, and dioxane, using such azide sources as NaN_3, LiN_3, and TMS-N_3. Full conversion towards product **12a** was observed by HPLC with NaN_3 in anhydrous DMF. However, precipitation, direct, and reversed-phase column chromatography provided low yields (Scheme 5) due to the degradation of the product. Compounds **12** did not tolerate aqueous conditions or high temperatures and have also been observed to degrade under direct sunlight.

Next, a stepwise one-pot approach was investigated to increase the overall yield (Scheme 6). The reaction in anhydrous DMF

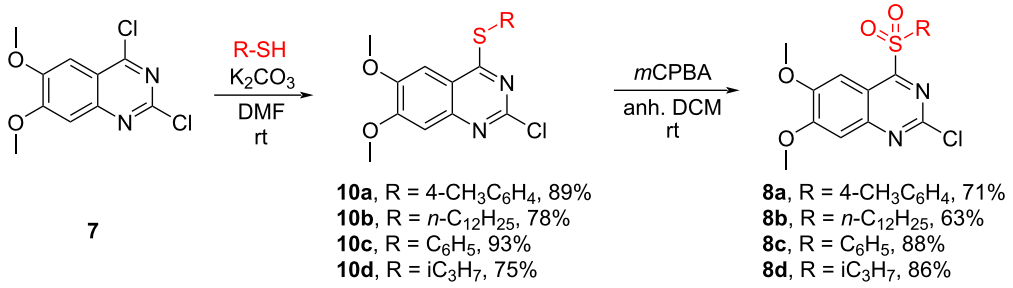

Scheme 4: Alternative synthesis pathway for 2-chloro-6,7-dimethoxy-4-sulfonylquinazoline derivatives **8**.

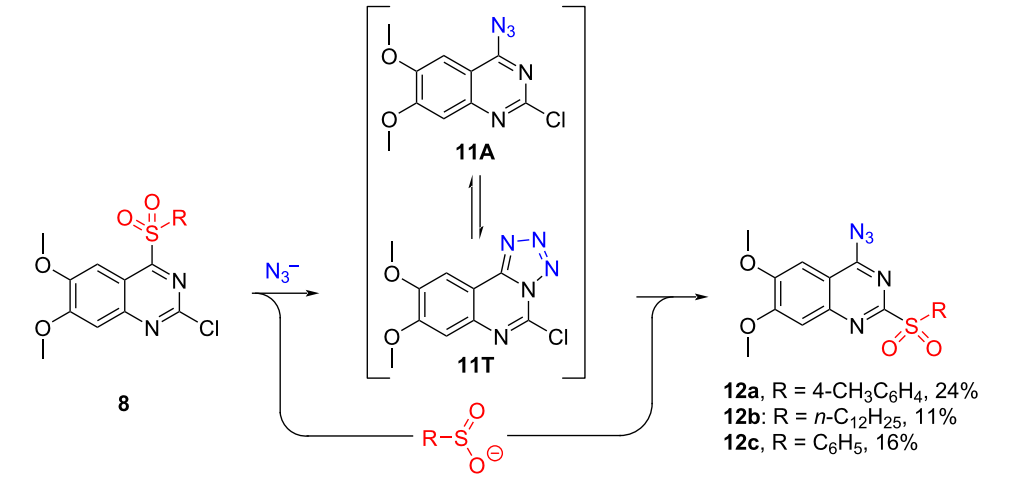

Scheme 5: Sulfonyl group dance using 2-chloro-6,7-dimethoxy-4-sulfonylquinazolines **8**.

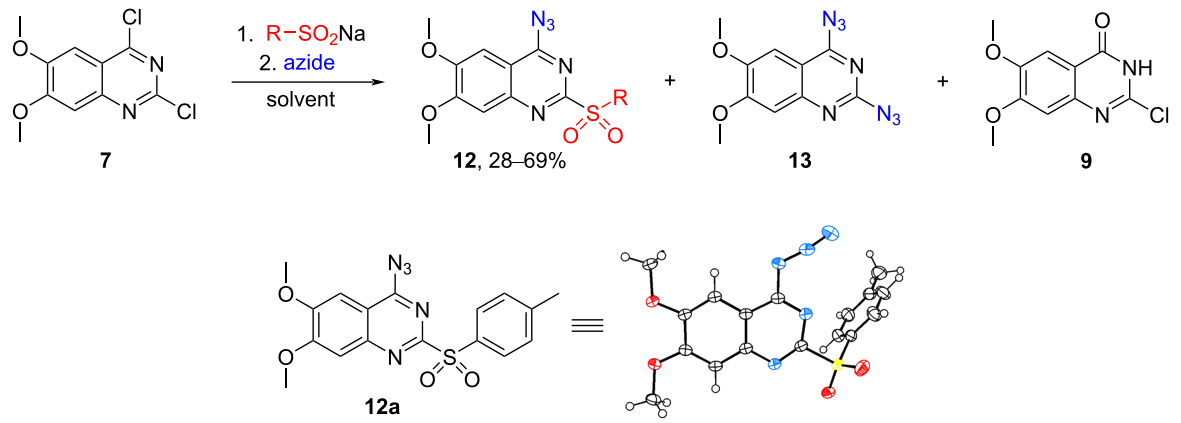

Scheme 6: One-pot synthesis of 4-azido-6,7-dimethoxy-2-sulfonylquinazolines **12**. The crystallographic information for **12a** has been submitted to the Cambridge Crystallographic Data Centre and is available as supplementary publication No. CCDC-2312750.

yielded a mixture of the desired product **12a**, diazide **13**, and hydrolysis product **9** [25] which were inseparable using common purification methods (Table 1).

The pivotal advancement occurred when attempting the reaction in DMSO (Table 1). In the case of **8a** (R = 4-$CH_3C_6H_4$), the product precipitated out when full conversion was reached. Filtration of this precipitate yielded the pure desired product **12a** in 39% yield (Table 1, entry 2). Incremental additions of NaN_3, coupled with HPLC analysis following each addition, facilitated the achievement of full conversion of the starting material after 0.7–0.8 equivalents of NaN_3. This approach limited the formation of diazide **13** and significantly elevated the yield of the desired product to 69% over two steps. When other sufinates were employed, the product failed to precipitate, necessitating isolation through preparative HPLC. Quantitative nuclear magnetic resonance (qNMR) yields were consequently reported.

To reduce the formation of diazide **13**, an overnight addition of the azide solution via a dispenser was employed at a rate of 0.1 equivalents of NaN_3 per hour. This strategy improved the ratio of product **12** to diazide **13**. For arylsulfinates, the addition time was finally reduced to 2 hours without compromising selectivity. Although tetrabutylammonium azide (TBAA) is better soluble in DMSO than NaN_3, practical challenges associated with its use led to the preference for NaN_3.

Confirmation of regioselectivity for the sulfonyl group dance products

The regioselectivity and the structure of 4-azido-6,7-dimethoxy-2-sulfonylquinazoline derivatives **12** were proven by chemical synthesis of the regioisomers **15** (Scheme 7) and X-ray analysis of **12a** (Scheme 6). 6,7-Dimethoxy-2,4-diazidoquinazoline (**13**) was synthesized from commercially available dichloroquinazoline **7** in 93% yield. Further, thioether substituents were installed in the presence of K_2CO_3. For alkylthiols, DMF was

Table 1: Conditions for one-pot synthesis of 4-azido-6,7-dimethoxy-2-sulfonylquinazolines **12**.

Entry	Solvent	Azide source	Time, h	R	Yield, %
1	anh. DMF	1.0 equiv NaN_3[a]	1	4-$CH_3C_6H_4$	–[b]
2	anh. DMSO	0.6 equiv NaN_3[a]	1	4-$CH_3C_6H_4$	**12a**, 39
3	anh. DMSO	0.8 equiv NaN_3[a]	4	4-$CH_3C_6H_4$	**12a**, 69
4	anh. DMSO	0.8 equiv NaN_3[c]	2	4-$CH_3C_6H_4$	**12a**, 66[d]
5	anh. DMSO	0.8 equiv NaN_3[c]	12	*n*-$C_{12}H_{25}$	**12b**, 28
6	anh. DMSO	0.8 equiv NaN_3[c]	12	iC_3H_7	**12d**, 63[e]
7	anh. DMSO	0.8 equiv NaN_3[c]	2	C_6H_5	**12c**, 50[e]

[a]Added in portions; [b]a mixture of products **12** and **13** (Scheme 6); [c]0.5 M solution of NaN_3 in anh. DMSO added over 2 hours; [d]5.8 mmol scale; [e]qNMR yield.

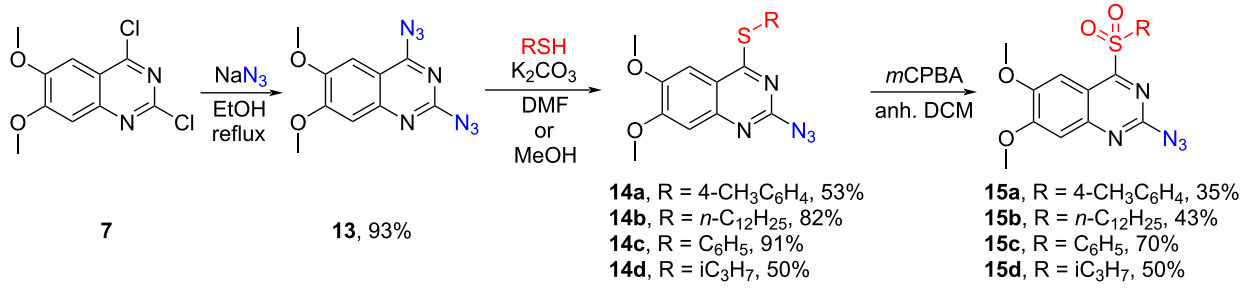

Scheme 7: Synthesis of 2-azido-4-sulfonyl-6,7-dimethoxyquinazolines **15**.

used, but arylthiols required milder conditions with MeOH and cooling to acquire regioselectivity to the C4 position which resulted in yields up to 91%. Oxidation with purified *m*CPBA (commercial *m*CPBA with 68% purity was washed with pH 7.4 phosphate buffer to reach 96% purity [26]) yielded the regioisomers **15** of the sulfonyl group dance products at a lower yield than the previously mentioned oxidation step, which was most likely caused by the high reactivity of product **14**, but the reaction conditions were not further optimized since the products were only needed for analytical purposes.

Two different pyrrolidine-substituted derivatives were additionally synthesized to prove the regioselectivity of the sulfonyl group dance products (Scheme 8). Compound **16** was obtained in the C4-selective S_NAr reaction between diazidoquinazoline **13** and pyrrolidine in 93% yield. A cross peak for the H–C5 position of quinazoline and CH_2 groups of pyrrolidine at the second position was observed in the NOESY spectrum and unequivocally proved the structure **16**. Selective C2 substitution was achieved between sulfonylquinazoline **12** and pyrrolidine in $CHCl_3$ yielding product **17a**. No NOESY signals were seen between the quinazoline core and the pyrrolidine moiety. Interestingly, the C4 substitution was achieved when DMF was used as a solvent in the transformation **12** → **18**, resulting in product **18**.

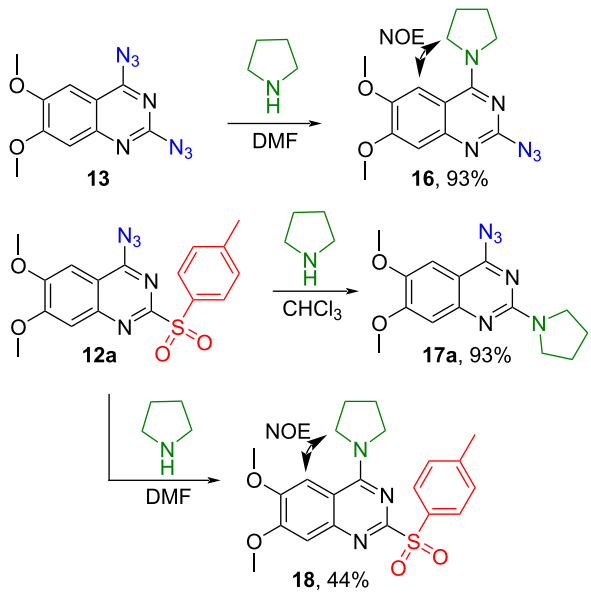

Scheme 8: Synthesis of 6,7-dimethoxyquinazoline derivatives **16**, **17a** and **18**.

In addition, the reaction **12a** + pyrrolidine in MeCN and THF gave only product **17a**, but in DMSO resulted in the mixture of **17a**/**18**/6,7-dimethoxy-2,4-di(pyrrolidin-1-yl)quinazoline = 36:15:48% (HPLC analysis). The selectivity of **17a**/**18** was interesting but was not further developed in the scope of this study.

Consequently, an investigation into the azide–tetrazole equilibrium of product **12a** was initiated, revealing a singular form present in all solvents. Despite attempts to increase the amount of the azide form with the increase of the temperature in NMR experiments [27], no observable alteration in the tautomeric equilibrium was observed. FTIR analysis of **12a** in $CHCl_3$ and DMSO solutions revealed the absence of the azide form (see Supporting Information File 1), precluding an explanation of the reactivity of **12a** through the tautomeric equilibrium. The presence of electron-donating methoxy groups in the structure was proposed as a plausible explanation for the present tetrazole form in the solutions. Surprisingly, FTIR and X-ray analyses of **12a** in the solid state indicated the existence of **12a** in the azide form.

In subsequent experiments it was discovered that for less nucleophilic *N*-nucleophiles (piperidine, morpholine, *N*-methylpiperazine) C2 selectivity was reached only in polar solvents such as DMF, DMSO, and MeCN. In other solvents, no reactivity was observed at the C2 or C4 positions.

Selective modification of the C2 position of 6,7-dimethoxyquinazoline

Products **12** are useful intermediates to achieve selective modification at the C2 position of quinazolines. A scope of 2-amino-4-azido-6,7-dimetoxyquinazolines **17** was synthesized. For pyrrolidine, selective C2 substitution was achieved in a non-polar solvent such as $CHCl_3$. Less nucleophilic amines gave C2-selective S_NAr in MeCN.

To apply the developed technique to the synthesis of pharmaceutically active substances such as terazosin and prazosin, nucleophilic substitution at the C2 position was carried out with the corresponding amines – piperazin-1-yl(tetrahydrofuran-2-yl)methanone and furan-2-yl(piperazin-1-yl)methanone to give products **17e** and **17f**. Products **17e**,**f** can be obtained through the aromatic nucleophilic substitution of 2-azido-4-sulfonylquinazoline **12a** or by performing three subsequent S_NAr reactions starting from 2,4-dichloroquinazoline **7** in a one-pot procedure [28] (Scheme 9, Table 2).

The resulting products exist in an azide–tetrazole equilibrium in solution, but in solid form can be in either the azide (**17e**, **17f**) or tetrazole form (**17a–d**).

With derivatives **17e**,**f** in hand, the reduction of the azido group in the C4 position was carried out by bubbling hydrogen through the solution in the presence of palladium on charcoal. In the last step, the product was acidified with a 4 M HCl solution in iPrOH, forming the respective hydrochlorides of terazosin [29,30] and prazosin [31,32] (Scheme 10).

In addition, we explored some other reactions of the azido group, and derivatives **17** were used in CuAAC and Staudinger reactions, yielding products **20** and **21** (Scheme 11).

For CuAAC reactions no conversion towards the desired triazolyl product **20** was observed in systems such as $CuSO_4{\cdot}5H_2O$/sodium ascorbate/*t*-BuOH/H_2O, $CuSO_4{\cdot}5H_2O$/sodium ascorbate/THF/H_2O, CuI/DIPEA/DCM. Instead, triazolyl derivatives **20** were synthesized using $[Cu(MeCN)_4]PF_6$/TBTA (tris(benzyltriazolylmethyl)amine) [33] in toluene.

Table 2: Diversity and yields for 2-amino-4-azido-6,7-dimethoxyquinazolines **17**.

Entry	R^1R^2NH	Solvent	Yield
1		$CHCl_3$	**17a**, 93[a]
2	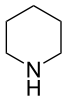	MeCN	**17b**, 73[a]
3	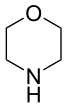	MeCN	**17c**, 75[a]
4	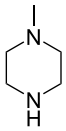	MeCN	**17d**, 77[a]
5	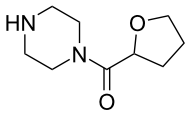	DMSO	**17e**, 80[a], 41[b]
6	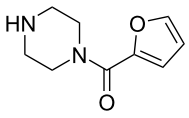	DMSO	**17f**, 75[a], 49[b]

[a]Yield **12a**→**17**, %; [b]yield **7**→**17**, % (over 3 steps).

Conclusion

To summarize, an approach toward 4-azido-6,7-dimethoxy-2-alkyl/arylsulfonylquinazolines was developed employing a sulfonyl group dance caused by the azide–tetrazole equilibrium in quinazolines. 4-Azido-6,7-dimethoxy-2-alkyl/arylsulfonylquinazolines were obtained using two pathways: 1) S_NAr reaction between 2-chloro-6,7-dimethoxy-4-sulfonylquinazoline derivatives and NaN_3; 2) S_NAr reaction between 2,4-dichloro-6,7-dimethoxyquinazoline and alkyl/arylsulfinates, followed by substitution with NaN_3. 4-Azido-6,7-dimethoxy-2-alkyl/arylsulfonylquinazolines serve as valuable precursors for the C2-regioselective modification in quinazolines. Furthermore, the de-

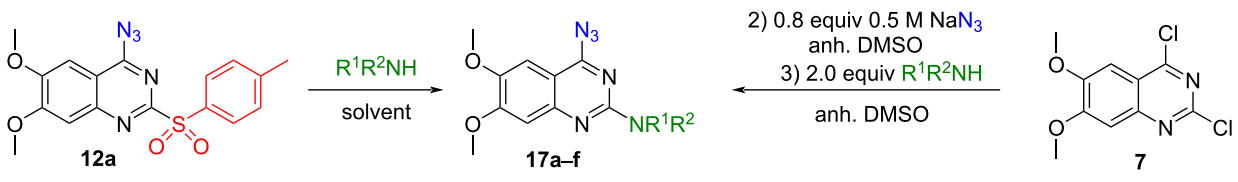

Scheme 9: Synthesis of 2-amino-4-azido-6,7-dimethoxyquinazolines **17**.

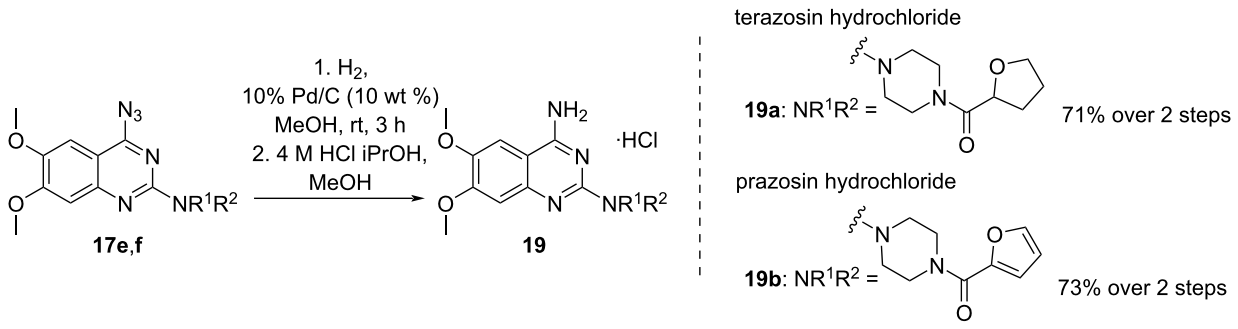

Scheme 10: Synthesis of terazosin and prazosin hydrochlorides **19a** and **19b**.

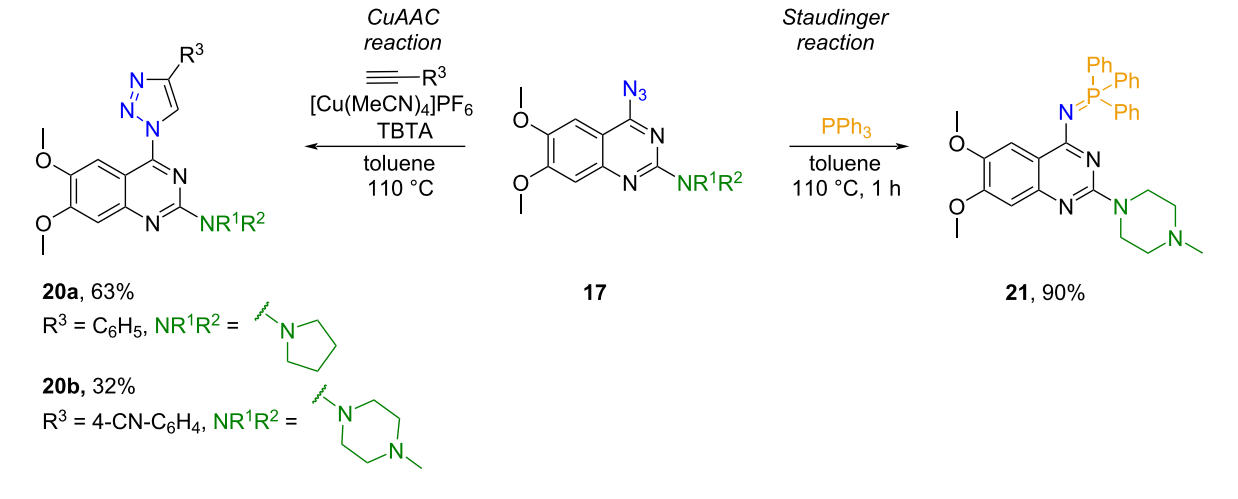

Scheme 11: Modifications of derivatives **17**.

veloped methodology was valorized by successfully employing it in the synthesis of adrenoblockers terazosin and prazosin.

Supporting Information

Supporting Information File 1

Experimental, copies of spectra and crystal data, data collection and structure refinement details for compound **12a**.
[https://www.beilstein-journals.org/bjoc/content/supplementary/1860-5397-20-61-S1.pdf]

Supporting Information File 2

Checkcif for compound **12a**.
[https://www.beilstein-journals.org/bjoc/content/supplementary/1860-5397-20-61-S2.pdf]

Supporting Information File 3

Crystallographic information file (CIF) for compound **12a**.
[https://www.beilstein-journals.org/bjoc/content/supplementary/1860-5397-20-61-S3.cif]

Acknowledgements

The authors thank Dr. chem. Kristīne Lazdoviča for IR analysis.

Funding

The authors thank the Latvian Council of Science Grant LZP-2020/1-0348 for financial support.

ORCID® iDs

Dāgs Dāvis Līpiņš - https://orcid.org/0009-0007-8216-0890
Anatoly Mishnev - https://orcid.org/0000-0001-9905-3257
Māris Turks - https://orcid.org/0000-0001-5227-0369
Irina Novosjolova - https://orcid.org/0000-0002-9607-2222

Data Availability Statement

All data that supports the findings of this study is available in the published article and/or the supporting information to this article.

References

1. Karan, R.; Agarwal, P.; Sinha, M.; Mahato, N. *ChemEngineering* **2021,** *5,* 73. doi:10.3390/chemengineering5040073
2. Gomaa, H. A. M. *Chem. Biol. Drug Des.* **2022,** *100,* 639–655. doi:10.1111/cbdd.14129
3. Minarini, A.; Bolognesi, M. L.; Tumiatti, V.; Melchiorre, C. *Expert Opin. Drug Discovery* **2006,** *1,* 395–407. doi:10.1517/17460441.1.5.395
4. Leonardi, A.; Motta, G.; Boi, C.; Testa, R. Quinazolinyl-amino derivatives having α-antagonist activity. WO Patent WO95/25726, Sept 28, 1995.
5. Li, B.; Wang, Z.; Su, S.-J.; Guo, F.; Cao, Y.; Zhang, Y. *Adv. Opt. Mater.* **2019,** *7,* 1801496. doi:10.1002/adom.201801496
6. Li, P.; Xiang, Y.; Gong, S.; Lee, W.-K.; Huang, Y.-H.; Wang, C.-Y.; Yang, C.; Wu, C.-C. *J. Mater. Chem. C* **2021,** *9,* 12633–12641. doi:10.1039/d1tc02633j
7. Li, B.; Li, Z.; Guo, F.; Song, J.; Jiang, X.; Wang, Y.; Gao, S.; Wang, J.; Pang, X.; Zhao, L.; Zhang, Y. *ACS Appl. Mater. Interfaces* **2020,** *12,* 14233–14243. doi:10.1021/acsami.9b20162
8. Khan, I.; Ibrar, A.; Ahmed, W.; Saeed, A. *Eur. J. Med. Chem.* **2015,** *90,* 124–169. doi:10.1016/j.ejmech.2014.10.084
9. Tamatam, R.; Kim, S.-H.; Shin, D. *Front. Chem. (Lausanne, Switz.)* **2023,** *11,* 1140562. doi:10.3389/fchem.2023.1140562
10. Shui, H.; Zhong, Y.; Ouyang, L.; Luo, N.; Luo, R. *Synthesis* **2022,** *54,* 2876–2884. doi:10.1055/a-1755-4700
11. Connolly, D. J.; Cusack, D.; O'Sullivan, T. P.; Guiry, P. J. *Tetrahedron* **2005,** *61,* 10153–10202. doi:10.1016/j.tet.2005.07.010
12. Gheidari, D.; Mehrdad, M.; Maleki, S. *Sustainable Chem. Pharm.* **2022,** *27,* 100696. doi:10.1016/j.scp.2022.100696
13. Tamatam, R.; Shin, D. *Molecules* **2023,** *28,* 3227. doi:10.3390/molecules28073227
14. Faisal, M.; Saeed, A. *Front. Chem. (Lausanne, Switz.)* **2021,** *8,* 594717. doi:10.3389/fchem.2020.594717
15. Chen, X.; Luo, X.; Wang, K.; Liang, F.; Wang, P. *Synlett* **2021,** *32,* 733–737. doi:10.1055/a-1294-0158
16. Xie, D.; Liu, Y.; Liu, X.; Yang, Q.; Peng, Y. *Eur. J. Org. Chem.* **2024,** *27,* e202300993. doi:10.1002/ejoc.202300993
17. Jeminejs, A.; Goliškina, S. M.; Novosjolova, I.; Stepanovs, D.; Bizdēna, Ē.; Turks, M. *Synthesis* **2021,** *53,* 1543–1556. doi:10.1055/s-0040-1706568
18. Jeminejs, A.; Novosjolova, I.; Bizdēna, Ē.; Turks, M. *Org. Biomol. Chem.* **2021,** *19,* 7706–7723. doi:10.1039/d1ob01315g
19. Zaķis, J. M.; Ozols, K.; Novosjolova, I.; Vilšķersts, R.; Mishnev, A.; Turks, M. *J. Org. Chem.* **2020,** *85,* 4753–4771. doi:10.1021/acs.joc.9b03518
20. Bottini, A.; De, S. K.; Wu, B.; Tang, C.; Varani, G.; Pellecchia, M. *Chem. Biol. Drug Des.* **2015,** *86,* 663–673. doi:10.1111/cbdd.12534
21. El Guesmi, N.; Berionni, G.; Asghar, B. H. *Monatsh. Chem.* **2013,** *144,* 1537–1545. doi:10.1007/s00706-013-1030-7
22. Marenich, A. V.; Cramer, C. J.; Truhlar, D. G. *J. Phys. Chem. B* **2009,** *113,* 6378–6396. doi:10.1021/jp810292n
23. Mizukawa, Y.; Ikegami-Kawai, M.; Horiuchi, M.; Kaiser, M.; Kojima, M.; Sakanoue, S.; Miyagi, S.; Nanga Chick, C.; Togashi, H.; Tsubuki, M.; Ihara, M.; Usuki, T.; Itoh, I. *Bioorg. Med. Chem.* **2021,** *33,* 116018. doi:10.1016/j.bmc.2021.116018
24. Nguyen, V. D.; Nguyen, V. T.; Haug, G. C.; Dang, H. T.; Arman, H. D.; Ermler, W. C.; Larionov, O. V. *ACS Catal.* **2019,** *9,* 4015–4024. doi:10.1021/acscatal.9b00464
25. Feng, J.; Zhang, Z.; Wallace, M. B.; Stafford, J. A.; Kaldor, S. W.; Kassel, D. B.; Navre, M.; Shi, L.; Skene, R. J.; Asakawa, T.; Takeuchi, K.; Xu, R.; Webb, D. R.; Gwaltney, S. L., II. *J. Med. Chem.* **2008,** *51,* 4357. doi:10.1021/jm8006799
26. Horn, A.; Kazmaier, U. *Eur. J. Org. Chem.* **2018,** 2531–2536. doi:10.1002/ejoc.201701645
27. Sebris, A.; Turks, M. *Chem. Heterocycl. Compd.* **2019,** *55,* 1041–1043. doi:10.1007/s10593-019-02574-7
28. Līpiņš, D. D.; Jeminejs, A.; Novosjolova, I.; Turks, M. The use of the sulfonyl group dance in quinazolines for the synthesis of 2-amino substituted 6,7-dimetoxyquinazolines. Latvian Patent LVP2023/000121, Nov 27, 2023.
29. Joshi, S. V.; Soni, M. N.; Fulwala, K. M.; Jalani, H. B.; Prajapati, K. K. Process for preparing anhydrous terazosin hydrochloride. Indian Patent 2004MU01090, April 27, 2007.
30. Schwartz, E.; Mendelovici, M.; Gershon, N. Process for the preparation of terazosin hydrochloride dihydrate. U.S. Patent US6248888B1, June 19, 2001.
31. Honkanen, E.; Pippuri, A.; Kairisalo, P.; Thaler, H.; Koivisto, M.; Tuomi, S. *J. Heterocycl. Chem.* **1980,** *17,* 797–798. doi:10.1002/jhet.5570170436
32. Petty, A.; Idippily, N.; Bobba, V.; Geldenhuys, W. J.; Zhong, B.; Su, B.; Wang, B. *Eur. J. Med. Chem.* **2018,** *143,* 1261–1276. doi:10.1016/j.ejmech.2017.10.026
33. Chan, T. R.; Hilgraf, R.; Sharpless, K. B.; Fokin, V. V. *Org. Lett.* **2004,** *6,* 2853–2855. doi:10.1021/ol0493094

License and Terms

BEILSTEIN JOURNAL OF ORGANIC CHEMISTRY

Enantioselective synthesis of β-aryl-γ-lactam derivatives via Heck–Matsuda desymmetrization of *N*-protected 2,5-dihydro-1*H*-pyrroles

Arnaldo G. de Oliveira Jr.‡, Martí F. Wang‡, Rafaela C. Carmona, Danilo M. Lustosa, Sergei A. Gorbatov and Carlos R. D. Correia*

Full Research Paper

Open Access

Address:
Department of Organic Chemistry, Chemistry Institute, University of Campinas, Rua Josué de Castro, 13083-970 Campinas, São Paulo, Brazil

Email:
Carlos R. D. Correia* - croque@unicamp.br

* Corresponding author ‡ Equal contributors

Keywords:
desymmetrization; enantioselective Heck–Matsuda reaction; lactam synthesis; *N,N*-ligands; palladium

Beilstein J. Org. Chem. **2024,** *20,* 940–949.
https://doi.org/10.3762/bjoc.20.84

Received: 27 December 2023
Accepted: 11 April 2024
Published: 29 April 2024

This article is part of the thematic issue "5th International Symposium on Synthesis and Catalysis (ISySyCat 2023)".

Guest Editor: A. Burke

Abstract

We report herein an enantioselective palladium-catalyzed Heck–Matsuda reaction for the desymmetrization of *N*-protected 2,5-dihydro-1*H*-pyrroles with aryldiazonium salts, using the chiral *N*,*N*-ligand (*S*)-PyraBox. This strategy has allowed straightforward access to a diversity of 4-aryl-γ-lactams via Heck arylation followed by a sequential Jones oxidation. The overall method displays a broad scope and good enantioselectivity, favoring the (*R*) enantiomer. The applicability of the protocol is highlighted by the efficient enantioselective syntheses of the selective phosphodiesterase-4-inhibitor rolipram and the commercial drug baclofen as hydrochloride.

Introduction

Desymmetrization reactions consist in the modification of a molecule with the loss of one or more symmetry elements, such as those which preclude chirality as in the transformation of a prochiral molecular entity into a chiral one [1]. It is a powerful and elegant strategy in asymmetric synthesis [2], which combined with the use of chiral ligands and transition-metal catalysts enabled many valuable transformations to increase molecular complexity in a synthetic route. The palladium-catalyzed coupling of arenediazonium salts with olefins, the Heck–Matsuda reaction, has been instrumental in this strategy involving the desymmetrization of cyclic systems [3], especially five-membered substrates [4-7]. As we have demonstrated previously, key five-membered olefins bearing heteroatoms can provide direct access to chiral sulfones, sulfoxides, phosphine oxides [8], phthalides, isochromanones, and lactones [9] in a very efficient and convenient manner. Despite

our previous results in this area, the desymmetrization of 2,5-dihydro-1*H*-pyrroles posed some challenges due to substrate instability and undesirable side reactions. In 2003, we reported the Heck–Matsuda arylation of *N*-protected 2,5-dihydro-1*H*-pyrroles [10] to obtain 4-aryl-γ-lactams in a racemic manner [11], thus demonstrating the feasibility of this transformation. The γ-lactam ring is a privileged scaffold widely present in drugs and natural products [12-14], as shown in Scheme 1.

Herein, we report the effective desymmetrization strategy of *N*-protected 2,5-dihydro-1*H*-pyrroles using aryldiazonium salts and the chiral *N*,*N*-ligand (*S*)-PyraBox (Scheme 2). The obtained Heck adducts (methyl *N*,*O*-acetals) were efficiently converted into several arylated γ-lactams by a simple oxidation procedure (Jones oxidation). To demonstrate the applicability of the strategy, two of the chiral aryl-lactams were further derivatized to provide the selective phosphodiesterase-4 inhibitor (*R*)-

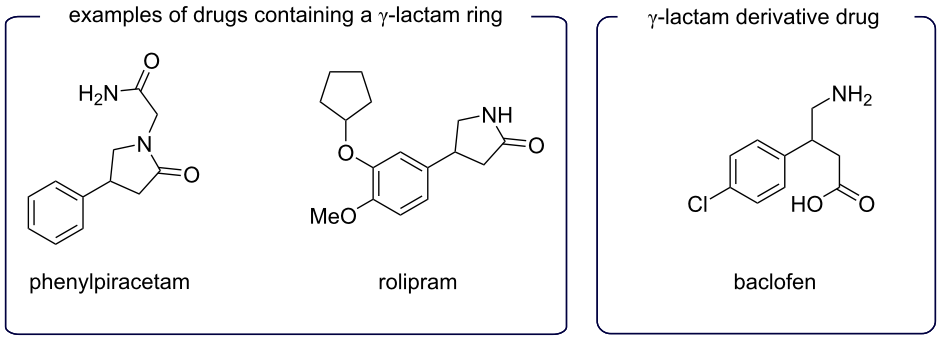

Scheme 1: Examples of drugs containing a γ-lactam and derivative.

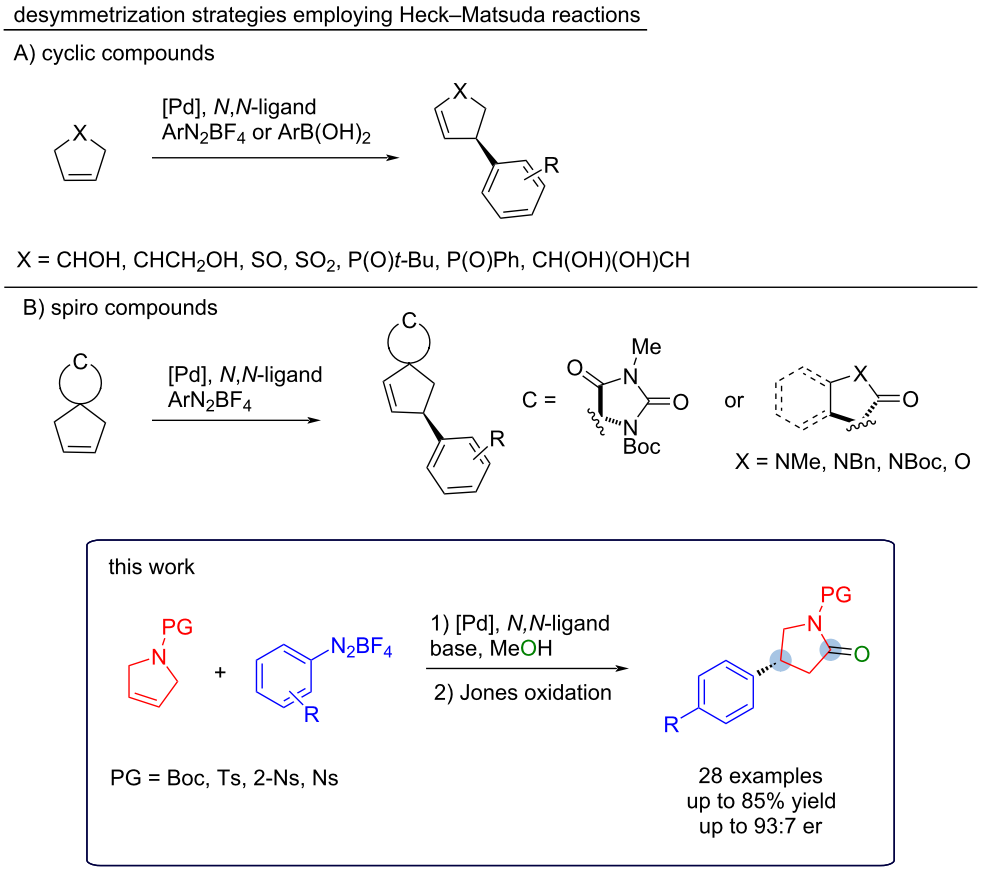

Scheme 2: Desymmetrization strategies employing Heck-Matsuda reactions.

rolipram (**5b**) [15], and the commercial drug (*R*)-baclofen hydrochloride (**6**), used to treat muscle spasticity from spinal cord injury and multiple sclerosis [16].

Results and Discussion

Desymmetrization of *N*-protected 2,5-dihydro-1*H*-pyrroles

Some initial results and reaction optimization

Based on our previous results regarding the desymmetrization of hidantoins [17], we started this study with the *N*-Boc-protected dihydropyrrole **1a** using different electronic-demanding aryldiazonium salts and the standard reaction conditions for similar Heck–Matsuda reactions (Scheme 3), i.e., $Pd(TFA)_2$ as the palladium source in combination with the pyrazinebisoxazoline ligand, (*S*)-PyraBox (**L1**), zinc carbonate as base, and methanol as solvent at 40 °C.

These initial conditions furnished 2-methoxypyrrolidines arylated at the 4-position, compound **3**, as Heck products as illustrated in Scheme 3. The presence of a methoxy group after the Heck–Matsuda reaction indicates methanolysis after arylation. Given the importance of the lactam rings, we envisioned a sequential Jones oxidation protocol without isolation of the methyl *N*,*O*-acetal products to obtain the corresponding lactams **4**. As observed in previous works [18], the oxidation step is practical and high-yielding, and the overall yield can be reported based on the isolated lactams.

By evaluating the electronics of the diazonium salt, we observed that the electron-donating *p*-OMe substituent performed better (**4aa**, 68% yield) when compared to neutral (**4ab**, 34% yield) and electron-withdrawing (**4ac**, 27% yield) ones, but no significant changes in the enantiomeric ratio were observed (Scheme 3).

Despite the formation of the hemiaminal ether as the major product, the formation of a minor *N*-Boc pyrrole was also observed as a side-product. To circumvent this side reaction, we envisioned that a more electron-withdrawing protecting group could reduce the tendency of the starting olefin to oxidation. Therefore, the *N*-tosylated 2,5-dihydro-1*H*-pyrrole **1b** was evaluated under the same reaction conditions with the same three aryldiazonium salts used before. Before exploring the reactivity of the olefin towards other aryldiazonium salts, we performed a brief optimization of the process by testing several other *N*,*N*-ligands. Therefore, five other *N*,*N*-ligands were evaluated as follows: PyraBox (**L2**), QuinOx (**L3**), PyOx **L4** and **L5**, and PyriBOx (**L6**) (Figure 1).

However, neither one of these new ligands performed better than **L1** (see Table 1 below). In an attempt to enhance the protocol performance, we also evaluated the palladium source as indicated in Table 1. Switching $Pd(TFA)_2$ by $Pd(OAc)_2$ led to a minor increase in the yield, but without any changes in the er. $Pd(acac)_2$ and $Pd(MeCN)_2(OTs)_2$ were also tested without significant improvements.

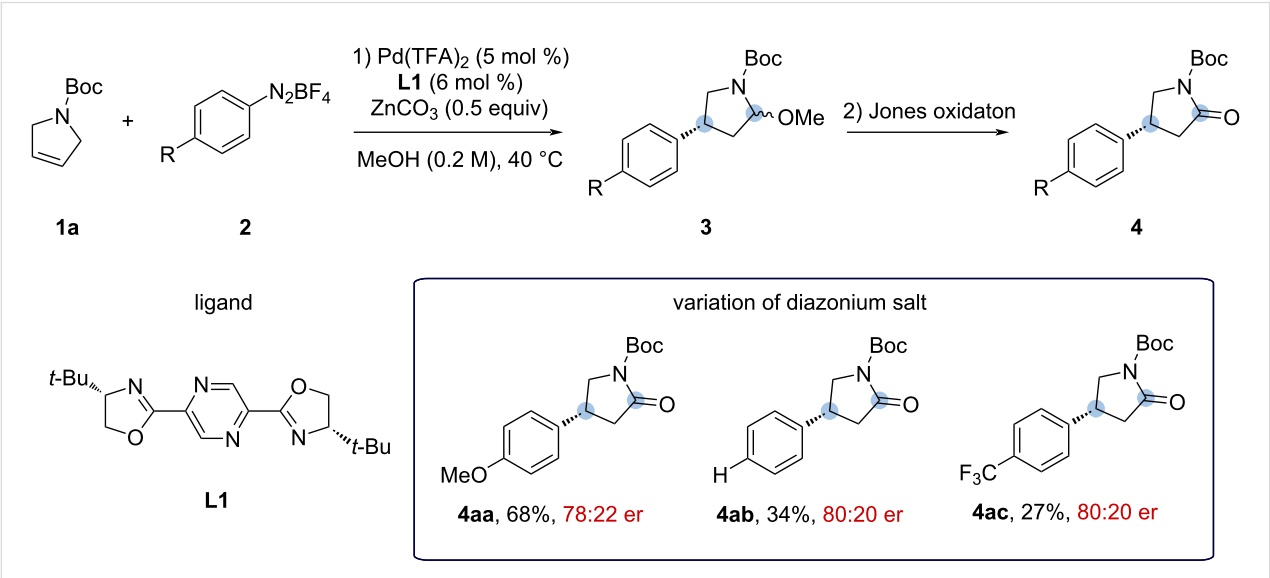

Scheme 3: Heck–Matsuda reaction (1) and Jones oxidation (2) of the *N*-Boc-protected 2,5-dihydro-1*H*-pyrrole **1a**. Reaction conditions: 1) pyrroline **1a** (0.30 mmol, 1.0 equiv), aryldiazonium salt **2** (0.60 mmol, 2.0 equiv), $Pd(TFA)_2$ (5 mol %), **L1** (*S*)-PyraBox (6 mol %), $ZnCO_3$ (0.15 mmol, 0.5 equiv), and MeOH (1.5 mL, 0.2 M) at 40 °C, 4 h; 2) 1.0 mL of the Jones solution 2.5 M, 6 mL of acetone/water 3:1 (v/v), 1.5 h. Isolated yields were calculated from an average of two runs. Enantiomeric ratios (er) were determined by high-performance liquid chromatography (HPLC) analysis of the purified compounds.

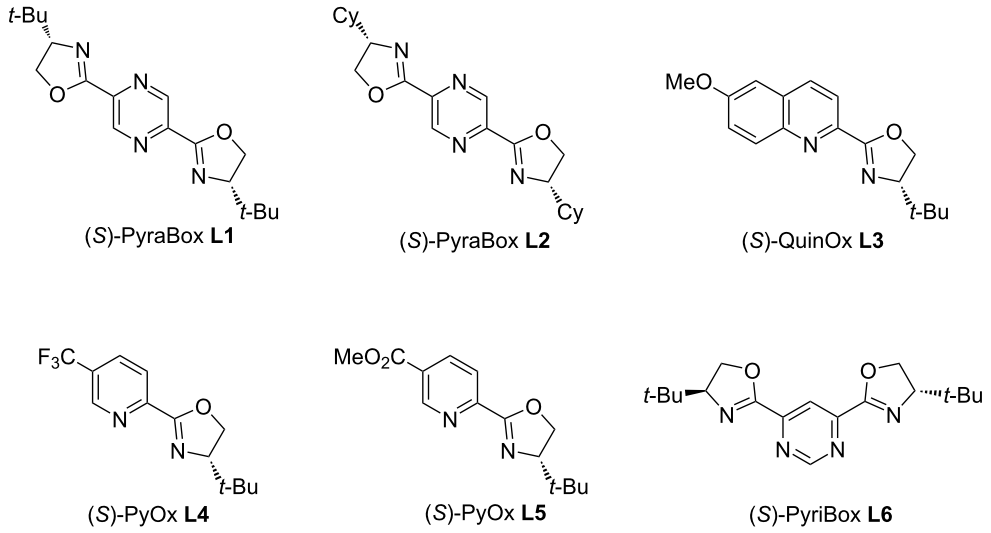

Figure 1: *N*,*N*-Ligands evaluated in this work.

Table 1: Optimization of the reaction conditions with tosyl-protected pyrroline **1b**.[a]

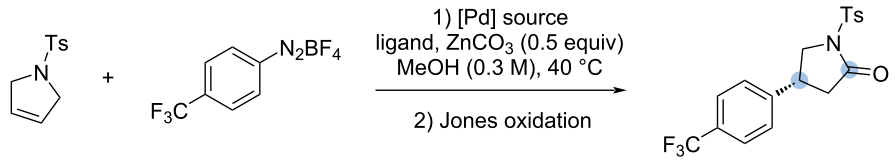

1b **2c** **4bc**

Entry	Ligand	[Pd] source	**4bc** %[b]	er[c]
1	**L1**[d]	**$Pd(TFA)_2$**	**62**	**85:15**
2	L2[d]	$Pd(TFA)_2$	56	57:43
3	L3[e]	$Pd(TFA)_2$	49	56:44
4	L4[e]	$Pd(TFA)_2$	57	77:23
5	L5[e]	$Pd(TFA)_2$	54	72:28
6	L6[d]	$Pd(TFA)_2$	51	69:31
7	L1[d]	$Pd(OAc)_2$	65	85:15
8	L1[d]	Pd_2dba_3	64	84:16
9	L1[d]	$Pd(acac)_2$	68	84:16
10	L1[d]	$Pd(MeCN)_2(OTs)_2$	62	83:17

[a]Reaction conditions: pyrroline **1b** (0.30 mmol, 1.0 equiv), 4-(trifluoromethyl)benzenediazonium tetrafluoroborate (**2c**, 0.60 mmol, 2.0 equiv), $Pd(TFA)_2$ (5 mol %), ligand, $ZnCO_3$ (0.15 mmol, 0.5 equiv), MeOH (1.0 mL, 0.3 M), 40 °C, 4 h. Jones conditions: 1.0 mL Jones solution 2.5 M, 6 mL of acetone/water 3:1 (v/v), 1.5 h. [b]NMR yields. [c]Determined by HPLC analysis. [d]Ligand: 6 mol %. [e]Ligand: 11 mol %.

Despite the fact that palladium acetate slightly better performed as shown in Table 1, we decided to continue with palladium trifluoroacetate due to its higher reactivity in forming palladium complexes with *N*,*N*-ligands. Therefore, we decided to maintain our initial conditions using $Pd(TFA)_2$ and proceeded to the evaluation of the scope of the Heck–Matsuda arylation as shown in Scheme 4. Gratifyingly, the new reaction conditions with the tosylpyrroline **1b** showed significant improvements in yield and enantioselectivities (**4ba** and **4bc** in Scheme 4). Somewhat surprisingly, no enhancement in the enantiomeric ratio was observed for the lactam **4bb**.

With the optimized conditions in hand, we evaluated the scope of the method by varying the aryldiazonium salts. For aryldia-

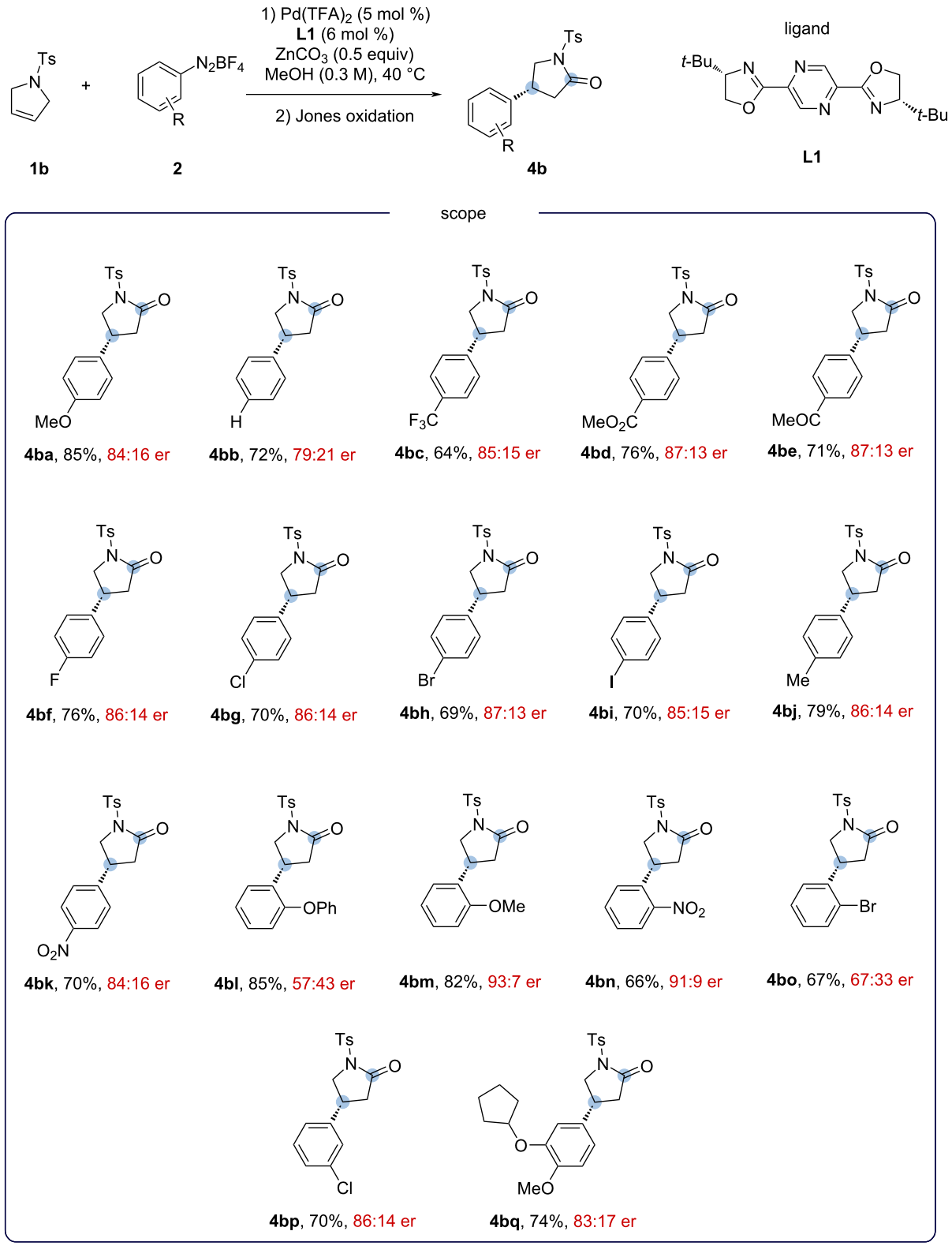

Scheme 4: Heck–Matsuda reaction of *N*-tosyl-2,5-dihydro-1*H*-pyrrole (**1b**). Reaction conditions: 1) pyrroline **1b** (0.30 mmol, 1.0 equiv), aryldiazonium salts **2** (0.60 mmol, 2.0 equiv), $Pd(TFA)_2$ (5 mol %), **L1** (6 mol %), $ZnCO_3$ (0.15 mmol, 0.5 equiv), MeOH (1.0 mL, 0.3 M), 40 °C, 4 h. 2) 1.0 mL Jones solution 2.5 M, 6 mL of acetone/water 3:1 (v/v), 1.5 h. Isolated yields were calculated from an average of two runs. Enantiomeric ratio (er) determined by high-performance liquid chromatography (HPLC) analysis of the purified compounds.

zonium salts bearing *p*-substituted groups, there is very little influence in the enantiomeric ratios, although electron-donating groups performed slightly better in terms of yield, as observed before for the *N*-Boc-protected pyrrolines. Weak electron-donating groups such as the methyl group furnished compound **4bj** in a higher yield and good er. Carbonyl-containing electron-withdrawing groups such as methyl ester and ketone did not show much of an effect in the outcome of the reaction, providing compounds **4bd** and **4be** in high yields and good er. On the other hand, product **4bq** was obtained in a higher yield but with a lower er. The *p*-halogen-containing derivatives **4bf**, **4bg**, **4bh**, and **4bi** were all obtained in high yields and good er. We also evaluated the change of some substituents to the *ortho* position. This change furnished compound **4bm** in higher yield and excellent er. However, when the bulkiness of the substituent was increased, as in compounds **4bl** and **4bo** (*o*-phenoxy and *o*-bromo group, respectively), the er dropped considerably. Finally, a strong electron-withdrawing group in the *ortho* position such as nitro (**4bn**) was met with a decrease in yield (66%), but with a higher er.

During the development of the scope, the hemiaminal ethers (Heck–Matsuda products) were found to be somehow unstable when concentrated to dryness during work-up. We hypothesize that a possible cause of such instability might consist in the formation of a highly electrophilic iminium ion upon protonation of the hemiaminal ether by silica or glassware acidity and further elimination of methanol favored by the evaporation process. The instability of hemiaminal ethers was previously described in literature [19] during work-up. We then found that careful control of the drying conditions, thus avoiding complete drying of the crude mixture prevents degradation of the Heck products. We then established a robust protocol consisting of successive additions of acetone to the crude mixture, followed by careful rotaevaporation. This procedure gradually removes most of the methanol, allowing the sequential Jones oxidation step to take place without any significant losses (see Supporting Information File 1 for details).

Given the presence of the 4-aryl-γ-lactam motif in the phosphodiesterase-4 inhibitor rolipram, and in a synthetic intermediate for the baclofen drug, the Heck products **4bg** and **4bq** were used as starting material for their syntheses. *N*-Tosylated lactams **4bg** and **4bq** were then submitted to deprotection protocols as described in the literature [20,21]. However, the removal of the tosyl group of pyrroline **1b** proved to be a challenging task. After several unsuccessful attempts to remove the tosyl group, we decided to evaluate the (*p*-nitrophenyl)sulfonyl (Ns) and (*o*-nitrophenyl)sulfonyl (2-Ns) as alternative protecting groups of 2,5-dihydro-1*H*-pyrrole (Scheme 5). Although the results with the 2-Ns protecting group were somewhat disappointing, the results with 4-Ns group were more promising, even with a welcome increase in the enantiomeric ratio in some cases (**4dd** and **4de**).

Synthesis of (*R*)-baclofen hydrochloride (**6**) from **4dd** and (*R*)-rolipram (**5b**) from **4de**

To further demonstrate the applicability of this method, the aryl-lactams **4dd** and **4de** were successfully converted into the selective phosphodiesterase-4 inhibitor (*R*)-rolipram (**5b**) [15], and the commercial drug (*R*)-baclofen for the treatment of muscle spasticity from spinal cord injury and multiple sclerosis [16]. Among all the sulfonyl-protecting groups used in this work, the removal of the *N*-nosyl group required milder conditions [22]. Deprotection of *N*-nosylated **4dd** and **4de** with thiophenol and K_2CO_3 at room temperature gave the NH-unprotected γ-lactam **5a** and the drug (*R*)-rolipram **5b** in 79% and 97% yields, respectively, with excellent enantioselectivity. Hydrolysis of γ-lactam **5a** in 6 N HCl aqueous solution at 100 °C for 10 hours then led to the formation of (*R*)-baclofen hydrochloride (**6**) in 76% yield (Scheme 6). The total yields were determined to be 49% for (*R*)-baclofen hydrochloride (**6**) and 61% (*R*)-rolipram (**5b**) from starting pyrrolidine **1d**.

Determination of the absolute stereochemistry of the Heck adducts/lactams and rationalization of the enantioselectivity

The absolute stereochemistry of the products was determined by the correlation of their optical rotations with that of the previously reported aryl-lactam **4bb** [23], and its deprotected analog [24], as well as with the intermediates **5b**, **5a**, and **6** in the (*R*)-rolipram (**5b**) and (*R*)-baclofen hydrochloride (**6**) [25] syntheses. Assignment of the stereochemistry of all other lactams as *R* was done by analogy. The assignment of the absolute stereochemistry allowed us to propose a rationale for the Heck–Matsuda reaction (Scheme 7). Upon activation of the catalyst (**I**), oxidative addition of aryldiazonium salt and subsequent nitrogen release generates the cationic palladium(II)–*N,N*-ligand complex (**II**), to which the pyrrolidine substrate coordinates (**III**). Next, migratory insertion takes place generating the alkylpalladium species (**IV**), which upon a sequence of β-elimination (**V**) and hydride insertion leads to alkylpalladium intermediate (**VI**). Finally, upon methanolysis, the hemiaminal ether product **3** is formed. We hypothesize that the enantioselectivity-determining step consists of the migratory insertion of the aryl group bonded to palladium to the pyrroline. The steric effect of the *t*-Bu group favors the coordination of the pyrroline with the protecting group upward, therefore creating an asymmetric center with absolute configuration (*R*), in accordance with experimental results. A rationalization for the transition state that would lead to the observed outcome is depicted in Figure 2.

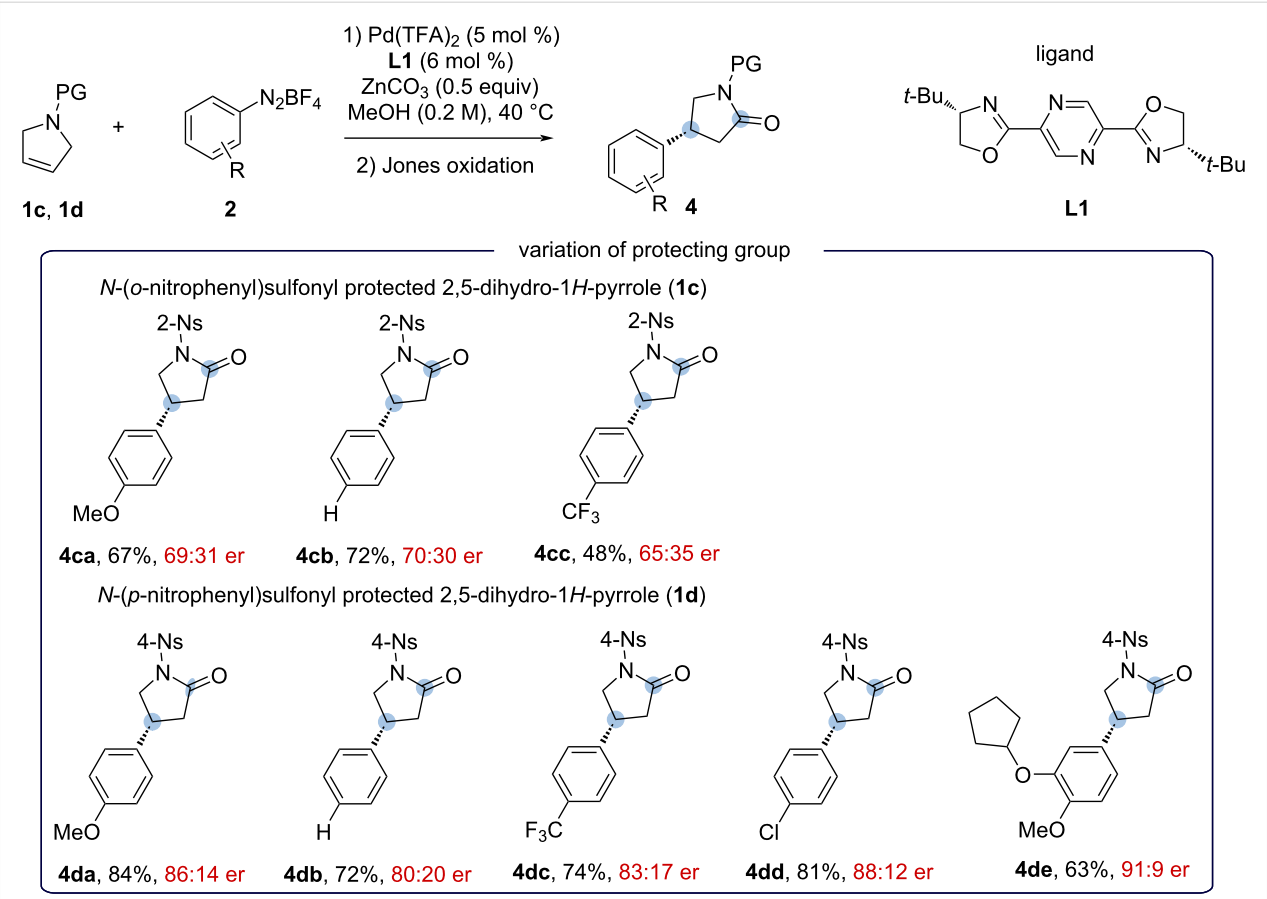

Scheme 5: Heck–Matsuda reaction of the protected 2,5-dihydro-1*H*-pyrrole with Ns and 2-Ns groups (pyrrolines **1c**, **1d**). Reaction conditions: 1) pyrroline **1c** or **1d** (0.30 mmol, 1.0 equiv), aryldiazonium salts **2** (0.60 mmol, 2.0 equiv), $Pd(TFA)_2$ (5 mol %), **L1** (6 mol %), $ZnCO_3$ (0.15 mmol, 0.5 equiv), MeOH (1.5 mL, 0.2 M), 40 °C, 4 h. 2) 1.0 mL Jones solution 2.5 M, 6 mL of acetone/water 3:1 (v/v), 1.5 h. Isolated yields were calculated from an average of two runs. Enantiomeric ratio (er) determined by high-performance liquid chromatography (HPLC) analysis of the purified compounds.

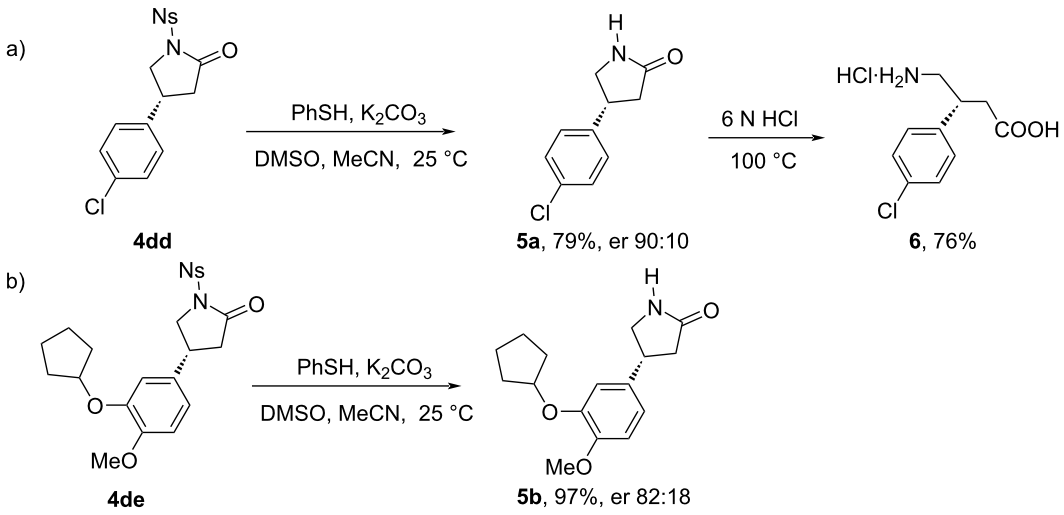

Scheme 6: Synthesis of (*R*)-baclofen hydrochloride (**6**) from **4dd** and (*R*)-rolipram (**5b**) from **4de**. Reaction conditions: a) **4dd** (0.20 mmol, 1.0 equiv), PhSH (0.30 mmol, 1.5 equiv), K_2CO_3 (0.40 mmol, 2 equiv), MeCN (2 mL), DMSO (0.75 mL), 25 °C, 2 h, then 6 N HCl (0.5 mL), 100 °C, 10 h. Reaction conditions: b) **4de** (0.105 mmol, 1.0 equiv), PhSH (0.16 mmol, 1.5 equiv), K_2CO_3 (0.21 mmol, 2 equiv), MeCN (1 mL), DMSO (0.4 mL), 25 °C, 2 h. Enantiomeric ratio (er) determined by high-performance liquid chromatography (HPLC) analysis of the purified compounds.

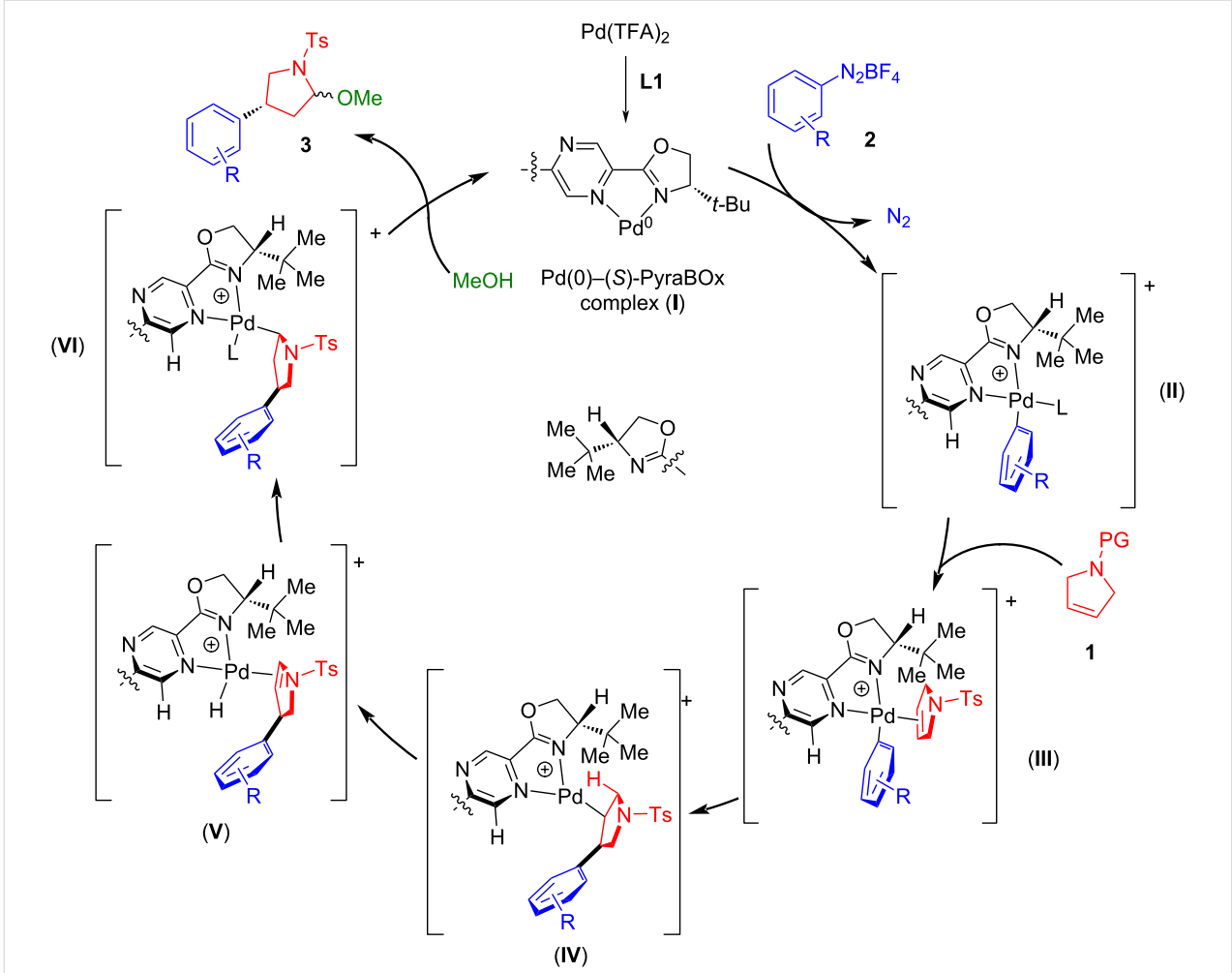

Scheme 7: A rationale for the catalytic cycle for the Heck–Matsuda reaction of the protected 2,5-dihydro-1*H*-pyrroles with aryldiazonium salts catalyzed by a (*S*)-PyraBox–palladium complex.

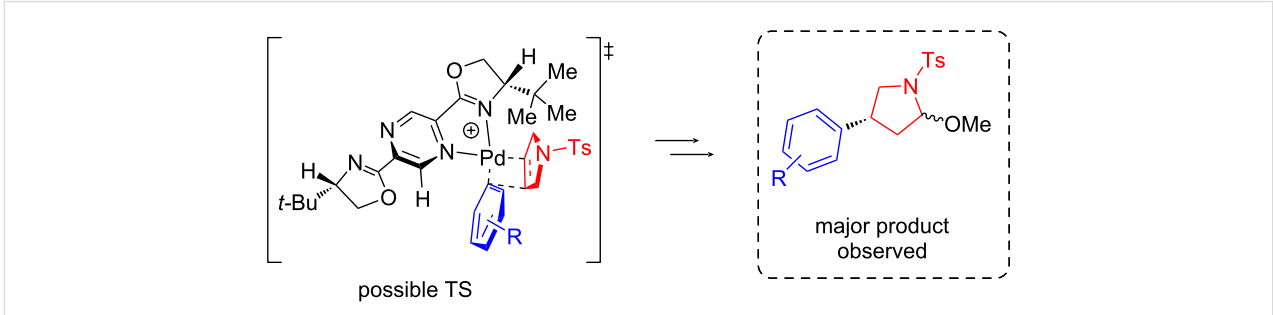

Figure 2: Rationalization of the enantioselectivity obtained in the Heck–Matsuda reaction of protected 2,5-dihydro-1*H*-pyrrole with aryldiazonium salts catalyzed by the (*S*)-PyraBox–palladium complex.

Conclusion

The palladium-catalyzed Heck–Matsuda desymmetrization of *N*-protected 2,5-dihydro-1*H*-pyrroles with aryldiazonium salts was successfully accomplished. The synthetic protocol employed the *N*,*N*-ligand (*S*)-PyraBox to provide several 4-substituted γ-lactams in an enantioselective fashion, with broad scope and good enantioselectivities, with yields up to 85% and er up to 93:7. The methodology was shown to be robust, allowing the use of different protecting groups at the nitrogen of the 4-pyrroline substrate. We also report straightforward synthetic routes to

obtain (*R*)-rolipram (**5b**, 61% overall yield, 3 steps, 82:18 er) and (*R*)-baclofen hydrochloride (**6**, 49% overall yield, 4 steps, 90:10 er) using the Heck–Matsuda reaction as a key step for constructing the stereogenic center.

Supporting Information

Supporting Information File 1

Experimental procedures and characterization data for the new compounds.
[https://www.beilstein-journals.org/bjoc/content/supplementary/1860-5397-20-84-S1.pdf]

Acknowledgements

We acknowledge the Ph.D. student Otto Daolio Köster for the fruitful discussions and assistance with the experimental work, and Mr. Anderson S. Pedrosa for technical assistance with NMR analysis.

Funding

We thank the financial support of the São Paulo Research Foundation (FAPESP, grants: 2017/21494-2 [MFW]; 2023/00025-5 [SAG]; 2014/25770-6, 2013/07600-3, 2014/25770-6 [CRDC], and 2018/00271-8 [RCC]) and the Brazilian National Research Council (CNPq, grants 406643/2018-0, 306773/2018-0 [CRDC]).

Author Contributions

Arnaldo G. de Oliveira Jr.: investigation; validation; writing – original draft. Martí F. Wang: investigation; validation. Rafaela C. Carmona: investigation; validation. Danilo M. Lustosa: investigation. Sergei A. Gorbatov: investigation; writing – original draft. Carlos R. D. Correia: conceptualization; funding acquisition; methodology; project administration; resources; supervision; writing – original draft; writing – review & editing.

ORCID® iDs

Arnaldo G. de Oliveira Jr. - https://orcid.org/0000-0002-2158-1110
Sergei A. Gorbatov - https://orcid.org/0000-0002-8077-3913
Carlos R. D. Correia - https://orcid.org/0000-0001-5564-6675

Data Availability Statement

All data that supports the findings of this study is available in the published article and/or the supporting information to this article.

Preprint

A non-peer-reviewed version of this article has been previously published as a preprint: https://doi.org/10.3762/bxiv.2023.66.v1

References

1. Kotani, S.; Nakajima, M. C–X Bond Formation: Organocatalytic Enantioselective Halogenation of Meso Epoxides. *Comprehensive Chirality;* Elsevier: Amsterdam, Netherlands, 2012; Vol. 6, pp 506–517. doi:10.1016/b978-0-08-095167-6.00624-8
2. Nájera, C.; Foubelo, F.; Sansano, J. M.; Yus, M. *Tetrahedron* **2022,** *106–107,* 132629. doi:10.1016/j.tet.2022.132629
3. Angnes, R. A.; Thompson, L. M.; Mashuta, M. S.; Correia, C. R. D.; Hammond, G. B. *Adv. Synth. Catal.* **2018,** *360,* 3760–3767. doi:10.1002/adsc.201800785
4. de Oliveira, V. C.; Angnes, R. A.; Batista, J. M., Jr.; Correia, C. R. D. *Eur. J. Org. Chem.* **2023,** *26,* e202300550. doi:10.1002/ejoc.202300550
5. de Oliveira Silva, J.; Angnes, R. A.; Menezes da Silva, V. H.; Servilha, B. M.; Adeel, M.; Braga, A. A. C.; Aponick, A.; Correia, C. R. D. *J. Org. Chem.* **2016,** *81,* 2010–2018. doi:10.1021/acs.joc.5b02846
6. de Oliveira, J. M.; Angnes, R. A.; Khan, I. U.; Polo, E. C.; Heerdt, G.; Servilha, B. M.; Menezes da Silva, V. H.; Braga, A. A. C.; Correia, C. R. D. *Chem. – Eur. J.* **2018,** *24,* 11738–11747. doi:10.1002/chem.201801910
7. Angnes, R. A.; Oliveira, J. M.; Oliveira, C. C.; Martins, N. C.; Correia, C. R. D. *Chem. – Eur. J.* **2014,** *20,* 13117–13121. doi:10.1002/chem.201404159
8. de Azambuja, F.; Carmona, R. C.; Chorro, T. H. D.; Heerdt, G.; Correia, C. R. D. *Chem. – Eur. J.* **2016,** *22,* 11205–11209. doi:10.1002/chem.201602572
9. Kattela, S.; de Lucca, E. C., Jr.; Correia, C. R. D. *Chem. – Eur. J.* **2018,** *24,* 17691–17696. doi:10.1002/chem.201804958
10. Montes De Oca, A. C. B.; Correia, C. R. D. *ARKIVOC* **2003,** No. x, 390–403. doi:10.3998/ark.5550190.0004.a37
11. Garcia, A. L. L.; Carpes, M. J. S.; de Oca, A. C. B. M.; dos Santos, M. A. G.; Santana, C. C.; Correia, C. R. D. *J. Org. Chem.* **2005,** *70,* 1050–1053. doi:10.1021/jo0484880
12. Caruano, J.; Muccioli, G. G.; Robiette, R. *Org. Biomol. Chem.* **2016,** *14,* 10134–10156. doi:10.1039/c6ob01349j
13. Rivas, F.; Ling, T. *Org. Prep. Proced. Int.* **2016,** *48,* 254–295. doi:10.1080/00304948.2016.1165059
14. Spencer, J. *ChemMedChem* **2016,** *11,* 1107. doi:10.1002/cmdc.201600133
15. Krause, W.; Kühne, G.; Sauerbrey, N. *Eur. J. Clin. Pharmacol.* **1990,** *38,* 71–75. doi:10.1007/bf00314807
16. Draulans, N.; Vermeersch, K.; Degraeuwe, B.; Meurrens, T.; Peers, K.; Nuttin, B.; Kiekens, C. *Clin. Rehabil.* **2013,** *27,* 1137–1143. doi:10.1177/0269215513488607
17. de Oliveira, V. C.; de Oliveira, J. M.; Menezes da Silva, V. H.; Khan, I. U.; Correia, C. R. D. *Adv. Synth. Catal.* **2020,** *362,* 3395–3406. doi:10.1002/adsc.202000443
18. Oliveira, C. C.; Pfaltz, A.; Correia, C. R. D. *Angew. Chem., Int. Ed.* **2015,** *54,* 14036–14039. doi:10.1002/anie.201507927
19. Ciou, J.-M.; Zhu, H.-F.; Chang, C.-W.; Chen, J.-Y.; Lin, Y.-F. *RSC Adv.* **2020,** *10,* 40421–40427. doi:10.1039/d0ra08527h
20. Nagashima, H.; Ozaki, N.; Washiyama, M.; Itoh, K. *Tetrahedron Lett.* **1985,** *26,* 657–660. doi:10.1016/s0040-4039(00)89172-8
21. Shu, C.; Liu, M.-Q.; Wang, S.-S.; Li, L.; Ye, L.-W. *J. Org. Chem.* **2013,** *78,* 3292–3299. doi:10.1021/jo400127x
22. Hajra, S.; Bhosale, S. S.; Hazra, A.; Kanaujia, N. *Org. Biomol. Chem.* **2019,** *17,* 8140–8148. doi:10.1039/c9ob01570a

23. Ghorai, M. K.; Tiwari, D. P. *J. Org. Chem.* **2010,** *75,* 6173–6181. doi:10.1021/jo101004x
24. Nakamura, S.; Tokunaga, A.; Saito, H.; Kondo, M. *Chem. Commun.* **2019,** *55,* 5391–5394. doi:10.1039/c9cc02443c
25. Thakur, V. V.; Nikalje, M. D.; Sudalai, A. *Tetrahedron: Asymmetry* **2003,** *14,* 581–586. doi:10.1016/s0957-4166(03)00024-7

License and Terms

BEILSTEIN JOURNAL OF ORGANIC CHEMISTRY

Novel analogues of a nonnucleoside SARS-CoV-2 RdRp inhibitor as potential antivirotics

Luca Julianna Tóth[1,2], Kateřina Krejčová[2], Milan Dejmek[2], Eva Žilecká[2], Blanka Klepetářová[2], Lenka Poštová Slavětínská[2], Evžen Bouřa[2] and Radim Nencka[*2]

Full Research Paper

Open Access

Address:
[1]Department of Organic Chemistry, Faculty of Science, Charles University, Hlavova 2030/8, 128 43 Prague, Czech Republic and [2]Institute of Organic Chemistry and Biochemistry of the Czech Academy of Sciences, Flemingovo náměstí 542/2, 166 10 Prague, Czech Republic

Email:
Radim Nencka[*] - radim.nencka@uochb.cas.cz

* Corresponding author

Keywords:
antivirotics; nonnucleotide inhibitor; RNA-dependent RNA polymerase; SARS-CoV-2

Beilstein J. Org. Chem. **2024,** *20,* 1029–1036.
https://doi.org/10.3762/bjoc.20.91

Received: 14 January 2024
Accepted: 09 April 2024
Published: 06 May 2024

This article is part of the thematic issue "5th International Symposium on Synthesis and Catalysis (ISySyCat 2023)".

Guest Editor: A. Burke

Abstract

The RNA-dependent RNA polymerase (RdRp) represents a prominent target in the discovery and development of new antivirotics against RNA viruses, inhibiting the replication process. One of the most targeted RNA viruses of the last years is, without doubt, SARS-CoV-2, the cause of the recent COVID-19 pandemic. HeE1-2Tyr, a known inhibitor of flaviviral RdRp, has been discovered to also have antiviral potency against this coronavirus. In this study, we report three distinct modifications of HeE1-2Tyr: conversion of the core from a benzothiazole to a benzoxazole moiety and two different scaffold simplifications, respectively. We provide a novel synthetic approach and, in addition, evaluate the final molecules in an in vitro polymerase assay for biological activity.

Introduction

Epidemics caused by various viral infections, such as AIDS, Zika fever, Dengue fever, or Ebola, are a constant threat to communities of all sizes [1]. The COVID-19 pandemic, caused by the newly emerged severe acute respiratory syndrome coronavirus type 2 (SARS-CoV-2), has put an enormous pressure on the healthcare system worldwide and called for immediate action in prevention and treatment, which in turn required the discovery of new effective therapeutic options. It seems to be clear that the widespread use of vaccines is able to stop the acute phase of the pandemic. However, antiviral therapy for COVID-19 is indispensable in case of vaccine failure, virus mutation or suppressed immunity of some patients [2].

SARS-CoV-2 is part of the *Coronaviridae* family, a group of enveloped +ssRNA viruses. The genome can directly act as a viral messenger RNA and encodes essential enzymes for repli-

cation [3]. Inhibiting these nonstructural proteins that are part of the replication complex has already shown great success in antiviral therapy [4-7].

The viral RNA-dependent RNA polymerase (RdRp) is encoded in all RNA viruses and plays a crucial role in viral RNA replication. In the proteome of SARS-CoV-2, the catalytic subunit nsp12, expressed together with the cofactors nsp7 and nsp8, constitutes the RdRp [8]. RdRp is usually targeted by nucleotide analogue inhibitors (NAIs) [9]. This class of antivirals can inhibit the replication by acting as a delayed chain terminator or by causing genetic corruption in the viral RNA and includes the first FDA-approved antiviral drugs in the therapy of COVID-19 patients, remdesivir [10] and molnupiravir [11]. The usability of NAIs may largely depend on the metabolic activation, and they also compete with the intracellular pool of natural nucleoside triphosphates (NTPs). Nonnucleotide analogue inhibitors (NNAIs) do not face these challenges as they bind to both active but also allosteric sites of the RdRp, and therefore they represent a promising NAI alternative [12].

Since the beginning of the pandemic, a variety of heterocyclic small molecules – either of natural or synthetic origin – was reported as promising inhibitors of the SARS-CoV-2 RdRp [13-15]. However, compounds with a sufficient combination of high potency and suitable pharmacokinetic properties are still scarce. Recently, many studies have been focusing on drug repurposing or screening libraries of already approved biologically active compounds [16,17]. This approach might represent a very promising strategy in the case of targeting the coronaviral RdRp due to the highly conserved structure of the polymerase, not only across the CoV group but also in other RNA viruses [13]. A great example of this phenomenon is remdesivir, which was originally developed as a therapeutic agent against Ebola virus [18,19].

HeE1-2Tyr (**1**) was originally identified by Tarantino et al. [20] as a potent inhibitor of RdRp from all members of the genus *Orthoflavivirus* [20-23] and was crystallized in complex with the RdRp from DENV-3 [20]. In 2021, our group reported this compound to also exhibit inhibitory activity against feline infectious peritonitis virus (FIPV) and SARS-CoV-2 RdRp and to hinder viral replication in cell-based antiviral assays [24]. That study highlighted the beneficial role of the tyrosine residue and the indispensable role of the C-2 substitution.

In this work, we report the synthesis and biological evaluation of further analogues of HeE1-2Tyr (**1**) against the SARS-CoV-2 RdRp. We focused on the modification of the central heterocyclic core and on the simplification and truncation of the relatively large molecule **1** (Figure 1).

In this work, replacing the sulfur atom with a (bio)isosteric oxygen atom yielded two novel structural analogues, whilst our effort towards more simple molecules led to a series of pyridone derivatives. Out of these, **3a** had already been synthesized by a different approach [22]. However, this study presents a novel and notably simpler synthetic route. Furthermore, as part of the systematic truncation of the core, we synthesized thiazolopyridone and thiadiazolopyridone derivatives because molecules based on these cores have already shown promising antimicrobial activities [25,26].

Results and Discussion

Synthesis of HeE1-2Tyr (**1**) structural analogues

Modification of the core: synthesis of pyridobenzoxazole derivatives

The synthesis of the pyridobenzoxazole derivative **2** was designed based on the modified approach published by Dejmek et al. (Scheme 1) [24].

In this work, we first synthesized the intermediate **6** from readily available 2′,5′-dihydroxyacetophenone (**5**) following a published procedure [27]. This compound was then easily converted to the suitably decorated benzoxazole derivative **12a**. The benzoxazole core showed increased sensitivity towards a basic environment, resulting in the ring-opened side product **13** through saponification of the ester function of compound **12a**. The identification of this side product proved to be challenging due to insufficient evidence provided even by meticulous NMR analysis and eventually had to be confirmed by X-ray crystallography (Figure S1, Supporting Information File 1). Changing the ester function from an ethyl to an allyl group enabled a very mild cleavage using a Pd-mediated reaction with triethylsilane [28], and thus avoiding the use of base, leading to the desired intermediate **14** in good yield. Compound **14** was then coupled with L-tyrosine methyl ester followed by deprotection of the amino acid carboxyl group by $LiOH{\cdot}H_2O$. As in the previous base-mediated saponification, here we also received a product of the benzoxazole ring-opening reaction, namely **16**.

Simplification of the hit molecule: synthesis of pyridone derivatives

We decided to simplify the relatively large structure of HeE1-2Tyr (**1**) in order to obtain smaller, more accessible inhibitors with similar or better properties. The employed novel synthetic strategy leading to pyridones bearing different aryl substituents is described in Scheme 2. During the Suzuki–Miyaura cross-coupling reaction, which introduced the substituents in the C-5 position, the methyl ester protection of

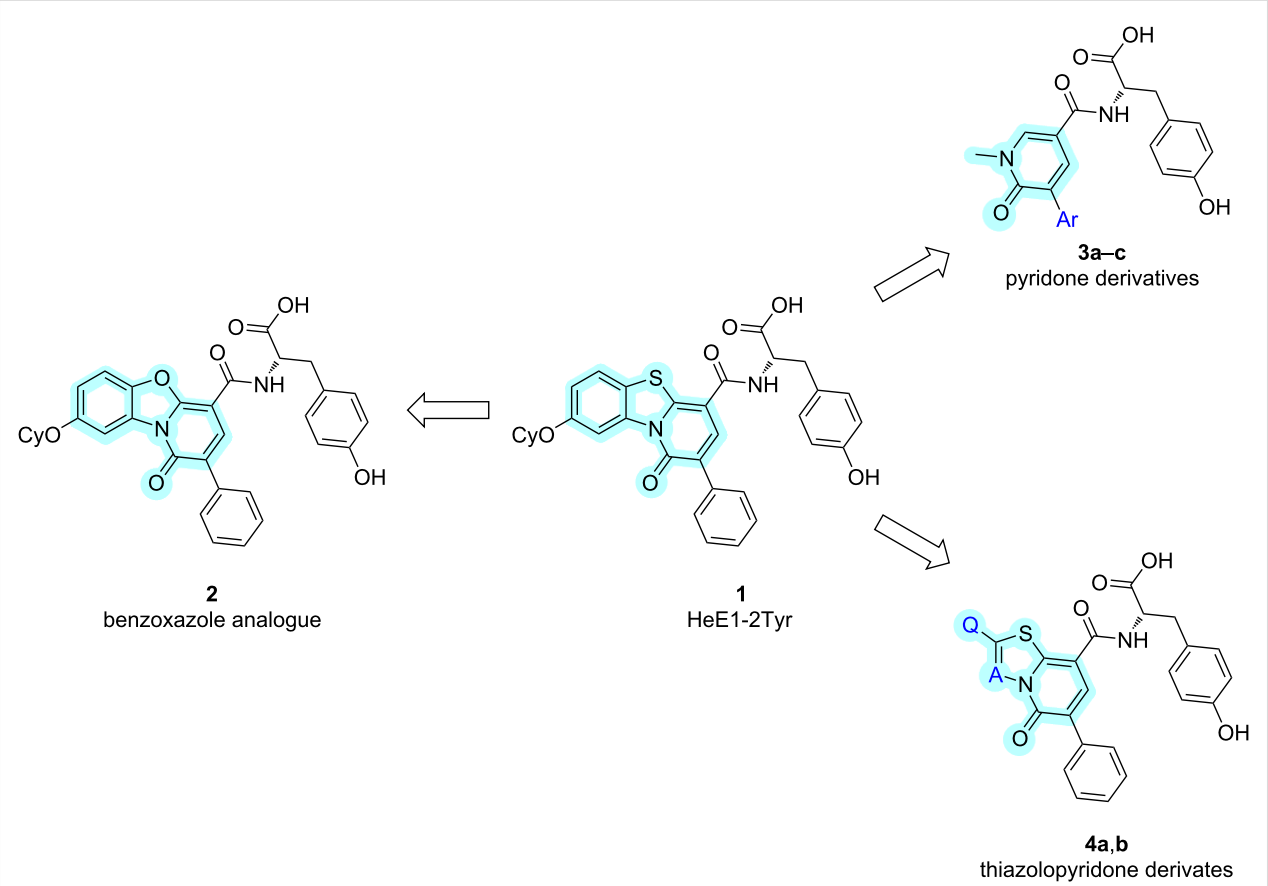

Figure 1: Structure of HeE1-2Tyr (**1**) and of the derivatives synthesized in this work.

the amino acid moiety was also cleaved, leading directly to the final compounds **3a** (first reported by Cannalire et al. [22]) and **3b**,**c**.

Simplification of the hit molecule: synthesis of thiazolopyridone derivatives

Further, a novel type of inhibitor containing a thiazolopyridone core and the corresponding azo derivative, namely **4a**,**b**, were synthesized. The synthetic route was designed based on the work reported by Potts et al. [29] and is described in Scheme 3. The 2-bromo-2-phenylacetyl chloride, necessary for the first step of the synthesis, was prepared from readily available phenylacetic acid [30,31]. The reaction with the 5-membered heterocycles **21** and **26**, respectively, led to two crucial mesoionic compounds, **22** and **27**. The recrystallized intermediates then underwent a formal cycloaddition with ethyl acrylate, followed by the elimination of H_2S, forming the desired heterocyclic core structures (intermediates **23** and **28**, respectively). A subsequent saponification step led to the corresponding carboxylic acids **24** and **29**, and from there, the desired final compounds **4a**,**b** were obtained in a straightforward two-step synthesis.

Biochemical study: inhibition of SARS-CoV-2 RdRp

We aimed to determine the inhibitory activity of the final compounds **2**, **16**, **3a–c** and **4a**,**b** against SARS-CoV-2 RdRp. The RdRp was prepared recombinantly, and the inhibitory activity was measured using a primer extension polymerase assay. This assay was also used to determine the IC_{50} values (Figure 2 and Figure S2, Supporting Information File 1). The benzoxazole analogue **2** was devoid of any activity, while the ring-opened derivative **16** showed inhibition with IC_{50} = 114.2 µM. It seemed that the significantly smaller size of the oxygen atom in the benzoxazole derivative compared to sulfur in HeE1-2Tyr (**1**) led to an unfavorable molecular shape, while the analogue with the open ring was able to compensate this difference. The pyridone derivatives **3a–c** exerted an activity resulting in IC_{50} values of 128.7 µM, 203.8 µM and 88.1 µM, respectively, highlighting that even significantly truncated molecules are capable of RdRp inhibition. A thiophene substituent in position 5 (i.e., **3c**) proved to be the most successful modification. The potential of the truncated derivatives was further illustrated by the thiazolopyridone and thiadiazolopyridone compounds **4a**,**b**, which showed inhibition with IC_{50} = 88.1 µM and 128.7 µM, respectively.

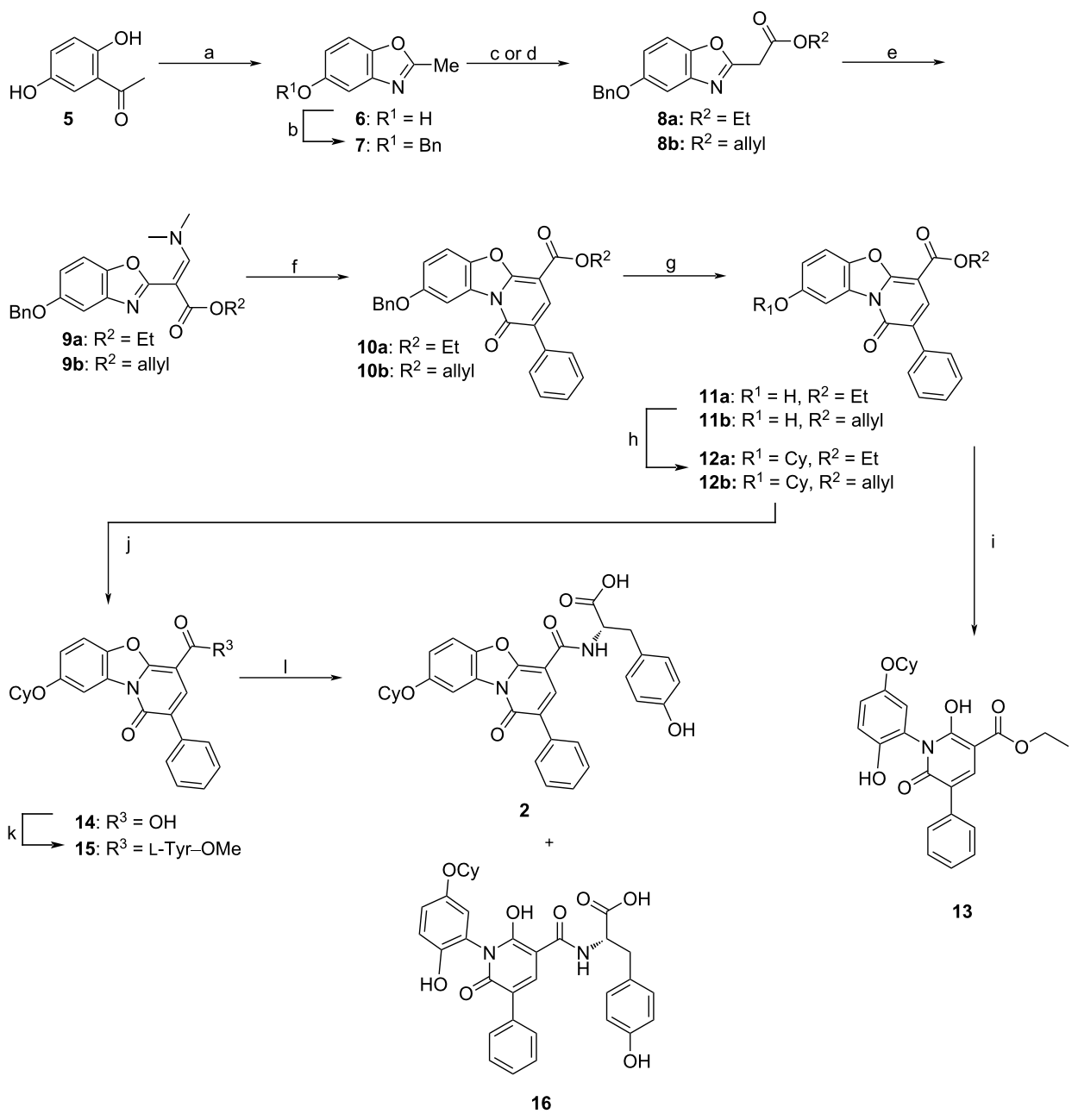

Scheme 1: Synthetic pathway to benzoxazole analogue **2** of HeE1-2Tyr (**1**). Reagents and conditions: a) $TMSN_3$, TfOH, DCM, rt, overnight, b) BnBr, NaH, DMF, 0 °C to rt, 1 h, c) (R = Et) diethyl carbonate, LiHMDS, THF, –78 to 0 °C, 1 h, d) (R = allyl) allyl chloroformate, LiHMDS, THF, –78 to 0 °C, 1 h, e) $POCl_3$, DMF, 90 °C, 30 min, f) $(BnCO)_2O$, 100 °C, 1.5 h, g) methanesulfonic acid, DCM, 0 °C to rt, 4 h, h) CyOH, PPh_3, DIAD, 1,4-dioxane, 50 °C, overnight, i) (R = Et) NaOH, H_2O, EtOH, 75 °C, 3 h, j) (R = allyl) Et_3SiH, PPh_3, $Pd(OAc)_2$, ACN, rt, k) H–L-Tyr–OMe, HOBt, EDCI, TEA, DCM, DMF, rt, 12 h, l) $LiOH{\cdot}H_2O$, H_2O, 1,4-dioxane, rt, 45 min. Cy = cyclohexyl.

Even though the measured inhibitory concentration was higher than that of HeE1-2Tyr (**1**), it must be considered that the synthesized ligands were significantly smaller in size. Normalization of the obtained results using the binding efficiency index (BEI) [32] suggest that both ligand types, **3a**–**c** and **4a**,**b**, bind more efficiently to the SARS-CoV-2 RdRp when compared to **1**.

Conclusion

In this study, novel analogues of the antiviral HeE1-2Tyr (**1**) were synthesized and evaluated with respect to the in vitro inhibitory activity towards SARS-CoV-2 RdRp. To obtain the benzoxazole analogue, a new synthetic strategy avoiding base-mediated hydrolysis was successfully applied. For the simplified structural derivatives, the applied routes were optimized for

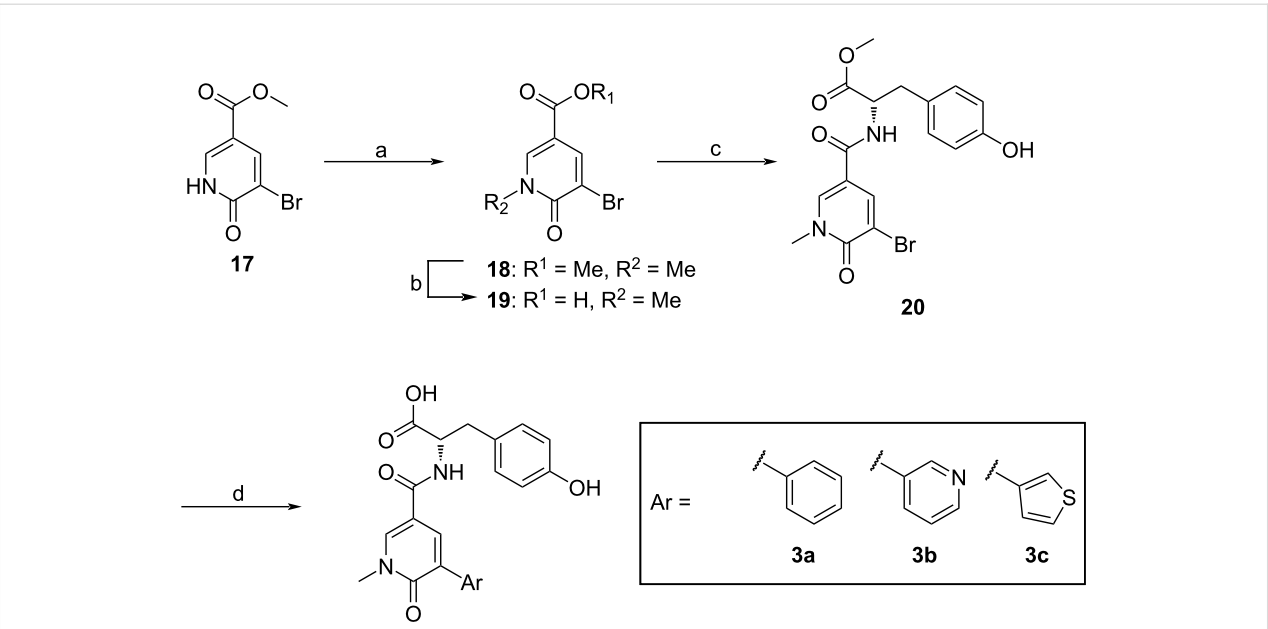

Scheme 2: Synthetic pathway to pyridone derivatives **3a–c** of HeE1-2Tyr (**1**). Reagents and conditions: a) MeI, K_2CO_3, DMF, rt, 2.5 h, b) LiOH·H_2O, H_2O, 1,4-dioxane, rt, 15 min, c) H–L-Tyr–OMe, HOBt, EDCI, TEA, DCM, DMF, rt, 12 h, d) $ArB(OH)_2$, Pd(dppf)Cl_2.CH_2Cl_2, Cs_2CO_3, DMF, H_2O, 80 °C, overnight.

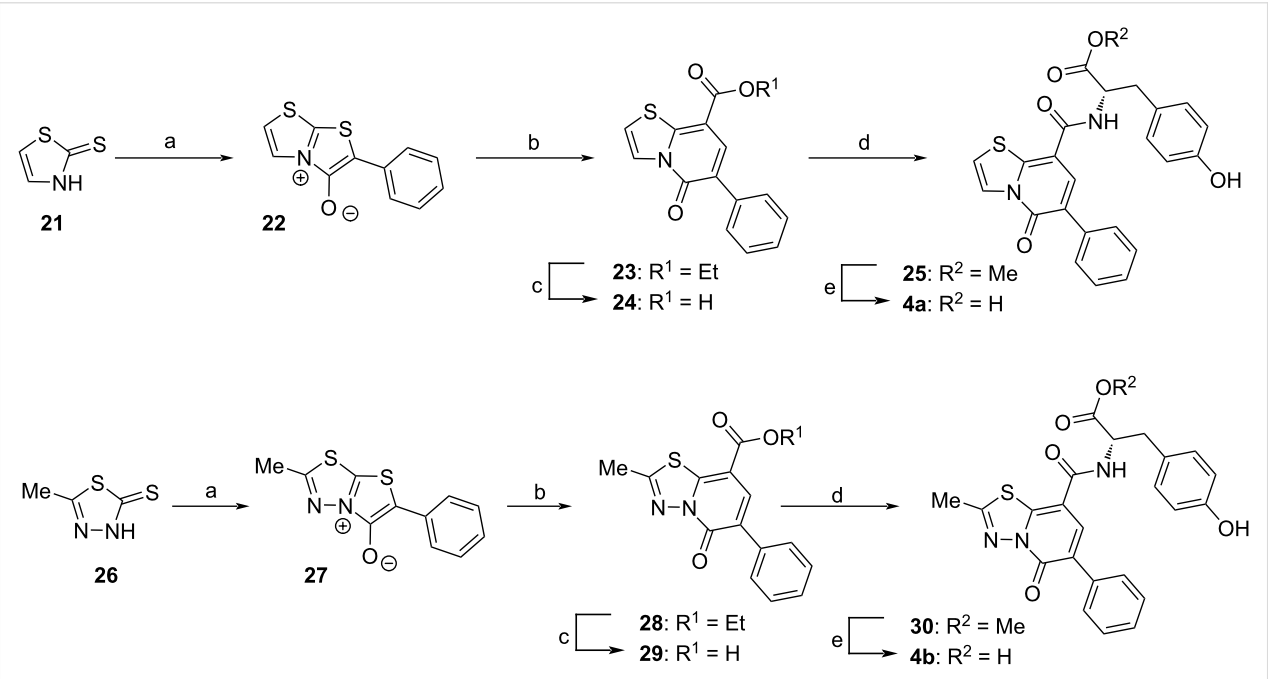

Scheme 3: Synthetic pathway to thiazolopyridone derivatives **4a**,**b** of HeE1-2Tyr (**1**). Reagents and conditions: a) 2-bromo-2-phenylacetyl chloride, TEA, THF, rt, 1 h, b) ethyl acrylate, toluene, 110 °C, 24 h, c) NaOH, H_2O, MeOH, 70 °C, 2 h, d) H–L-Tyr–OMe, HOBt, EDCI, TEA, DCM, DMF, rt, 12 h, e) LiOH·H_2O, H_2O, 1,4-dioxane, rt, 2 h.

maximal efficacy of the synthetic work. Regarding the inhibitory activity, six of the novel compounds showed inhibition in the fluorescence-based primer extension assay. The two simplified molecules were the most promising inhibitors, with an IC_{50} value below 90 µM, and the compounds **3a–c** and **4a**,**b** exerted stronger BEIs than **1**. The obtained results provide important information about the structural requirements for the heterocyclic inhibitors based on HeE1-2Tyr (**1**), which

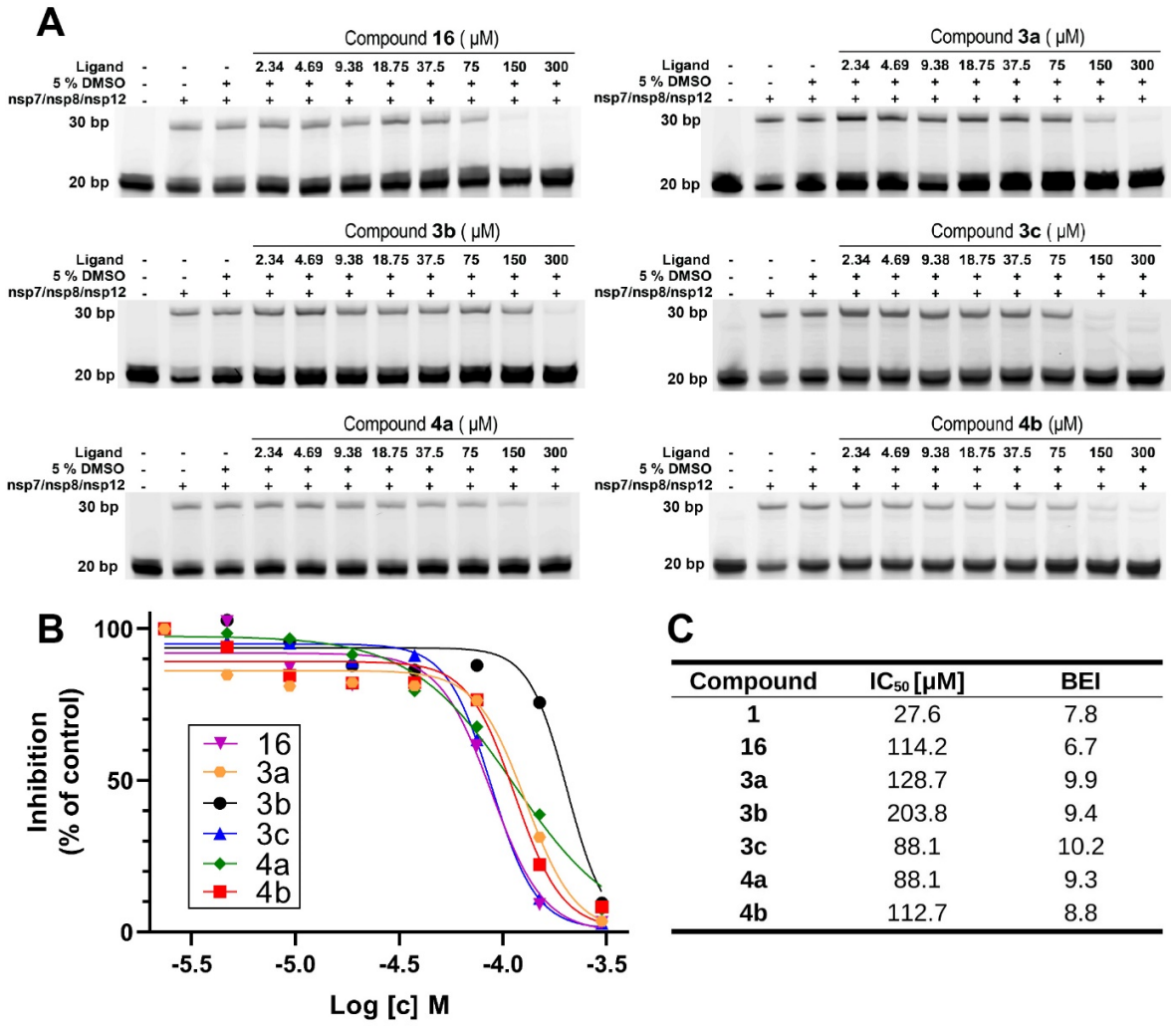

Compound	IC_{50} [µM]	BEI
1	27.6	7.8
16	114.2	6.7
3a	128.7	9.9
3b	203.8	9.4
3c	88.1	10.2
4a	88.1	9.3
4b	112.7	8.8

Figure 2: Analysis of inhibitory activity against SARS-CoV-2 RdRp using primer extension assay. A) Gel-based polymerase assay with a constant concentration of fluorescently labeled template/primer RNA (0.5 µM) and the polymerase complex (nsp7, nsp8 3 µM and nsp12 1 µM), along with increasing concentrations of compounds as indicated at the top. Reactions were initiated by adding 10 µM NTPs and run for 1 h at 30 °C. The reactions were stopped by adding stop buffer, and the products were separated on a 20% denaturing gel. B) Graphical representation of the inhibitory activity of selected compounds evaluated from the gels obtained in the primer extension assay. The percentage of inhibition (against control) was plotted against the logarithm of the concentration of compounds. The results were fitted to sigmoidal dose–response curves. C) The IC_{50} values were determined using the GraphPad algorithm (IC_{50} value of compound **1** was published by Dejmek et al. [24]), the BEI was calculated using the function pIC_{50} [mol/L]/MW [kDa].

we will use in the design of further generations of such antivirals.

Supporting Information

Supporting Information File 1

Experimental procedures, spectra and X-ray data.
[https://www.beilstein-journals.org/bjoc/content/supplementary/1860-5397-20-91-S1.pdf]

Acknowledgements

We thank Lucie Bednárová from the Institute of Organic Chemistry and Biochemistry of the Czech Academy of Sciences for the help with the analysis of compound **13**.

Funding

The work was supported by the National Institute of Virology and Bacteriology (Program EXCELES, ID Project No. LX22NPO5103) and funded by the European Union NextGenerationEU scheme and the Czech Academy of Sciences (RVO: 61388963).

ORCID® iDs

Luca Julianna Tóth - https://orcid.org/0009-0008-7709-8268
Kateřina Krejčová - https://orcid.org/0000-0002-7503-7954
Milan Dejmek - https://orcid.org/0000-0002-8195-971X
Eva Žilecká - https://orcid.org/0000-0003-0285-3843
Evžen Bouřa - https://orcid.org/0000-0002-9652-4065
Radim Nencka - https://orcid.org/0000-0001-6167-0380

Data Availability Statement

The data that supports the findings of this study is available from the corresponding author upon reasonable request.

References

1. Bekheit, M. S.; Panda, S. S.; Girgis, A. S. *Eur. J. Med. Chem.* **2023,** *252,* 115292. doi:10.1016/j.ejmech.2023.115292
2. Shiraki, K.; Sato, N.; Sakai, K.; Matsumoto, S.; Kaszynski, R. H.; Takemoto, M. *Pharmacol. Ther.* **2022,** *235,* 108121. doi:10.1016/j.pharmthera.2022.108121
3. Sorouri, F.; Emamgholipour, Z.; Keykhaee, M.; Najafi, A.; Firoozpour, L.; Sabzevari, O.; Sharifzadeh, M.; Foroumadi, A.; Khoobi, M. *Mini-Rev. Med. Chem.* **2022,** *22,* 273–311. doi:10.2174/1389557521666210308144302
4. Shiraki, K.; Daikoku, T. *Pharmacol. Ther.* **2020,** *209,* 107512. doi:10.1016/j.pharmthera.2020.107512
5. Keating, G. M. *Drugs* **2014,** *74,* 1127–1146. doi:10.1007/s40265-014-0247-z
6. Izquierdo, L.; Helle, F.; Francois, C.; Castelain, S.; Duverlie, G.; Brochot, E. *Pharmacogenomics Res. Pers. Med.* **2014,** *7,* 241–249. doi:10.2147/pgpm.s52715
7. Hessel, M. H. M.; Cohen, A. F.; Rissmann, R. *Br. J. Clin. Pharmacol.* **2016,** *82,* 878–879. doi:10.1111/bcp.13011
8. Hillen, H. S.; Kokic, G.; Farnung, L.; Dienemann, C.; Tegunov, D.; Cramer, P. *Nature* **2020,** *584,* 154–156. doi:10.1038/s41586-020-2368-8
9. Astasio-Picado, Á.; Zabala-Baños, M. d. C.; Jurado-Palomo, J. *Appl. Sci.* **2023,** *13,* 4471. doi:10.3390/app13074471
10. Kokic, G.; Hillen, H. S.; Tegunov, D.; Dienemann, C.; Seitz, F.; Schmitzova, J.; Farnung, L.; Siewert, A.; Höbartner, C.; Cramer, P. *Nat. Commun.* **2021,** *12,* 279. doi:10.1038/s41467-020-20542-0
11. Kabinger, F.; Stiller, C.; Schmitzová, J.; Dienemann, C.; Kokic, G.; Hillen, H. S.; Höbartner, C.; Cramer, P. *Nat. Struct. Mol. Biol.* **2021,** *28,* 740–746. doi:10.1038/s41594-021-00651-0
12. Jamal, Q. M. S. *Int. J. Mol. Sci.* **2022,** *23,* 13564. doi:10.3390/ijms232113564
13. Gao, S.; Song, L.; Xu, H.; Fikatas, A.; Oeyen, M.; De Jonghe, S.; Zhao, F.; Jing, L.; Jochmans, D.; Vangeel, L.; Cheng, Y.; Kang, D.; Neyts, J.; Herdewijn, P.; Schols, D.; Zhan, P.; Liu, X. *Molecules* **2022,** *28,* 160. doi:10.3390/molecules28010160
14. Brindani, N.; Munafò, F.; Menichetti, A.; Donati, E.; Nigro, M.; Ottonello, G.; Armirotti, A.; De Vivo, M. *Bioorg. Med. Chem.* **2023,** *80,* 117179. doi:10.1016/j.bmc.2023.117179
15. Miropolskaya, N.; Kozlov, M.; Petushkov, I.; Prostova, M.; Pupov, D.; Esyunina, D.; Kochetkov, S.; Kulbachinskiy, A. *Biochimie* **2023,** *206,* 81–88. doi:10.1016/j.biochi.2022.10.007
16. Jade, D.; Alzahrani, A.; Critchley, W.; Ponnambalam, S.; Harrison, M. A. *Struct. Chem.* **2023,** *34,* 1005–1019. doi:10.1007/s11224-022-02072-1
17. Shahabadi, N.; Zendehcheshm, S.; Mahdavi, M.; Khademi, F. *Inform. Med. Unlocked* **2023,** *36,* 101147. doi:10.1016/j.imu.2022.101147
18. Wang, J.; Reiss, K.; Shi, Y.; Lolis, E.; Lisi, G. P.; Batista, V. S. *Biochemistry* **2021,** *60,* 1869–1875. doi:10.1021/acs.biochem.1c00292
19. Warren, T. K.; Jordan, R.; Lo, M. K.; Ray, A. S.; Mackman, R. L.; Soloveva, V.; Siegel, D.; Perron, M.; Bannister, R.; Hui, H. C.; Larson, N.; Strickley, R.; Wells, J.; Stuthman, K. S.; Van Tongeren, S. A.; Garza, N. L.; Donnelly, G.; Shurtleff, A. C.; Retterer, C. J.; Gharaibeh, D.; Zamani, R.; Kenny, T.; Eaton, B. P.; Grimes, E.; Welch, L. S.; Gomba, L.; Wilhelmsen, C. L.; Nichols, D. K.; Nuss, J. E.; Nagle, E. R.; Kugelman, J. R.; Palacios, G.; Doerffler, E.; Neville, S.; Carra, E.; Clarke, M. O.; Zhang, L.; Lew, W.; Ross, B.; Wang, Q.; Chun, K.; Wolfe, L.; Babusis, D.; Park, Y.; Stray, K. M.; Trancheva, I.; Feng, J. Y.; Barauskas, O.; Xu, Y.; Wong, P.; Braun, M. R.; Flint, M.; McMullan, L. K.; Chen, S.-S.; Fearns, R.; Swaminathan, S.; Mayers, D. L.; Spiropoulou, C. F.; Lee, W. A.; Nichol, S. T.; Cihlar, T.; Bavari, S. *Nature* **2016,** *531,* 381–385. doi:10.1038/nature17180
20. Tarantino, D.; Cannalire, R.; Mastrangelo, E.; Croci, R.; Querat, G.; Barreca, M. L.; Bolognesi, M.; Manfroni, G.; Cecchetti, V.; Milani, M. *Antiviral Res.* **2016,** *134,* 226–235. doi:10.1016/j.antiviral.2016.09.007
21. Cannalire, R.; Tarantino, D.; Piorkowski, G.; Carletti, T.; Massari, S.; Felicetti, T.; Barreca, M. L.; Sabatini, S.; Tabarrini, O.; Marcello, A.; Milani, M.; Cecchetti, V.; Mastrangelo, E.; Manfroni, G.; Querat, G. *Antiviral Res.* **2019,** *167,* 6–12. doi:10.1016/j.antiviral.2019.03.004
22. Cannalire, R.; Ki Chan, K. W.; Burali, M. S.; Gwee, C. P.; Wang, S.; Astolfi, A.; Massari, S.; Sabatini, S.; Tabarrini, O.; Mastrangelo, E.; Barreca, M. L.; Cecchetti, V.; Vasudevan, S. G.; Manfroni, G. *ACS Med. Chem. Lett.* **2020,** *11,* 773–782. doi:10.1021/acsmedchemlett.9b00619
23. Felicetti, T.; Burali, M. S.; Gwee, C. P.; Ki Chan, K. W.; Alonso, S.; Massari, S.; Sabatini, S.; Tabarrini, O.; Barreca, M. L.; Cecchetti, V.; Vasudevan, S. G.; Manfroni, G. *Eur. J. Med. Chem.* **2021,** *210,* 112992. doi:10.1016/j.ejmech.2020.112992
24. Dejmek, M.; Konkoľová, E.; Eyer, L.; Straková, P.; Svoboda, P.; Šála, M.; Krejčová, K.; Růžek, D.; Boura, E.; Nencka, R. *Viruses* **2021,** *13,* 1585. doi:10.3390/v13081585
25. Wardakhan, W. W.; El-Sayed, N. N. E. *Phosphorus, Sulfur Silicon Relat. Elem.* **2009,** *184,* 790–804. doi:10.1080/10426500802274534
26. Targowska-Duda, K. M.; Maj, M.; Drączkowski, P.; Budzyńska, B.; Boguszewska-Czubara, A.; Wróbel, T. M.; Laitinen, T.; Kaczmar, P.; Poso, A.; Kaczor, A. A. *ChemMedChem* **2022,** *17,* e202100721. doi:10.1002/cmdc.202100721
27. Nimnual, P.; Tummatorn, J.; Thongsornkleeb, C.; Ruchirawat, S. *J. Org. Chem.* **2015,** *80,* 8657–8667. doi:10.1021/acs.joc.5b01305
28. Goldberg, J. A.; Nguyen, H.; Kumar, V.; Spencer, E. J.; Hoyer, D.; Marshall, E. K.; Cmolik, A.; O'Shea, M.; Marshall, S. H.; Hujer, A. M.; Hujer, K. M.; Rudin, S. D.; Domitrovic, T. N.; Bethel, C. R.; Papp-Wallace, K. M.; Logan, L. K.; Perez, F.; Jacobs, M. R.; van Duin, D.; Kreiswirth, B. M.; Bonomo, R. A.; Plummer, M. S.; van den Akker, F. *J. Med. Chem.* **2020,** *63,* 5990–6002. doi:10.1021/acs.jmedchem.0c00255
29. Potts, K. T.; Kanemasa, S. *J. Org. Chem.* **1979,** *44,* 3808–3811. doi:10.1021/jo01336a014
30. Walkinshaw, A. J.; Xu, W.; Suero, M. G.; Gaunt, M. J. *J. Am. Chem. Soc.* **2013,** *135,* 12532–12535. doi:10.1021/ja405972h

31. Dvorak, K. A.; Swanson, D. M.; Wong, V. D. Piperazinyl Derivatives Useful as Modulators of the Neuropeptide Y_2 Receptor. U.S. Patent US8338426B2, June 26, 2008.
32. Schultes, S.; de Graaf, C.; Haaksma, E. E. J.; de Esch, I. J. P.; Leurs, R.; Krämer, O. *Drug Discovery Today: Technol.* **2010,** *7,* e157–e162. doi:10.1016/j.ddtec.2010.11.003

License and Terms

BEILSTEIN JOURNAL OF ORGANIC CHEMISTRY

The Ugi4CR as effective tool to access promising anticancer isatin-based α-acetamide carboxamide oxindole hybrids

Carolina S. Marques*[1], Aday González-Bakker[2] and José M. Padrón[2]

Full Research Paper

Open Access

Address:
[1]LAQV-REQUIMTE, University of Évora, Institute for Research and Advanced Studies, Rua Romão Ramalho, 59, 7000-641, Évora, Portugal and [2]BioLab, Instituto Universitario de Bio-Orgánica Antonio González (IUBO-AG), Universidad de La Laguna, PO Box 456, 38200, La Laguna, Spain

Email:
Carolina S. Marques* - carolsmarq@uevora.pt

* Corresponding author

Keywords:
cancer; GI_{50}; isatin; oxindole; Ugi4CR

Beilstein J. Org. Chem. **2024,** *20,* 1213–1220.
https://doi.org/10.3762/bjoc.20.104

Received: 12 December 2023
Accepted: 13 May 2024
Published: 27 May 2024

This article is part of the thematic issue "5th International Symposium on Synthesis and Catalysis (ISySyCat 2023)".

Guest Editor: A. Burke

Abstract

Considering early-stage drug discovery programs, the Ugi four-component reaction is a valuable, flexible, and pivotal tool, facilitating the creation of two new amide bonds in a one-pot fashion to effectively yield the desired α-aminoacylamides. Here, we highlight the reputation of this reaction approach to access number and scaffold diversity of a library of isatin-based α-acetamide carboxamide oxindole hybrids, promising anticancer agents, in a mild and fast sustainable reaction process. The library was tested against six human solid tumor cell lines, among them, non-small cell lung carcinoma, cervical adenocarcinoma, breast cancer and colon adenocarcinoma. The most potent compounds **8d**, **8h** and **8k** showed GI_{50} values in the range of 1–10 μM.

Introduction

Meticulous attention has been given by chemists regarding process formation of new bonds and synthesis of new scaffolds. In drug discovery and development, medicinal chemists struggle everyday towards the creation of new synthetic methods, driven by the increasing complexity of the molecules and taking into consideration economic and social aspects. Multicomponent reactions (MCRs) are remarkable tools which demonstrated great potential for more sustainable production of active pharmaceutical ingredients (API's). These flexible and versatile one-pot transformations in which three or more reagents are combined to access a new complex scaffold with remarkable atom economy, cost and time-effective and mainly diminishing waste production is a conscientious boost for structural diversity and sustainability [1-3]. The well-known Passerini, Ugi, Mannich, Biginelli, Hantzsch and Strecker reactions are some examples of the classic MCRs, representing the easygoing generation of a collection of small-molecules essential for structure–activity relationships (SAR). The isocyanide-based Ugi reaction is one of the most resourceful tools and still broadly studied MCR, generating multifunctional libraries of α-aminoacylamide derivatives, or Ugi adducts, with stereochemistry control [4,5]. Unquestionable potential of application

in the pharmaceutical industry is recognizable by the number of APIs obtained by this reaction approach [6,7]. The oxindole framework is a privileged unit, recognized massively by its extensive biological applications [8,9]. In the last few years we have been active in isatin modification using new synthetic approaches, anticipating the creation of new libraries of small-molecule hybrids with potential as cholinesterase inhibitors [10-13], important to treat neurodegenerative diseases, and anticancer agents [14-16] (Figure 1).

Cancer is a complex, cureless and fatal disease, oftentimes diagnosed worldwide. Being one of the leading causes of death worldwide, it is expected an increase of 47% with 28.4 million cases diagnosed, in 2040 [17,18]. Despite long years of research, there is still an urgent need to find novel, effective and safe drugs for cancer therapy.

Recently, focusing on the design of more potent anticancer drug candidates using more sustainable synthetic processes, we report a new Ugi four-component reaction approach for easy access to Ugi-derived isatin-peptoids in moderate to excellent yields (up to 99% yield). Some selected compounds were screened against five human solid tumor cell lines: lung (A549), breast (HBL-100 and T-47D), cervix (HeLa) and colon (WiDr). Preliminary SAR studies have revealed the preference of the *N*-benzylisatin structure over the 3,3-protected-oxindole, aliphatic chain on the acid component and small aliphatic chain on the aldehyde component to increase the antiproliferative activity. Also, benzyl isocyanide was favored over the aliphatic one (Scheme 1A) [16]. Considering the value of amide groups in drug discovery [19], the feasibility of running the isatin-based Ugi reaction [16,20-23] and the potential of the bis-amide-oxindole type derivatives as anticancer agents, a second family was synthesized, and screened for their anticancer activities (Scheme 1B).

Results and Discussion

Synthesis

Underlining sustainability and economically favored processes, a second family of α-acetamide carboxamide oxindole derivatives **5** was obtained using the previously optimized Ugi4CR approach [16] (Scheme 2 and Figure 2). Taking into account the preliminary SAR studies reported for the first family of Ugi-derived isatin-peptoids, the second family was obtained using 5-amino-1-benzyl-3,3-dimethoxyindolin-2-one (**1**) [12] and benzyl isocyanide (**4**), as amine and isocyanide components, respectively. Different carboxylic acids **2** and aldehydes/ketones **3** were evaluated using ZnF_2 as catalyst (10 mol %) and MeOH as the solvent (Scheme 2 and Figure 2).

A library of α-acetamide carboxamide oxindole hybrids **5** was obtained in moderate yields (26–63%), at room temperature, in

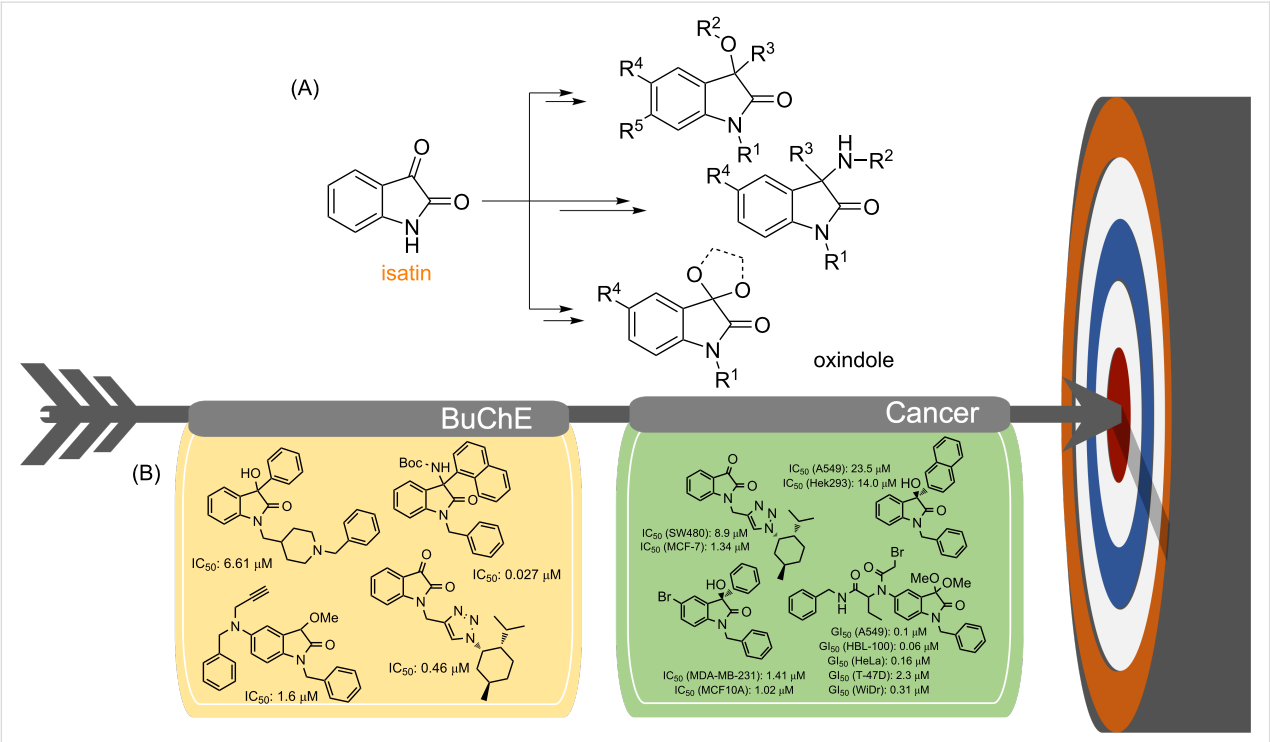

Figure 1: (A) Accessing libraries of oxindole hybrids using commercially available isatin as starting material and (B) most potent oxindole derivatives as BuChE inhibitors and anticancer agents, by Marques et al. [10-16].

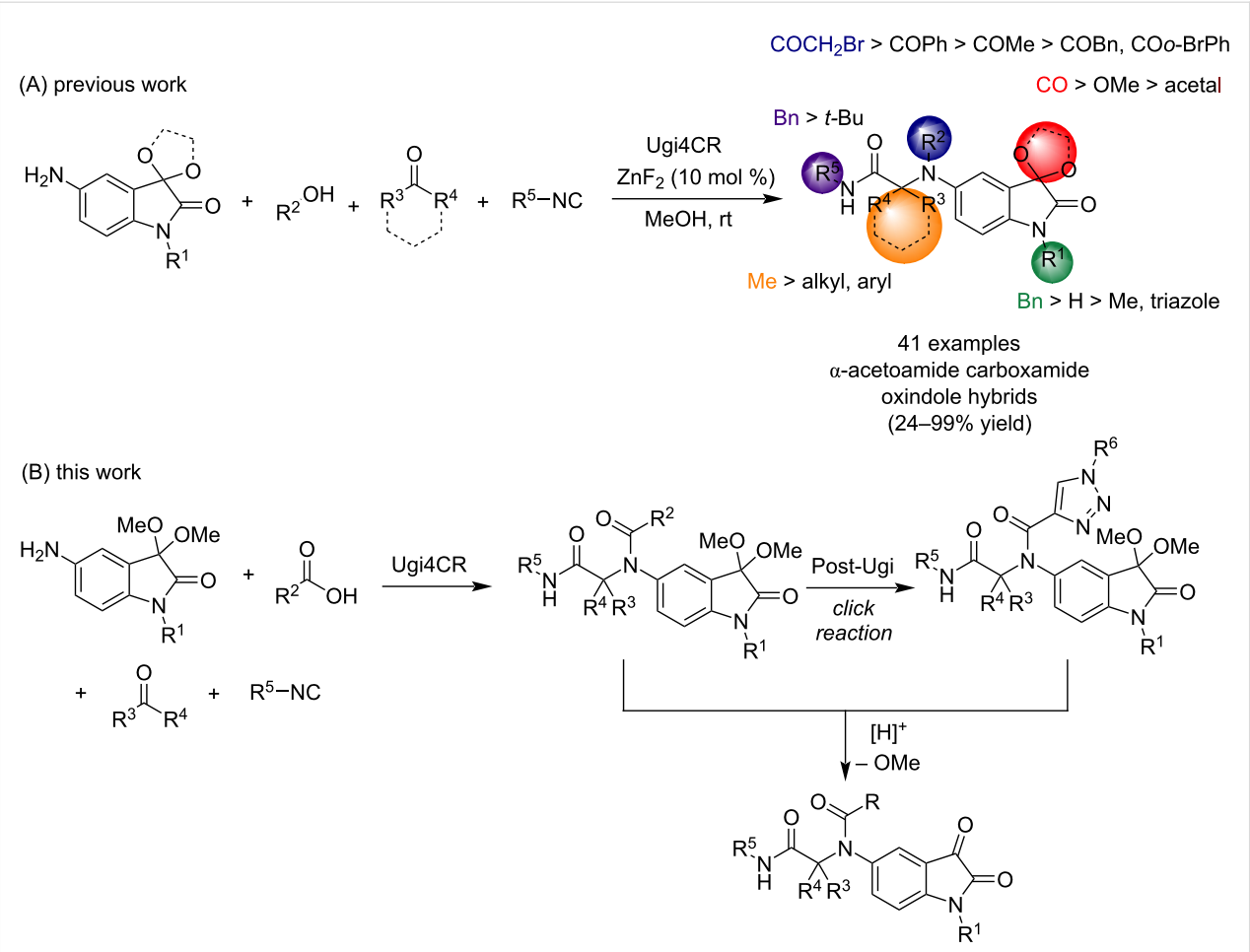

Scheme 1: (A) Library of isatin-based α-acetamide carboxamide oxindole derivatives obtained using an Ugi four-component reaction (Ugi4CR). (B) The synthetic strategy reported in this work.

short time (2 hours), proving the efficiency and the generality of this methodology. Aliphatic (**2a**, **2c** and **2m**), aromatic (**2d**, **2f**, **2g**, **2k** and **2l**), heterocyclic (**2e**, **2h**, **2i**, **2n** and **2o**), alkyne **2b** and alkene **2j** carboxylic acids were used successfully in this MCR, demonstrating a great reaction scope (Scheme 2 and Figure 2). Remarkably, the best yields were obtained when heterocyclic carboxylic acid components like 1*H*-pyrrole-3-carboxylic acid (**2n**), 2-furoic acid (**2o**) and 5-nitrofuran-2-carboxylic acid (**2e**) were used. The corresponding products **5nb**, **5ob** and **5ec** were achieved in 63, 51 and 49% yields, respectively. 1-Boc-azetidine-3-carboxylic acid (**2i**) also gave the corresponding product **5ib** in 54% yield. Considering the carbonyl component, 1-chloropropan-2-one (**3a**) was used to access the corresponding Ugi adduct **5aa** in 42% yield (Scheme 2 and Figure 2). Interestingly, *N*-benzyl-2-(*N*-(1-benzyl-3,3-dimethoxy-2-oxoindolin-5-yl)acetamido)-3-hydroxy-2-methylpropanamide (**5aa**) was obtained rather than the predictable compound with a 3-chloro-2-methylpropanamide group. We believe that a nucleophilic substitution occurs due to the presence of acetic acid (**2a**) as reaction component. Aliphatic aldehydes with small chains (**3b** and **3c**) were used successfully in the reaction approach, as expected. Also, aromatic 2-chlorobenzaldehyde (**3d**) was used and the desired compound **5ad** was obtained in 36% yield (Scheme 2 and Figure 2).

Like the oxindole scaffold, 1,2,3-triazole is also considered a privileged unit in drug discovery since compounds having this structure have a broad spectrum of biological activities, and have been widely used to create anticancer drug candidates [24,25]. The copper-catalyzed azide–alkyne cycloaddition (CuAAC) reaction, or commonly entitled “click” reaction, is a widely and straightforward tool to access the 1,2,3-triazole ring [26,27]. Due to the presence of an alkyne group on the Ugi-adduct **5bb** (Scheme 2) we decided to use the CuAAC reaction to introduce a 1,2,3-triazole unit into the scaffold. Benzyl azide (**6**), obtained using a previously reported procedure [27], was used in the CuAAC reaction. The α-acetamide carboxamide

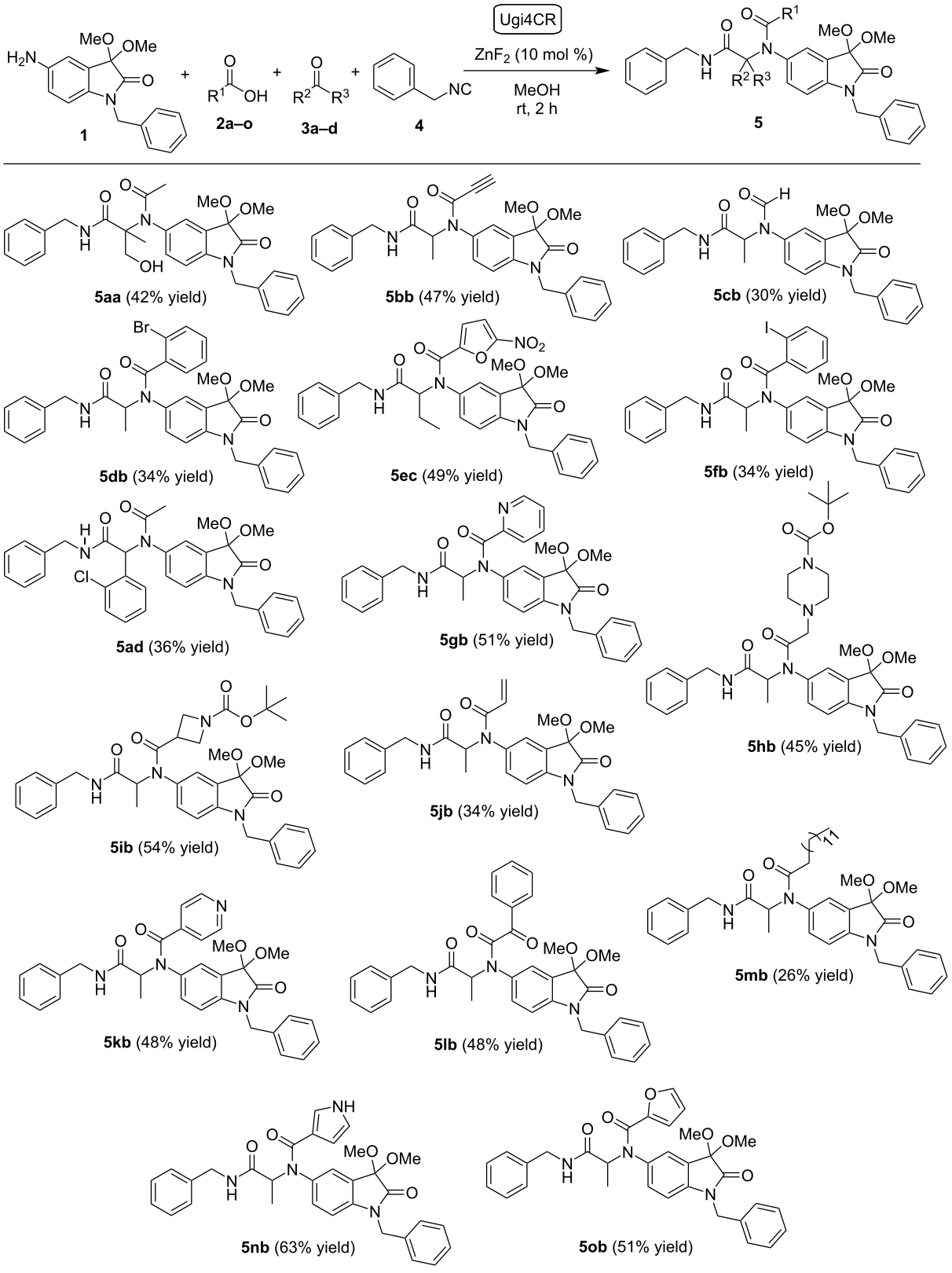

Scheme 2: Library of α-acetamide carboxamide oxindole hybrids **5** accessed via the Ugi4CR.

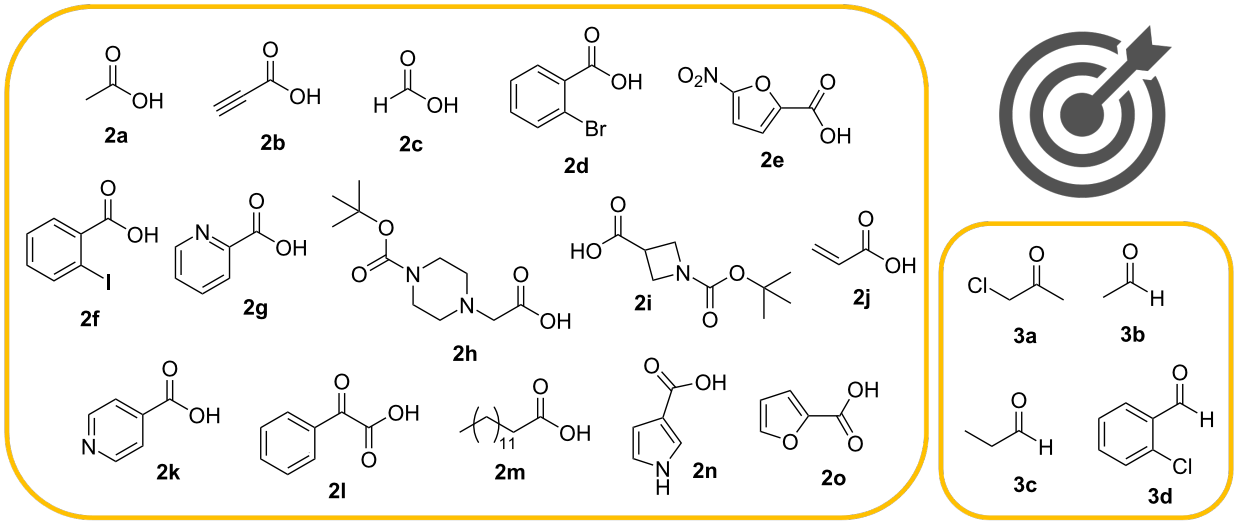

Figure 2: Carboxylic acids **2** and aldehydes/ketones **3** used in the Ugi4CR.

1,2,3-triazole oxindole hybrid **7** was easily obtained in 61% yield using $Cu(OAc)_2$ as catalyst, ascorbic acid, DMF as solvent, and microwave reaction conditions (120 ºC, 30 minutes) (Scheme 3).

Resourcefulness of the Ugi4CR and preliminary SAR studies [16] lead us to synthesize a third library of oxindole derivatives, using trifluoroacetic acid (TFA), under mild reaction conditions, to afford the corresponding α-acetamide carboxamide isatin hybrids **8** from the 3-protected oxindole counterparts **5** and **7**, in moderate to good yields (Scheme 4). The best yield was obtained when 3-protected oxindole derivatives **5** possess an aromatic or heterocyclic unit substituted in the 5-amide position of the oxindole ring. Compounds **8c**, **8d**, **8e** and **8m** were obtained in 83, 72, 74 and 84% yield, respectively. An exception was noticed for *N*-heterocycle units (pyridine and 1*H*-pyrrole) substituted in the same position, since compounds **8g**, **8l** and **8i** were obtained in 56, 51 and 36% yield, respectively. The 1,2,3-triazole hybrid isatin compound **8n** was obtained in 56% yield. Compounds **5ib** and **5hb**, with *N*-Boc protected-heterocycle units in the 5-amide position of the oxindole ring (Scheme 2) failed to afford the corresponding 3-deprotected isatin hybrids, since only decomposition byproducts (not identified) were obtained.

Antiproliferative activity

Considering the potential antiproliferative activity of these compounds, we screened 14 α-acetamide carboxamide isatin hybrids against six human solid tumor cell lines. The panel of cell lines comprised non-small cell lung carcinoma A549 and SW1573, cervical adenocarcinoma HeLa, breast cancer HBL-100 and T-47D, and colon adenocarcinoma WiDr. The half-maximal growth inhibitory concentration (GI_{50}) values after 48 hours of exposure were calculated for each compound (Table

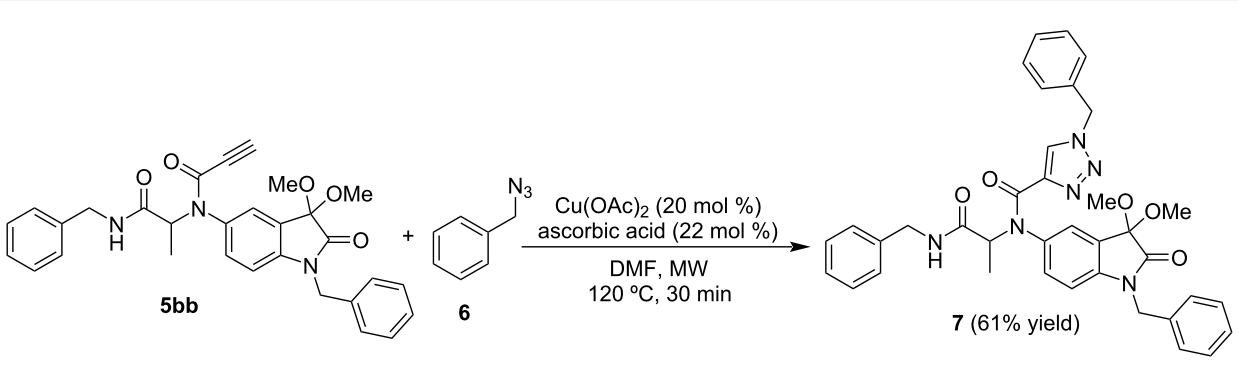

Scheme 3: Microwave-assisted CuAAC reaction to access α-acetamide carboxamide 1,2,3-triazole oxindole hybrid **7**.

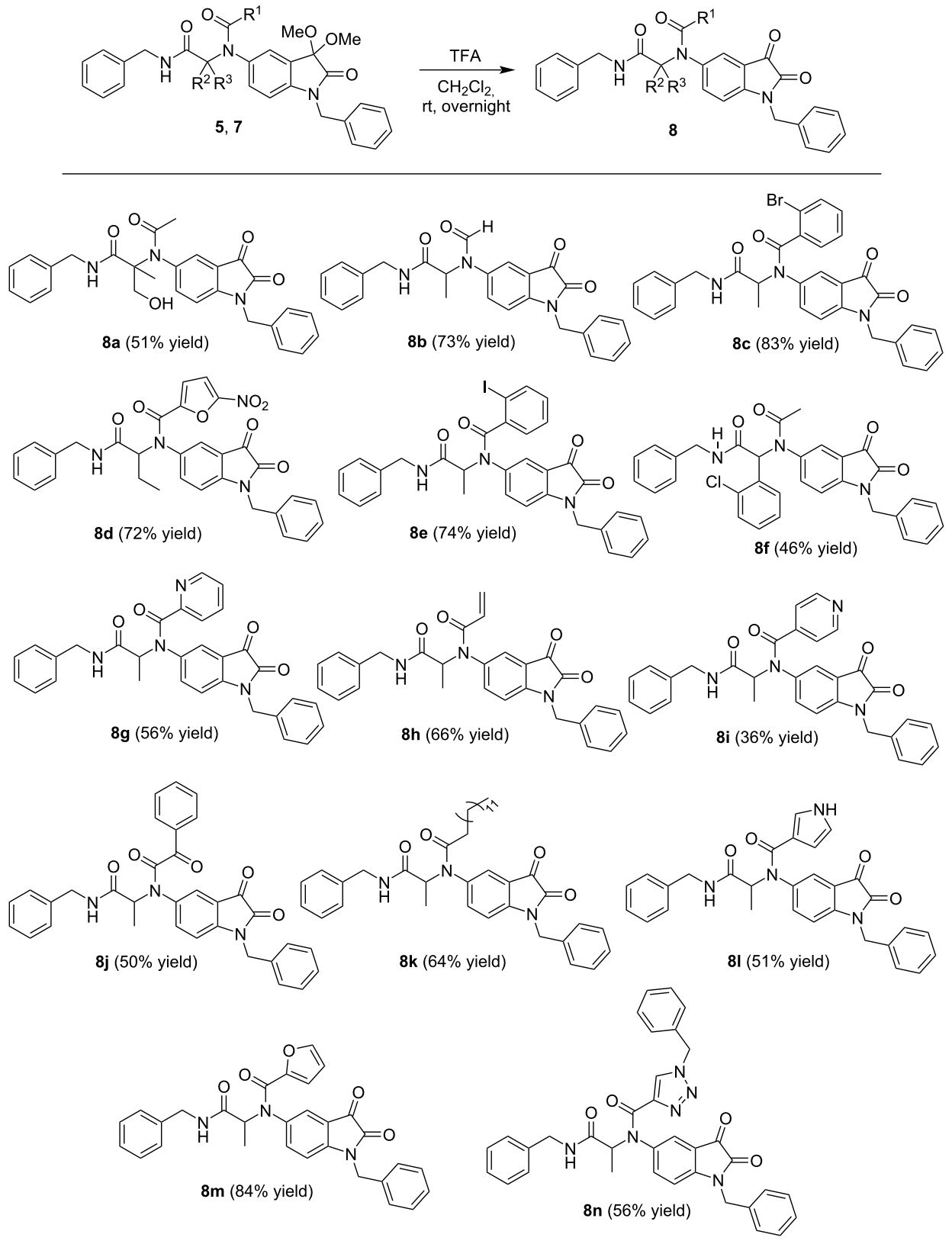

Scheme 4: Library of α-acetamide carboxamide isatin hybrids **8** easy accessed via deprotection reaction on the Ugi-adducts **5** and **7**. TFA: trifluoroacetic acid.

S1, Supporting Information File 1). The standard anticancer drug cisplatin (CDDP) was used as positive control. The results are viewed as GI_{50} range plot (Figure 3). The compounds were classified in three groups according to the GI_{50} range plot. The first group included the most active compounds **8d**, **8h** and **8k**. These compounds exhibited antiproliferative effects in the range of 1–10 μM against all cell lines. The second group comprised the less potent compounds, which were **8a**, **8b**, **8g** and **8i**. In this group, the GI_{50} values were higher than 10 μM in all cell lines tested. Finally, the third group enclosed the compounds that displayed a larger GI_{50} range with relevant activity against some cell lines (GI_{50} < 10 μM), but less potent against the others (GI_{50} > 10 μM). Some structure–activity relationships derived from the GI_{50} values. The presence of a nitro group at the furan moiety enhanced the activity (**8d** > **8m**). Presumably, the nitro group made **8d** the most potent analogue bearing an aromatic amide (**8c**, **8e**, **8g**, **8i**, **8l–n**). For the aliphatic amides, the most potent derivatives were **8h** and **8k**. The former is an α,β-unsaturated amide, which could react with nucleophiles inside the cell and thus explain its relative potency. The latter bears a long aliphatic side chain (thirteen carbon atoms), which could allow anchoring to cell membranes, representing a potential target. Overall, the results of the biological activity allow speculating that the compounds from the series **8a–n** might exhibit diverse mode of actions. Taking all these considerations as a whole, further studies of the biological activity of compounds **8d**, **8h** and **8k** might provide insights into the mode of action. Generally, the biological results point out the relevance of these isatin hybrids as privileged scaffolds for the development of new therapeutically relevant substances.

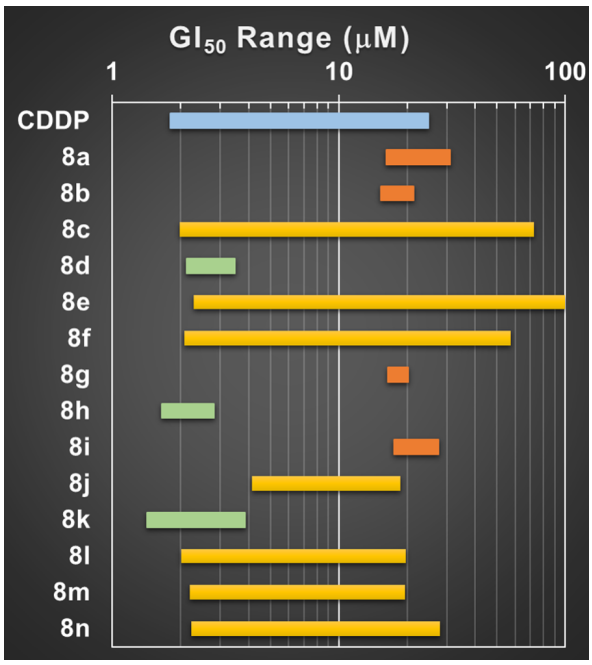

Figure 3: GI_{50} range plot against human solid tumor cell lines of investigated α-acetamide carboxamide isatin hybrids. Green most potent, yellow intermediate, red less potent.

Conclusion

Two new families of α-acetamide carboxamide oxindole and isatin hybrids were synthesized efficiently using the sustainable and efficient Ugi4CR approach. Easy access to isatin from the 3-protected oxindole scaffold was demonstrated using mild reaction conditions. Flexibility of the carboxylic acid component and also the carbonyl one (ketone/aldehyde) was exhibited in the library of Ugi adducts obtained in moderate to good yields, in a fast and clean reaction process. Among the library of α-acetamide carboxamide isatin hybrids, 14 were tested regarding their antiproliferative activity. Compounds **8d**, **8h** and **8k** were found to be the most potent ones, with GI_{50} values in the range of 1–10 μM. Further studies on the mode of action and lead-discovery are in progress and will be reported shortly.

Supporting Information

Supporting Information File 1

Experimental procedures, analytical data, NMR spectra and biological assays.
[https://www.beilstein-journals.org/bjoc/content/supplementary/1860-5397-20-104-S1.pdf]

Funding

C. S. M. thanks the Norma transitória for funding through the program DL 57/2016 (project UIDB/50006/2020|UIDP/50006/2020). A.G.-B. thanks the Asociación Española Contra el Cáncer (AECC) de Santa Cruz de Tenerife for predoctoral grant PRDTF233958GONZ. This work received financial support from PT national funds from Fundação para a Ciência e Tecnologia/Ministério da Ciência, Tecnologia e Ensino Superior (FCT/MCTES) 2022.02910.PTDC and the Spanish Government (Project PID2021-123059OB-I00 funded by MCIN/AEI / 10.13039/501100011033 / FEDER, UE).

ORCID® iDs

Carolina S. Marques - https://orcid.org/0000-0003-1697-7871
Aday González-Bakker - https://orcid.org/0000-0002-9792-5194
José M. Padrón - https://orcid.org/0000-0001-6268-6552

Data Availability Statement

All data that supports the findings of this study is available in the published article and/or the supporting information to this article.

Preprint

A non-peer-reviewed version of this article has been previously published as a preprint: https://doi.org/10.3762/bxiv.2023.60.v1

References

1. Herrera, R. P.; Marqués-López, E. *Multicomponent Reactions: Concepts and Applications for Design and Synthesis;* John Wiley & Sons: Hoboken, NJ, USA, 2015. doi:10.1002/9781118863992
2. Cores, Á.; Clerigué, J.; Orocio-Rodríguez, E.; Menéndez, J. C. *Pharmaceuticals* **2022,** *15,* 1009. doi:10.3390/ph15081009
3. Buskes, M. J.; Coffin, A.; Troast, D. M.; Stein, R.; Blanco, M.-J. *ACS Med. Chem. Lett.* **2023,** *14,* 376–385. doi:10.1021/acsmedchemlett.3c00012
4. Fouad, M. A.; Abdel-Hamid, H.; Ayoup, M. S. *RSC Adv.* **2020,** *10,* 42644–42681. doi:10.1039/d0ra07501a
5. Rocha, R. O.; Rodrigues, M. O.; Neto, B. A. D. *ACS Omega* **2020,** *5,* 972–979. doi:10.1021/acsomega.9b03684
6. Kalinski, C.; Lemoine, H.; Schmidt, J.; Burdack, C.; Kolb, J.; Umkehrer, M.; Ross, G. *Synthesis* **2008,** 4007–4011. doi:10.1055/s-0028-1083239
7. Younus, H. A.; Al-Rashida, M.; Hameed, A.; Uroos, M.; Salar, U.; Rana, S.; Khan, K. M. *Expert Opin. Ther. Pat.* **2021,** *31,* 267–289. doi:10.1080/13543776.2021.1858797
8. Khetmalis, Y. M.; Shivani, M.; Murugesan, S.; Chandra Sekhar, K. V. G. *Biomed. Pharmacother.* **2021,** *141,* 111842. doi:10.1016/j.biopha.2021.111842
9. Kaur, M. Oxindole: A Nucleus Enriched with Multitargeting Potential Against Complex Disorders. In *Key Heterocycle Cores for Designing Multitargeting Molecules;* Silakari, O., Ed.; Elsevier: Amsterdam, Netherlands, 2018; pp 211–246. doi:10.1016/b978-0-08-102083-8.00006-6
10. Totobenazara, J.; Bacalhau, P.; San Juan, A. A.; Marques, C. S.; Fernandes, L.; Goth, A.; Caldeira, A. T.; Martins, R.; Burke, A. J. *ChemistrySelect* **2016,** *1,* 3580–3588. doi:10.1002/slct.201600932
11. Marques, C. S.; López, Ó.; Bagetta, D.; Carreiro, E. P.; Petralla, S.; Bartolini, M.; Hoffmann, M.; Alcaro, S.; Monti, B.; Bolognesi, M. L.; Decker, M.; Fernández-Bolaños, J. G.; Burke, A. J. *Bioorg. Chem.* **2020,** *98,* 103753. doi:10.1016/j.bioorg.2020.103753
12. Marques, C. S.; López, Ó.; Leitzbach, L.; Fernández-Bolaños, J. G.; Stark, H.; Burke, A. J. *Synthesis* **2022,** *54,* 4304–4319. doi:10.1055/s-0041-1737343
13. Hofmanova, T.; Marques, C.; García-Sosa, A. T.; López, Ó.; Leitzbach, L.; Carreiro, E. P.; González-Bakker, A.; Puerta, A.; Stark, H.; Padrón, J. M.; Fernández-Bolaños, J. G.; Burke, A. J. *Results Chem.* **2023,** *6,* 101032. doi:10.1016/j.rechem.2023.101032
14. Marques, C. S.; Busto, N.; Gaudio, E.; Bertoni, F.; Burke, A. J. Novel N-(1,2,3-triazolmethylisatin and N-(1,2,3-triazolmethyl)-3-hydroxy-3-aryloxindoles with cytotoxic and anti-tumor activity. Eur. Pat. Appl. EP3400938A1, Nov 14, 2018.
15. Busto, N.; Leitão-Castro, J.; García-Sosa, A. T.; Cadete, F.; Marques, C. S.; Freitas, R.; Burke, A. J. *RSC Med. Chem.* **2022,** *13,* 970–977. doi:10.1039/d2md00044j
16. Marques, C. S.; González-Bakker, A.; Padrón, J. M.; Burke, A. J. *New J. Chem.* **2023,** *47,* 743–750. doi:10.1039/d2nj03627d
17. Sung, H.; Ferlay, J.; Siegel, R. L.; Laversanne, M.; Soerjomataram, I.; Jemal, A.; Bray, F. *Ca-Cancer J. Clin.* **2021,** *71,* 209–249. doi:10.3322/caac.21660
18. Chhikara, B. S.; Parang, K. *Chem. Biol. Lett.* **2023,** *10,* 451.
19. Roughley, S. D.; Jordan, A. M. *J. Med. Chem.* **2011,** *54,* 3451–3479. doi:10.1021/jm200187y
20. Brandão, P.; Marques, C.; Burke, A. J.; Pineiro, M. *Eur. J. Med. Chem.* **2021,** *211,* 113102. doi:10.1016/j.ejmech.2020.113102
21. Brandão, P.; López, Ó.; Leitzbach, L.; Stark, H.; Fernández-Bolaños, J. G.; Burke, A. J.; Pineiro, M. *ACS Med. Chem. Lett.* **2021,** *12,* 1718–1725. doi:10.1021/acsmedchemlett.1c00344
22. Brandão, P.; Marques, C. S.; Carreiro, E. P.; Pineiro, M.; Burke, A. J. *Chem. Rec.* **2021,** *21,* 924–1037. doi:10.1002/tcr.202000167
23. Brandão, P.; Puerta, A.; Padrón, J. M.; Kuznetsov, M. L.; Burke, A. J.; Pineiro, M. *Asian J. Org. Chem.* **2021,** *10,* 3434–3455. doi:10.1002/ajoc.202100684
24. Cai, J. H.; Zhu, X. Z.; Guo, P. Y.; Rose, P.; Liu, X. T.; Liu, X.; Zhu, Y. Z. *Front. Chem. (Lausanne, Switz.)* **2023,** *11,* 1114970. doi:10.3389/fchem.2023.1114970
25. Jiang, X.; Hao, X.; Jing, L.; Wu, G.; Kang, D.; Liu, X.; Zhan, P. *Expert Opin. Drug Discovery* **2019,** *14,* 779–789. doi:10.1080/17460441.2019.1614910
26. Haldón, E.; Nicasio, M. C.; Pérez, P. J. *Org. Biomol. Chem.* **2015,** *13,* 9528–9550. doi:10.1039/c5ob01457c
27. Marques, C. S.; Burke, A. J. *ChemCatChem* **2016,** *8,* 3518–3526. doi:10.1002/cctc.201600901

License and Terms

BEILSTEIN JOURNAL OF ORGANIC CHEMISTRY

New triazinephosphonate dopants for Nafion proton exchange membranes (PEM)

Fátima C. Teixeira*[1], António P. S. Teixeira[2] and C. M. Rangel[1]

Full Research Paper

Open Access

Address:
[1]Laboratório Nacional de Energia e Geologia, I.P., Estrada do Paço do Lumiar, 22, 1649-038 Lisboa, Portugal, and [2]Departamento de Ciências Médicas e da Saúde, Escola de Saúde e Desenvolvimento Humano & LAQV- REQUIMTE, IIFA, Universidade de Évora, R. Romão Ramalho, 59, 7000-671 Évora, Portugal

Email:
Fátima C. Teixeira* - fatima.teixeira@lneg.pt; António P. S. Teixeira - apsteix@uevora.pt; C. M. Rangel - carmen.rangel@lneg.pt

* Corresponding author

Keywords:
electrolyser; fuel cells; Nafion-modified membranes; phosphonates; proton exchange membranes; triazine

Beilstein J. Org. Chem. **2024,** *20,* 1623–1634.
https://doi.org/10.3762/bjoc.20.145

Received: 25 February 2024
Accepted: 05 July 2024
Published: 17 July 2024

This article is part of the thematic issue "5th International Symposium on Synthesis and Catalysis (ISySyCat 2023)".

Guest Editor: A. Burke

Abstract

A new paradigm for energy is underway demanding decarbonized energy systems. Some of them rely on emerging electrochemical devices, crucial in hydrogen technologies, including fuel cells, CO_2 and water electrolysers, whose applications and performances depend on key components such as their separators/ion-exchange membranes. The most studied and already commercialized Nafion membrane shows great chemical stability, but its water content limits its high proton conduction to a limited range of operating temperatures. Here, we report the synthesis of a new series of triazinephosphonate derivatives and their use as dopants in the preparation of new modified Nafion membranes. The triazinephosphonate derivatives were prepared by substitution of chlorine atoms in cyanuric chloride. Diverse conditions were used to obtain the trisubstituted (4-hydroxyphenyl)triazinephosphonate derivatives and the (4-aminophenyl)triazinephosphonate derivatives, but with these amino counterparts, only the disubstituted compounds were obtained. The new modified Nafion membranes were prepared by casting incorporation of the synthesized 1,3,5-triazinephosphonate (TPs) derivatives. The evaluation of the proton conduction properties of the new membranes and relative humidity (RH) conditions and at 60 °C, showed that they present higher proton conductivities than the prepared Nafion membrane and similar or better proton conductivities than commercial Nafion N115, in the same experimental conditions. The Nafion-doped membrane with compound **TP2** with a 1.0 wt % loading showed the highest proton conductivity with 84 $mS{\cdot}cm^{-1}$.

Introduction

Decarbonized energy sources are the new paradigm in a world with increasing energy demands, primarily powered by fossil fuels, being proposed as a key strategy for restricting the detrimental effects of climate change. Vast efforts are being made to fulfil this crucial challenge of the 21st century. Clean, renewable, and environmental-friendly technological processes are

being considered using electrochemical devices which convert chemical to electric energy and/or vice versa that, when associated to renewable energy sources, can promote sustainable energy systems [1-4]. Among them are included proton exchange membrane devices [5,6], such as proton exchange membrane fuel cells (PEMFCs) [3,7-9], due to their high-power density and high power-to-weight ratio, and CO_2 electrolysers, which can reduce the polluting gas CO_2 and produce syngas from the co-electrolysis of CO_2 and water [10,11], or water electrolysers that allow the generation of green hydrogen [12,13]. The technology behind these electrochemical devices still relies on the membrane as a key component that defines the applications and the conditions to its use [14]. Both fuel cells and water electrolyser devices depend on proton exchange membranes to ensure a high proton conduction or leading to an efficient reaction production of hydrogen and oxygen gases, with no risk of electrolyte leakage and restricted gas-crossover [15-17].

Also, besides their conductivity and their low permeability to fuel and oxidant, the chemical and structural properties of the membranes restrain their stability and durability, their humidity and temperature application conditions, and their efficiency and consequently, the performance of fuel cells or eletrolysers [18,19].

Many organic polymers with acidic functional groups have been developed as membranes for these electrochemical devices [14,20]. However, many technological limitations remain due to the high dependence of the membrane's performance on the presence of water or other electrolyte content. To overcome these limitations, the modification of the membrane can be done by the incorporation of other compounds into these polymeric materials to participate in the proton conduction or to surpass the water or electrolyte dependency [15,21].

The most studied and commercially available proton exchange membranes consist of Nafion, a hydrophobic perfluorosulfonated polymer with sulfonic acid groups [22]. These membranes have an excellent chemical stability, but their high proton conduction is dependent of the water content of the membranes which limits their operating temperature range to 80 °C [23].

The importance of the membranes for the new sustainable energy sources fostered the efforts and investments in the research and development of new membranes that might be able to surpass the actual limitations. Our studies started with the synthesis of phosphonate and phosphonic acid compounds to be used as membrane dopants [24,25]. These studies were followed by the incorporation of bisphosphonic acids as dopants in Nafion membranes that led to an increase on the proton conduction of the new membranes, since these compounds are good proton carriers due to their proton donor and acceptor behavior [26-29]. In addition, the increase in the proton conduction of the doped membranes has been shown to be dependent of the chemical structure of the dopant.

Triazines are a class of heteroaromatic compounds with three nitrogen atoms on a six-membered ring, with the general formula $C_3N_3H_3$. According to the position of the nitrogen atoms in the ring, they constitute 1,2,3-, 1,2,4- and 1,3,5-triazine isomers [30]. There have been reported several and diverse applications to a large number of compounds with a triazine moiety, ranging from biological applications [31-34], such as fungicide, herbicide, antiviral, antimicrobial, antitumor, to their use in organic synthesis, including combinatorial chemistry [35], in analytical chemistry, in electrochemical redox processes, in crystal engineering, and as fluorescent, light emitting, corrosion inhibitors or several other materials [36-42].

The most used triazine is 1,3,5-triazine (or *s*-triazine) that can provide symmetrical monosubstituted derivatives, or di- or trisubstituted symmetrical or asymmetrical derivatives. The C_3 symmetry of 1,3,5-triazine makes it a popular heterocyclic core for the synthesis of star-shaped molecules [43-45], which was being used to the construction of triangular molecules, including molecular cages [46,47] and at porous materials, as linkers in metal-organic frameworks (MOFs) [48], used in the evaluation of the cycloaddition of CO_2 to epoxides [49] and CO_2 uptake [50].

Taking in consideration the strategy of the incorporation of dopants to promote the proton conduction in Nafion membranes, new triazinephosphonate (TPs) derivatives were prepared to be applied as dopants through their incorporation into new doped membranes. To this purpose, the present work reports on the synthesis and characterization of a new series of 1,3,5-triazinephosphonate (TPs) derivatives in the anticipation that these dopants can act both as a source of protons and proton acceptors, facilitating the intermolecular proton conduction. The rational of the strategy behind the use of amino- and hydroxyphenyl spacers is twofold: i) their inclusion in the structure separates the bulky phosphonate groups from the triazine moiety, giving the membrane more structural flexibility; ii) nitrogen and oxygen atoms of these groups can also participate in the proton conduction of the membranes. The new membranes were prepared by casting incorporation of the synthesized 1,3,5-triazinephosphonate (TPs) derivatives. Proton conduction properties of new membranes were evaluated by electrochemical impedance spectroscopy (EIS) at 60 °C at different relative humidity (RH) conditions. The results showed

higher proton conductivities than recast Nafion membrane and similar or better proton conductivities than commercial Nafion N115, in the same experimental conditions.

Results and Discussion

Preparation of triazine derivatives

The synthesis of 1,3,5-triazinephosphonate (TP) derivatives, to be used as dopants on new membranes, were carried out from the commercially available cyanuric chloride (**1**), through the substitution of chlorine atoms by different nucleophiles. The devised strategy involved the attack of the O or N atoms of the arylphosphonate nucleophile at the position of the chlorine atom of triazine, at its 2, 4 and 6 carbon positions (Figure 1). Most of these nucleophiles bearing a phosphonate group were not commercially available and were prepared from 4-hydroxyphenyl- or 4-aminophenyl-based derivatives.

The first nucleophile to be synthesized was diethyl (4-hydroxyphenyl)phosphonate (**2**) [51], starting from 4-bromophenol (**3**) and triethyl phosphite. When this reaction was carried out in the presence of nickel(II) bromide, it afforded compound **2** with a very low yield (2%). When the phosphonation was performed with diethyl phosphonate in the presence of $Pd(PPh_3)_4$ as catalyst and trimethylamine, compound **2** was formed with a good yield (72%) (Scheme 1).

The corresponding (4-nitrophenyl)phosphonate derivative **6** [51] was also prepared, using the same reaction conditions, by the reaction between 1-bromo-4-nitrobenzene (**5**) and diethyl phosphonate, in the presence of $Pd(PPh_3)_4$ as catalyst and triethylamine, since the use of triethyl phosphite in the presence on nickel(II) bromide do not allow the formation of the desired product. Compound **6** [51] was subsequently reduced to the corresponding aniline derivative **4** [52] in the presence of H_2 and Pd/C (Scheme 1).

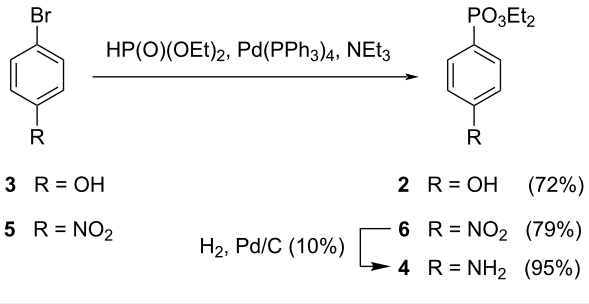

Scheme 1: Synthesis of diethyl phenylphosphonates **2, 4** and **6**.

The synthesis of diethyl (4-hydroxyphenyl)methylphosphonate (**7**) [53] started from [4-(benzyloxy)phenyl]methanol (**8**). Compound **8** was submitted to a nucleophilic substitution using hydrobromic acid, as a 33% solution in acetic acid, to afford the corresponding bromide derivative **9** [54] (Scheme 2). Subsequently 1-(benzyloxy)-4-(bromomethyl)benzene (**9**) underwent Michaelis–Arbuzov reaction with triethyl phosphite to afford diethyl [4-(benzyloxy)phenyl]methylphosphonate (**10**). The

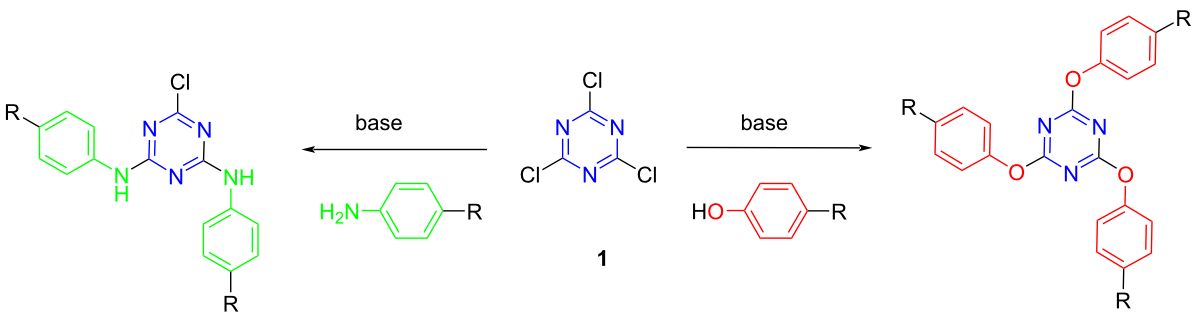

Figure 1: General synthesis of triazinephosphonate compounds.

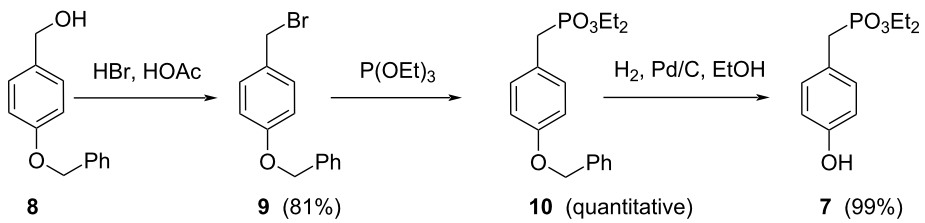

Scheme 2: Synthesis of (4-hydroxyphenyl)methylphosphonate **7** starting from [4-(benzyloxy)phenyl]methanol (**8**).

following hydrogenolysis under H_2/Pd/C conditions in ethanol, afforded the desired diethyl (4-hydroxyphenyl)methylphosphonate (**7**), in an overall yield of 80%.

The synthesis of diethyl [hydroxy(4-hydroxyphenyl)methyl]phosphonate (**11**) [55] started with the reaction of 4-hydroxybenzaldehyde (**12**) with diethyl phosphonate. Several attempts were carried out under different conditions, using several bases or an acidic resin, but only complex mixtures of products were obtained from which it was not possible to isolate the product. The reaction of 4-hydroxybenzaldehyde (**12**) with triethyl phosphite in the presence of zinc(II) bromide allowed the formation of diethyl [hydroxy(4-hydroxyphenyl)methyl]phosphonate (**11**) and tetraethyl [(4-hydroxyphenyl)methylene]bis(phosphonate) (**13**), which were separated by column chromatography (Scheme 3).

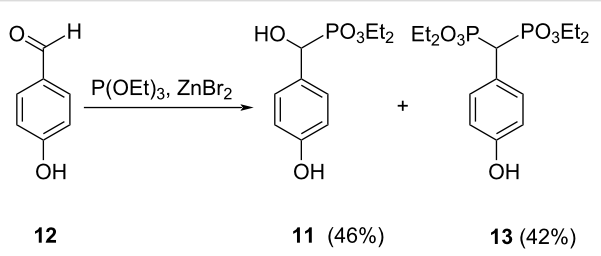

Scheme 3: Synthesis of diethyl [hydroxy(4-hydroxyphenyl)methyl]phosphonate (**11**) and tetraethyl [(4-hydroxyphenyl)methylene]bis(phosphonate) (**13**).

The synthesis of pure tetraethyl [(4-hydroxyphenyl)methylene]bis(phosphonate) (**13**) [56] was successfully achieved, with high yield, by the reaction of diethyl phosphonate with 4-hydroxybenzaldehyde (**12**) in the presence of sodium metal.

A reaction to obtain the corresponding amino derivative **14** [57] was carried out starting from 4-nitrobenzaldehyde (**15**). Compound **15** reacted with diethyl phosphonate in the presence of a strong base (sodium methoxide) to afford diethyl [hydroxy(4-nitrophenyl)methyl]phosphonate (**16**) in 81% yield (Scheme 4). The hydrogenolysis of this compound under H_2 on Pd/C afforded quantitatively diethyl [hydroxy(4-aminophenyl)methyl]phosphonate (**14**) (Scheme 4). With the starting compound **15**, the Michaelis-Arbuzov reaction did not afford the tetraethyl bisphosphonate derivative.

To reach the star-shaped *s*-triazine derivatives bearing a phosphonate group, it was considered that the best strategy was to carry out the substitution of chlorine atoms of 2,4,6-trichloro-1,3,5-triazine (cyanuric chloride, **1**) by the previously synthesized nucleophiles. The general scheme to obtain the desired triazinephosphonates (TPs) from the synthesized amino nucleophiles are represented in Scheme 5.

Initially, the 4-aminophenyl derivatives were synthesized in a THF solution, using DIPEA as base. The first reaction was carried out between more than 3 equiv of (4-aminophenyl)phosphonate **4** and cyanuric chloride (**1**). This reaction did not afford the desired trisubstituted triazine; instead, only the disubstituted derivative was achieved (compound **TP1**), in low yield, with a chlorine atom remaining bonded to the triazine ring (Scheme 5). The spectroscopic data of the isolated compound are in accordance with the proposed structure for compound **TP1**. The MS spectrum confirms the presence of a chlorine atom, with a molecular ion MH^+ and a $MH^+ + 2$ peak for ^{35}Cl and ^{37}Cl isotopes, respectively, with an approximately 3/4 and 1/4 proportion. The symmetry of the obtained compound **TP1** gives simple NMR spectra, with the ^{31}P NMR spectrum showing a singlet signal (Figure 2) and the signal at 169.5 ppm, on the ^{13}C NMR spectrum, confirming the presence of a chlorine atom bonded to a carbon atom in the proposed structure. Other synthetic attempts were carried out with different reaction conditions, but they usually gave complex mixtures, whose compounds could not be separated, and the trisubstituted triazine derivative was not achieved.

The reaction of cyanuric chloride (**1**) with (4-aminophenyl)methylphosphonate **17** also afforded the disubstituted triazine derivative **TP2** (Scheme 5). Other reactions were carried out at different conditions, but they did not afford the desired trisubstituted derivative. The spectroscopic data are in

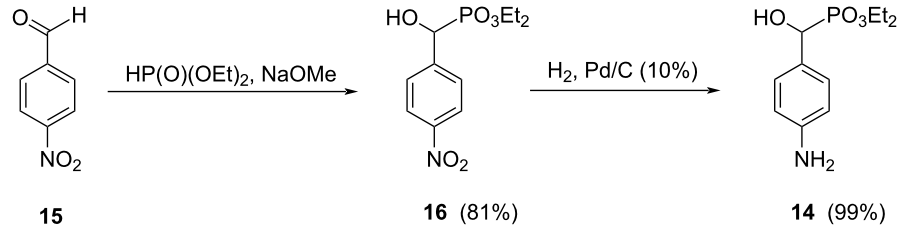

Scheme 4: Synthesis of diethyl phenylphosphonates **16** and **14**.

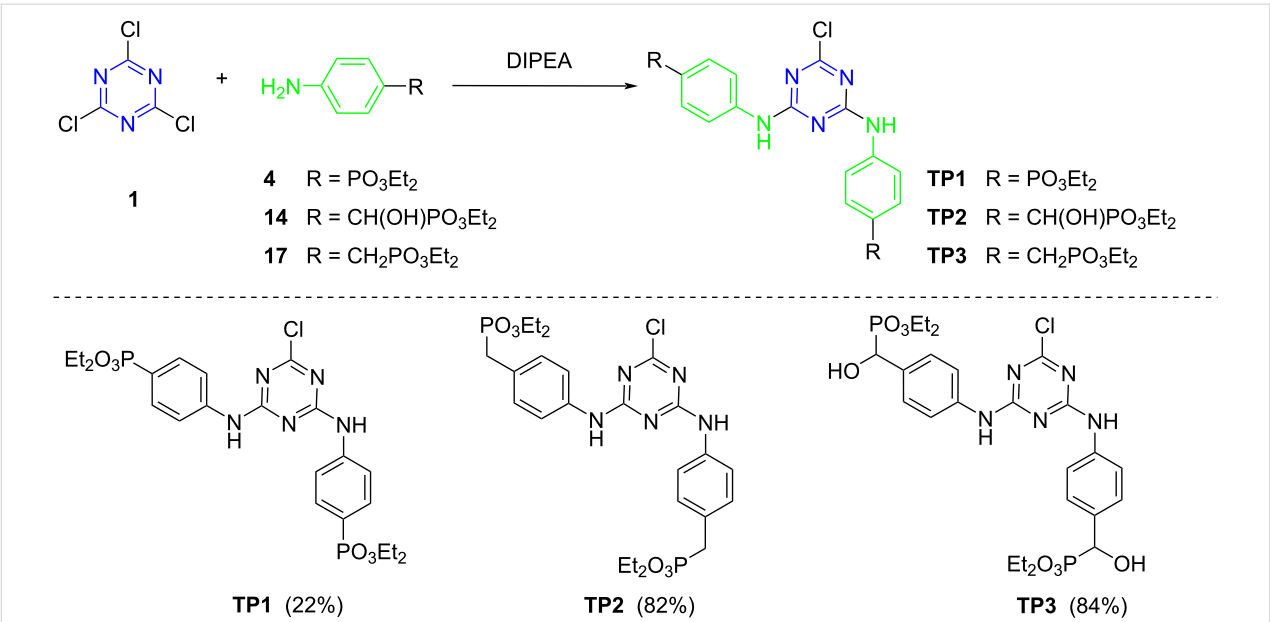

Scheme 5: Synthesis of 4-aminophenyltriazinephosphonate derivatives **TP1–TP3**.

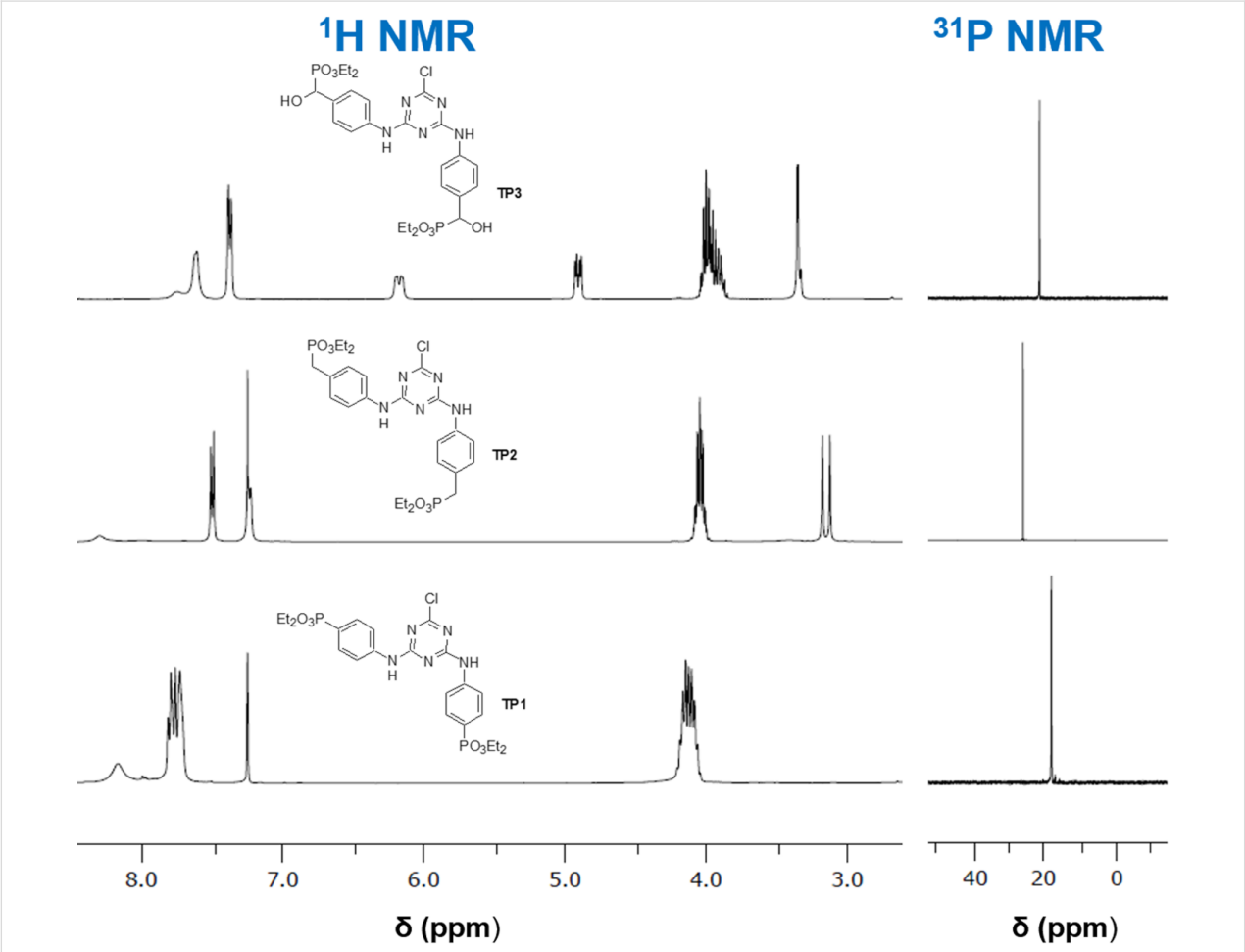

Figure 2: Partial view of ^{1}H and ^{31}P NMR spectra of 4-aminophenyltriazinephosphonate derivatives **TP1–TP3**.

agreement with the proposed disubstitution pattern, with MS showing MH^+ and $MH^+ + 2$ isotope peaks due to the presence of chlorine in the molecule. In the ^1H NMR spectrum, the CH_2P protons appear as a doublet signal at 3.14 ppm, due to the coupling with the ^{31}P atom of the phosphonate group (Figure 2). The chemical shift of the ^{31}P atoms is observed as a singlet for both phosphorus atoms (Figure 2) and the carbon atom bonded to the chlorine atom is observed at 167.8 ppm.

Also, the reaction with diethyl [hydroxy(4-aminophenyl)methyl]phosphonate (**14**) only afforded the disubstituted derivative **TP3** (Scheme 5), despite the different conditions tested. The spectroscopic data are in agreement with the proposed structure for compound **TP3** (Scheme 5), namely the presence of the chlorine atom in the mass spectrum, due to the presence of isotope peaks, the signal at 168.2 ppm at ^{13}C NMR spectrum attributed to the carbon atom bonded to chlorine, and the singlet signal of the phosphorus atom at the ^{31}P NMR spectrum.

The synthesis of the corresponding 4-hydroxyphenylphosphonate derivatives followed the same strategy of the amino counterparts' preparation (Scheme 6). The initial reaction between cyanuric acid (**1**) and diethyl 4-hydroxyphenylphosphonate (**2**) in THF, with DIPEA as base, gave a mixture of products which was purified by column chromatography to afford the desired

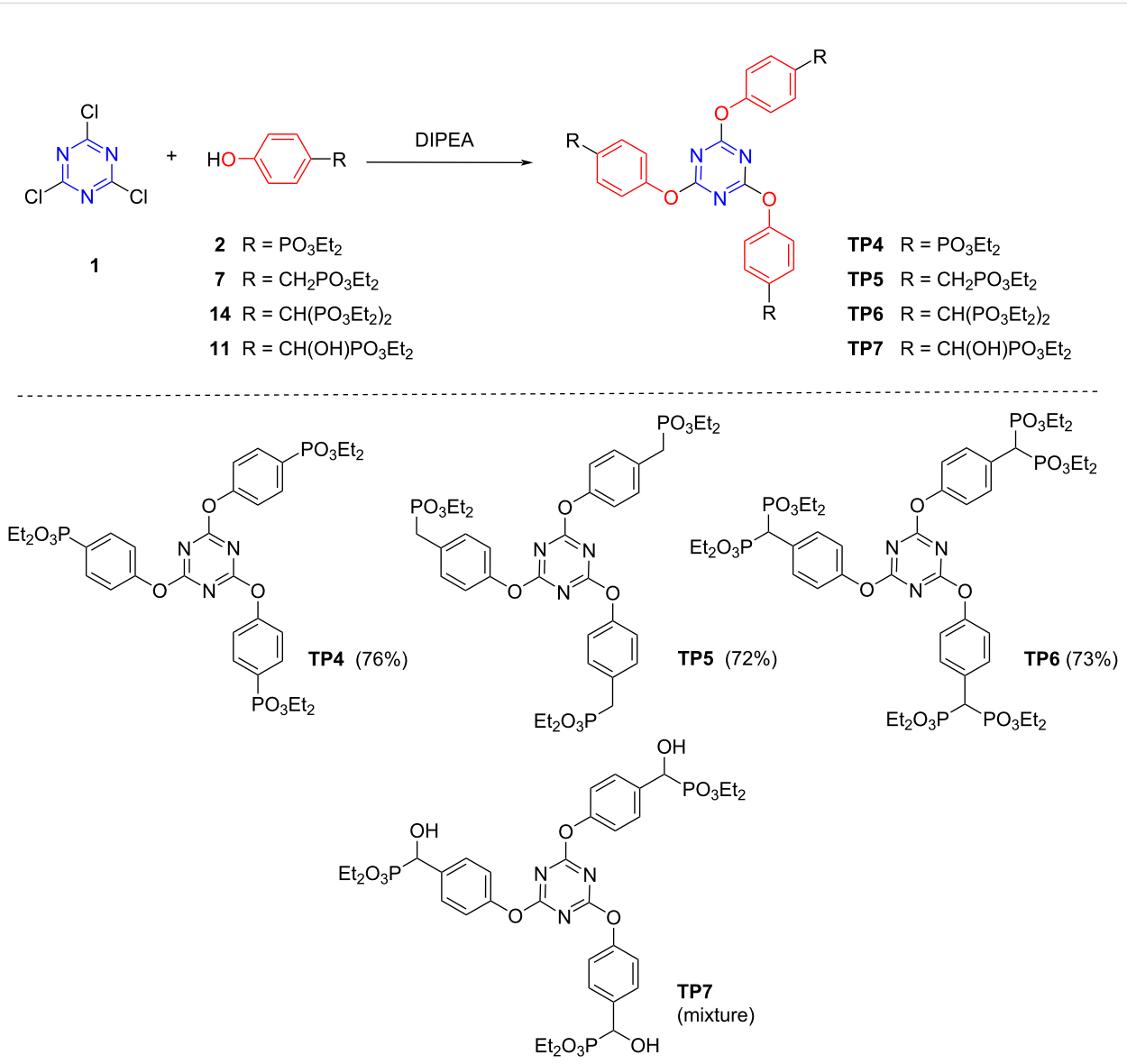

Scheme 6: Synthesis of (4-hydroxyphenyl)triazinephosphonate derivatives **TP4**–**TP6**.

trisubstituted compound **TP4** (Scheme 6). Since this reaction had a very low yield (17%), another base, Na_2CO_3, was used and compound **TP4** was obtained in a good yield (76%). No isotope peaks were observed at the MS of the compound, in agreement with the full displacement of the chlorine atoms. The NMR spectra (Figure 3) presented a similar pattern of the corresponding 4-amino derivative **TP1**. The ^{31}P NMR spectrum shows only one singlet in accordance with the symmetry of the molecule, with magnetically equivalent phosphorus atoms.

The synthesis of other 4-hydroxyphenyltriazinephosphonate derivatives **TP5** and **TP6**, starting from diethyl [(4-hydroxyphenyl)methyl]phosphonate (**7**) and tetraethyl [(4-hydroxyphenyl)methylene]bisphosphonate (**13**), were carried out using the same conditions of the previous reaction, including Na_2CO_3 as base. These reactions afforded the desired trisubstituted triazine derivatives, compounds **TP5** and **TP6**, respectively, in good yields (>70%) (Scheme 6). The **TP5** was also prepared using DIPEA as a base, but in low yield (25%). All spectra of

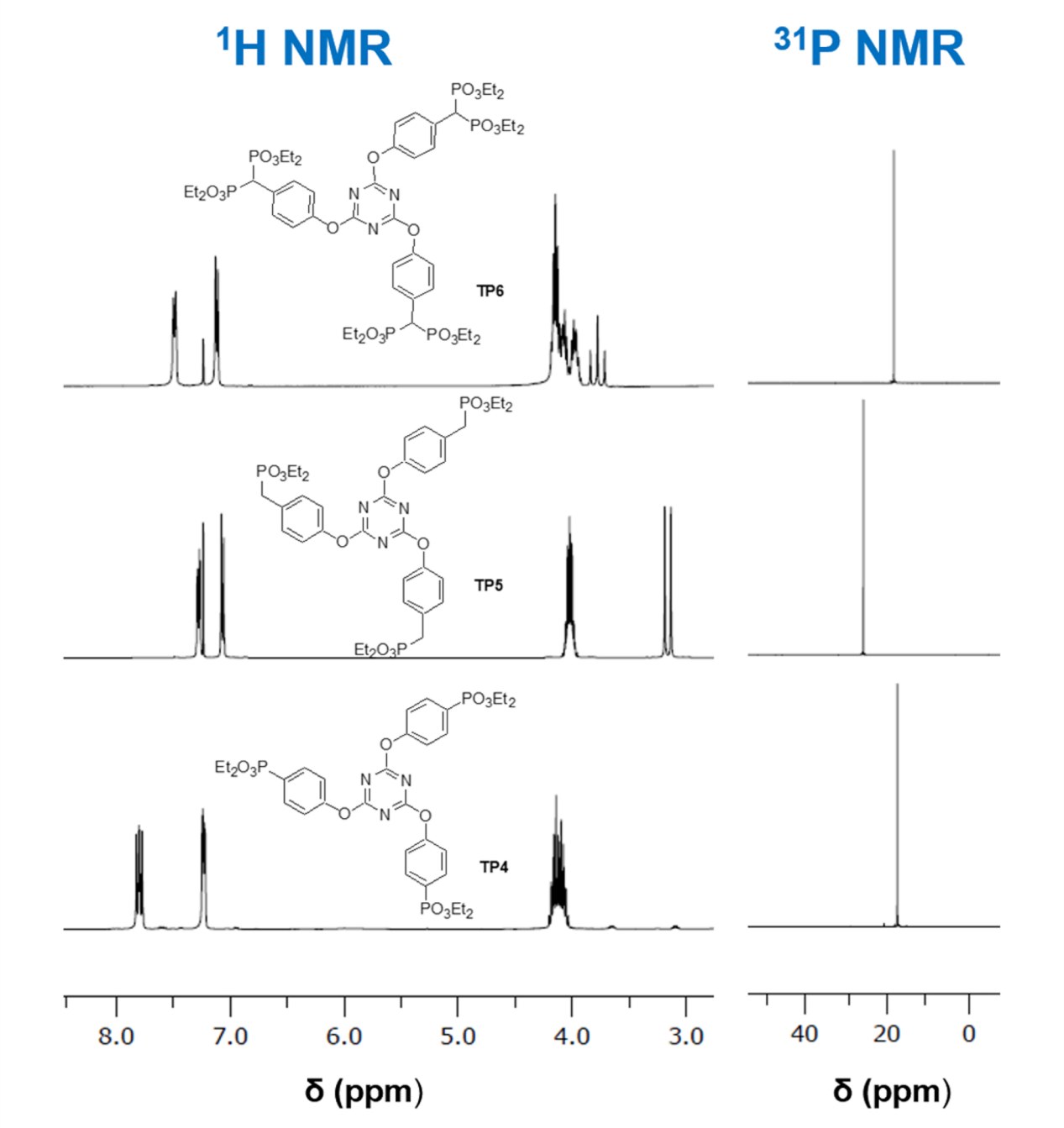

Figure 3: Partial view of ^{1}H and ^{31}P NMR spectra of (4-hydroxyphenyl)triazinephosphonate derivatives **TP4**–**TP6**.

these compounds are in agreement with the proposed structures (Figure 3).

Several attempts were carried out to prepare triazinephosphonate **TP7** derivative from diethyl [hydroxy(4-hydroxyphenyl)methyl]phosphonate (**11**). However, all the attempts to isolate triazinephosphonate **TP7** derivative failed. The initial reactions between cyanuric acid (**1**) and compound **11**, using Na_2CO_3 as base, gave a mixture of products, which were not possible to separate. The data obtained from these mixtures suggest that triazine derivatives with different substitutions patterns are obtained, and that the displacement of the chlorine atom occurred by several substitution degrees by both the oxygen atom of hydroxyphenyl or the hydroxymethyl group of compound **11**, giving a complex mixture. The use of DIPEA as base, under the previous conditions, gave the desired trisubstituted compound **TP7** (crude, 47%) (Scheme 6). However, purification of the crude product by column chromatography led to the decomposition of compound **TP7**.

Another strategy was devised to obtain the desired triazinephosphonate **TP7**: The first step was the nucleophilic substitution of the chlorine atoms of triazine **1** by 4-hydroxybenzaldehyde (**12**), followed by the phosphonation of the aldehyde group. To implement this strategy, a reaction between 4-hydroxybenzaldehyde (**12**) and cyanuric chloride (**1**) was performed, in toluene with Na_2CO_3 as base, to obtain compound **19** [58] in very good yield (87%) (Scheme 7). Compound **19** was subjected to similar reaction conditions that led to phosphonates **11** and **16**, using diethyl phosphonate in the presence of a base, such as Et_3N and $NaOCH_3$, or even sodium metal, to obtain compound **TP7** (Scheme 7). Unfortunately, these reactions afforded complex mixtures of products and by column chromatography was isolated only compound **20** in low yield (13%). It was not possible to isolate neither di- or triphosphonate derivatives and with this compound it was not possible to prepare a doped membrane (Scheme 7).

Preparation and proton conduction of doped membranes

Previous studies in our group [26-29] have shown that the incorporation of phosphonic acid derivatives into commercial Nafion polymers increment their proton conduction properties. The synthesized compounds (**TP1**–**TP6**) were attempted to be applied as dopants in the preparation of new proton exchange membranes.

With this in mind, new doped membranes were prepared by incorporation of the chosen dopants into a Nafion polymer using a casting method (Figure 4). It was expected that the dopants could act as proton carriers, improving the proton conduction of the membranes. The new membranes had a 1 wt % loading of **TPs** since our previous [27] results showed that 1 wt % is usually the best weight loading for doped Nafion membranes.

The FTIR-ATR spectra of Nafion membranes (Supporting Information File 1, Figure S1) showed the characteristic very strong and broad absorption bands of Nafion near 1200 and 1145 cm^{-1} due to the C–F stretching vibration [59-63]. The phosphonate compounds also present their strongest bands in this region, but they are overlapped by the more intense Nafion bonds due to the small wt % loading of the dopants. As a result, despite the visible slight dark-brown color, observed by a visual inspection of the membranes, only discrete changes are observed in the spectra of new membranes compared to commercial Nafion [64]. Other characteristic bands of S–O group, CF_2–CF and C–O–C are observed at near 1050, 980 and 960 cm^{-1}, respectively, in the FTIR spectra [63].

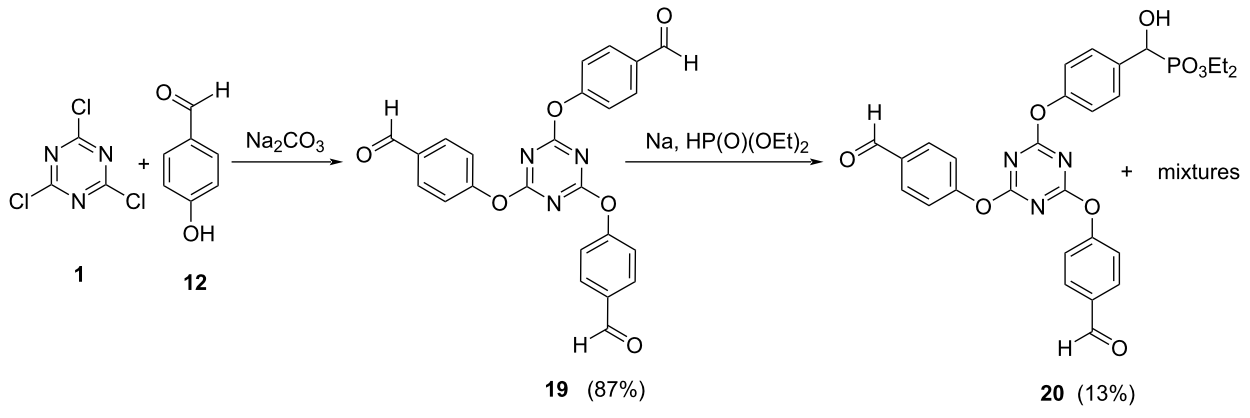

Scheme 7: Attempted synthesis of triazinephosphonate **TP7**.

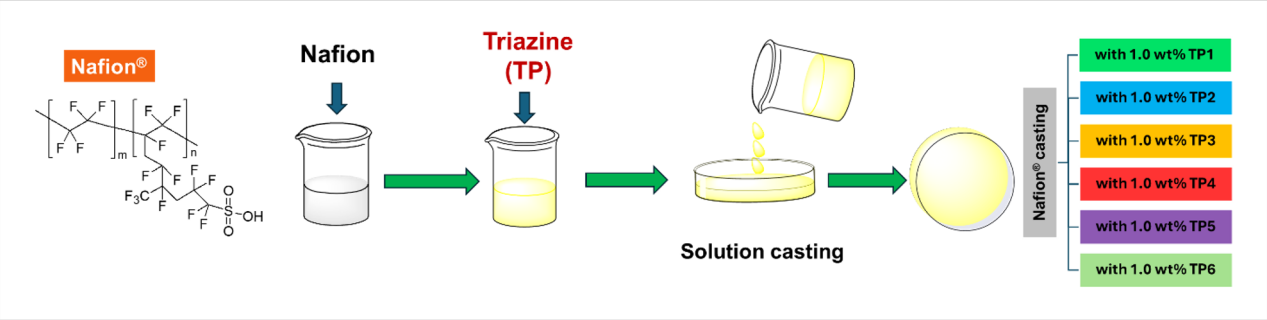

Figure 4: Preparation of the new doped membranes.

The proton conductivity of the new proton exchange membrane is a key property relevant, for example, to the performance of fuel cells. The study of the protonic conductivities of the new modified membranes were determined, in-plane, at 60 ºC, in different relative humidity (RH) conditions (40, 60 and 80%), through electrochemical impedance spectroscopy (EIS) (Figure 5). A prepared recast Nafion and a commercial Nafion N115 membrane were also submitted to EIS analysis, under the same experimental conditions of the prepared membranes, for comparison of their proton conductivities.

An increase in the proton conductivity of all membranes with increasing of RH was observed. All membranes showed a near 4-fold increment in their proton conductivities between 40% to 80% RH conditions.

All membranes showed a better proton conductivity than the recast Nafion membrane. Also, all prepared membranes, with exception of the membrane doped with **TP4**, showed better proton conductivity than commercial Nafion N115.

It was also observed that the membranes doped with aminophenylphosphonate derivatives (**TP1**, **TP2** and **TP3**) show slightly higher proton conductivities compared with hydroxyphenyl derivatives (**TP4**, **TP5** and **TP6**). In both series (aminophenylphosphonate or hydroxyphenylphosphonate derivatives), the membranes doped with phenylphosphonates (**TP1** and **TP4**) showed the lowest proton conductivity compared with the membranes doped with other amino- or hydroxy derivatives. In the case of the membrane doped with triazine **TP6**, with a methylbisphosphonate structure, it is observed similar results compared to the membrane doped with **TP3** with a hydroxymethylphosphonate structure. The best value was observed for the Nafion membrane doped with compound **TP2**, at 80% RH, with a proton conductivity of 83.8 $mS \cdot cm^{-1}$.

Conclusion

This study presents the synthesis of several triazinephosphonates with 4-aminophenyl or 4-hydroxyphenyl moieties, used as dopants in the preparation of new Nafion membranes. The synthesis of these triazinephosphonate derivatives were achieved through the substitution of chlorine atoms of cyanuric chloride (**1**). In these syntheses, different bases were used with different results, with Na_2CO_3 being used to obtain 4-hydroxyphenyl derivatives **TP4**, **TP5** and **TP6**, while DIPEA was used to prepare the 4-aminophenyl counterparts and **TP7**. In the case of the 4-aminophenyl derivatives, only the disubstituted triazine compounds **TP1**–**TP3** were isolated. The proposed structures for these compounds were supported by the spectroscopic data, including NMR, FTIR and MS spectra.

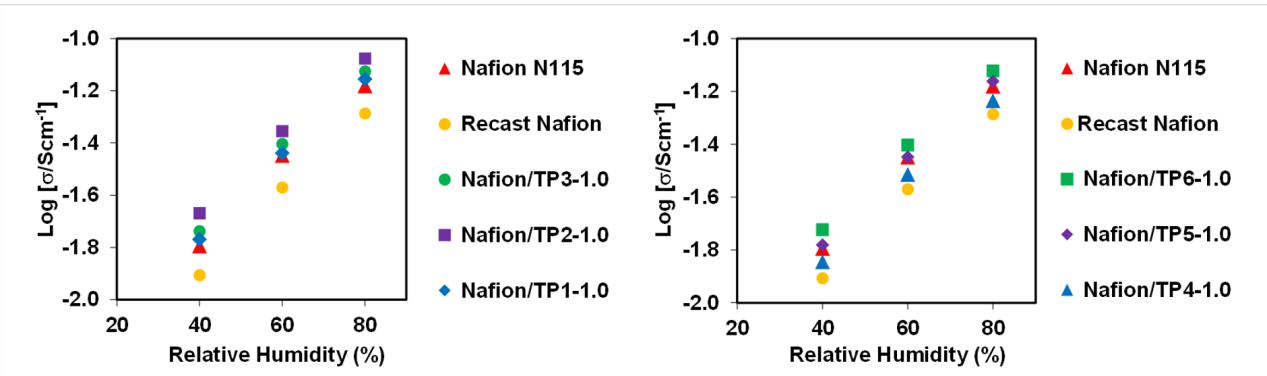

Figure 5: Comparison of in-plane proton conductivity vs RH of Nafion doped membranes, at 60 °C.

New doped Nafion membranes were prepared, with a 1 wt % loading of the dopant, by a casting method developed previously in our group. The proton conduction properties of the new membranes were evaluated by EIS, under different RH conditions, at 60 ºC. The EIS results of the new membranes endorse the proposed strategy delivering new membranes with a better proton conductivity. These results showed that the incorporation of the dopants promotes an increase in the proton conduction of the new membranes, with higher proton conductivity values than recast Nafion and commercial Nafion N115 (with the exception of the membrane doped with **TP4**) under the same experimental conditions. The RH marks a strong influence with large increments in the proton conductivity of all membranes with the increase of RH, up to 4.2-fold, when the measurements were done at 80% RH compared with 40% RH results. Also, disubstituted (4-aminophenyl)triazinephosphonate-doped membranes showed better proton conductivities than trisubstituted (4-hydroxyphenyl)triazinephosphonate-doped membranes in the same experimental conditions. The highest proton conductivity was observed for Nafion doped membrane with compound **TP2**, with a 1.0 wt % loading, with 84 $mS \cdot cm^{-1}$.

Experimental

Materials and methods

Cyanuric chloride (**1**) and diethyl (4-aminophenyl)methylphosphonate (**17**) are commercially available (Sigma-Aldrich, Alfa Aesar). Other acquired reagents and deuterated solvents were used as received, without further purification. Solvents and air-sensitive reagents were distilled under a dry nitrogen atmosphere. Dry THF was distilled from sodium benzophenone ketyl.

A Nafion N115 film was acquired from FuelCell Store and a 20 wt % mixture in lower aliphatic alcohols and water (34%) of Nafion perfluorinated resin solution was purchased from Sigma-Aldrich.

Purification of reaction products was done by column chromatography on silica gel (230–400 mesh) with the appropriate eluent mixture and using a positive pressure of nitrogen.

Spectroscopic characterization

The characterization of the dopants was carried out by Fourier-transform infrared spectroscopy (FTIR), nuclear magnetic resonance (NMR) spectroscopy and mass spectrometry (MS). ^{1}H, ^{13}C and ^{31}P NMR characterization was done using different one- and two-dimensional techniques, and were obtained on a Bruker Avance III HD 400 (^{1}H 400 MHz, ^{13}C NMR 100 MHz, ^{31}P 162 MHz) spectrometer, with the chemical shifts (δ) indicated in ppm, and coupling constants (*J*) in Hz.

The FTIR characterization of the dopants was done on a PerkinElmer FT-IR Spectrum BX Fourier Transform spectrometer, using KBr discs, and the characterization of the membranes was carried out on a Perkin Elmer Spectrum Two, with an attenuated total reflectance (ATR) module, with a wavenumber range from 450 to 4000 cm^{-1}, and their band wavelengths are quoted in cm^{-1}.

Low-resolution and high-resolution (HRMS) mass spectra (MS) were performed on an APEX-Q (Bruker Daltonics) instrument at 'C.A.C.T.I. - Unidad de Espectrometria de Masas', at the University of Vigo, Spain. Melting points were determined on a Reichert Thermovar melting point apparatus and are uncorrected.

Proton conductivity

In-plane proton conductivity (σ) evaluation of the new membranes was performed by electrochemical impedance spectroscopy (EIS), on a commercial BT-112 BekkTech conductivity cell (Scribner Associates Inc.), with a frequency response analyzer Solartron 1250, coupled to a Solartron 1286 electrochemical interface. The measurements were performed with a test signal amplitude of 10 mV, over a frequency range of 65 kHz to 5 Hz. The bulk resistance (R_b) of the membranes were calculated using the ZView software (Version 2.6b, Scribner Associates). A Binder KBF 115 climatic chamber was used to perform the measurements at a temperature of 60 °C and different relative humidity (RH) conditions (40, 60 and 80%). The measurements were performed directly from the temperature-controlled humidity chamber, after a 2 h equilibration period.

The proton conductivity (σ) was calculated using Equation 1

$$\sigma = \frac{L}{AR_b}, \tag{1}$$

where L – distance between the two electrodes (cm), R_b – bulk resistance (Ω), and A - cross-sectional area (cm^2).

Preparation of the dopants

The preparation of all compounds is described in Supporting Information File 1.

Membrane preparation

Membranes were prepared by a casting method using Nafion®/DMAc solutions, based on our previous works, using 1 wt % loading of **TP** dopants. The 20 wt % Nafion solution was dried under reduced pressure, at 40 °C, until a dry residue was obtained. A new 10 wt % solution of Nafion was obtained by dissolution of the dried Nafion in the required amount of *N,N*-

dimethylacetamide (DMAc). The **TP** dopant quantity was added to DMAC solution and the mixture was stirred during 1–5 h, in an ultrasonic bath, to guarantee the complete dissolution of dopants. The resulting solutions were casted on a 5 cm diameter Petri dish and slowly evaporated, until obtaining homogeneous membranes. The resulting membranes were dried in a vacuum oven at 60 °C, and were followed by their annellation for 2 h, at 140 °C. The membranes were activated by a sequential treatment, with 1 h for each step, by boiling them in H_2O_2 solution (3%), washing with hot deionized water, boiling in a 0.5 M sulfonic acid solution, and washing again with hot deionized water. After activation, the membranes were kept in deionized water until their use. The new membranes were labelled as Nafion/TP*i*-1.0, respectively, where *i* indicates the specific triazine used, and 1.0 specifies the wt % of dopant. Recast Nafion films were also prepared, for comparison, without the incorporation of TPs.

Supporting Information

Supporting Information File 1

Experimental data.
[https://www.beilstein-journals.org/bjoc/content/supplementary/1860-5397-20-145-S1.pdf]

Funding

This work was financed by national funds through FCT – Fundação para a Ciência e a Tecnologia, I.P., within the scope of the project PTDC/EQU-EPQ/2195/2021 - CO2RED, and LAQV-REQUIMTE, project UIDB/50006/2020 and UIDP/50006/2020.

ORCID® iDs

Fátima C. Teixeira - https://orcid.org/0000-0003-0801-2068
António P. S. Teixeira - https://orcid.org/0000-0001-7448-0893
C. M. Rangel - https://orcid.org/0000-0001-7996-8142

Data Availability Statement

All data that supports the findings of this study is available in the published article and/or the supporting information to this article.

References

1. Singla, M. K.; Nijhawan, P.; Oberoi, A. S. *Environ. Sci. Pollut. Res.* **2021,** *28,* 15607–15626. doi:10.1007/s11356-020-12231-8
2. Feng, Q.; Yuan, X.-Z.; Liu, G.; Wei, B.; Zhang, Z.; Li, H.; Wang, H. *J. Power Sources* **2017,** *366,* 33–55. doi:10.1016/j.jpowsour.2017.09.006
3. Li, H.; Zhao, H.; Jian, S.; Tao, B.; Gu, S.; Xu, G.; Wang, G.; Chang, H. *J. Mater. Chem. A* **2023,** *11,* 17373–17391. doi:10.1039/d3ta02545d
4. Hossain, M. B.; Islam, M. R.; Muttaqi, K. M.; Sutanto, D.; Agalgaonkar, A. P. *J. Energy Storage* **2023,** *62,* 106842. doi:10.1016/j.est.2023.106842
5. Fan, L.; Tu, Z.; Chan, S. H. *Energy Rep.* **2021,** *7,* 8421–8446. doi:10.1016/j.egyr.2021.08.003
6. Jiang, S.; Sun, H.; Wang, H.; Ladewig, B. P.; Yao, Z. *Chemosphere* **2021,** *282,* 130817. doi:10.1016/j.chemosphere.2021.130817
7. Wang, Y.; Pang, Y.; Xu, H.; Martinez, A.; Chen, K. S. *Energy Environ. Sci.* **2022,** *15,* 2288–2328. doi:10.1039/d2ee00790h
8. Sun, J.; Han, D.; Mohideen, M. M.; Li, S.; Wang, C.; Hu, P.; Liu, Y. *Int. J. Hydrogen Energy* **2024,** *50,* 1456–1480. doi:10.1016/j.ijhydene.2023.10.342
9. Jiao, K.; Xuan, J.; Du, Q.; Bao, Z.; Xie, B.; Wang, B.; Zhao, Y.; Fan, L.; Wang, H.; Hou, Z.; Huo, S.; Brandon, N. P.; Yin, Y.; Guiver, M. D. *Nature* **2021,** *595,* 361–369. doi:10.1038/s41586-021-03482-7
10. Zhang, Z.; Huang, X.; Chen, Z.; Zhu, J.; Endrődi, B.; Janáky, C.; Deng, D. *Angew. Chem., Int. Ed.* **2023,** *62,* e202302789. doi:10.1002/anie.202302789
11. Habibzadeh, F.; Mardle, P.; Zhao, N.; Riley, H. D.; Salvatore, D. A.; Berlinguette, C. P.; Holdcroft, S.; Shi, Z. *Electrochem. Energy Rev.* **2023,** *6,* 26. doi:10.1007/s41918-023-00183-9
12. Shirvanian, P.; van Berkel, F. *Electrochem. Commun.* **2020,** *114,* 106704. doi:10.1016/j.elecom.2020.106704
13. Paidar, M.; Fateev, V.; Bouzek, K. *Electrochim. Acta* **2016,** *209,* 737–756. doi:10.1016/j.electacta.2016.05.209
14. Ran, J.; Wu, L.; He, Y.; Yang, Z.; Wang, Y.; Jiang, C.; Ge, L.; Bakangura, E.; Xu, T. *J. Membr. Sci.* **2017,** *522,* 267–291. doi:10.1016/j.memsci.2016.09.033
15. Mayadevi, T. S.; Goo, B.-H.; Paek, S. Y.; Choi, O.; Kim, Y.; Kwon, O. J.; Lee, S. Y.; Kim, H.-J.; Kim, T.-H. *ACS Omega* **2022,** *7,* 12956–12970. doi:10.1021/acsomega.2c00263
16. Wang, Y.; Ruiz Diaz, D. F.; Chen, K. S.; Wang, Z.; Adroher, X. C. *Mater. Today* **2020,** *32,* 178–203. doi:10.1016/j.mattod.2019.06.005
17. Kim, Y. S. *ACS Appl. Polym. Mater.* **2021,** *3,* 1250–1270. doi:10.1021/acsapm.0c01405
18. Zhang, H.; Shen, P. K. *Chem. Rev.* **2012,** *112,* 2780–2832. doi:10.1021/cr200035s
19. Chen, Y.; Liu, C.; Xu, J.; Xia, C.; Wang, P.; Xia, B. Y.; Yan, Y.; Wang, X. *Small Struct.* **2023,** *4,* 2200130. doi:10.1002/sstr.202200130
20. Hwang, S.; Lee, H.; Jeong, Y.-G.; Choi, C.; Hwang, I.; Song, S.; Nam, S. Y.; Lee, J. H.; Kim, K. *Int. J. Mol. Sci.* **2022,** *23,* 14252. doi:10.3390/ijms232214252
21. Prykhodko, Y.; Fatyeyeva, K.; Hespel, L.; Marais, S. *Chem. Eng. J.* **2021,** *409,* 127329. doi:10.1016/j.cej.2020.127329
22. Karimi, M. B.; Mohammadi, F.; Hooshyari, K. *Int. J. Hydrogen Energy* **2019,** *44,* 28919–28938. doi:10.1016/j.ijhydene.2019.09.096
23. Kusoglu, A.; Weber, A. Z. *Chem. Rev.* **2017,** *117,* 987–1104. doi:10.1021/acs.chemrev.6b00159
24. Teixeira, F. C.; Rangel, C. M.; Teixeira, A. P. S. *New J. Chem.* **2013,** *37,* 3084–3091. doi:10.1039/c3nj00585b
25. Teixeira, F. C.; Rangel, C. M.; Teixeira, A. P. S. *Heteroat. Chem.* **2015,** *26,* 236–248. doi:10.1002/hc.21254
26. Teixeira, F. C.; de Sá, A. I.; Teixeira, A. P. S.; Rangel, C. M. *Appl. Surf. Sci.* **2019,** *487,* 889–897. doi:10.1016/j.apsusc.2019.05.078
27. Teixeira, F. C.; de Sá, A. I.; Teixeira, A. P. S.; Rangel, C. M. *New J. Chem.* **2019,** *43,* 15249–15257. doi:10.1039/c9nj03405f
28. Teixeira, F. C.; de Sá, A. I.; Teixeira, A. P. S.; Ortiz-Martínez, V. M.; Ortiz, A.; Ortiz, I.; Rangel, C. M. *Int. J. Hydrogen Energy* **2021,** *46,* 17562–17571. doi:10.1016/j.ijhydene.2020.01.212

29. Teixeira, F. C.; Teixeira, A. P. S.; Rangel, C. M. *Renewable Energy* **2022,** *196,* 1187–1196. doi:10.1016/j.renene.2022.07.054
30. Afonso, C. A. M.; Lourenço, N. M. T.; Rosatella, A. D. A. *Molecules* **2006,** *11,* 81–102. doi:10.3390/11010081
31. Ali, M. I.; Naseer, M. M. *RSC Adv.* **2023,** *13,* 30462–30490. doi:10.1039/d3ra05953g
32. Patel, R. V.; Kumari, P.; Rajani, D. P.; Pannecouque, C.; De Clercq, E.; Chikhalia, K. H. *Future Med. Chem.* **2012,** *4,* 1053–1065. doi:10.4155/fmc.12.57
33. Gavade, S. N.; Markad, V. L.; Kodam, K. M.; Shingare, M. S.; Mane, D. V. *Bioorg. Med. Chem. Lett.* **2012,** *22,* 5075–5077. doi:10.1016/j.bmcl.2012.05.111
34. Sharma, A.; Sheyi, R.; de la Torre, B. G.; El-Faham, A.; Albericio, F. *Molecules* **2021,** *26,* 864. doi:10.3390/molecules26040864
35. Blotny, G. *Tetrahedron* **2006,** *62,* 9507–9522. doi:10.1016/j.tet.2006.07.039
36. Chauhan, D. S.; Quraishi, M. A.; Nik, W. B. W.; Srivastava, V. *J. Mol. Liq.* **2021,** *321,* 114747. doi:10.1016/j.molliq.2020.114747
37. Dávila Cerón, V.; Illicachi, L. A.; Insuasty, B. *Molecules* **2023,** *28,* 257. doi:10.3390/molecules28010257
38. Zuo, P.; Ye, C.; Jiao, Z.; Luo, J.; Fang, J.; Schubert, U. S.; McKeown, N. B.; Liu, T. L.; Yang, Z.; Xu, T. *Nature* **2023,** *617,* 299–305. doi:10.1038/s41586-023-05888-x
39. Xiong, P.; Zhang, S.; Wang, R.; Zhang, L.; Ma, Q.; Ren, X.; Gao, Y.; Wang, Z.; Guo, Z.; Zhang, C. *Energy Environ. Sci.* **2023,** *16,* 3181–3213. doi:10.1039/d3ee01360j
40. Yu, J.; Sun, X.; Xu, X.; Zhang, C.; He, X. *Appl. Catal., B* **2019,** *257,* 117935. doi:10.1016/j.apcatb.2019.117935
41. Branowska, D.; Olender, E.; Wysocki, W.; Karczmarzyk, Z.; Bancerz, I.; Ledwon, P.; Lapkowski, M.; Mirosław, B.; Urbańczyk-Lipkowska, Z.; Kalicki, P. *Electrochim. Acta* **2016,** *214,* 19–30. doi:10.1016/j.electacta.2016.08.019
42. Xiang, Y.; Gong, S.; Zhao, Y.; Yin, X.; Luo, J.; Wu, K.; Lu, Z.-H.; Yang, C. *J. Mater. Chem. C* **2016,** *4,* 9998–10004. doi:10.1039/c6tc02702d
43. Diab, H. M.; Abdelmoniem, A. M.; Shaaban, M. R.; Abdelhamid, I. A.; Elwahy, A. H. M. *RSC Adv.* **2019,** *9,* 16606–16682. doi:10.1039/c9ra02749a
44. Diab, H. M.; Salem, M. E.; Abdelhamid, I. A.; Elwahy, A. H. M. *RSC Adv.* **2020,** *10,* 44066–44078. doi:10.1039/d0ra09025e
45. Sharma, A.; El-Faham, A.; de la Torre, B. G.; Albericio, F. *Front. Chem. (Lausanne, Switz.)* **2018,** *6,* 516. doi:10.3389/fchem.2018.00516
46. Zhang, R.-F.; Hu, W.-J.; Liu, Y. A.; Zhao, X.-L.; Li, J.-S.; Jiang, B.; Wen, K. *J. Org. Chem.* **2016,** *81,* 5649–5654. doi:10.1021/acs.joc.6b01115
47. Tominaga, M.; Noda, A.; Ohara, K.; Yamaguchi, K.; Itoh, T. *Chem. Lett.* **2016,** *45,* 773–775. doi:10.1246/cl.160347
48. Klinkebiel, A.; Beyer, O.; Malawko, B.; Lüning, U. *Beilstein J. Org. Chem.* **2016,** *12,* 2267–2273. doi:10.3762/bjoc.12.219
49. Liu, T.-T.; Liang, J.; Huang, Y.-B.; Cao, R. *Chem. Commun.* **2016,** *52,* 13288–13291. doi:10.1039/c6cc07662a
50. Dey, S.; Bhunia, A.; Esquivel, D.; Janiak, C. *J. Mater. Chem. A* **2016,** *4,* 6259–6263. doi:10.1039/c6ta00638h
51. Gooßen, L. J.; Dezfuli, M. K. *Synlett* **2005,** 445–448. doi:10.1055/s-2005-862372
52. Kim, Y.-C.; Brown, S. G.; Harden, T. K.; Boyer, J. L.; Dubyak, G.; King, B. F.; Burnstock, G.; Jacobson, K. A. *J. Med. Chem.* **2001,** *44,* 340–349. doi:10.1021/jm9904203
53. Boyer, S. H.; Jiang, H.; Jacintho, J. D.; Reddy, M. V.; Li, H.; Li, W.; Godwin, J. L.; Schulz, W. G.; Cable, E. E.; Hou, J.; Wu, R.; Fujitaki, J. M.; Hecker, S. J.; Erion, M. D. *J. Med. Chem.* **2008,** *51,* 7075–7093. doi:10.1021/jm800824d
54. Chow, H.-F.; Mak, C. C. *J. Org. Chem.* **1997,** *62,* 5116–5127. doi:10.1021/jo970383s
55. Rao, K. U. M.; Sundar, C. S.; Prasad, S. S.; Rani, C. R.; Reddy, C. S. *Bull. Korean Chem. Soc.* **2011,** *32,* 3343–3347. doi:10.5012/bkcs.2011.32.9.3343
56. Vovk, A. I.; Kalchenko, V. I.; Cherenok, S. A.; Kukhar, V. P.; Muzychka, O. V.; Lozynsky, M. O. *Org. Biomol. Chem.* **2004,** *2,* 3162–3166. doi:10.1039/b409526j
57. Németh, G.; Greff, Z.; Sipos, A.; Varga, Z.; Székely, R.; Sebestyén, M.; Jászay, Z.; Béni, S.; Nemes, Z.; Pirat, J.-L.; Volle, J.-N.; Virieux, D.; Gyuris, Á.; Kelemenics, K.; Áy, É.; Minarovits, J.; Szathmary, S.; Kéri, G.; Őrfi, L. *J. Med. Chem.* **2014,** *57,* 3939–3965. doi:10.1021/jm401742r
58. Tahmassebi, D. C.; Sasaki, T. *J. Org. Chem.* **1994,** *59,* 679–681. doi:10.1021/jo00082a034
59. Danilczuk, M.; Lin, L.; Schlick, S.; Hamrock, S. J.; Schaberg, M. S. *J. Power Sources* **2011,** *196,* 8216–8224. doi:10.1016/j.jpowsour.2011.05.067
60. Giffin, G. A.; Haugen, G. M.; Hamrock, S. J.; Di Noto, V. *J. Am. Chem. Soc.* **2013,** *135,* 822–834. doi:10.1021/ja3099799
61. Gruger, A.; Régis, A.; Schmatko, T.; Colomban, P. *Vib. Spectrosc.* **2001,** *26,* 215–225. doi:10.1016/s0924-2031(01)00116-3
62. Singh, R. K.; Kunimatsu, K.; Miyatake, K.; Tsuneda, T. *Macromolecules* **2016,** *49,* 6621–6629. doi:10.1021/acs.macromol.6b00999
63. Liang, Z.; Chen, W.; Liu, J.; Wang, S.; Zhou, Z.; Li, W.; Sun, G.; Xin, Q. *J. Membr. Sci.* **2004,** *233,* 39–44. doi:10.1016/j.memsci.2003.12.008
64. Jung, J.; Cho, E. H.; Hwang, S. S.; Won, J. *ChemistrySelect* **2018,** *3,* 5769–5777. doi:10.1002/slct.201800020

License and Terms

BEILSTEIN JOURNAL OF ORGANIC CHEMISTRY

2-Heteroarylethylamines in medicinal chemistry: a review of 2-phenethylamine satellite chemical space

Carlos Nieto*, Alejandro Manchado, Ángel García-González, David Díez and Narciso M. Garrido

Review

Open Access

Address:
Department of Organic Chemistry, Faculty of Chemical Sciences, University of Salamanca, Pl. Caídos, s/n, 37008 Salamanca, Spain

Email:
Carlos Nieto* - eneas@usal.es

* Corresponding author

Keywords:
bioisosteres; 2-heteroarylethylamines; medicinal chemistry; 2-phenethylamine; scaffold hopping

Beilstein J. Org. Chem. **2024,** *20,* 1880–1893.
https://doi.org/10.3762/bjoc.20.163

Received: 30 April 2024
Accepted: 19 July 2024
Published: 02 August 2024

This article is part of the thematic issue "5th International Symposium on Synthesis and Catalysis (ISySyCat 2023)".

Guest Editor: A. Burke

Abstract

The concept of bioisostere replacement is of paramount importance in medicinal chemistry, as it can be employed as a rational to expand bioactive chemical space to tackle lead optimization issues like lack of potency, efficacy, and selectivity or pharmacokinetic/dynamic issues. One of the most important building blocks (in the sense of participating in a vast area of chemical space of biological importance) in medicinal chemistry is the 2-phenethyl moiety, a key component of diverse drug-like entities. Although the core 2-phenethylamine structure has been recognized by the drug discovery community, little attention has been given to the various ring-based rescaffolding procedures that can be conducted with this unit. In this regard, a review on the use of 2-heteroarylethylamines displaying pharmacological activity is reported. A detailed description of flexible, amine-opened motifs is provided, that describes therapeutic targets and other potent bioactive examples, which will be a valuable repository of phenyl, heteroaryl, and other replacement units of high value to the drug discovery community.

Introduction

One of the major hit-2-lead exploration techniques in any medicinal chemistry program – knowledge-based or computationally aided – is bioisosteric replacement, where a particular arrangement of atoms, such as a functional group, chain, ring, linker, etc., is substituted by motifs with size, electronic, and physicochemical characteristics comparable to the original [1]. The main purpose of this approach is quality improvement, such as activity, selectivity, bioavailability, metabolism, and/or toxicity, while expanding the chemical space surrounding bioactive compounds [2,3]. Benzene-to-heteroaromatic ring replacement represents a classical structural hopping strategy, as five- or six-membered heterocyclic aromatic rings are widespread entities in

drug discovery [4]. In this sense, any bioactive molecule enclosing a benzene ring in its initial optimization stages could undergo a heteroaromatic replacement.

2-Phenethylamines are notable bioactive compounds towards different disease-related receptors, as it was described in our previous work [5]. By means of benzene ring aromatic rescaffolding, it is possible to access the 2-heteroarylethylamine neighboring space. This satellite chemical region is rich not only in structures displaying affinity to key phenethylamine targets like adrenergic or histamine-type receptors, but also to novel ones such as TAAR1 (trace-amine-associated receptor 1), σ1/2 (sigma receptors 1 and 2), or AChE (acetylcholinesterase). Similar to our previous review, a descriptive, simple scope is presented below to outline which structural motifs are included in this work and which ones are discarded (Scheme 1). In detail, this review encompasses bioactive compounds which satisfy:

- flexible, open chain-substituted 5/6-membered heteroaromatic scaffolds with decorations,
- condensed heteroaromatic or polycyclic systems featuring an exocyclic amine (and their substitutions).

Systems out of scope of this review are those, where:

- non-basic ethylamine systems are present (featuring other functionalities due to oxidation states),
- condensed or polycyclic systems are present and featuring a key amine embedded in a (poly)cycle.

Consequently, a dedicated review covering the 2-heteroarylethylamine space is presented here. This work is divided into subsections covering individual heteroaryl replacements and target bioactive deployment, rather than a pure disease-related target division as in our previous review. The absence of a specific heteroaromatic subsection indicates no biologically relevant data has been reported up to date.

Review

2-Heteroarylethylamine scaffolds of biological importance

Six-membered heteroaromatic rings

Pyridines: *IL4I1*, interleukin-4 induced gene 1, encodes L-phenylalanine oxidase IL4I1 present in the tumor bed of a vast diversity of human tumor types. As phenylalanine is the preferred substrate of IL4I1 catalytic activity, Presset et al. [6] reported novel phenylalanine derivatives as a strategy to inhibit IL4I1 activity, as this enzyme has a preference for hydrophobic amino acids. Among them, commercial compound **1** (Scheme 2) represents a rescaffolding exercise to pyridine retaining low inhibitory activity although it was found toxic in in vitro assays on a human T-cell line and PBMCs (periferal blood mononuclear cells).

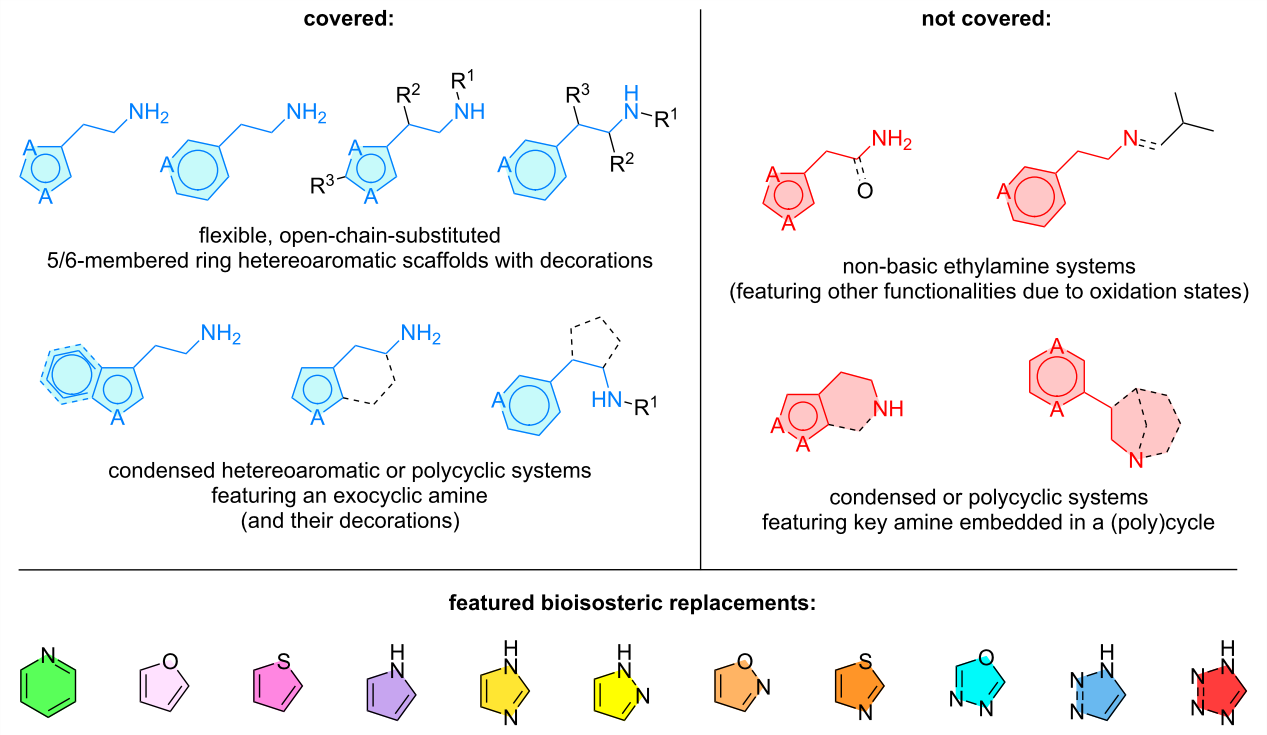

Scheme 1: Description of the 2-heteroarylethylamine scope of the present review featuring appropriate heteroaromatic systems (A = O, N, S).

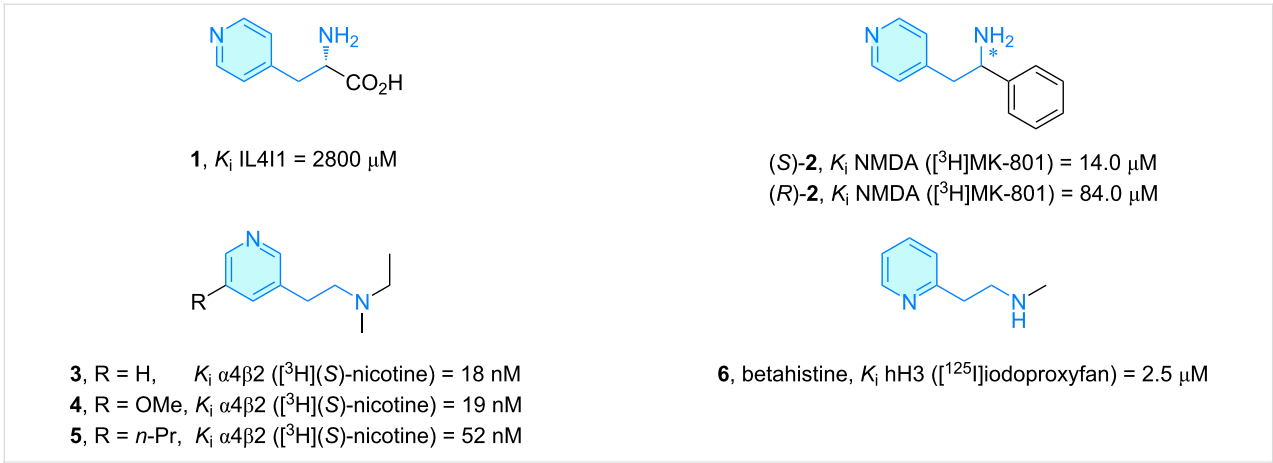

Scheme 2: 2-Aminoethylpyridine derivatives with therapeutic activity.

The derivatives (*R*)-**2** and (*S*)-**2** were elaborated by Berger et al. [7] in the course of an extensive screening of NMDA (*N*-methyl-D-aspartate) channel blockers resembling 1,2-diphenylethylamines. A channel pharmacophore description was envisaged collecting data from stereoisomers of 1,2-diphenylethylamine derivatives and 1,2-dicyclohexylethylamine derivatives. Among them, isomer (*S*)-**2**, also called lanicemine, AZD6765 or AR-R15896AR, was described as a competitive ketamine alternative without psychotomimetic side effects, although potency and selectivity were significantly lower (Scheme 2) [8,9].

Dukat et al. [10] developed flexible 3-(2-aminoethyl)pyridine (AEP) analogs **3**–**5** as α4β2 nicotinic cholinergic receptor ligands with nanomolar activities in rat brain homogenates (Scheme 2). The idea behind these AEP structures was to check activity correlation against a nicotine series. The comparison of K_i values of both series showed a moderate correlation, which opens the possibility of different binding topologies to the α4β2 receptor.

Betahistine (**6**) is an orally active 2-(2-aminoethyl)pyridine drug indicated for vestibular disorders like Meniere's disease, whose patients exhibit acute vertigo attacks (Scheme 2) [11,12]. Gbahou et al. [13] demonstrated histaminergic synapse improvement through inverse agonism at histamine receptor 3 (H_3) using recombinant isoforms. This finding corrects their previous assumption of betahistidine acting as an antagonist. Inhibition of cAMP formation and [^{3}H]arachidonic acid release concluded the inverse agonist role.

Five-membered heteroaromatic rings

Furans: Racemic heteroarylisopropylamines were described as MAO inhibitors (monoamine oxidase) by Vallejos et al. [14] as a natural extension of their previous QSAR studies using phenylisopropylamines [15]. The authors supported their aryl-to-heteroaryl group hopping due to the success of similar replacements leading to novel MAO-A bioactive entities [16,17]. The brominated analogue **8** showed moderate MAO-A activity compared to the parent 2-furyl compound **7**, as a result of increased polarizability. The condensed benzofuran **9** revealed submicromolar MAO-A potency, a resemblance to the indole system of 5-hydroxytryptamine (a MAO-A substrate), in a molecular docking experiment tested against serotonin (Scheme 3).

A similar class of benzofuran systems with attractive binding properties are those represented by 4-amino-3-(benzo[*b*]furan-2-yl)butanoic acids, baclofen analogs, elaborated to elucidate the structural requirements for access to γ-aminobutyric receptor type B ($GABA_B$) [18]. Amino acids **10**–**12** were demonstrated [19-21] to act as substrates of $GABA_B$ (Scheme 3), key metabotropic receptors from the G-protein-coupled receptor superfamily responsible for CNS inhibitory synapses [22]. The authors concluded that a heteroaromatic ring bound to the C3 position of the GABA chain is well tolerated for activity.

Thiophenes: Back to the MAO-A scenario, Vallejo et al. [14] also developed thienyl-substituted isopropylamines **13**–**16**, which were found to bind to MAO-A with IC_{50} values in the micromolar range with better inhibitory data than for the aforementioned furyl analogues (Scheme 4). The authors suggested the replacement of furyl by a more polarizable aromatic ring such as thienyl as prospective origin of the observed IC_{50} downward shift.

Berthelot et al. [23,24] expanded their studies on $GABA_B$ inhibitors from furanyl derivatives to thienyl-substituted compounds **17**–**23** in the search to elucidate structural features for accessing

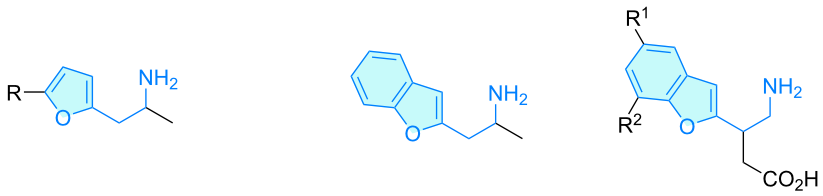

7, R = H, IC_{50} MAO-A > 100 μM
8, R = Br, IC_{50} MAO-A = 44.8 μM

9, IC_{50} MAO-A = 0.8 μM

10, R^1 = H, R^2 = Me, IC_{50} $GABA_B$ (*rac*-[^{3}H]-baclofen) = 5.4 μM
11, R^1 = Cl, R^2 = H, IC_{50} $GABA_B$ (*rac*-[^{3}H]-baclofen) = 17.0 μM
12, R^1 = OMe, R^2 = H, IC_{50} $GABA_B$ (*rac*-[^{3}H]-baclofen) = 5.6 μM

Scheme 3: 2-Aminoethylfuran derivatives with therapeutic activity.

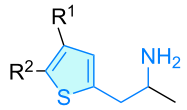

13, R^1 = H, R^2 = H, IC_{50} MAO-A > 100 μM
14, R^1 = Br, R^2 = H, IC_{50} MAO-A = 17.8 μM
15, R^1 = H, R^2 = Br, IC_{50} MAO-A = 15.8 μM

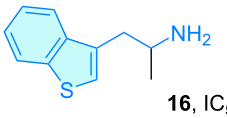

16, IC_{50} MAO-A = 16.2 μM

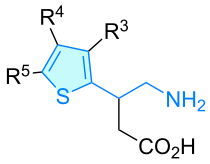

compound	R^3	R^4	R^5	IC_{50} $GABA_B$ ((*R*)-[^{3}H]-baclofen)
17	H	H	H	9.72 μM
18	H	H	Me	1.34 μM
19	Me	H	H	124 μM
20	H	H	Br	1.86 μM
21	H	Br	H	39.1 μM
22	H	H	Cl	0.61 μM
23	H	Cl	H	45.3 μM

Scheme 4: 2-Aminoethylthiophene derivatives with therapeutic activity, part 1.

this receptor (Scheme 4). The chloride- and bromide-substituted thienyl derivatives encompassed micromolar to submicromolar activities in radioligand binding assays based on (*R*)-[^{3}H]-baclofen displacement. QSAR studies have been developed in order to examine the pivotal role of the aromatic moiety of baclofen-like compounds [25]. In this sense, the QSAR equation revealed HOMO/LUMO orbital energies are critical for a high correlation with binding strength.

An in vivo antihypertensive activity was demonstrated for a series of flexible secondary amines incorporating terminal aromatic rings by Bagli et al. [26]. A blood pressure lowering effect was observed for 2-hydroxy-2-thienylethylamines **24**–**26** (Scheme 5), which was related to typical antihypertensive pathways like adrenergic system interference, catecholamine depletion, or plasma volume lowering.

The 20S proteasome core particle represents a critical degradation machinery for cellular homeostasis [27]. A set of (thiophen-2-yl)cycloalkyl(phenoxypropanol)amines **27**–**29** was tested against caspase-like and chymotrypsin-like activities of this supramolecular complex (Scheme 5), with positive in vitro activities in 20S proteasome core particles isolated from rabbit erythrocytes [28].

The sulfonamide **30** (Scheme 6) has been evaluated as inhibitor of human carbonic anhydrase I/II (hCA I and II), which catalyze the reversible hydration reaction of carbon dioxide to bicarbonate, cyanates to carbamic acids, aldehydes to *gem*-diols, etc., and represent a potential therapeutic target for diseases like osteoporosis, edema, obesity or cancer [29]. Alım et al. [30] evaluated a series of thiophene sulfonamides based on the high stability of this aromatic ring. Molecular docking studies combined with in vitro studies showed that only the thiophene-based phenethylamine derivative **30** possesses a weak hCA I/II activity compared with analogues lacking the 2-aminoethyl moiety.

Carrol et al. [31,32] explored bupropion analogues for their capacity to antagonize human nAChRs (nicotinic acetylcholine

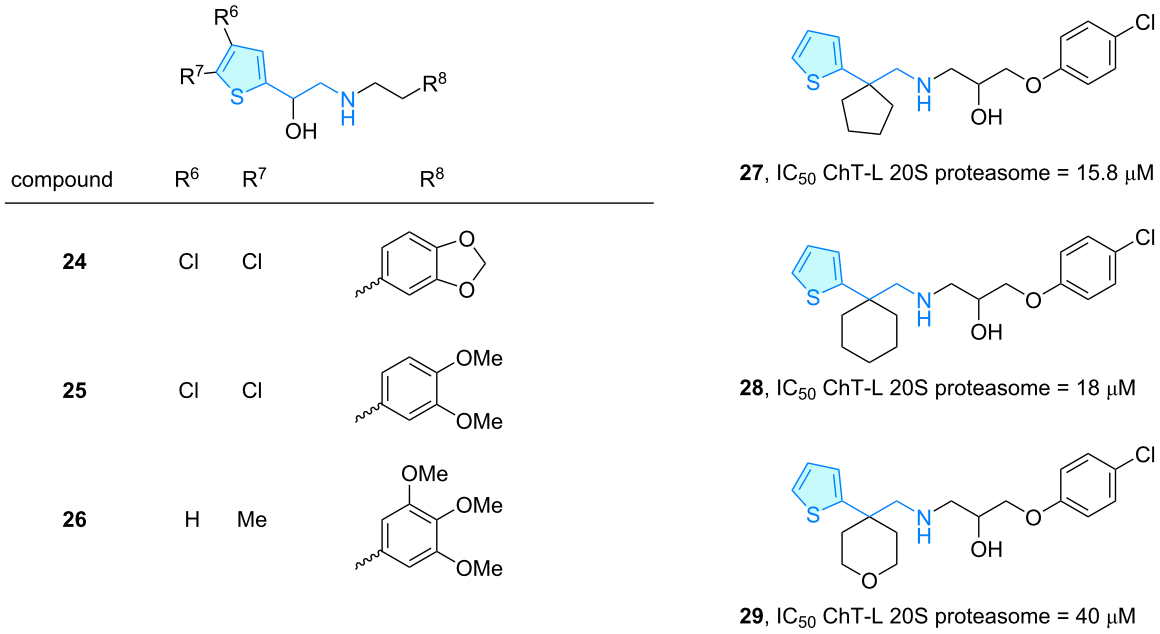

Scheme 5: 2-Aminoethylthiophene derivatives with therapeutic activity, part 2.

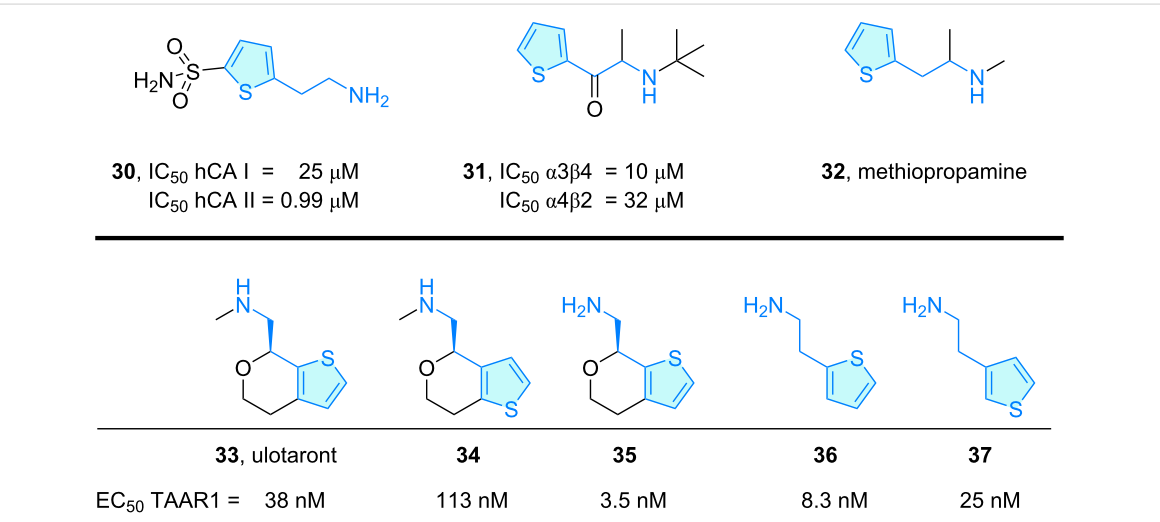

Scheme 6: 2-Aminoethylthiophene derivatives with therapeutic activity, part 3.

receptor) as these are of clinical importance in developing tobacco-derived diseases. From the range of propiophenone derivatives elaborated tackling dopaminergic activities, thiophene **31** showed weak inhibitory activity towards α3β4 and α4β2 (Scheme 6).

Methiopropamine (**32**) [33] is an emergent psychoactive substance structurally similar to methamphetamine, where the aromatic moiety was rescaffolded from benzene to thiophene (Scheme 6). First synthesized in 1942 [34], it irrupted into the recreational drug market in 2011 [35], with acute toxicity reports in hospital admissions. Nguyen et al. [36] investigated its effects in mice, demonstrating neurotoxicity via dopamine receptors, while Tuv et al. [37] studied the compound's phamarcokinetics, pharmacodynamics, and mode of action in comparison to methamphetamine, which revealed a significantly lower potency of **32**.

Ulotaront (**33**, SEP-363856) [38] is a phase-3 clinical lead for the treatment of schizophrenia, displaying TAAR1 (trace-amine-associated receptor 1) [39] and 5-HT1A agonism as mode of action, lacking dopamine D2 and 5-HT2A antagonism.

SAR exploration of the ulotaront family was envisaged by Heffernan et al. [40], including human TAAR1 agonist activity and structural evaluation via homology model development followed by molecular docking and molecular dynamics studies (Scheme 6). Structural features like sulfur location and ring opening of the aminoethyl section were investigated computationally, identifying key interactions to understand TAAR1 agonism.

Pyrroles: New histamine-related compounds were synthesized and evaluated towards activation of human carbonic anhydrase isoforms (hCA), aiming at potency and selectivity enhancement by Chiaramonte et al. [41]. Among them, a discrete set of 2-aminoethylpyrrole (Scheme 7) hits were elaborated and tested in a stopped-flow CO_2 hydrase assay. Comparing this pyrrole family with original histamine inferred a decrease in selectivity towards the hCA VII isoform, while activity was not affected significantly.

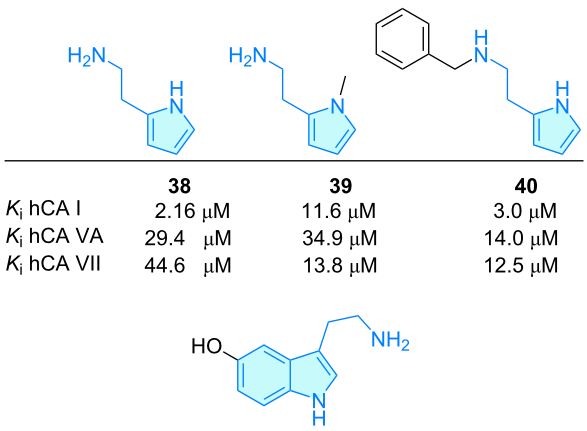

Scheme 7: 2-Aminoethylpyrrole derivatives with therapeutic activity.

Tryptamine derivatives, i.e., compounds derived from 2-(indole-3-yl)ethylamine, comprise a huge number of indole compounds such as serotonin (**41**) [42] (Scheme 7). These compounds play an important role for a variety of biological targets, from 5-HT (serotonin receptors) to RAS [43,44], and are used to treat disorders as diverse as obesity, oncology, CNS disorders, etc. Following these overwhelming features, these are not included in this work as capturing an adequate group of representatives, even selecting only the most prominent ones, would mask other heteroaromatic structures.

Imidazoles: Probably, the pinnacle of the 2-heteroarylethylamine chemical space is constituted by the biogenic amine histamine (**43**). In a similar fashion as dopamine and epinephrine produced from L-phenylalanine along the catecholamine pathway, histamine is generated from the amino acid L-histidine (**42**) via enzymatic decarboxylation promoted by L-histidine decarboxylase (Scheme 8) [45-47]. Histamine is commonly degradated by two enzymes: diamine oxidase (DAO) to produce (imidazol-4-yl)acetic acid (**44**), or histamine *N*-methyltransferase (HMT) to *N*-methylhistamine **45**. Monoamine oxidase B (MAO-B) transforms *N*-methylhistamine into (*N*-methylimidazol-4-yl)acetic acid (**46**). The major source of histamine are mast cells, although it is additionally biosynthesized in basophils, other immune cells, and tissues like intestinal mucosa, skin, or the heart [45,48].

Histamine plays many pivotal roles in the onset of allergies via Th2 cytokine secretion and inhibition of Th1 cytokine,

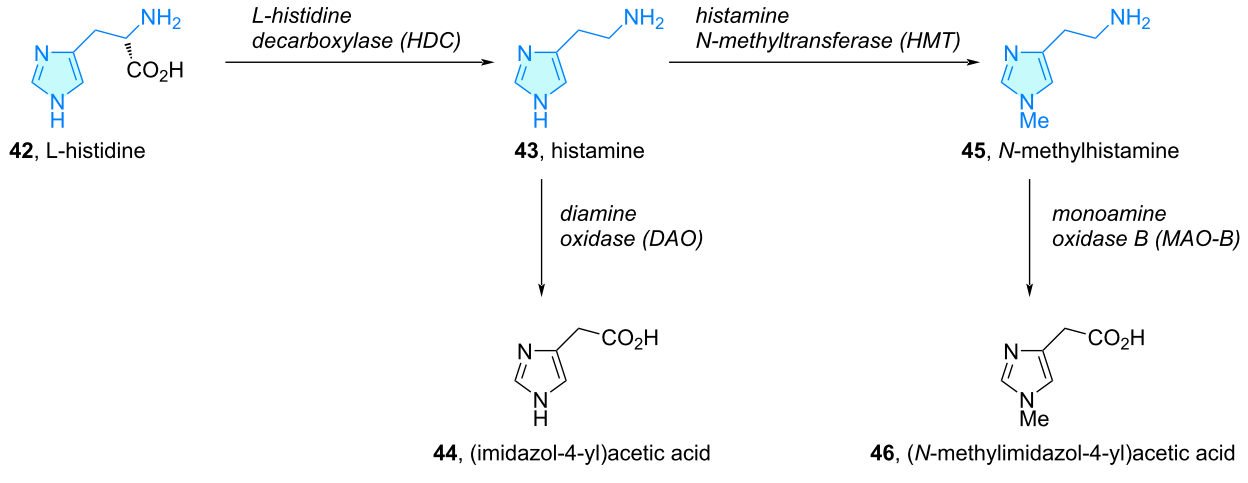

Scheme 8: Histamine metabolic pathway.

leukotriene and chemokines release, or IL-6 induction. Histamine targets histamine receptors H1–4, triggering pro-inflammatory or anti-inflammatory events depending on the receptor type and cells involved [45,49]. Histamine also plays a critical role in both vertebrates and invertebrates as neurotransmitter, in the so called histaminergic synapses [50]. As a consequence, histamine has been used as a template to rationally design histamine receptor agonists/antagonists capable to modulate their extensive range of capabilities.

(*R*)-α-Methylhistamine (**51**) is an H_3 receptor agonist approximately 15-fold more active than histamine (Scheme 9). Gannellin et al. [51] performed a discrete H_3 SAR study starting from compound **51** and investigated the effect of the position of the methyl group on the agonist activity. Analogues **50** and **53**, having the methyl group in the aminoethyl side chain, showed almost a 3-fold potency compared to histamine, while the derivatives **47**–**49** with a methyl group attached to the imidazole core demonstrated lower relative potency. The derivative **54** was investigated towards its effect against the H_4 receptor, recently [52-54]. Furthermore, an antagonistic H_3 SAR study was achieved creating *N*-arylimidazolethylamine counterparts **55**–**59** (Scheme 9). It was shown, that electron-withdrawing substituents at the pyridine 5-position lowered the antagonistic activity for this small family.

Conformationally restricted cyclopropylhistamine analogues were disclosed by De Esch et al. [55] and by Kazuta el al. [56]. The primary aim was the design of a new class of highly H_3-selective agonists lacking H_4 affinity by restricting the flexibility of the aminoethyl chain. Previous structure–activity exercises demonstrated an impact on selectivity upon introducing a stereocenter into the flexible aminoethyl chain [57]. Radioligand binding assays showed activities in the nanomolar range for the four diastereomers, while functional assays demonstrated only H_3-subtype activity for compound **63**, with no H_4 subtype activity, which was the original goal (Scheme 10).

Histaprodifen **64** is a potent H_1 receptor agonist with a 3,3-diphenylpropyl moiety at position 2 of the imidazole ring characterized by Elz and co-workers [58]. The authors showed parent compound **64** and methylated derivatives **65** and **66** were

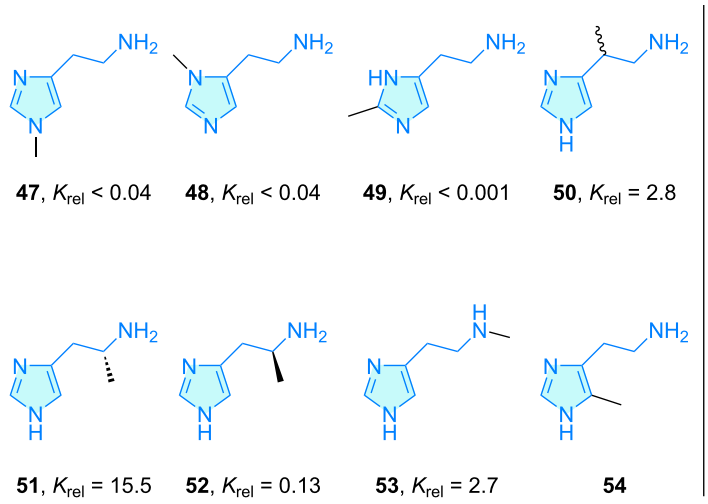

compound	55	56	57	58	59
R	–H	–NO_2	–CF_3	–CO_2Me	–NH_2
K_i (nM)	200	29	17	42	186

Scheme 9: 2-Aminoethylimidazole derivatives with therapeutic activity, part 1. K_{rel} is referred as histamine relative potency (basal reference 1.0).

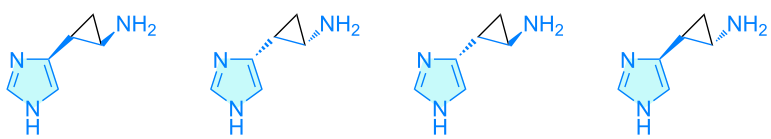

compound	**60**	**61**	**62**	**63**
K_i H_3 ([^{3}H]-*N*-α-methylhistamine) (nM)	91	1380	42	4.30

Scheme 10: Conformationally restricted 2-aminoethylimidazole derivatives with therapeutic activity, part 2.

potent H_1 receptor agonists in pithed and anaesthetized rats (Scheme 11). Later, the authors expanded the histaprodifen family by SAR exploration of small substituents in the phenyl rings (compounds **67**–**78**, Scheme 11) [59,60]. While pEC_{50} values varied very subtle, a histamine relative potency screening revealed a general reduction in potency. Following the same assay, Menghin and co-workers [61] explored flexible chain incorporations at the terminal nitrogen of histaprodifen generating hits **79**–**86** (Scheme 11). Finally, the *N*,*N*-bis(2-imidazolyl)ethyl)-substituted amine superhistaprodifen **87** cluster was exhaustively synthesized and tested for their agonist activity against the H_1 receptor by Straßer et al. [62]. From the set of compounds, biological assays revealed pK_i values of 4.5–7.5 in human, rat, bovine, and guinea pig H_1 receptor activities. Additional modelling studies via CoMFA (comparative molecular field analysis) and posterior comparison with experi-

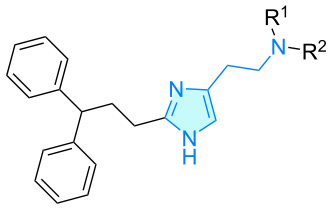

compound	pED_{50}
64, histaprodifen (R^1 = R^2 = H)	7.55
65, methylhistaprodifen (R^1 = H, R^2 = Me)	8.43
66, dimethylhistaprodifen (R^1 = R^2 = Me)	8.12

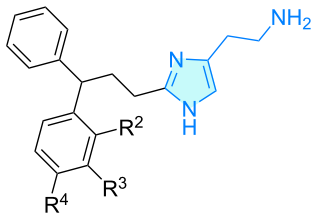

compound	R^2	R^3	R^4	pEC_{50}	relative potency (histamine)
67	F	H	H	5.66	0.09
68	H	F	H	6.66	0.92
69	H	H	F	6.33	0.43
70	Cl	H	H	6.18	0.30
71	H	Cl	H	6.65	0.89
72	H	H	Cl	5.72	0.10
73	Br	H	H	6.31	0.41
74	H	Br	H	6.42	0.52
75	H	H	Br	5.61	0.08
76	Me	H	H	6.25	0.35
77	H	Me	H	5.99	0.20
78	H	CF_3	H	5.27	0.04

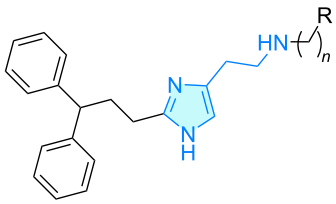

compound	*n*	R	pEC_{50}	relative potency (histamine)
79	2	4-imidazolyl	8.26	36.30
80	3	4-imidazolyl	7.87	14.68
81	4	4-imidazolyl	6.91	1.63
82	4	2-pyridyl	8.16	28.56
83	5	2-pyridyl	7.81	12.97
84	3	3-pyridyl	6.93	1.69
85	4	3-pyridyl	7.87	14.79
86	4	4-pyridyl	7.62	8.32

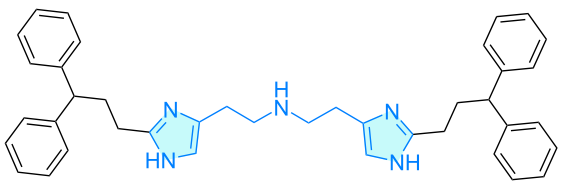

87 superhistaprodifen-like compounds

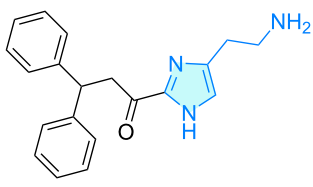

88, pEC_{50} H_1 = 5.78 μM

Scheme 11: 2-Aminoethylimidazole derivatives with therapeutic activity, part 3.

mental data showed good agreement, suggesting two different binding topologies. Patil et al. [63] synthesized compound **88**, an oxidized version at position 1 of the propyl chain, and observed H-type agonism in guinea pig ileum assays (Scheme 11).

The sulfur-containing histidine compounds ovothiol (**90**) and thiohistidine (**89**) were evaluated for skincare anti-inflammatory properties by Brancaccio et al. (Scheme 12) [64]. These compounds, biosynthesized by microalgae, bacteria and marine invertebrates feature skin protection via Nrf2 activation (nuclear factor erythroid 2-related factor 2).

Antimalarial properties against chloroquine-sensitive and resistant *Plasmodium falciparium* strains in mice were reported by Jain and co-workers [65]. Initially, these authors developed simple halohistidine derivatives as first generation analogues showing successful in vitro antimalarial activity. Prompted by these findings, a second generation series, i.e., compounds **91**–**94** (Scheme 12), featuring simple hydrocarbon substituents was elaborated. This collection showed good activities, demonstrating the tolerance of introducing bulky moieties at position C2 or N1 of the imidazole ring. Researchers also described positive membrane diffusion features related to these changes.

The amino acid L-histidine has attracted the attention of the medicinal chemistry community due to its properties not only in the aforementioned histaminergic system, but also as metal-ion chelator, proton buffering modulator, and antioxidant. Considering the importance and applications of ring-modified histidines, Sharma et al. [66] reviewed the design, synthesis, and medicinal chemistry of these motifs covering antimicrobial, antiplasmodial, CNS and anticancer applications among others.

Pyrazoles: Betazole (**95**) is a pyrazole-like histamine analogue with H_2 receptor agonist activity (Scheme 13) and is employed as a stimulant of gastric secretion, with a 10-fold weaker activity compared to parent histamine [67]. Betazole and its isomer **96** were also found to be moderately active in the activation of human carbonic anhydrase isoforms as reported by Chiaramonte et al. (Scheme 13) [41].

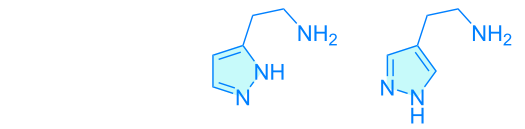

	95, betazole	**96**
K_a hCA I	11.6 μM	28.4 μM
K_a hCA VA	37.9 μM	51.0 μM
K_a hCA VII	32.8 μM	23.7 μM

Scheme 13: 2-Aminoethylpyrazole derivatives with therapeutic activity.

Isoxazole: Homoibotenic acid (HIBO) analogues are known ligands with pharmacological bioactive profile towards ionotropic and metabotropic glutamate receptors (iGluR and mGluR). 4-Substituted HIBO compounds **97** and **98** (Scheme 14) portrayed by Madsen et al. [68] and Kromann et al. [69] were investigated to search new selectivity profiles. They presented different affinities towards glutamate receptors, with good potencies for the Glu1, Glu2 and Glu5 receptors. The high selectivity achievement is related to neuroprotective or neurotoxic applications following authors studies.

Thiazoles: 2-Thiazolylethylamine was characterized as a more selective and potent histamine H_1 agonist [70]. Based on this,

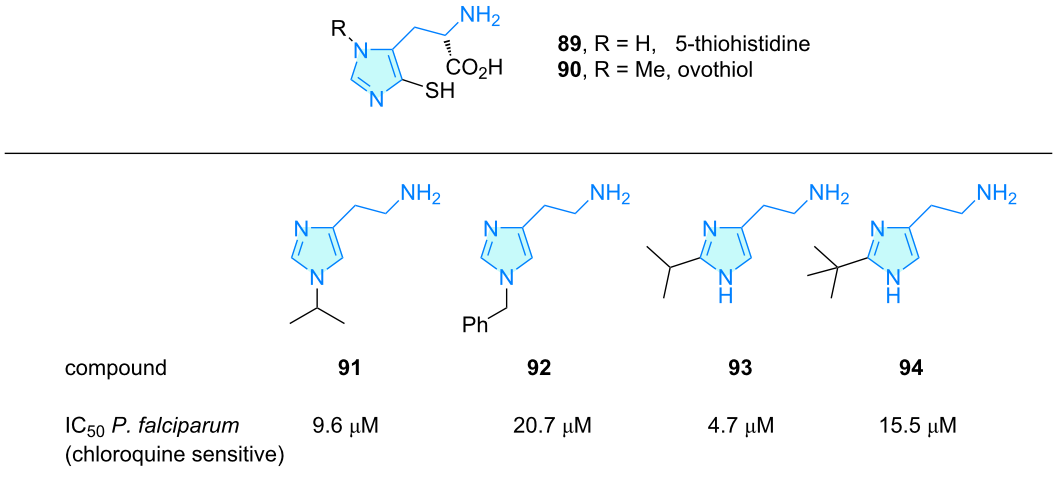

Scheme 12: 2-Aminoethylimidazole derivatives with therapeutic activity, part 4.

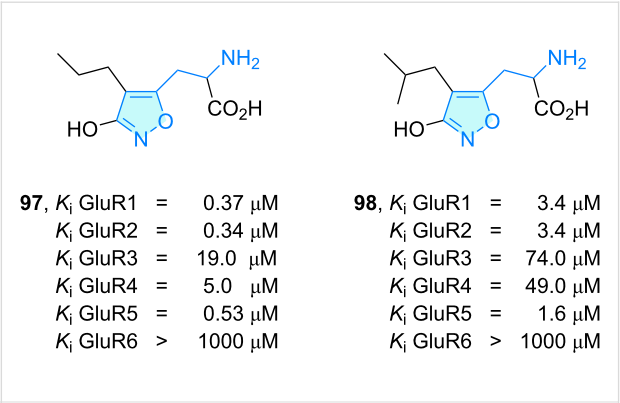

Scheme 14: 2-Aminoethylisoxazole derivatives with therapeutic activity.

Govoni et al. [71] analyzed the pharmacological profile of several histamine H_1 antagonists, with a section covering thiazole-based compounds. 2-(Thiazol-4-yl)ethylamine (**99**) presented a low H_1 affinity, whereas the 2-substituted candidates **100**–**103** displayed a borderline, marginal activity (Scheme 15). A similar derivative described as a histamine H_2 full agonist used to study gastric secretion was amthamine (**104**) [72].

Pramipexole (**105**, SND 919) is a dopamine agonist approved for the treatment of Parkinson´s symptoms like rigidity, tremor, and bradykinesia [73]. Mierau et al. [74] showed that the compound has a high affinity for the dopamine D_3 receptor (Scheme 15).

Jonczyk and co-workers [75] evaluated a series of 1-[2-thiazol-5-yl-(2-aminoethyl)]-4-*N*-propylpiperazine and 1-[2-thiazol-4-yl-(2-aminoethyl)]-4-*N*-propylpiperazine derivatives as substrates for acetylcholinesterase (AChE) and butyrylcholinesterase (BuChE). Compounds **106** and **107** showed good inhibitory potency as multitarget-directed ligands (MTD, Scheme 15).

Oxadiazole: In their seminal work, Chiaramonte and co-workers [41] also tested 1,3,4-oxadiazole **108** and 1,2,4-oxadiazole **109** histamine congeners towards carbonic anhydrase isoforms, finding moderate potencies among them, with **109** 3 times more potent than histamine in CA type VII (Scheme 16).

Oxolamine (**110**, Scheme 16) is a cough suppressant originally synthesized by Palazzo et al. [76] and several other deriv-

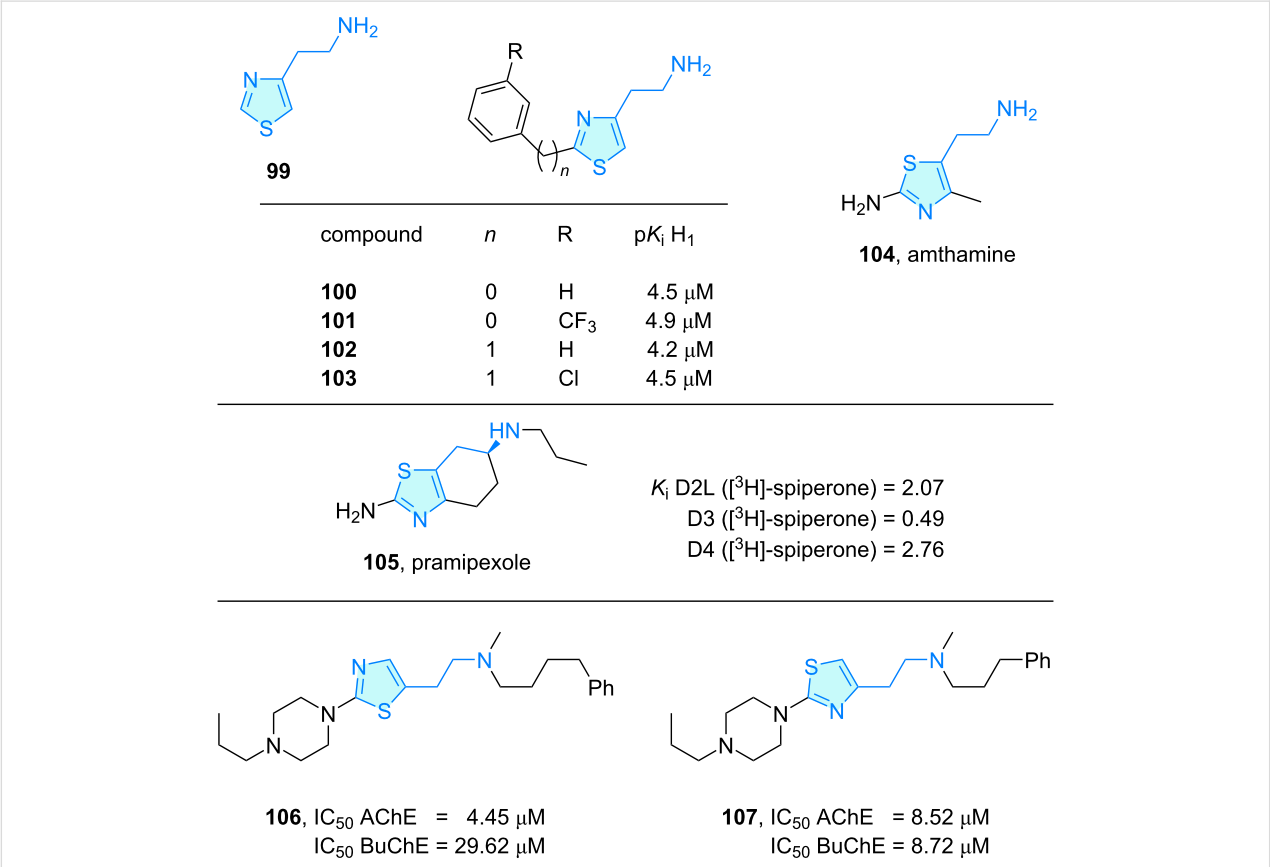

Scheme 15: 2-Aminoethylthiazole derivatives with therapeutic activity.

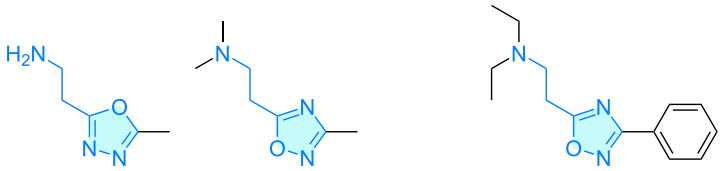

	108	109	110, oxolamine
K_a hCA VA	21.7 μM	28.6 μM	
K_a hCA VII	23.0 μM	12.1 μM	

Scheme 16: 2-Aminoethyloxadiazole derivatives with therapeutic activity.

atives were developed based on ethylamine-chain homologation [77].

Triazoles: Hall and co-workers [78] developed 1,2,3-triazolyl analogues **111** of L-histidine for L-type amino acid transporter 1 (LAT1) activity, a sodium-independent membrane solute carrier protein which is used as strategic target for blood–brain-barrier drug delivery. In general, the authors found the compounds less potent than the natural substrate L-tryptophan, with exception of derivative **112** (Scheme 17).

111 **112**

Scheme 17: 2-Aminoethyltriazole derivatives with therapeutic activity.

Tetrazoles: Taking advantage of using tetrazoles not as a phenyl-ring bioisostere, but as carboxylic acid one, Schwarz et al. [79] developed tetrazole-based pregabalin bioisosteres **113**–**118** (Scheme 18). The target protein α2-δ is involved in neurotransmitters release reduction, as a model of anxiety and neuropathic pain. In general, submicromolar affinities were observed for this family of tetrazole scaffolds.

Conclusion

The present review focuses on an examination of the expanded 2-phenethylamine chemical space, highlighting heteroaromatic structures with reported pharmacological profiles. The close inspection of each of the phenyl and other heteroaryl ring systems reveals a conserved pattern: most of the changes are related to bioisostere structure–activity exploration of the chemical space from original phenyl hits. The results with the imidazole analogues are different, since the L-histidine unit marks a non-phenyl-based scaffold hopping.

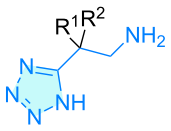

compound	R^1	R^2	K_i α2–δ
113	H	H	>10 μM
114	iPr	H	0.13 μM
115	Bn	H	7.6 μM
116	*c*-C_5H_9	H	0.018 μM
117	Me	Me	>10 μM
118	Bn	Me	0.90 μM

Scheme 18: 2-Aminoethyloxadiazole derivatives with therapeutic activity.

The main goal of these SAR expansions is creating new chemical matter with appealing potency and selectivity profiles. The impact of the scaffold hopping exercise in these target biomarkers depends on the nature of the targets themselves. It is noteworthy, that the use of molecular modelling tools, especially molecular docking or QSAR calculations to describe the bioisostere, impact and rationalize the observed experimental binding or efficacy measurements.

As it was stated in the introduction, only the rings described in this review, are the ones with reported activity, but there exists a plethora of other analogues containing a wide variety of heteroaryls which still need to be bioassayed. These examples, will be covered in another article on the 2-heteroaryl- (and phenyl)ethylamine series. As a final conclusion, this review of 2-heteroarylethylamines serves as an updated repository of bioisosteric rescaffolding of 2-phenethylamine derivatives evaluating affinity and aromatic core diversity.

Funding

The authors gratefully acknowledge the financial support of this work provided by Ministerio de Ciencia e Innovación

(PID2020-118303GB-I00 MCIN/AEI/10.13039/501100011033) and Junta de Castilla y Leon (SA0076P20). C.T.N. thanks Junta de Castilla y Leon for a postdoctoral contract (SA0076P20).

Author Contributions

Carlos Nieto: conceptualization; data curation; funding acquisition; investigation; project administration; supervision; visualization; writing – original draft; writing – review & editing. Alejandro Manchado: writing – review & editing. Ángel García-González: writing – review & editing. David Díez: funding acquisition; writing – review & editing. Narciso M. Garrido: conceptualization; funding acquisition; writing – review & editing.

ORCID® iDs

Carlos Nieto - https://orcid.org/0000-0001-5041-8825
Alejandro Manchado - https://orcid.org/0000-0002-6090-8147
Ángel García-González - https://orcid.org/0000-0002-9100-3869
David Díez - https://orcid.org/0000-0002-7261-8454
Narciso M. Garrido - https://orcid.org/0000-0002-1704-8073

Data Availability Statement

Data sharing is not applicable as no new data was generated or analyzed in this study.

References

1. Brown, N. Bioisosterism in Medicinal Chemistry. In *Bioisosteres in Medicinal Chemistry;* Brown, N., Ed.; Wiley-VCH: Weinheim, Germany, 2012; pp 1–14. doi:10.1002/9783527654307.ch1
2. Smith, D. A.; Millan, D. S. Consequences of Bioisosteric Replacement. In *Bioisosteres in Medicinal Chemistry;* Brown, N., Ed.; Wiley-VCH: Weinheim, Germany, 2012; pp 31–51. doi:10.1002/9783527654307.ch3
3. Barillari, C.; Brown, N. Classical Bioisosteres. In *Bioisosteres in Medicinal Chemistry;* Brown, N., Ed.; Wiley-VCH: Weinheim, Germany, 2012; pp 15–29. doi:10.1002/9783527654307.ch2
4. Subbaiah, M. A. M.; Meanwell, N. A. *J. Med. Chem.* **2021,** *64,* 14046–14128. doi:10.1021/acs.jmedchem.1c01215
5. Nieto, C. T.; Manchado, A.; Belda, L.; Diez, D.; Garrido, N. M. *Molecules* **2023,** *28,* 855. doi:10.3390/molecules28020855
6. Presset, M.; Djordjevic, D.; Dupont, A.; Le Gall, E.; Molinier-Frenkel, V.; Castellano, F. *Bioorg. Chem.* **2020,** *94,* 103463. doi:10.1016/j.bioorg.2019.103463
7. Berger, M. L.; Schweifer, A.; Rebernik, P.; Hammerschmidt, F. *Bioorg. Med. Chem.* **2009,** *17,* 3456–3462. doi:10.1016/j.bmc.2009.03.025
8. Sanacora, G.; Smith, M. A.; Pathak, S.; Su, H.-L.; Boeijinga, P. H.; McCarthy, D. J.; Quirk, M. C. *Mol. Psychiatry* **2014,** *19,* 978–985. doi:10.1038/mp.2013.130
9. Ye, S.; Han, Y.; Wei, Z.; Li, J. *Molecules* **2023,** *28,* 4346. doi:10.3390/molecules28114346
10. Dukat, M.; Ramunno, A.; Banzi, R.; Damaj, M. I.; Martin, B.; Glennon, R. A. *Bioorg. Med. Chem. Lett.* **2005,** *15,* 4308–4312. doi:10.1016/j.bmcl.2005.06.053
11. Al-Tamimi, D. J.; Ammoo, A. M.; Alani, M. E.; Ibraheem, J. J. *Sci. Pharm.* **2020,** *88,* 13. doi:10.3390/scipharm88010013
12. Lacour, M.; Sterkers, O. *CNS Drugs* **2001,** *15,* 853–870. doi:10.2165/00023210-200115110-00004
13. Gbahou, F.; Davenas, E.; Morisset, S.; Arrang, J.-M. *J. Pharmacol. Exp. Ther.* **2010,** *334,* 945–954. doi:10.1124/jpet.110.168633
14. Vallejos, G.; Fierro, A.; Rezende, M. C.; Sepúlveda-Boza, S.; Reyes-Parada, M. *Bioorg. Med. Chem.* **2005,** *13,* 4450–4457. doi:10.1016/j.bmc.2005.04.045
15. Vallejos, G.; Rezende, M. C.; Cassels, B. K. *J. Comput.-Aided Mol. Des.* **2002,** *16,* 95–103. doi:10.1023/a:1016344030772
16. Morón, J. A.; Pérez, V.; Pastó, M.; Lizcano, J. M.; Unzeta, M. *J. Pharmacol. Exp. Ther.* **2000,** *292,* 788–794.
17. Kagaya, T.; Kajiwara, A.; Nagato, S.; Akasaka, K.; Kubota, A. *J. Pharmacol. Exp. Ther.* **1996,** *278,* 243–251.
18. Humeniuk, R. E.; Ong, J.; Kerr, D. I. B.; White, J. M. *Gen. Pharmacol.* **1995,** *26,* 417–424. doi:10.1016/0306-3623(94)00175-m
19. Ansar, M.; Al Akoum Ebriki, S.; Mouhoub, R.; Berthelot, P.; Vaccher, C.; Vaccher, M. P.; Flouquet, N.; Caignard, D. H.; Renard, P.; Pirard, B.; Rettori, M. C.; Evrard, G.; Durant, F.; Debaert, M. *Eur. J. Med. Chem.* **1996,** *31,* 449–460. doi:10.1016/0223-5234(96)85165-8
20. Berthelot, P.; Vaccher, C.; Musadad, A.; Flouquet, N.; Debaert, M.; Luyckx, M. *J. Med. Chem.* **1987,** *30,* 743–746. doi:10.1021/jm00387a031
21. Pirard, B.; Paquet, B.; Evrard, G.; Berthelot, P.; Vaccher, C.; Ansard, M. H.; Debaert, M.; Durant, F. *Eur. J. Med. Chem.* **1995,** *30,* 851–857. doi:10.1016/0223-5234(96)88304-8
22. Benarroch, E. E. *Neurology* **2012,** *78,* 578–584. doi:10.1212/wnl.0b013e318247cd03
23. Pirard, B.; Carrupt, P.-A.; Testa, B.; Tsai, R.-S.; Berthelot, P.; Vaccher, C.; Debaert, M.; Durant, F. *Bioorg. Med. Chem.* **1995,** *3,* 1537–1545. doi:10.1016/0968-0896(95)00144-6
24. Berthelot, P.; Vaccher, C.; Flouquet, N.; Debaert, M.; Luyckx, M.; Brunet, C. *J. Med. Chem.* **1991,** *34,* 2557–2560. doi:10.1021/jm00112a033
25. Costantino, G.; Macchiarulo, A.; Entrena Guadix, A.; Pellicciari, R. *J. Med. Chem.* **2001,** *44,* 1827–1832. doi:10.1021/jm0100133
26. Bagli, J. F.; Mackay, W. D.; Ferdinandi, E.; Cayen, M. N.; Vavra, I.; Pugsley, T.; Lippmann, W. *J. Med. Chem.* **1976,** *19,* 876–882. doi:10.1021/jm00229a004
27. Kumar Deshmukh, F.; Yaffe, D.; Olshina, M. A.; Ben-Nissan, G.; Sharon, M. *Biomolecules* **2019,** *9,* 190. doi:10.3390/biom9050190
28. Hovhannisyan, A. A.; Pham, T. H.; Bouvier, D.; Tan, X.; Touhar, S.; Mkryan, G. G.; Dallakyan, A. M.; El Amri, C.; Melikyan, G. S.; Reboud-Ravaux, M.; Bouvier-Durand, M. *Bioorg. Med. Chem. Lett.* **2017,** *27,* 5172–5178. doi:10.1016/j.bmcl.2017.10.055
29. Alım, Z.; Kılınç, N.; İşgör, M. M.; Şengül, B.; Beydemir, Ş. *Chem. Biol. Drug Des.* **2015,** *86,* 857–863. doi:10.1111/cbdd.12561
30. Alım, Z.; Köksal, Z.; Karaman, M. *Pharmacol. Rep.* **2020,** *72,* 1738–1748. doi:10.1007/s43440-020-00149-4
31. Carroll, F. I.; Blough, B. E.; Mascarella, S. W.; Navarro, H. A.; Eaton, J. B.; Lukas, R. J.; Damaj, M. I. *J. Med. Chem.* **2010,** *53,* 2204–2214. doi:10.1021/jm9017465
32. Carroll, F. I.; Blough, B. E.; Abraham, P.; Mills, A. C.; Holleman, J. A.; Wolckenhauer, S. A.; Decker, A. M.; Landavazo, A.; McElroy, K. T.; Navarro, H. A.; Gatch, M. B.; Forster, M. J. *J. Med. Chem.* **2009,** *52,* 6768–6781. doi:10.1021/jm901189z

33. Lee, H. M. D.; Wood, D. M.; Hudson, S.; Archer, J. R. H.; Dargan, P. I. *J. Med. Toxicol.* **2014,** *10,* 299–302. doi:10.1007/s13181-014-0399-y
34. Blicke, F. F.; Burckhalter, J. H. *J. Am. Chem. Soc.* **1942,** *64,* 477–480. doi:10.1021/ja01255a001
35. Foti, F.; Bilel, S.; Tirri, M.; Arfè, R.; Boccuto, F.; Bernardi, T.; Serpelloni, G.; De-Giorgio, F.; Marti, M. *Psychopharmacology (Heidelberg, Ger.)* **2021,** *238,* 1847–1856. doi:10.1007/s00213-021-05813-y
36. Nguyen, P.-T.; Dang, D.-K.; Tran, H.-Q.; Shin, E.-J.; Jeong, J. H.; Nah, S.-Y.; Cho, M. C.; Lee, Y. S.; Jang, C.-G.; Kim, H.-C. *Chem.-Biol. Interact.* **2019,** *305,* 134–147. doi:10.1016/j.cbi.2019.03.017
37. Tuv, S. S.; Bergh, M. S.-S.; Andersen, J. M.; Steinsland, S.; Vindenes, V.; Baumann, M. H.; Huestis, M. A.; Bogen, I. L. *Int. J. Mol. Sci.* **2021,** *22,* 12002. doi:10.3390/ijms222112002
38. Achtyes, E. D.; Hopkins, S. C.; Dedic, N.; Dworak, H.; Zeni, C.; Koblan, K. *Eur. Arch. Psychiatry Clin. Neurosci.* **2023,** *273,* 1543–1556. doi:10.1007/s00406-023-01580-3
39. Costa, V. M.; Grando, L. G. R.; Milandri, E.; Nardi, J.; Teixeira, P.; Mladěnka, P.; Remião, F.; on behalf of The OEMONOM. *Biomolecules* **2022,** *12,* 1793. doi:10.3390/biom12121793
40. Heffernan, M. L. R.; Herman, L. W.; Brown, S.; Jones, P. G.; Shao, L.; Hewitt, M. C.; Campbell, J. E.; Dedic, N.; Hopkins, S. C.; Koblan, K. S.; Xie, L. *ACS Med. Chem. Lett.* **2022,** *13,* 92–98. doi:10.1021/acsmedchemlett.1c00527
41. Chiaramonte, N.; Gabellini, A.; Angeli, A.; Bartolucci, G.; Braconi, L.; Dei, S.; Teodori, E.; Supuran, C. T.; Romanelli, M. N. *Molecules* **2022,** *27,* 545. doi:10.3390/molecules27020545
42. Pithadia, A. B.; Jain, S. M. *J. Clin. Med. Res.* **2009,** *1,* 72–80. doi:10.4021/jocmr2009.05.1237
43. Hoyer, D. *Neuropharmacology* **2020,** *179,* 108233. doi:10.1016/j.neuropharm.2020.108233
44. Hoyer, D. 5-Hydroxytryptamine Receptors. In *xPharm: The Comprehensive Pharmacology Reference;* Enna, S. J.; Bylund, D. B., Eds.; Elsevier: New York, NY, USA, 2007; pp 1–7. doi:10.1016/b978-008055232-3.60122-9
45. Thangam, E. B.; Jemima, E. A.; Singh, H.; Baig, M. S.; Khan, M.; Mathias, C. B.; Church, M. K.; Saluja, R. *Front. Immunol.* **2018,** *9,* 1873. doi:10.3389/fimmu.2018.01873
46. Marquardt, D. L. *Clin. Rev. Allergy* **1983,** *1,* 343–351. doi:10.1007/bf02991225
47. Moro, J.; Tomé, D.; Schmidely, P.; Demersay, T.-C.; Azzout-Marniche, D. *Nutrients* **2020,** *12,* 1414. doi:10.3390/nu12051414
48. Neumann, J.; Grobe, J. M.; Weisgut, J.; Schwelberger, H. G.; Fogel, W. A.; Marušáková, M.; Wache, H.; Bähre, H.; Buchwalow, I. B.; Dhein, S.; Hofmann, B.; Kirchhefer, U.; Gergs, U. *Front. Pharmacol.* **2021,** *12,* 582916. doi:10.3389/fphar.2021.582916
49. Carthy, E.; Ellender, T. *Front. Neurosci.* **2021,** *15,* 680214. doi:10.3389/fnins.2021.680214
50. Stuart, A. E.; Borycz, J.; Meinertzhagen, I. A. *Prog. Neurobiol.* **2007,** *82,* 202–227. doi:10.1016/j.pneurobio.2007.03.006
51. Ganellin, C. R.; Fkyerat, A.; Hosseini, S. K.; Khalaf, Y. S.; Piripitsi, A.; Tertiuk, W.; Arrang, J. M.; Garbarg, M.; Ligneau, X.; Schwartz, J. C. *J. Pharm. Belg.* **1995,** *50,* 179–187.
52. Ahmad, S. F.; Zoheir, K. M. A.; Ansari, M. A.; Korashy, H. M.; Bakheet, S. A.; Ashour, A. E.; Attia, S. M. *Immunobiology* **2015,** *220,* 341–349. doi:10.1016/j.imbio.2014.10.014
53. Gbahou, F.; Vincent, L.; Humbert-Claude, M.; Tardivel-Lacombe, J.; Chabret, C.; Arrang, J.-M. *Br. J. Pharmacol.* **2006,** *147,* 744–754. doi:10.1038/sj.bjp.0706666
54. Igel, P.; Dove, S.; Buschauer, A. *Bioorg. Med. Chem. Lett.* **2010,** *20,* 7191–7199. doi:10.1016/j.bmcl.2010.10.041
55. De Esch, I. J. P.; Vollinga, R. C.; Goubitz, K.; Schenk, H.; Appelberg, U.; Hacksell, U.; Lemstra, S.; Zuiderveld, O. P.; Hoffmann, M.; Leurs, R.; Menge, W. M. P. B.; Timmerman, H. *J. Med. Chem.* **1999,** *42,* 1115–1122. doi:10.1021/jm9810912
56. Kazuta, Y.; Hirano, K.; Natsume, K.; Yamada, S.; Kimura, R.; Matsumoto, S.-i.; Furuichi, K.; Matsuda, A.; Shuto, S. *J. Med. Chem.* **2003,** *46,* 1980–1988. doi:10.1021/jm020415q
57. Krause, M.; Stark, H.; Schunack, W. Medicinal chemistry of histamine H3 receptor agonists. In *Pharmacochemistry Library;* Leurs, R.; Timmerman, H., Eds.; Elsevier: Amsterdam, Netherlands, 1998; pp 175–196. doi:10.1016/s0165-7208(98)80030-5
58. Malinowska, B.; Piszcz, J.; Schlicker, E.; Kramer, K.; Elz, S.; Schunack, W. *Naunyn-Schmiedeberg's Arch. Pharmacol.* **1999,** *359,* 11–16. doi:10.1007/pl00005316
59. Schlicker, E.; Kozłowska, H.; Kwolek, G.; Malinowska, B.; Kramer, K.; Pertz, H.; Elz, S.; Schunack, W. *Naunyn-Schmiedeberg's Arch. Pharmacol.* **2001,** *364,* 14–20. doi:10.1007/s002100100414
60. Elz, S.; Kramer, K.; Leschke, C.; Schunack, W. *Eur. J. Med. Chem.* **2000,** *35,* 41–52. doi:10.1016/s0223-5234(00)00105-7
61. Menghin, S.; Pertz, H. H.; Kramer, K.; Seifert, R.; Schunack, W.; Elz, S. *J. Med. Chem.* **2003,** *46,* 5458–5470. doi:10.1021/jm0309147
62. Straßer, A.; Wittmann, H.-J. *Mol. Inf.* **2010,** *29,* 333–341. doi:10.1002/minf.200900036
63. Patil, R.; Elz, S.; Reiser, O. *Bioorg. Med. Chem. Lett.* **2006,** *16,* 672–676. doi:10.1016/j.bmcl.2005.10.030
64. Brancaccio, M.; Milito, A.; Viegas, C. A.; Palumbo, A.; Simes, D. C.; Castellano, I. *Free Radical Biol. Med.* **2022,** *192,* 224–234. doi:10.1016/j.freeradbiomed.2022.09.017
65. Jain, R.; Vangapandu, S.; Jain, M.; Kaur, N.; Singh, S.; Pal Singh, P. *Bioorg. Med. Chem. Lett.* **2002,** *12,* 1701–1704. doi:10.1016/s0960-894x(02)00289-5
66. Sharma, K.; Sharma, K. K.; Mahindra, A.; Sehra, N.; Bagra, N.; Aaghaz, S.; Parmar, R.; Rathod, G. K.; Jain, R. *Med. Res. Rev.* **2023,** *43,* 775–828. doi:10.1002/med.21936
67. Durant, G. J.; Ganellin, C. R.; Parsons, M. E. *J. Med. Chem.* **1975,** *18,* 905–909. doi:10.1021/jm00243a009
68. Madsen, U.; Pickering, D. S.; Nielsen, B.; Bräuner-Osborne, H. *Neuropharmacology* **2005,** *49,* 114–119. doi:10.1016/j.neuropharm.2005.05.007
69. Kromann, H.; Sløk, F. A.; Stensbøl, T. B.; Bräuner-Osborne, H.; Madsen, U.; Krogsgaard-Larsen, P. *J. Med. Chem.* **2002,** *45,* 988–991. doi:10.1021/jm010443t
70. Yokoyama, H.; Onodera, K.; Iinuma, K.; Watanabe, T. *Pharmacol., Biochem. Behav.* **1994,** *47,* 503–507. doi:10.1016/0091-3057(94)90151-1
71. Govoni, M.; Bakker, R. A.; van de Wetering, I.; Smit, M. J.; Menge, W. M. B. P.; Timmerman, H.; Elz, S.; Schunack, W.; Leurs, R. *J. Med. Chem.* **2003,** *46,* 5812–5824. doi:10.1021/jm030936t
72. Coruzzi, G.; Timmerman, H.; Adami, M.; Bertaccini, G. *Naunyn-Schmiedeberg's Arch. Pharmacol.* **1993,** *348,* 77–81. doi:10.1007/bf00168540
73. Constantinescu, R. *Neuropsychiatr. Dis. Treat.* **2008,** *4,* 337–352. doi:10.2147/ndt.s2325

74. Mierau, J.; Schneider, F. J.; Ensinger, H. A.; Chio, C. L.; Lajiness, M. E.; Huff, R. M. *Eur. J. Pharmacol., Mol. Pharmacol. Sect.* **1995,** *290,* 29–36. doi:10.1016/0922-4106(95)90013-6
75. Jończyk, J.; Lodarski, K.; Staszewski, M.; Godyń, J.; Zaręba, P.; Soukup, O.; Janockova, J.; Korabecny, J.; Sałat, K.; Malikowska-Racia, N.; Hebda, M.; Szałaj, N.; Filipek, B.; Walczyński, K.; Malawska, B.; Bajda, M. *Bioorg. Chem.* **2019,** *90,* 103084. doi:10.1016/j.bioorg.2019.103084
76. Palazzo, G.; Tavella, M.; Strani, G.; Silvestrini, B. *J. Med. Pharm. Chem.* **1961,** *4,* 351–367. doi:10.1021/jm50018a009
77. Cao, X.; Yao, Z.; Dou, F.; Zhang, Y.; Qiu, Y.; Zhao, S.; Xu, X.; Liu, X.; Liu, B.-F.; Chen, Y.; Zhang, G. *Chem. Biodiversity* **2019,** *16,* e1800599. doi:10.1002/cbdv.201800599
78. Hall, C.; Wolfe, H.; Wells, A.; Chien, H.-C.; Colas, C.; Schlessinger, A.; Giacomini, K. M.; Thomas, A. A. *Bioorg. Med. Chem. Lett.* **2019,** *29,* 2254–2258. doi:10.1016/j.bmcl.2019.06.033
79. Schwarz, J. B.; Colbry, N. L.; Zhu, Z.; Nichelson, B.; Barta, N. S.; Lin, K.; Hudack, R. A.; Gibbons, S. E.; Galatsis, P.; DeOrazio, R. J.; Manning, D. D.; Vartanian, M. G.; Kinsora, J. J.; Lotarski, S. M.; Li, Z.; Dickerson, M. R.; El-Kattan, A.; Thorpe, A. J.; Donevan, S. D.; Taylor, C. P.; Wustrow, D. J. *Bioorg. Med. Chem. Lett.* **2006,** *16,* 3559–3563. doi:10.1016/j.bmcl.2006.03.083

License and Terms

BEILSTEIN JOURNAL OF ORGANIC CHEMISTRY

A new platform for the synthesis of diketopyrrolopyrrole derivatives via nucleophilic aromatic substitution reactions

Vitor A. S. Almodovar and Augusto C. Tomé*

Full Research Paper

Open Access

Address:
LAQV-REQUIMTE, Department of Chemistry, University of Aveiro, 3810-193 Aveiro, Portugal

Email:
Augusto C. Tomé* - actome@ua.pt

* Corresponding author

Keywords:
diketopyrrolopyrrole; fluorescent dye; nucleophilic aromatic substitution; phenol; thiol

Beilstein J. Org. Chem. **2024,** *20,* 1933–1939.
https://doi.org/10.3762/bjoc.20.169

Received: 11 March 2024
Accepted: 30 July 2024
Published: 08 August 2024

This article is part of the thematic issue "5th International Symposium on Synthesis and Catalysis (ISySyCat 2023)".

Guest Editor: A. Burke

Abstract

Diketopyrrolopyrroles (DPPs) are a versatile group of dyes and pigments with valuable optoelectronic properties. In this work we report the synthesis of highly fluorescent DPP derivatives through straightforward nucleophilic aromatic substitution reactions with thiols and phenols. These nucleophilic substitutions occur at room temperature and manifest a remarkable selectivity for the 4-position of the pentafluorophenyl groups. Both symmetrical (disubstitution) and non-symmetrical (monosubstitution) DPP derivatives are formed in excellent overall yields. The optical properties of the newly synthesized compounds are also discussed. The new platform may be useful for bioorthogonal chemistry.

Introduction

Diketopyrrolopyrroles (DPPs) are a class of organic pigments discovered by serendipity in the 1970s [1,2]. Generally, N-unsubstituted DPP derivatives exhibit high melting points, low solubility in most solvents, and strong absorption in the visible region [3,4]. In turn, N-substituted DPP derivatives are soluble in common organic solvents, exhibit large molar extinction coefficients, Stokes shifts in the range of 10–70 nm and high fluorescence quantum yields [5-7].

Due to their outstanding photophysical properties, DPP-based dyes have been used in a wide range of applications, namely as organic semiconductors [8], acceptors for organic solar cells [9,10], as fluorescent probes [11-13], or as photosensitizers for photodynamic therapy and antimicrobial photodynamic therapy [14-17]. DPP derivatives with improved performance or novel properties can be prepared by conventional chemical modifications of simple DPP derivatives [3,18]. The most frequently used transformations include: i) N-alkylation with adequately functionalized alkyl groups [19-22], ii) N-arylation [23-25], and functionalization at the 3,6-di(het)aryl groups via Suzuki–Miyaura [26-28] or Sonogashira [29-31] reactions.

In this study, we report a straightforward method to obtain a diverse array of N-substituted DPP derivatives through a two-step process. Firstly, the N-alkylation of Pigment Red 254 (DPP **1**) is achieved using pentafluorobenzyl bromide, followed by a nucleophilic aromatic substitution (S_NAr) with thiols and phenols. This approach is based on the well-established reactivity of perfluoroaromatic compounds in nucleophilic aromatic substitutions [32-35]. By varying the reaction conditions and the number of equivalents of the nucleophile, it is possible to promote the substitution of one or more fluorine atoms. Nucleophilic substitution of fluorine atoms often necessitates harsh conditions such as elevated temperatures, strong bases, or strong nucleophiles, but our findings demonstrate that this process can be conducted under remarkably mild conditions.

Results and Discussion

The initial step of our method involved the N-alkylation of DPP **1** with pentafluorobenzyl bromide (Scheme 1). Although a similar reaction had been previously reported for other DPP derivatives, the experimental conditions used (DMF, K_2CO_3, 120 °C, 2 h) resulted in very low yields (6–16%) for the formation of *N*,*N*'-bis(pentafluorobenzyl)-DPP derivatives [36]. Changing the base to NaH and performing the reaction at a lower temperature, enabled to obtain DPP **2** in a reasonable yield (61%) and allowed us to use it as a starting material for generating new DPP derivatives through nucleophilic aromatic substitution reactions with thiols and phenols.

The main objective of this study was to employ the *N*,*N*'-bis(pentafluorobenzyl)-DPP **2** as an electrophile and investigate its reactivity with thiols and phenols (Scheme 1). All S_NAr reactions were performed in dry DMF at room temperature, in the presence of a base (K_2CO_3 or Cs_2CO_3). Room temperature was chosen due to the observed rapid degradation of the starting material at elevated temperatures. The work described herein allowed us to assess the potential of DPP **2** as a novel platform for obtaining functionalized DPP derivatives. As anticipated, it displayed reactivity with thiols and phenols through nucleo-

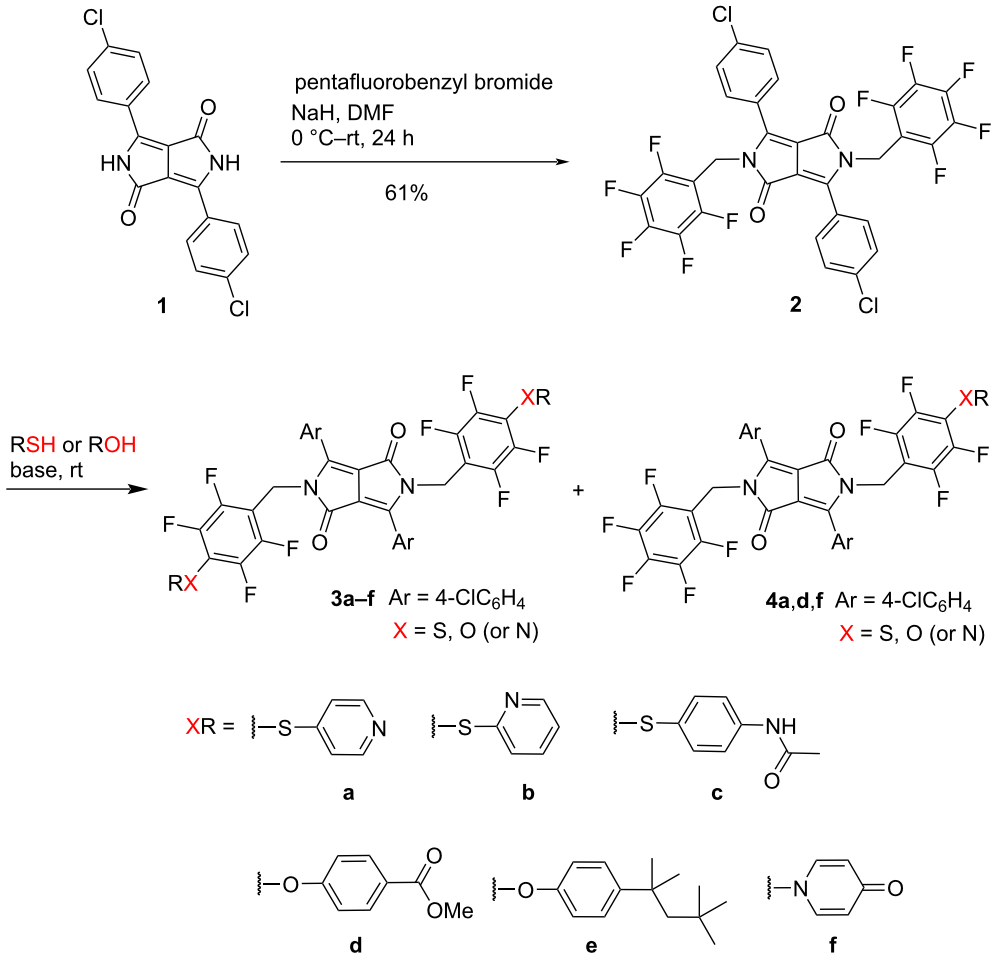

Scheme 1: Synthesis of new diketopyrrolopyrroles via nucleophilic aromatic substitution.

philic aromatic substitution at the pentafluorobenzyl groups, yielding both symmetrical (disubstitution) and non-symmetrical (monosubstitution) derivatives in satisfactory yields (Scheme 1).

Thiols are excellent nucleophiles and generally react under mild conditions, resulting in the substitution of the 4-F atom of the pentafluorophenyl groups. In this case, reactions with thiols were performed in dry DMF and K_2CO_3 was used as the base. Three different thiols were tested: pyridine-4-thiol, pyridine-2-thiol and 4-(acetylamino)benzenethiol. The reaction with pyridine-4-thiol yielded a mixture of the di- and monosubstituted compounds **3a** and **4a** in 51% and 23% yields, respectively. Conversely, for the reaction with pyridine-2-thiol, exclusively produced the disubstituted compound **3b** in an 85% yield. Furthermore, the reaction with 4-(acetylamino)benzenethiol led to the selective formation of the disubstituted compound **3c** in 53% yield.

Phenols are less nucleophilic than thiols and, depending on the substitution pattern, a stronger base is often required to generate the corresponding alkoxide, which is the effective nucleophile. So, in this case, Cs_2CO_3 was employed as the base. The reaction of DPP **2** with methyl 4-hydroxybenzoate yielded compounds **3d** and **4d** in 56% and 14% yield, respectively. When reacting with 4-(2,4,4-trimethylpentan-2-yl)phenol, the disubstituted compound **3e** was obtained in 63% yield. In contrast to the reaction with pyridine-4-thiol, which resulted in the S-substituted product **3a**, the reaction with 4-hydroxypyridine led exclusively to the formation of the pyridin-4-one-derived compounds **3f** and **4f,** in 45% and 13% yield, respectively. The substitution occurred at the nitrogen atom rather than the oxygen due to the preferential existence of 4-hydroxypyridine in the pyridin-4-one tautomeric form [37-39]. The structures of dyes **3a–f**, **4a**, **4d** and **4f** were unambiguously established through their ^{1}H, ^{13}C and ^{19}F NMR and mass spectra.

The ^{1}H NMR spectra of the symmetrical compounds displayed a characteristic signal for the N–CH_2 protons as a singlet at approximately δ 5.10 ppm. Signals of the 4-chlorophenyl groups appeared as AB systems centred at around δ 7.9 ppm. For the non-symmetrical derivatives, two singlets were observed at approximately δ 5.05 and 5.10 ppm, corresponding to the protons of the N–$CH_2C_6F_5$ and N–$CH_2C_6F_4XR$ groups, respectively. All ^{19}F NMR spectra confirmed the selective substitution of the 4-fluorine atoms (in one or in two rings) by the disappearance of the signal corresponding to the resonance of those atoms. Mass spectra of compounds **3a–f**, **4a**, **4d** and **4f** consistently displayed the protonated molecular ion $[M + H]^+$ as the base peak.

The UV–vis and fluorescence spectra of DPP derivatives **3a–f**, **4a**, **4d** and **4f** in DMF are presented in Figure 1, and their photophysical properties are summarized in Table 1. These compounds are highly fluorescent, and their UV–vis spectra are very similar. These results indicate that substituents with different functional groups can be attached to DPP **2** without significant modification of their optical properties. The observed Stokes shifts for dyes **3** and **4** averaged in the range of 60–70 nm. All compounds exhibited high fluorescence quantum yields, ranging from 0.66 to 0.83, confirming their potential applications in fluorescence imaging, sensors, and optoelectronic devices. A comprehensive discussion of the potential uses of these fluorescent substances in areas such as materials science, biology, or chemistry may provide a deeper understanding of their significance.

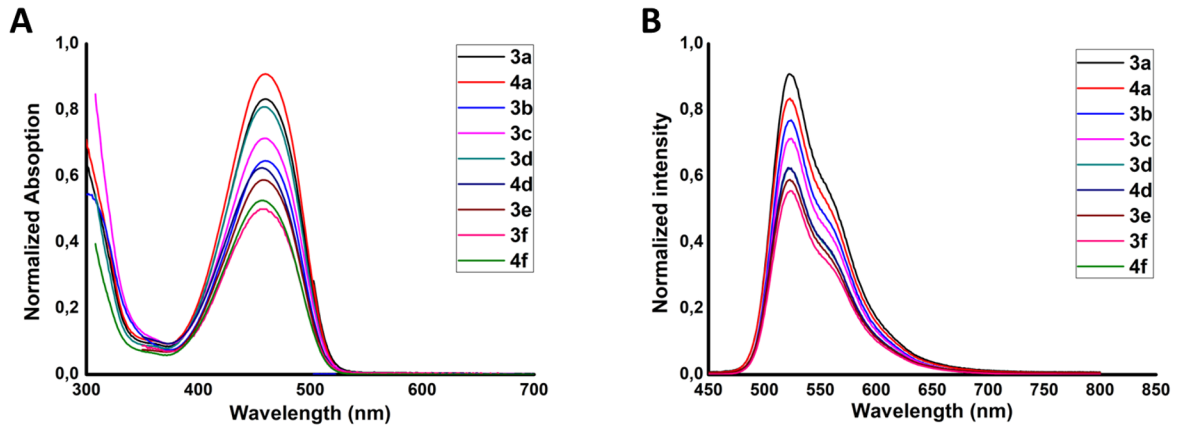

Figure 1: (A) Absorption and (B) fluorescence spectra of compounds **3a–f**, **4a**, **4d** and **4f**, in DMF. Different concentrations of the compounds were used to allow visualization of each spectrum.

Table 1: Spectroscopic data for the new compounds (between 1 × 10^{-6} M and 4 × 10^{-5} M in DMF).

Compound	Absorption λ_{max} (nm)	Log ε (M^{-1} cm^{-1})	Emission λ_{max} (nm)	Stokes shift (cm^{-1})	Φ_F (DMF)[a]
3a	460	4.15	521	2545	0.69
4a	460	4.11	522	2582	0.68
3b	461	4.17	524	2608	0.83
3c	461	4.25	525	2644	0.78
3d	457	4.43	522	2687	0.73
4d	459	4.46	521	2593	0.72
3e	460	4.03	522	2547	0.71
3f	456	4.33	523	2809	0.83
4f	458	4.32	524	2750	0.66

[a]Excitation at 436 nm. *N,N'*-Dibenzyl-DPP was used as the fluorescence quantum yield reference: Φ_F = 0.88, in chloroform [40].

Conclusion

In conclusion, novel DPP derivatives were synthesized through the reaction of a *N*,*N*'-bis(pentafluorobenzyl)-DPP with thiols and phenols. The nucleophilic aromatic substitution reactions took place under exceptionally mild experimental conditions, and the resulting compounds were isolated in reasonable yields. The newly synthesized compounds display high fluorescence quantum yields and moderate Stokes shifts, which are crucial attributes for their potential application in diverse fields, particularly in biological or technical applications. Additionally, it is crucial to highlight the chemical versatility of compound **2**, which allows the attachment of various functional units without significantly altering its optical properties. This versatility holds significant promise in the design and synthesis of innovative molecules tailored for specific purposes. This study not only contributes to the expansion of accessible N-substituted DPP derivatives but also reveals that such transformations can be achieved with outstanding efficiency and environmental sensitivity by employing mild reaction conditions.

Experimental

Chemicals and instrumentation

The reagents used in this work were purchased from Merck Life Science (Algés, Portugal) or TCI Europe N.V. (Belgium) and were used as received. Pigment Red 254 was purchased from TCI Europe N.V. The solvents were used as received or distilled and dried by standard procedures. Analytical thin-layer chromatography (TLC) was carried out on precoated sheets with silica gel (Merck 60, 0.2 mm thick). Preparative TLC was carried out on 20 cm × 20 cm glass plates precoated with a layer of silica gel 60 (0.5 mm thick) and activated in an oven at 100 °C for 12 h. Melting points were determined with a Büchi B-540 apparatus. NMR spectra were recorded on a Bruker DRX 300 Avance operating at 300.13 MHz (for ^{1}H NMR), at 75.47 MHz (for ^{13}C NMR) and 282 MHz (for ^{19}F NMR). Deuterated chloroform ($CDCl_3$) was used as the solvent and tetramethylsilane (TMS) as the internal reference. The chemical shifts (δ) are expressed in parts per million (ppm) and the coupling constants (*J*) in hertz (Hz). UV–vis spectra were recorded on a Shimadzu UV-2501PC spectrophotometer using DMF as the solvent. The emission spectra were recorded with a Jasco FP-8300 spectrofluorometer using DMF as the solvent. Mass spectra were recorded using a Micromass Q-TOF-2TM mass spectrometer and $CHCl_3$ as the solvent. The NMR, absorption and emission spectra of the new compounds are shown in Supporting Information File 1.

Synthesis

3,6-Bis(4-chlorophenyl)-2,5-bis(pentafluorobenzyl)-2,5-dihydropyrrolo[3,4-*c*]pyrrole-1,4-dione (**2**)

A suspension of DPP **1** (1 g, 2.8 mmol) and NaH (11.2 mmol) in DMF (60 mL) was stirred at 0 °C under a nitrogen atmosphere for 30 min. At this temperature, and under vigorous stirring, a solution of pentafluorobenzyl bromide (1.7 mL, 11.2 mmol) in DMF (8 mL) was added dropwise. The mixture was stirred for 24 h at room temperature and then it was diluted with CH_2Cl_2 and water. The organic layer was separated and washed with water and brine. The product was isolated by column chromatography on silica gel using CH_2Cl_2 as the eluent. Yield: 61%; mp: 278–280 °C; ^{1}H NMR (300 MHz, $CDCl_3$) δ (ppm) 7.62–7.66 (m, 4H), 7.47–7.52 (m, 4H), 5.03 (s, 4H); ^{13}C NMR (75 MHz, $CDCl_3$) δ (ppm) 161.7, 147.2, 138.01, 129.8, 129.6, 125.6, 110.0, 29.7; ^{19}F NMR (282 MHz, $CDCl_3$) δ (ppm) −138.11 to −138.29 (m, 4F), −149.90 (t, *J* = 21.4 Hz, 2F), −157.63 to −157.91 (m, 4F); ESIMS *m*/*z*: 717.0 (M + H^+, 100%).

General procedure for the nucleophilic aromatic substitution reactions

The reactions of DPP **2** with thiols and phenols were carried out in dry DMF, at room temperature, and in the presence of K_2CO_3 or Cs_2CO_3. Once the starting DPP was completely con-

sumed (after 2–3 hours with thiols and 5–6 hours with phenols), the reaction mixtures were diluted with CH_2Cl_2 and water. The organic layer was then separated and washed with brine and water. The products were isolated by preparative TLC using CH_2Cl_2/hexane mixtures as the eluent.

Compound 3a. Yield: 51%; mp 274–276 °C; ^{1}H NMR ($CDCl_3$, 300 MHz) δ (ppm) 8.43 (AA'XX', *J* = 6 Hz, 4H), 7.68 (AA'BB', *J* = 8.7 Hz, 4H), 7.51 (AA'BB', *J* = 8.7 Hz, 4H), 6.91 (AA'XX', *J* = 6 Hz, 4H), 5.15 (s, 4H); ^{19}F NMR (282 MHz, $CDCl_3$) δ (ppm) −153.53 to −153.65 (m, 4F), −162.60 to −162.73 (m, 4F); ESIMS *m/z*: 899.1 (M + H^+, 100%).

Compound 4a. Yield: 23%; mp 269–273 °C; ^{1}H NMR (300 MHz, $CDCl_3$) δ (ppm) 8.45 (AA'XX', *J* = 6.3 Hz, 2H), 7.70–7.64 (m, 4H), 7.52 (AA'BB', *J* = 8.7 Hz, 4H), 7.07 (AA'XX', *J* = 6.3 Hz, 2H), 5.15 (s, 2H), 5.05 (s, 2H); ^{13}C NMR (125 MHz, $CDCl_3$) δ (ppm) 161.7, 149.7, 147.6, 146.95, 145.9, 138.1, 129.9, 129.6, 125.6, 121.1, 109.9, 109.7, 34.9, 34.5; ^{19}F NMR (282 MHz, $CDCl_3$) δ (ppm) −126.79 to −126.90 (m, 2F), –135.53 to –153.81 (m, 2F), −137.99 to −138.50 (m, 2F), −149.74 (t, *J* = 21.3 Hz, 1F), −157.60 to −157.78 (m, 2H); ESIMS *m/z*: 802.3 (M + H^+, 100%).

Compound 3b. Yield: 85%; mp 270–272 °C; ^{1}H NMR (300 MHz, $CDCl_3$) δ (ppm) 8.3–8.32 (m, 2H), 7.68 (AA'BB', *J* = 8.7 Hz, 4H), 7.55 (ddd, *J* = 8.1, 7.4, 1.9 Hz, 2H), 7.49 (AA'BB', *J* = 8.7 Hz, 4H), 7.15–7.02 (m, 4H), 5.13 (s, 4H); ^{13}C NMR (125 MHz, $CDCl_3$) δ (ppm) 161.8, 155.5, 150.0, 147.3, 137.9, 137.1, 129.9, 129.5, 125.8, 121.7, 121.1, 116.4, 110.0, 35.1; ^{19}F NMR (282 MHz, $CDCl_3$) δ (ppm) −127.66 to −127.79 (m 4F), −138.03 to −138.25 (m, 4F); ESIMS *m/z*: 899.0 (M + H^+, 100%).

Compound 3c. Yield: 53%; mp 252–256 °C; ^{1}H NMR (300 MHz, DMSO-d_6) δ (ppm) 10.08 (s, 2H), 7.78 (AA'BB', *J* = 8.7 Hz, 4H), 7.55–7.61 (m, 8H), 7.22 (AA'BB', *J* = (8.7 Hz, 4H), 5.09 (s, 4H), 2.03 (s, 6H); ^{13}C NMR (125 MHz, DMSO) δ (ppm) 169.1, 164.7, 161.2, 147.3, 139.9, 136.7, 131.6, 130.9, 130.6, 129.5, 126.4, 125.4, 120.4, 120.1, 109.3, 31.3, 24.5; ^{19}F NMR (282 MHz, DMSO-d_6) δ (ppm) −131.31 to −131.54 (m, 4F), −137.94 to −138.07 (m, 4F); ESIMS *m/z*: 1011.0 (M + H^+, 100%).

Compound 3d. Yield: 56%; mp 249–251 °C; ^{1}H NMR (300 MHz, $CDCl_3$) δ (ppm) 8.02 (AA'XX', *J* = 9 Hz, 4H), 7.68 (AA'BB', *J* = 8.7 Hz, 4H), 7.52 (AA'BB', *J* = 8.7 Hz, 4H), 6.88 (AA'XX', *J* = 9 Hz, 4H), 5.11 (s, 4H), 3.90 (s, 6H); ^{19}F NMR (282 MHz, $CDCl_3$) δ (ppm) −138.23 to −138.35 (m, 4F), −149.59 to −149.96 (m, 4F); ESIMS *m/z*: 981.0 (M + H^+, 100%).

Compound 4d. Yield: 14%; mp 255–257 °C; ^{1}H NMR (300 MHz, $CDCl_3$) δ (ppm) 8.02 (AA'XX', *J* = 9 Hz, 2H), 7.67–7.59 (m, 4H), 7.52–7.44 (m, 4H), 6.88 (AA'XX', *J* = 9 Hz, 2H), 5.10 (s, 2H), 5.03 (s, 2H), 3.92 (s, 3H); ^{19}F NMR (282 MHz, $CDCl_3$) δ (ppm) −138.14 to −138.37 (m, 4F), −149.82 to −150.01 (m, 3F), −157.70 to −157.85 (m, 2F); ESIMS *m/z*: 849.0 (M + H^+, 100%).

Compound 3e. Yield: 63%; mp 262–265 °C; ^{1}H NMR (300 MHz, $CDCl_3$) δ (ppm) 7.66 (AA'BB', *J* = 8.7 Hz, 4H), 7.47 (AA'BB', *J* = 8.7 Hz, 4H), 7.28 (AA'BB', *J* = 9 Hz, 4H), 6.75 (AA'BB', *J* = 9 Hz, 4H), 5.09 (s, 4H), 1.70 (s, 4H), 1.34 (s, 12H), 0.70 (s, 18H); ^{13}C NMR (125 MHz, DMSO) δ (ppm) 161.7, 154.7, 147.3, 145.8, 137.9, 129.9, 129.4, 127.4, 125.8, 114.8, 109.8, 57.0, 38.2, 34.5, 32.3, 31.8, 31.6; ^{19}F NMR (282 MHz, $CDCl_3$) δ (ppm) −139.07 to −139.30 (m, 4F), −150.36 to −150.46 (m, 4F); ESIMS *m/z*: 1089.2 (M + H^+, 100%).

Compound 3f. Yield: 45%; mp 253–255 °C; ^{1}H NMR (300 MHz, $CDCl_3$) δ (ppm) 7.69 (AA'BB', *J* = 8.7 Hz, 4H), 7.55 (AA'BB', *J* = 8.7 Hz, 4H), 7.25–7.21 (m, 4H), 6.48 (d, *J* = 8.1 Hz, 4H), 5.12 (s, 4H); ^{19}F NMR (282 MHz, $CDCl_3$) δ (ppm) −137.72 to −137.84 (m, 4F), −145.60 to −145.71 (m, 4F); ESIMS *m/z*: 867.1 (M + H^+, 100%).

Compound 4f. Yield: 13%; mp 248–250 °C; ^{1}H NMR (300 MHz, $CDCl_3$) δ (ppm) 7.73–7.58 (m, 4H), 7.58–7.46 (m, 4H), 7.28–7.25 (m, 2H), 6.53 (d, *J* = 7.8 Hz, 2H), 5.10 (s, 2H), 5.04 (s, 2H); ^{13}C NMR (125 MHz, DMSO) δ (ppm) 177.7, 161.2, 147.4, 141.8, 136.9, 131.1, 130.9, 129.6, 126.3, 118.0, 109.4, 34.9, 34.5; ^{19}F NMR (282 MHz, $CDCl_3$) δ (ppm): −135.56 to −135.69 (m, 2F), −138.23 to −138.34 (m, 2F), −144.36 to −144.49 (m, 2F), −149.67 (t, *J* = 20.8 Hz, 1F), −157.53 to −157.84 (m, 2F); ESIMS *m/z*: 792.1 (M + H^+, 100%).

Supporting Information

Supporting Information File 1

^{1}H NMR, ^{13}C NMR and ^{19}F NMR spectra; MS, UV–vis and emission spectra.
[https://www.beilstein-journals.org/bjoc/content/supplementary/1860-5397-20-169-S1.pdf]

Funding

Thanks are due to the University of Aveiro and FCT/MCTES for the financial support for LAQV-REQUIMTE. This work received financial support from FCT/MCTES (Fundação para a

Ciência e a Tecnologia and Ministério da Ciência, Tecnologia e Ensino Superior) through projects LA/P/0008/2020 doi:10.54499/LA/P/0008/2020, UIDP/50006/2020 doi:10.54499/UIDP/50006/2020 and UIDB/50006/2020 doi:54499/UIDB/50006/2020, through PT national funds within the PT2020 Partnership Agreement, and to the Portuguese NMR Network. Vítor A. S. Almodovar thanks FCT/MCTES for his doctoral grant (SFRH/BD/135598/2018).

ORCID® iDs

Vitor A. S. Almodovar - https://orcid.org/0000-0002-6019-4068
Augusto C. Tomé - https://orcid.org/0000-0003-4331-714X

Data Availability Statement

All data that supports the findings of this study is available in the published article and/or the supporting information to this article.

References

1. Farnum, D. G.; Mehta, G.; Moore, G. G. I.; Siegal, F. P. *Tetrahedron Lett.* **1974,** *15,* 2549–2552. doi:10.1016/s0040-4039(01)93202-2
2. Rochat, A. C.; Cassar, L.; Iqbal, A. Preparation of pyrrolo-(3,4-c)-pyrroles. Eur. Pat. Appl. EP0094911A2, Nov 23, 1983.
3. Grzybowski, M.; Gryko, D. T. *Adv. Opt. Mater.* **2015,** *3,* 280–320. doi:10.1002/adom.201400559
4. Głowacki, E. D.; Coskun, H.; Blood-Forsythe, M. A.; Monkowius, U.; Leonat, L.; Grzybowski, M.; Gryko, D.; White, M. S.; Aspuru-Guzik, A.; Sariciftci, N. S. *Org. Electron.* **2014,** *15,* 3521–3528. doi:10.1016/j.orgel.2014.09.038
5. Mizuguchi, J.; Wooden, G. *Ber. Bunsen-Ges.* **1991,** *95,* 1264–1274. doi:10.1002/bbpc.19910951016
6. Mizuguchi, J.; Rihs, G. *Ber. Bunsen-Ges.* **1992,** *96,* 597–606. doi:10.1002/bbpc.19920960414
7. Closs, F.; Gompper, R. *Angew. Chem., Int. Ed. Engl.* **1987,** *26,* 552–554. doi:10.1002/anie.198705521
8. Liu, Q.; Bottle, S. E.; Sonar, P. *Adv. Mater. (Weinheim, Ger.)* **2020,** *32,* 1903882. doi:10.1002/adma.201903882
9. Privado, M.; Dahiya, H.; de la Cruz, P.; Keshtov, M. L.; Langa, F.; Sharma, G. D. *J. Mater. Chem. C* **2021,** *9,* 16272–16281. doi:10.1039/d1tc02241e
10. Zhao, C.; Wang, J.; Jiao, J.; Huang, L.; Tang, J. *J. Mater. Chem. C* **2020,** *8,* 28–43. doi:10.1039/c9tc05567c
11. Kaur, M.; Choi, D. H. *Chem. Soc. Rev.* **2015,** *44,* 58–77. doi:10.1039/c4cs00248b
12. Auwalu, M. A.; Cheng, S. *Chemosensors* **2021,** *9,* 44. doi:10.3390/chemosensors9030044
13. Li, W.; Wang, L.; Tang, H.; Cao, D. *Dyes Pigm.* **2019,** *162,* 934–950. doi:10.1016/j.dyepig.2018.11.023
14. Schmitt, J.; Heitz, V.; Sour, A.; Bolze, F.; Kessler, P.; Flamigni, L.; Ventura, B.; Bonnet, C. S.; Tóth, É. *Chem. – Eur. J.* **2016,** *22,* 2775–2786. doi:10.1002/chem.201503433
15. Cai, Y.; Liang, P.; Tang, Q.; Yang, X.; Si, W.; Huang, W.; Zhang, Q.; Dong, X. *ACS Nano* **2017,** *11,* 1054–1063. doi:10.1021/acsnano.6b07927
16. Agazzi, M. L.; Almodovar, V. A. S.; Gsponer, N. S.; Bertolotti, S.; Tomé, A. C.; Durantini, E. N. *Org. Biomol. Chem.* **2020,** *18,* 1449–1461. doi:10.1039/c9ob02487e
17. Jiang, X.; Wang, L.; Tang, H.; Cao, D.; Chen, W. *Dyes Pigm.* **2020,** *181,* 108599. doi:10.1016/j.dyepig.2020.108599
18. Shaikh, S. A. L.; Birajdar, S. S.; Ambore, S. D.; Puyad, A. L.; Vijayanand, P.; Bhosale, S. V.; Bhosale, S. V. *Results Chem.* **2022,** *4,* 100473. doi:10.1016/j.rechem.2022.100473
19. Cai, Y.; Tang, Q.; Wu, X.; Si, W.; Zhang, Q.; Huang, W.; Dong, X. *ACS Appl. Mater. Interfaces* **2016,** *8,* 10737–10742. doi:10.1021/acsami.6b01533
20. Cai, Y.; Liang, P.; Tang, Q.; Si, W.; Chen, P.; Zhang, Q.; Dong, X. *ACS Appl. Mater. Interfaces* **2017,** *9,* 30398–30405. doi:10.1021/acsami.7b09025
21. Zheng, L.; Li, J.; Yu, M.; Jia, W.; Duan, S.; Cao, D.; Ding, X.; Yu, B.; Zhang, X.; Xu, F.-J. *J. Am. Chem. Soc.* **2020,** *142,* 20257–20269. doi:10.1021/jacs.0c10771
22. Sun, W.; Liu, X.-Y.; Ma, L.-L.; Lu, Z.-L. *ACS Appl. Mater. Interfaces* **2020,** *12,* 10193–10201. doi:10.1021/acsami.0c00652
23. Gutkowski, K.; Azarias, C.; Banasiewicz, M.; Kozankiewicz, B.; Jacquemin, D.; Gryko, D. T. *Eur. J. Org. Chem.* **2018,** 6643–6648. doi:10.1002/ejoc.201701593
24. Jiang, W.; Liu, Z.; Zhu, D.; Zheng, W.; Chen, L.; Zhang, X.; Zhang, G.; Yi, Y.; Jiang, L.; Zhang, D. *Angew. Chem., Int. Ed.* **2021,** *60,* 10700–10708. doi:10.1002/anie.202102131
25. Vala, M.; Krajčovič, J.; Luňák, S., Jr.; Ouzzane, I.; Bouillon, J.-P.; Weiter, M. *Dyes Pigm.* **2014,** *106,* 136–142. doi:10.1016/j.dyepig.2014.03.005
26. Beninatto, R.; Borsato, G.; De Lucchi, O.; Fabris, F.; Lucchini, V.; Zendri, E. *Dyes Pigm.* **2013,** *96,* 679–685. doi:10.1016/j.dyepig.2012.11.011
27. Almodôvar, V. A. S.; Tomé, A. C. *Molecules* **2021,** *26,* 4758. doi:10.3390/molecules26164758
28. Regeni, I.; Chowdhury, R.; Terlinden, K.; Horiuchi, S.; Holstein, J. J.; Feldmann, S.; Clever, G. H. *Angew. Chem., Int. Ed.* **2023,** *62,* e202308288. doi:10.1002/anie.202308288
29. Ogumi, K.; Nakagawa, T.; Okada, H.; Matsuo, Y. *Org. Electron.* **2019,** *71,* 50–57. doi:10.1016/j.orgel.2019.04.036
30. Du, X.; Ma, T.; Ge, T.; Chang, Q.; Liu, X.; Cheng, X. *J. Mol. Liq.* **2022,** *351,* 118605. doi:10.1016/j.molliq.2022.118605
31. Popli, C.; Patil, Y.; Misra, R. *Eur. J. Org. Chem.* **2018,** 6474–6481. doi:10.1002/ejoc.201801072
32. Costa, J. I. T.; Tomé, A. C.; Neves, M. G. P. M. S.; Cavaleiro, J. A. S. *J. Porphyrins Phthalocyanines* **2011,** *15,* 1116–1133. doi:10.1142/s1088424611004294
33. Brittain, W. D. G.; Coxon, C. R. *Chem. – Eur. J.* **2022,** *28,* e202103305. doi:10.1002/chem.202103305
34. Kikushima, K.; Koyama, H.; Kodama, K.; Dohi, T. *Molecules* **2021,** *26,* 1365. doi:10.3390/molecules26051365
35. Bhupathiraju, N. V. S. D. K.; Rizvi, W.; Batteas, J. D.; Drain, C. M. *Org. Biomol. Chem.* **2016,** *14,* 389–408. doi:10.1039/c5ob01839k
36. Calvo-Castro, J.; Morris, G.; Kennedy, A. R.; McHugh, C. J. *Cryst. Growth Des.* **2016,** *16,* 2371–2384. doi:10.1021/acs.cgd.6b00157
37. Costa, D. C. S.; Pais, V. F.; Silva, A. M. S.; Cavaleiro, J. A. S.; Pischel, U.; Tomé, J. P. C. *Tetrahedron Lett.* **2014,** *55,* 4156–4159. doi:10.1016/j.tetlet.2014.05.108
38. Khan, T. K.; Rao, M. R.; Ravikanth, M. *Eur. J. Org. Chem.* **2010,** 2314–2323. doi:10.1002/ejoc.200901460

39. Kocak, A.; Kurbanli, S.; Malkondu, S. *Synth. Commun.* **2007,** *37,* 3697–3708. doi:10.1080/00397910701569254
40. Kuwabara, J.; Yamagata, T.; Kanbara, T. *Tetrahedron* **2010,** *66,* 3736–3741. doi:10.1016/j.tet.2010.03.067

BEILSTEIN JOURNAL OF ORGANIC CHEMISTRY

Factors influencing the performance of organocatalysts immobilised on solid supports: A review

Zsuzsanna Fehér, Dóra Richter, Gyula Dargó and József Kupai*

Review

Open Access

Address:
Department of Organic Chemistry and Technology, Budapest University of Technology and Economics, Műegyetem rkp. 3., H-1111 Budapest, Hungary

Email:
József Kupai* - kupai.jozsef@vbk.bme.hu

* Corresponding author

Keywords:
asymmetric synthesis; catalyst recycling; heterogenisation; organocatalysis; solid support

Beilstein J. Org. Chem. **2024,** *20,* 2129–2142.
https://doi.org/10.3762/bjoc.20.183

Received: 30 March 2024
Accepted: 01 August 2024
Published: 26 August 2024

This article is part of the thematic issue "5th International Symposium on Synthesis and Catalysis (ISySyCat 2023)".

Guest Editor: A. Burke

Abstract

Organocatalysis has become a powerful tool in synthetic chemistry, providing a cost-effective alternative to traditional catalytic methods. The immobilisation of organocatalysts offers the potential to increase catalyst reusability and efficiency in organic reactions. This article reviews the key parameters that influence the effectiveness of immobilised organocatalysts, including the type of support, immobilisation techniques and the resulting interactions. In addition, the influence of these factors on catalytic activity, selectivity and recyclability is discussed, providing an insight into optimising the performance of immobilised organocatalysts for practical applications in organic chemistry.

Introduction

Organocatalysts are small molecules that do not contain a metal atom in the reaction centre and are able to increase the speed of reactions. They have proven their place among the efficient and robust catalysts on numerous occasions since the two seminal works [1,2] published in 2000. Since then, organocatalysis has been combined with many other areas of research, such as photocatalysis, electrochemistry and mechanochemistry [3-5], while List and MacMillan were awarded the Nobel Prize in 2021 for the development of asymmetric organocatalysis [6]. To date, industrial companies have used a number of asymmetric organocatalytic processes to synthesise pharmaceuticals and fine chemicals on large scales [7].

Catalyst recycling is key from both an economic and an environmental perspective. An efficient catalytic process is characterised by the fact that the catalyst can be easily and, if possible, completely separated from the reaction mixture. Catalysts can be classified into homogeneous and heterogeneous catalysts. In homogeneous catalysis, the reaction components and the catalyst are in the same phase. Active catalytic sites are readily accessible to the reactants and therefore generally result in higher catalytic activity and selectivity [8]. As a result, homogeneous catalysis is generally preferred to heterogeneous catalysis, especially in the fine chemical and pharmaceutical industries [9]. The limitation of homogeneous catalysts, however, is

their complex, time-consuming and energy-intensive recovery and subsequent recycling. Therefore, synthetic modification of catalysts is a commonly used method to aid their recovery.

Obstacles to the recycling of homogeneous catalysts can be addressed by heterogenisation of homogeneous catalysts [10], either following their application as homogeneous catalysts or before their application (heterogeneous catalysis). In heterogeneous catalysis, catalysts and reactants are present in different phases. Heterogeneous catalysts are easy to handle and can be easily separated from the reaction mixture by filtration, centrifugation or magnetic force, thus allowing catalysts to be recycled multiple times. Most highly stable and recyclable catalysts are attached to solid supports [11].

Solid supports are generally insoluble materials preferably with a large surface area to maximise the number of active sites for catalyst attachment. The advantages of such supports have been demonstrated by numerous reports on immobilised catalysts [12-14]. The type of support and the immobilisation technique have a major influence on the properties and thus performance of the resulting heterogeneous catalyst.

However, immobilisation and structural modification introduce additional steps in the synthesis of the catalyst. Moreover, the catalytic activity and selectivity of immobilised catalysts are often lower than those of the corresponding native catalysts. In addition, inactivation due to degradation may also occur. For long-term use, consistently high yields (and selectivity) are required over repeated runs, as these are indicative of the robust nature of the catalyst system.

A real challenge is to develop a supported organocatalyst whose catalytic efficiency can be reproduced over a sufficient number of reaction cycles. Despite the difficulty of the challenge, the design of heterogeneous, recyclable organocatalytic systems is of high interest [8]. The continued development of efficient catalytic recovery methods, such as the application of immobilised organocatalysts [14,15] and heterogeneous organocatalysis [16-18], could be a potential driver for the introduction of, for example, enantioselective organocatalysis in the pharmaceutical industry [19]. Knowledge of the factors that influence catalyst performance is crucial to the development of high performance immobilised organocatalysts.

Review

Characteristics of the solid support

Considering the support type, organic polymer-supported, silica-supported [20-25], glass beads [26] and magnetic nanoparticle-supported [27-32] organocatalysts are pivotal in the field of immobilised organocatalysts. Polymer-supported organocatalysts are commonly immobilised on polystyrene (PS) [28,33-38], as well as on other materials such as nylon 6,6 [15], chitosan [39,40], and polymethylhydrosiloxane (PMHS) [41]. The role of the polymers as supports for catalysts is not merely passive. These supports significantly influence the reaction environment and catalytic efficiency [42]. Attachment methods, spacer lengths, and polymer nature profoundly impact the catalyst's performance and recyclability. Various immobilization strategies, including covalent bonding and encapsulation, cater to different polymer types. Soluble polymers enhance diffusion, while insoluble ones ensure stability and high loading capacities [42]. Silica is also widely applied due to its ease of functionalisation and thermal stability [43]. The controllability of surface, geometry, and pore size makes silica-based materials sustainable and functionalisable supports for organocatalytic reactions [44].

The particle morphology of mesoporous silica can be tuned to various shapes, including spheres, tubes, and rods of various dimensions [45], by using a co-condensation method performed under low surfactant concentration conditions [46-50], changing the concentration, molecular size, and hydrophilicity/hydrophobicity of the organoalkoxysilane precursors [51]. Various morphologies of mesoporous silica, including fibre, platelet, rod, and film, can be generated by altering the reaction conditions during synthesis [52-57] or by using potassium chloride or ammonium fluoride salts as additives [58-60]. In a comprehensive study [61], the catalytic properties of three types (rope, rod and fibre) of mesoporous silica Santa Barbara Amorphous (SBA-15) and small pore-sized Mobil Composition of Matter (MCM-41) were applied and compared as supports of an organocatalyst. These silicas were modified by incorporating an organosulfonic acid group (propylenesulfonic acid) through a post-synthesis grafting method. Their catalytic performance was studied and compared in the esterification of methanol or glycerol with oleic acid (**1**). It was observed that substrate conversion and product yield also depended on the particle morphology. Rope-type propylsulfonic SBA-15 mesoporous silica gel showed the highest catalytic activity in both studied esterification reactions (Scheme 1).

By adjusting the pore size of the support, the catalyst selectivity can be influenced. To counteract the decrease in selectivity caused by catalyst immobilisation, the concept of “confinement” was introduced [62], which involves forcing the catalytic moieties into confined spaces. The confinement of the heterogeneous version of cinchona amine and thiourea catalysts was reported, leading to improved enantioselectivity values in the Michael addition of nitromethane (**5**) to chalcone (**6**) through modification of the pore size of mesoporous silica **8** or **9** (Scheme 2) [63]. Thus, for cinchona thiourea, enantioselectiv-

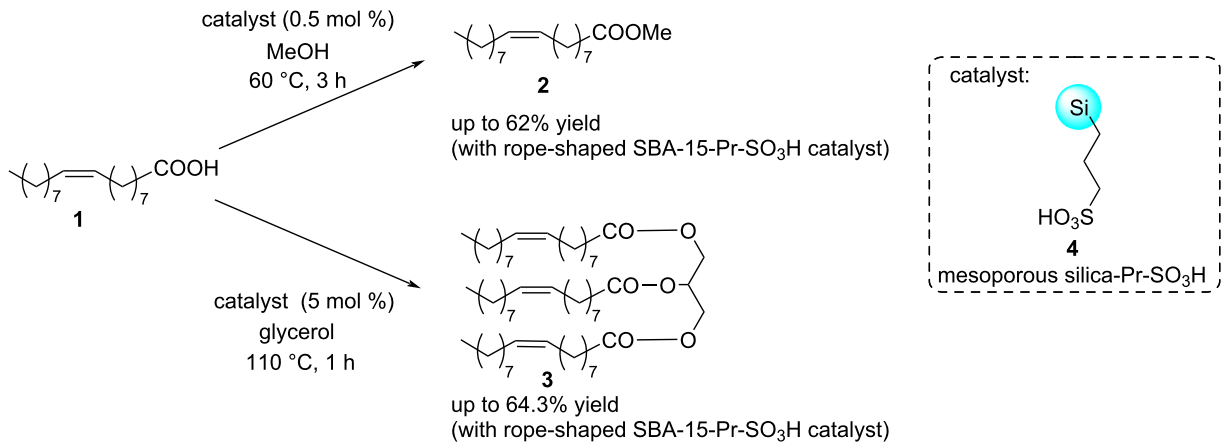

Scheme 1: Esterification of oleic acid (**1**) with propylsulfonic acid (Pr-SO_3H)-functionalised mesoporous silica catalyst **4**.

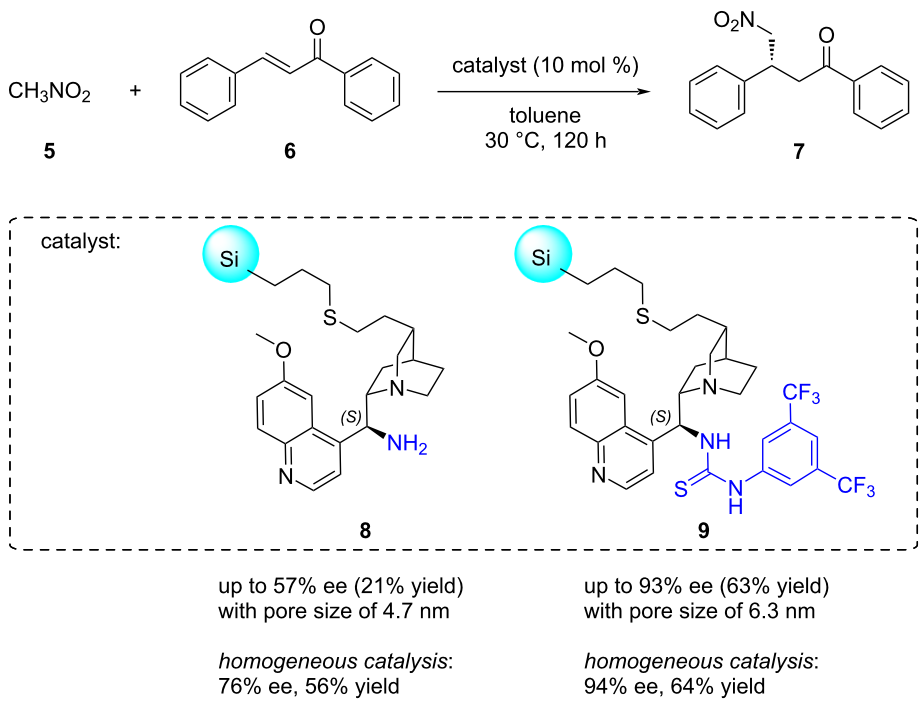

Scheme 2: Using confinement of organocatalytic units for improving the enantioselectivity of silica-supported organocatalysts in the Michael addition of nitromethane (**5**) to chalcone (**6**).

ity not only increased with reduced pore size but even reached the level of the homogeneous catalyst when the support pore size was reduced to 6.3 nm. This resulted in obtaining the (*R*)-configured product **7** with 63% yield and 93% ee, as opposed to a 55% yield and 39% ee for a pore size of 11.3 nm [64].

Catalyst supports must meet certain criteria, including being chemically inert, and the supported catalyst should exhibit high stability across various reaction conditions while also being easily recyclable [8,64]. When the solid support is not inert, it can lead to a decrease in selectivity.

Connon and co-workers have attached a cinchona thiourea organocatalyst to magnetic nanoparticles **13** for the Michael addition of dimethyl malonate (**10**) to *trans*-β-nitrostyrene (**11**) (Scheme 3) [31].

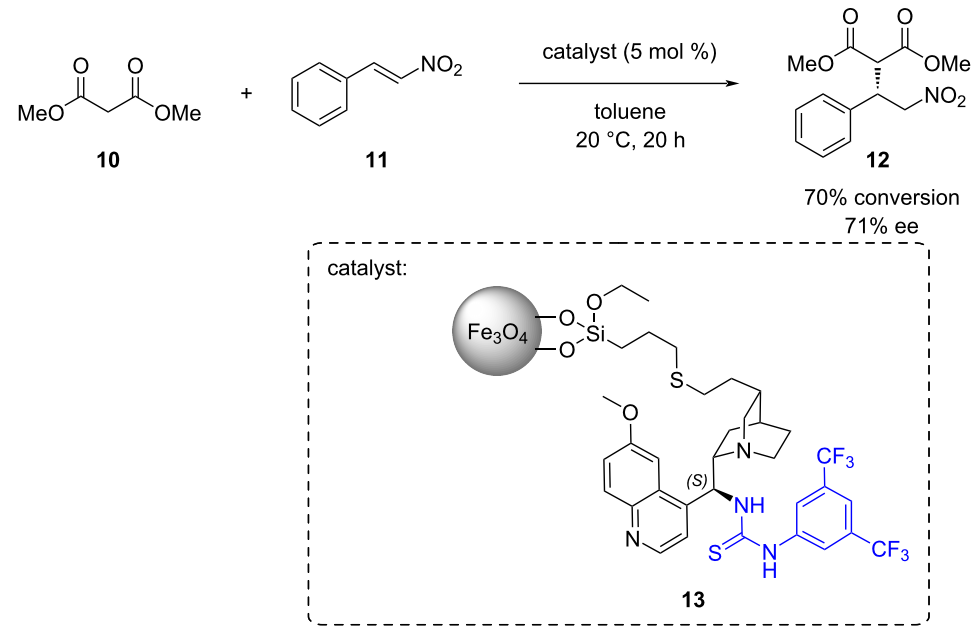

Scheme 3: Michael addition catalysed by cinchona thiourea immobilised on magnetic nanoparticles (**13**).

To explore the potential impact of nanoparticles on catalyst efficiency, experiments were conducted. It was discovered that the nanoparticles themselves catalysed the formation of the racemic product in the absence of the thiourea catalyst. This finding elucidates the relatively poor enantioselectivity observed in reactions catalysed by the magnetic nanoparticle-supported organocatalyst. To validate this hypothesis, the Michael addition was repeated in the presence of both unsupported thiourea **14** and the nanoparticles. The resulting product was isolated with only 84% ee, indicating that the nanoparticles compete with the thiourea catalyst **14** for the substrate under these conditions (Scheme 4).

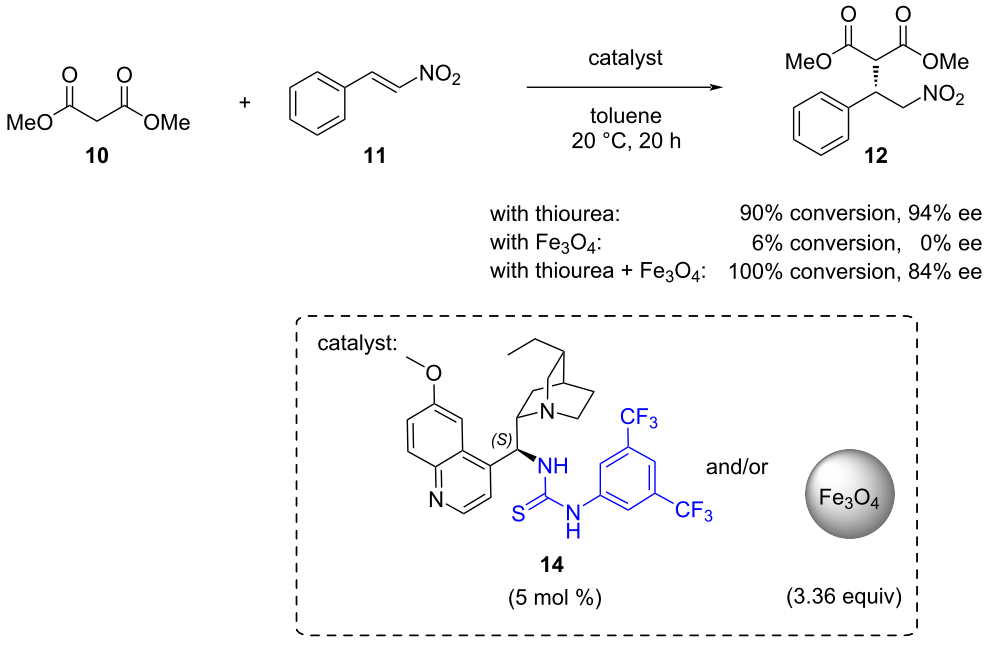

Scheme 4: Michael addition catalysed by cinchona thiourea in the presence of magnetic nanoparticles.

Thiel and co-workers examined *N*-benzylthiazolium salts **17** anchored covalently to mesoporous materials in a benzoin condensation reaction (Scheme 5) [65]. Initially good yields were observed, even after a short reaction time, but a drop in yield was seen after reusing the catalysts for a second run. This decrease was attributed to the use of a protic solvent, MeOH, in combination with basic Et_3N, which could degrade the surface of the support and result in the leaching of the active sites or the restructuring of the mesoporous material. This could have been avoided by performing reactions in a less protic and less polar solvent.

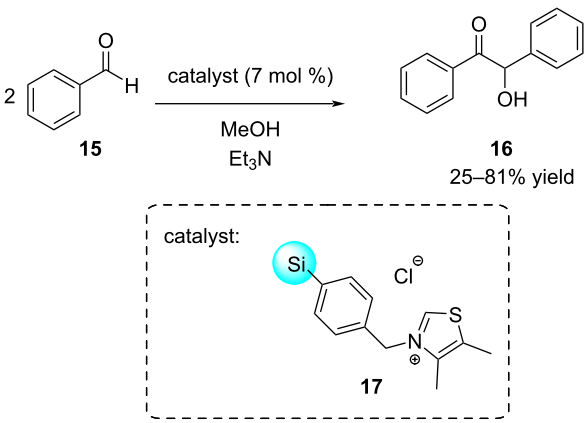

Scheme 5: Benzoin condensation catalysed by *N*-benzylthiazolium salt attached to mesoporous material.

Attaching catalysts to solid supports also offers the potential for enhancing catalyst stability. Boyer and co-workers reported the use of silica nanoparticle-supported eosin Y **21** as a photocatalyst in reversible addition fragmentation chain transfer (RAFT) photo-polymerisation reactions (Scheme 6) [24]. Previous endeavours utilising the homogeneous catalyst led to catalyst degradation or failure to remove the catalyst properly which resulted in the degradation of the polymer itself [66]. By employing the supported photocatalyst, reduced contamination was demonstrated in the final product and the catalyst could be recycled over five polymerisation cycles at ultralow catalyst loadings (6 ppm), thereby confirming the stability of the catalyst.

Immobilisation methods

Catalysts are generally immobilised via various interactions between the support and the active catalytic species. These methods can be classified into four categories: covalent bonding, non-covalent interactions (physisorption), ionic bonding, and encapsulation. The catalysts are connected to the support via strong chemical bonds in covalent bonding. In non-covalent interactions, the catalysts are adsorbed onto the support surface through weaker intermolecular forces, such as van der Waals forces and hydrogen bonding. Ionic catalysts form ionic bonds or those that can be ionised under immobilisation conditions. Encapsulation involves physically trapping the catalyst within the pores or cavities of the support [8,67].

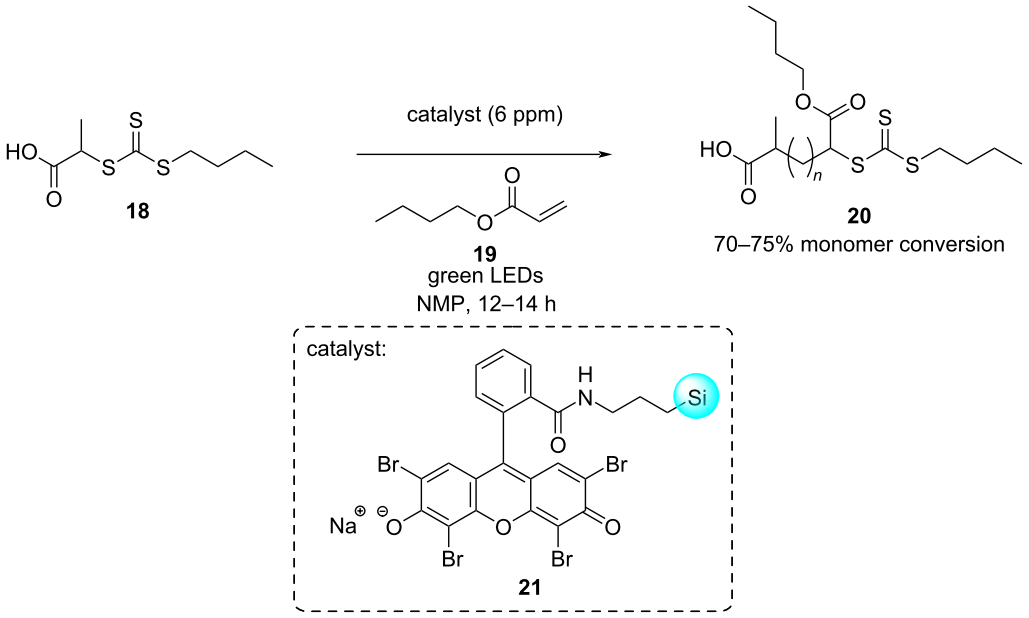

Scheme 6: Photoinduced RAFT polymerisation of *n*-butyl acrylate (**19**) catalysed by silica nanoparticle-supported eosin Y **21**, which could be recycled over five reaction cycles.

Adsorption is a non-covalent reversible technique for attaching organocatalysts to supports. It offers a facile and modular construction of immobilised chiral catalysts with maintained or even improved activity and stereoselectivity [68-70]. The main advantages of catalyst immobilisation by adsorption are that minimal modifications of the parent catalysts are required, few reagents are needed, and it is a relatively cheap and easily implemented method [69,71]. Therefore, adsorption is a popular method for immobilising catalysts. However, this method has a major drawback as the catalyst can easily leach into the solution as it reaches equilibrium between the absorbed species on the surface and the solubilised species. To improve the stability of the supported catalyst, it is important to modify the catalyst and support to enable hydrogen bonding.

This method can also bring the catalyst closer to the support, impacting electronic properties and ligand conformation. With large catalyst molecules, the pores of an ordered mesoporous material being similar in size to the catalyst can create significant diffusion barriers as the catalyst attempts to enter the pores. As a result, the pore channels that are distant from the pore openings are unlikely to be accessible to the catalyst [72].

Ionic bonding is a straightforward and economical immobilisation method. This form of non-covalent immobilisation can be reversed by altering the temperature and ionic strength [71]. Furthermore, the electrostatic interaction between the homogeneous catalyst and the support is robust enough to reduce leaching significantly [67,73]. However, a potential drawback of this technique is that the presence of a charged support can lead to complications, such as distortion of the catalyst structure and changes in the reaction kinetics.

The non-covalent immobilisation of chiral organocatalysts can also be carried out within deep eutectic solvents (DESs). Very recently, a cinchonidine-squaramide organocatalyst was immobilised in three types of natural DESs, namely betaine/sorbitol/water, betaine/xylitol/water, and betaine/mannitol/water [74]. In these systems, the recyclability of the organocatalyst was investigated and several reaction cycles were performed using the same DESs and organocatalyst. For example, in the Michael addition of methyl 2-oxocyclopentane-1-carboxylate and *trans*-β-nitrostyrene, the recyclability of the organocatalyst in the betaine/sorbitol/water DES system was demonstrated up to 10 cycles without any significant decrease in yield (up to 99%) or stereoselectivity (up to 96% ee).

Encapsulation is an irreversible method and the only catalyst immobilisation process that does not require any interaction between the catalyst and the support. Because of this, it is the sole technique which attempts to mimic the homogeneously catalysed reaction process [75]. It typically results in enhanced properties, e.g., augmented morphological stability, tailored physicochemical permeability, and reduced catalyst leakage [76].

When constructing a support around a catalyst, the catalyst must remain stable under the synthesis conditions of the support. If the catalyst can be easily synthesised in a few steps, assembling it within the pores is preferable. However, if the catalyst is difficult to synthesise but remains stable, forming the support around it is advisable [67]. Another limitation of the encapsulation method is that the size of the pore openings in the support must be smaller than the kinetic size of the immobilised catalyst [77].

Covalent tethering is a method of bonding that creates stable catalysts and minimises catalyst leaching. However, this technique has some limitations. Some covalent immobilisation methods involve complex synthetic manipulations, making them unsuitable for large-scale preparations. Furthermore, catalysts bound to carriers may experience restrictions in mobility, limiting their ability to undergo conformational changes necessary for catalysis, especially in the case of enzymes [72,78]. Overall, covalent tethering techniques are the preferred approach to designing stable heterogeneous organocatalysts, provided that the covalent modification does not involve complex synthetic steps.

Recent advancements in materials synthesis and nanotechnology have expanded the repertoire of techniques available for designing catalysts with controlled structures to promote complex reactions selectively. A recent review of Francuisco Zaera [79] discusses key research directions in the transition from homogeneous to heterogeneous catalysis. Special nanostructures, the so-called metal-organic frameworks (MOF), covalent organic frameworks (COF), porous organic frameworks (POF), and hyperbranched systems are formed with a special case of tethering. The ability to predesign both primary and high-order structures serves as a great advantage in these catalytic systems, making them easily fine tuneable. Catalytically active sites can be formed by direct condensation or post-synthetic modifications. In the case of catalyst immobilisation post-synthetic modifications play a more important role.

MOFs are a type of porous crystalline polymers where organic ligands are coordinated to metal clusters [80-90]. The framework can be post-synthetically modified by functional organic sites, often specifically chiral functionalities, giving easily recyclable asymmetric catalysts. The asymmetric sites can be different types, commonly they are binaphthyl-, biphenyl- [91-93] and proline-based [94,95].

COFs are a type of crystalline porous material, consisting of covalently linked organic ligands [96,97]. Since the framework only has organic building blocks, both condensation [98] and post-synthetic modification [99] methods can be used to immobilise organocatalysts. Asymmetric organocatalysis is commonly achieved by pyrrolidone ligands, with great results in a variety of reactions, such as Michael [100] and aldol [101] reactions.

POFs [102] are hydrocarbon systems that contain pores, of which COFs are a subgroup. POFs are widely applied in the fields of gas adsorption and storage, the separation of gases, catalysis, energy storage, photocatalysis, etc., and have many different types, such as hyper-cross-linked polymers (HCPs), polymers of intrinsic microporosity (PIMs), covalent organic frameworks (COFs), extrinsic porous molecules, and porous organic cages [103] etc. Since in terms of organocatalyst immobilisation COFs are the most important, further discussion of POFs is not included in this review.

Hyperbranched systems [104-106] and dendrimers [107-109] have also emerged as alternative soluble supports for catalyst immobilisation. In these systems the catalyst moieties can be built in at the core, at the periphery, or at intermediate positions, affecting the catalytic performances differently [110]. An advantage of dendrimer-supported organocatalysts are their enzyme-like properties [111,112]. Selective binding and cooperative catalysis can give the catalyst high selectivity and activity.

Interactions between the support and other components

The interaction between the solid support and the organocatalyst [113], reactants [114], product [115] or solvent [116] can significantly impact catalytic activity. These interactions often manifest in various forms of adsorption: physisorption, involving forces like van der Waals interactions and hydrogen bonding, or chemisorption, which may involve ionic or covalent bonding. These adsorptive interactions can alter the electronic properties and conformation of the supported organocatalyst, thereby influencing its catalytic activity compared to its homogeneous counterpart. For instance, Fotaras et al. showed that the incorporation of a tripeptide-like prolinamide-thiourea organocatalyst onto commercially available resins (JandaJel, polystyrene-divinylbenzene, and ChemMatrix) results in diminished catalytic activity, both in terms of yield and enantiomeric excess values, compared to the homogeneous analogue [117]. On the contrary, Dumesic and co-workers showed that the activity of a difunctional organocatalyst in lactose hydrolysis was improved 5.2-fold by immobilisation on different solid supports that mimic the active site channels of enzymes [113].

In a solid-supported system, the solvent can exert a different influence on the catalytic activity compared to a homogeneous catalyst. Solvent molecules present on the support surface might partially obstruct the active sites of the catalyst. Therefore, selecting the appropriate solvent may require adjustments to optimise the performance of the solid-supported organocatalyst [116]. Moreover, before the immobilisation of catalysts, it is necessary to consider whether the solid support itself can catalyse the desired or side reactions. This could be advantageous in some cases, i.e., when the solid support cooperatively helps the reaction [118], but in asymmetric synthesis, background activity of the solid support can lead to lower stereoselectivity, as previously shown in Scheme 4.

Solutions for limitations of solid-supported organocatalysts

The properties and applicability of an immobilised catalyst depend not only on the immobilisation method and the physicochemical characteristics, porosity, and dimensions of the support, but can also be influenced by several other factors. In a homogeneous system, rapid diffusion, and creation of catalyst–reactant interactions are possible because the organocatalyst is dissolved in the reaction mixture. However, in a solid-supported organocatalyst, the reactants need to diffuse to the active sites on the solid support. Diffusion limitations can decrease the effective concentration of reactants at the catalytic sites, resulting in lower reaction rates compared to the homogeneous catalyst. Thus, optimising reactor design, including appropriate mixing and flow characteristics, can help to minimise these limitations. Higher reactant concentrations may also be necessary to overcome diffusion limitations and maintain suitable concentrations at the active sites [119].

Fülöp and co-workers proved the diffusion dependence by employing the Koros–Nowak criterion test [120] in the conjugate addition of propanal (**22**) and *trans*-β-nitrostyrene (**11**) catalysed by a simple solid-supported peptidic catalyst **24** using a continuous flow reactor. To overcome the diffusion limitations, elevated pressure was applied. Increasing the pressure from atmospheric to 60 bar resulted in a 12% increase in yields, however, further increase in pressure proved to be non-beneficial. Moreover, increasing the temperature provided higher yields at optimised pressure (60 bar) but also led to lowered enantioselectivity (Scheme 7) [121].

Zhang and co-workers prepared a novel polymer with an ordered mesoporous system, resulting in a high surface area and uniform pore size. As a result, a high degree of dispersion of the piperazine active sites was achieved, leading to a catalyst exhibiting comparable activity and selectivity to that of a homogenous organocatalyst. Moreover, the hydrophobic surface of the

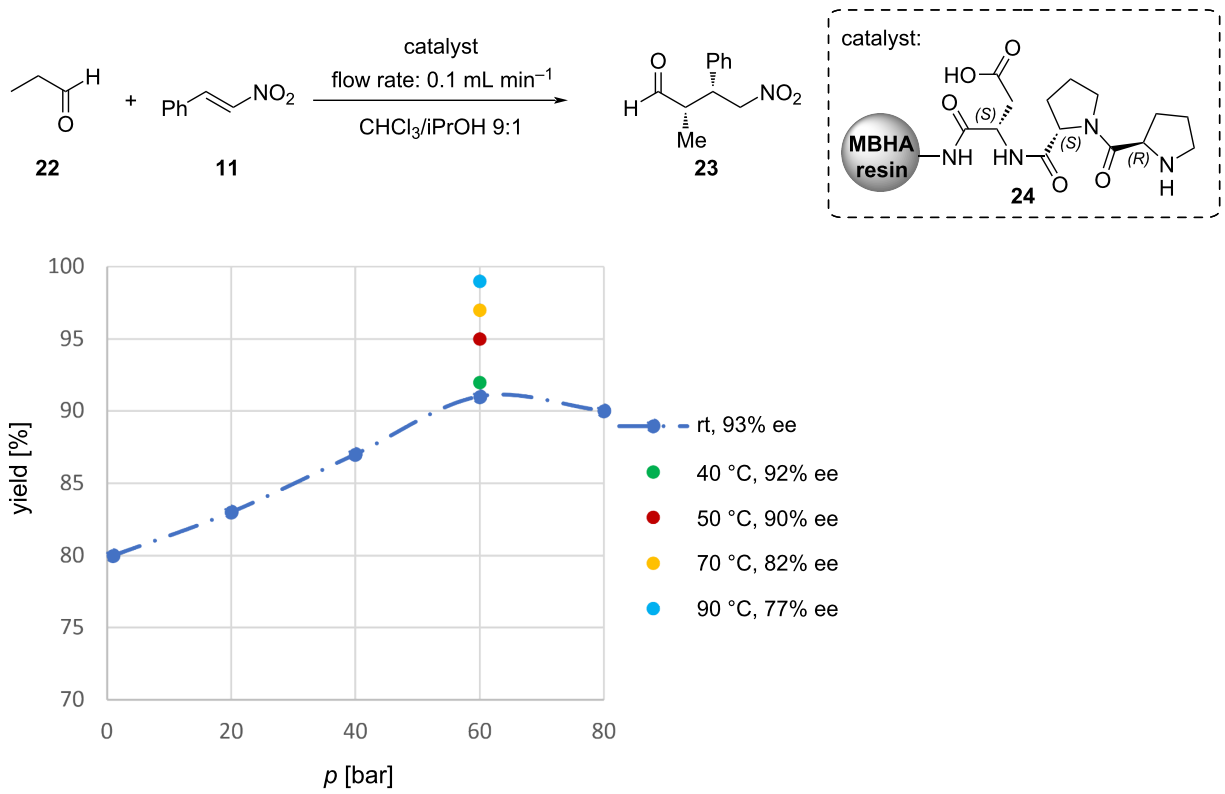

Scheme 7: Pressure and temperature dependence of the 1,4-addition of propanal to *trans*-β-nitrostyrene under continuous flow conditions.

catalyst enhanced the mass transport of organic reactants in water [122]. Based on similar mesoporous catalysts [123,124], it can be concluded that with a properly designed pore size resulting in a high density of active catalytic sites, diffusion control could be diminished.

Furthermore, the solid support may impose restrictions on access to the active sites of the organocatalyst. If the active sites are too close to the support backbone or situated within the porous structure of the support, they are less accessible for larger reactant molecules, thereby affecting the catalytic activity and selectivity. Proper design of the linker between the catalytic sites and the support surface, along with careful selection of the solid support, can help to optimise the accessibility of the active sites and mitigate this limitation [65,125].

Consequently, the properties of the supported organocatalyst also depend on the density of catalytic sites on the support surface, as well as the nature and length of the linker [8]. Additionally, the linker itself could serve as a competitive active site. In the case of enantioselective catalysis, the linker could promote the formation of racemic products, leading to lower stereoselectivity. Moreover, in catalyst co-polymerisation, the organocatalyst might be enclosed within the inner part of the polymer bead, rendering it inaccessible for reactants, or the repeating unit of the polymer could act as a competitive active site.

On the other hand, in some cases, the support surface can even impede unwanted side reactions. Pericàs and co-workers immobilised a thiourea organocatalyst on PS (**28**) and applied it in the enantioselective α-amination of 1,3-dicarbonyl compounds [36]. Unlike homogeneous thioureas, catalyst **28** is not irreversibly deactivated by azodicarboxylate reagents. In the attempt to recycle catalyst **28** for the reaction between ethyl 2-oxocyclopentanecarboxylate (**25**) and di-*tert*-butyl azodicarboxylate (**26**) (Scheme 8), a decline in catalytic activity was initially noticed. While this could be attributed to the nucleophilic deactivation of thioureas by azodicarboxylates in a homogeneous phase, as noted by Takemoto [126], it was suggested that this interaction would be significantly impeded by the polymer backbone. Alternatively, it was proposed that this degradation could be due to protonation of the basic tertiary amine unit. It was found that washing the resin with triethylamine between reaction cycles was sufficient to regenerate the catalyst. Consequently, high yields (85–94%) and enantiomeric excess values (90–92%) were consistently achieved over 9 reaction cycles.

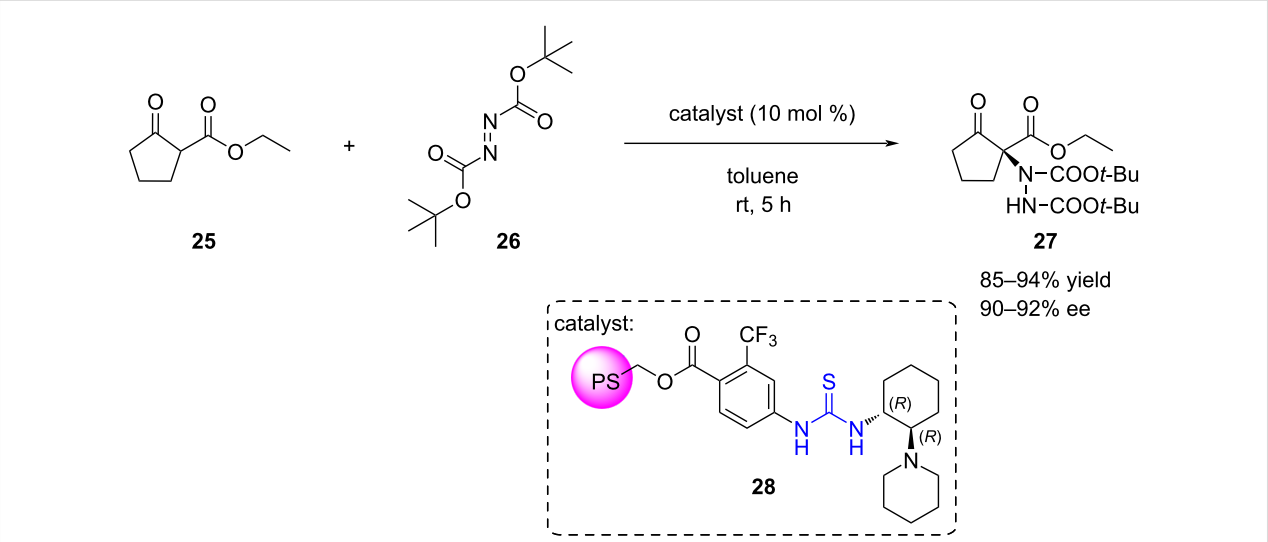

Scheme 8: α-Amination of ethyl 2-oxocyclopentanecarboxylate catalysed by PS-THU which could be recycled over 9 reaction cycles.

In a previous work conducted in our research group, we investigated the influence of various linkers of cinchona squaramide organocatalysts immobilised on a poly(glycidyl methacrylate) (PGMA) solid support [127]. The support consisted of well-defined monodispersed PGMA microspheres, which were prepared through thorough parameter optimisation. Three amine-functionalised cinchona derivatives **29–31** were immobilised on this polymer support by utilising its reactive epoxy groups (Scheme 9).

These structurally diverse precatalysts were prepared by modifying the cinchona skeleton at different positions to investigate

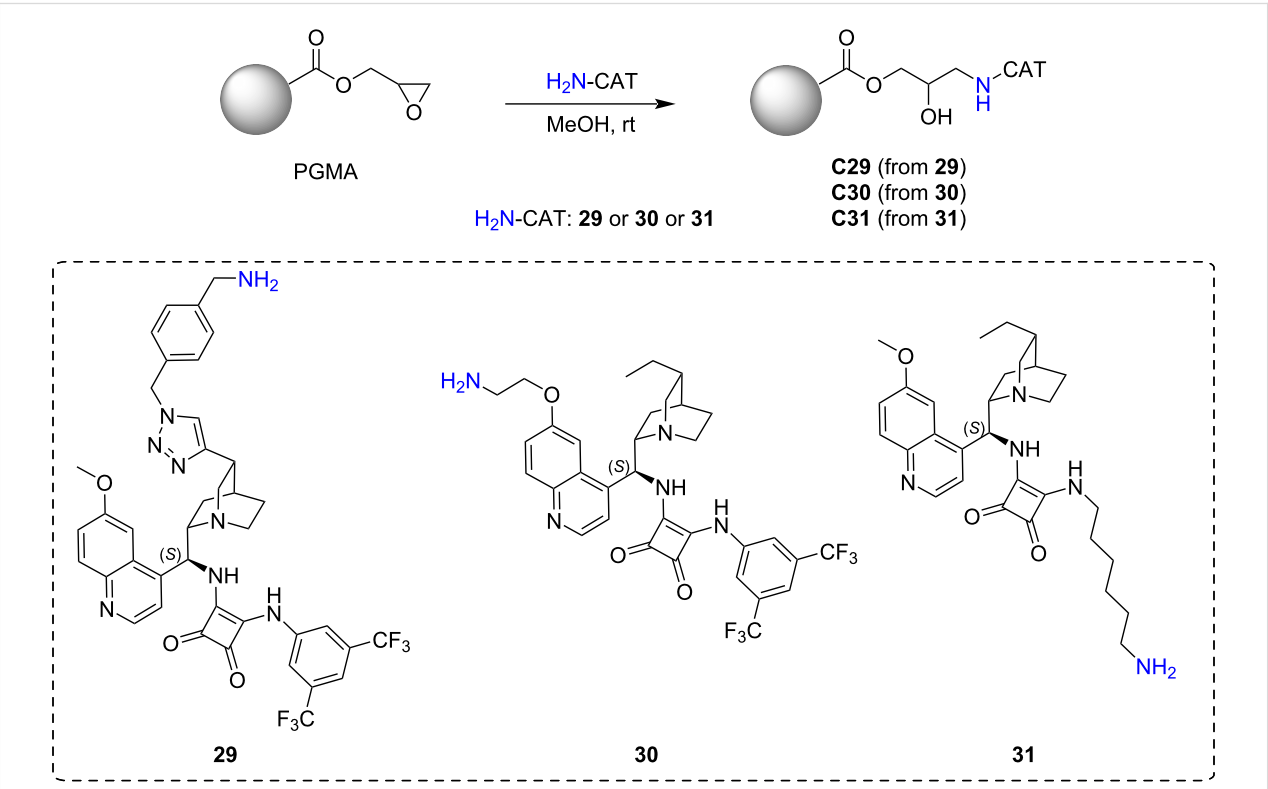

Scheme 9: Preparation of supported catalysts **C29–C31** from cinchona squaramides **29–31** modified with a primary amino group.

how the amino group-containing linker affects them. The immobilised organocatalysts' catalytic activities and enantioselectivity values were evaluated in the Michael addition of pentane-2,4-dione (**32**) and *trans*-β-nitrostyrene (**11**). The catalysts could be reused over five reaction cycles through centrifugation, without significant loss of activity (Scheme 10).

The catalysts showed no significant differences in terms of yields. However, catalysts **C30** and **C31** achieved higher enantiomeric excess values (up to 79% ee and 59% ee, respectively) compared to catalyst **C29** (up to 31% ee). Among the immobilised catalysts, **C30** produced the best results. Catalyst **C29**, which showed lower selectivity, features a 1,2,3-triazole-4-yl unit as the substituent at the tertiary amine-containing quinuclidine motif, whereas **C30** and **C31** have an ethyl group attached to the ring in this position. Additionally, catalyst **C31** has a longer-chain linker, but its squaramide NH groups are more acidic due to binding with an electron-withdrawing group. This acidity can result in stronger hydrogen bonds between the substrate and the catalyst **C30**, which contains a bis(trifluoromethyl)phenyl-modified squaramide moiety. This stronger interaction potentially enhances the catalyst–substrate interaction, allowing for more precise stereocontrol of the reaction [128-132]. Therefore, the difference in enantioselectivity values may be attributed to these electronic effects. Ultimately, the most favourable outcomes were achieved with catalyst **C30** at 0 °C, with yields reaching up to 84% and enantiomeric excess reaching 96%.

As highlighted in this review, different factors can aid in the design and optimisation of solid-supported organocatalysts, ensuring their catalytic activity is comparable or even superior to their homogeneous counterparts. A notable example of a highly recyclable solid-supported organocatalyst was demonstrated by List and co-workers, who showcased the robustness of a cinchona alkaloid-based sulfonamide organotextile catalyst **36** (immobilised on nylon 6,6) through hundreds of recycling experiments (Scheme 11) [15]. The organotextile catalyst **36** exhibited a very similar enantioselectivity (93% ee) to the homogeneous catalyst (94% ee) in the alcoholytic desymmetrisation of a cyclic anhydride **34** albeit requiring a slightly longer reaction time. Compared to polymer films, textile fibres offer a significantly higher surface area, potentially contributing to the maintenance of high enantioselectivity (>90% ee) for over 250 cycles.

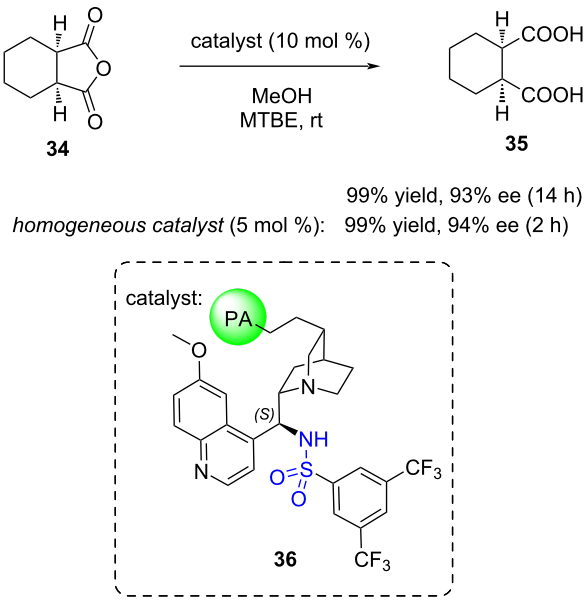

Scheme 11: Alcoholytic desymmetrisation of a cyclic anhydride **34** catalysed by polyamide-supported cinchona sulfonamide **36**.

Conclusion

Solid-supported organocatalysts can provide an environmentally friendly and economical solution even for industrial processes. To maximise their adoption by industry, efficient catalysts that can be easily recycled need to be developed. Immobilisation on solid supports such as polymers, silica, glass beads and magnetic nanoparticles has proven effective, although each method presents unique challenges regarding catalytic activity, selectivity and stability. A number of factors need to be taken

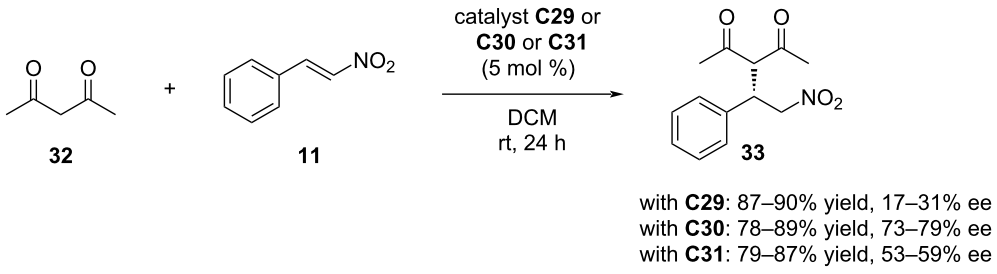

Scheme 10: Application of PGMA-supported organocatalysts **C29–C31** in the asymmetric Michael addition of pentane-2,4-dione (**32**) and *trans*-β-nitrostyrene (**11**).

into account during the development process. The surface area, morphology and pore size of the solid support have a strong influence on the catalytic properties. Innovative approaches such as confinement effects and advanced material designs such as MOFs, COFs and hyperbranched systems offer promising solutions to enhance catalyst efficiency and selectivity. It is also crucial that the supports meet certain requirements: they must be chemically inert, stable and easily recyclable. Examples can also be found where the stability of the catalyst is increased through the attachment to the support.

Of the immobilisation methods, covalent tethering is preferred because of the resulting stable immobilisation. However, simple catalyst grafting with few steps is important and favourable for industrial applications. Interactions between the support, the catalytically active site and other components must also be taken into account in catalyst development. Additionally, the selection of the appropriate solvent is critical.

To mitigate diffusion limitation, it is important to ensure appropriate mixing and flow characteristics and adequate concentration of reactants and catalytic units. Flow chemistry can be easily combined with solid-supported organocatalysis, while even elevated pressure can be applied to reduce diffusion limitations. The size, rigidity and character of the linker also play an important role in catalyst design.

Despite these advances, the development of highly efficient and recyclable organocatalysts remains a challenge. Trade-offs between immobilisation methods and the catalytic performance require further research. Future directions include improving immobilisation strategies, exploring new support materials and optimising reaction conditions to alleviate diffusion limitations and improve the availability of active sites.

In summary, the evolving development of solid-supported organocatalysts has significant potential for industrial applications, particularly in the pharmaceutical and fine chemical industry. The design of recyclable, robust and high-performance organocatalyst systems will continue to encourage innovation in this area, contributing to more sustainable and efficient catalytic processes.

Funding

This research was funded by the National Research, Development, and Innovation Office (grant number FK138037), the Jozsef Varga Foundation (J. K.), and the Richter Gedeon Excellence PhD Scholarship of the Richter Gedeon Talentum Foundation, Gedeon Richter Plc. (Z. F., D. R., G. D.). Project no. RRF-2.3.1-21-2022-00015 has been implemented with the support provided by the European Union.

Author Contributions

Zsuzsanna Fehér: conceptualization; methodology; visualization; writing – original draft; writing – review & editing. Dóra Richter: writing – original draft; writing – review & editing. Gyula Dargó: visualization; writing – original draft; writing – review & editing. József Kupai: conceptualization; funding acquisition; project administration; supervision; writing – review & editing.

ORCID® iDs

Zsuzsanna Fehér - https://orcid.org/0000-0001-8203-4711
Gyula Dargó - https://orcid.org/0000-0003-4997-5151
József Kupai - https://orcid.org/0000-0002-4212-4517

Data Availability Statement

Data sharing is not applicable as no new data was generated or analyzed in this study.

References

1. List, B.; Lerner, R. A.; Barbas, C. F. *J. Am. Chem. Soc.* **2000,** *122,* 2395–2396. doi:10.1021/ja994280y
2. Ahrendt, K. A.; Borths, C. J.; MacMillan, D. W. C. *J. Am. Chem. Soc.* **2000,** *122,* 4243–4244. doi:10.1021/ja000092s
3. Nicewicz, D. A.; MacMillan, D. W. C. *Science* **2008,** *322,* 77–80. doi:10.1126/science.1161976
4. Chauhan, P.; Chimni, S. S. *Beilstein J. Org. Chem.* **2012,** *8,* 2132–2141. doi:10.3762/bjoc.8.240
5. Némethová, V.; Krištofíková, D.; Mečiarová, M.; Šebesta, R. *Chem. Rec.* **2023,** *23,* e202200283. doi:10.1002/tcr.202200283
6. The Nobel Prize organisation; Press Release The Nobel Prize in Chemistry 2021. https://www.nobelprize.org/prizes/chemistry/2021/press-release/ (accessed March 27, 2024).
7. Bulger, P. G. Industrial Applications of Organocatalysis. *Comprehensive Chirality;* Elsevier: Amsterdam, Netherlands, 2012; Vol. 9, pp 228–252. doi:10.1016/b978-0-08-095167-6.00911-3
8. Piermatti, O.; Abu-Reziq, R.; Vaccaro, L. Strategies to Immobilized Catalysts. In *Catalyst Immobilization: Methods and Applications;* Benaglia, M.; Puglisi, A., Eds.; Wiley-VCH: Weinheim, Germany, 2019; pp 1–22. doi:10.1002/9783527817290.ch1
9. Hübner, S.; de Vries, J. G.; Farina, V. *Adv. Synth. Catal.* **2016,** *358,* 3–25. doi:10.1002/adsc.201500846
10. Collis, A. E. C.; Horváth, I. T. *Catal. Sci. Technol.* **2011,** *1,* 912–919. doi:10.1039/c1cy00174d
11. Molnár, Á.; Papp, A. *Coord. Chem. Rev.* **2017,** *349,* 1–65. doi:10.1016/j.ccr.2017.08.011
12. Munnik, P.; de Jongh, P. E.; de Jong, K. P. *Chem. Rev.* **2015,** *115,* 6687–6718. doi:10.1021/cr500486u
13. Fulgheri, T.; Della Penna, F.; Baschieri, A.; Carlone, A. *Curr. Opin. Green Sustainable Chem.* **2020,** *25,* 100387. doi:10.1016/j.cogsc.2020.100387
14. Rodríguez-Escrich, C.; Pericàs, M. A. *Chem. Rec.* **2019,** *19,* 1872–1890. doi:10.1002/tcr.201800097
15. Lee, J.-W.; Mayer-Gall, T.; Opwis, K.; Song, C. E.; Gutmann, J. S.; List, B. *Science* **2013,** *341,* 1225–1229. doi:10.1126/science.1242196

16. Wang, X.; Blechert, S.; Antonietti, M. *ACS Catal.* **2012,** *2,* 1596–1606. doi:10.1021/cs300240x
17. Liu, X.; Tang, B.; Long, J.; Zhang, W.; Liu, X.; Mirza, Z. *Sci. Bull.* **2018,** *63,* 502–524. doi:10.1016/j.scib.2018.03.009
18. Ötvös, S. B.; Pericàs, M. A.; Kappe, C. O. *Chem. Sci.* **2019,** *10,* 11141–11146. doi:10.1039/c9sc04752b
19. Han, B.; He, X.-H.; Liu, Y.-Q.; He, G.; Peng, C.; Li, J.-L. *Chem. Soc. Rev.* **2021,** *50,* 1522–1586. doi:10.1039/d0cs00196a
20. Huh, S.; Chen, H.-T.; Wiench, J. W.; Pruski, M.; Lin, V. S.-Y. *Angew. Chem., Int. Ed.* **2005,** *44,* 1826–1830. doi:10.1002/anie.200462424
21. Yu, P.; He, J.; Guo, C. *Chem. Commun.* **2008,** 2355–2357. doi:10.1039/b800640g
22. Brunelli, N. A.; Jones, C. W. *J. Catal.* **2013,** *308,* 60–72. doi:10.1016/j.jcat.2013.05.022
23. Leyva-Pérez, A.; García-García, P.; Corma, A. *Angew. Chem., Int. Ed.* **2014,** *53,* 8687–8690. doi:10.1002/anie.201403049
24. Shanmugam, S.; Xu, S.; Adnan, N. N. M.; Boyer, C. *Macromolecules* **2018,** *51,* 779–790. doi:10.1021/acs.macromol.7b02215
25. Erigoni, A.; Hernández-Soto, M. C.; Rey, F.; Segarra, C.; Díaz, U. *Catal. Today* **2020,** *345,* 227–236. doi:10.1016/j.cattod.2019.09.041
26. Amorim, A. C.; Fonseca, D. P.; Carreiro, E. P.; Hermann, G. J.; Federsel, H.-J.; Burke, A. J. *Synlett* **2022,** *33,* 1756–1762. doi:10.1055/a-1916-4858
27. Keller, M.; Perrier, A.; Linhardt, R.; Travers, L.; Wittmann, S.; Caminade, A.-M.; Majoral, J.-P.; Reiser, O.; Ouali, A. *Adv. Synth. Catal.* **2013,** *355,* 1748–1754. doi:10.1002/adsc.201300120
28. Riente, P.; Yadav, J.; Pericàs, M. A. *Org. Lett.* **2012,** *14,* 3668–3671. doi:10.1021/ol301515d
29. Wang, B. G.; Ma, B. C.; Wang, Q.; Wang, W. *Adv. Synth. Catal.* **2010,** *352,* 2923–2928. doi:10.1002/adsc.201000508
30. Riente, P.; Mendoza, C.; Pericás, M. A. *J. Mater. Chem.* **2011,** *21,* 7350–7355. doi:10.1039/c1jm10535c
31. Gleeson, O.; Davies, G.-L.; Peschiulli, A.; Tekoriute, R.; Gun'ko, Y. K.; Connon, S. J. *Org. Biomol. Chem.* **2011,** *9,* 7929–7940. doi:10.1039/c1ob06110k
32. Kong, Y.; Tan, R.; Zhao, L.; Yin, D. *Green Chem.* **2013,** *15,* 2422–2433. doi:10.1039/c3gc40772a
33. Rueping, M.; Sugiono, E.; Steck, A.; Theissmann, T. *Adv. Synth. Catal.* **2010,** *352,* 281–287. doi:10.1002/adsc.200900746
34. Kasaplar, P.; Riente, P.; Hartmann, C.; Pericàs, M. A. *Adv. Synth. Catal.* **2012,** *354,* 2905–2910. doi:10.1002/adsc.201200526
35. Whiteoak, C. J.; Henseler, A. H.; Ayats, C.; Kleij, A. W.; Pericàs, M. A. *Green Chem.* **2014,** *16,* 1552–1559. doi:10.1039/c3gc41919c
36. Kasaplar, P.; Ozkal, E.; Rodríguez-Escrich, C.; Pericàs, M. A. *Green Chem.* **2015,** *17,* 3122–3129. doi:10.1039/c5gc00496a
37. Cañellas, S.; Ayats, C.; Henseler, A. H.; Pericàs, M. A. *ACS Catal.* **2017,** *7,* 1383–1391. doi:10.1021/acscatal.6b03286
38. Rodríguez-Rodríguez, M.; Maestro, A.; Andrés, J. M.; Pedrosa, R. *Adv. Synth. Catal.* **2020,** *362,* 2744–2754. doi:10.1002/adsc.202000238
39. Andrés, J. M.; González, F.; Maestro, A.; Pedrosa, R.; Valle, M. *Eur. J. Org. Chem.* **2017,** 3658–3665. doi:10.1002/ejoc.201700582
40. de Gonzalo, G.; Franconetti, A.; Fernández, R.; Lassaletta, J. M.; Cabrera-Escribano, F. *Carbohydr. Polym.* **2018,** *199,* 365–374. doi:10.1016/j.carbpol.2018.07.009
41. Guizzetti, S.; Benaglia, M.; Siegel, J. S. *Chem. Commun.* **2012,** *48,* 3188–3190. doi:10.1039/c2cc17919a
42. Altava, B.; Burguete, M. I.; García-Verdugo, E.; Luis, S. V. *Chem. Soc. Rev.* **2018,** *47,* 2722–2771. doi:10.1039/c7cs00734e
43. Ferré, M.; Pleixats, R.; Wong Chi Man, M.; Cattoën, X. *Green Chem.* **2016,** *18,* 881–922. doi:10.1039/c5gc02579f
44. Corma, A.; Garcia, H. *Adv. Synth. Catal.* **2006,** *348,* 1391–1412. doi:10.1002/adsc.200606192
45. Huh, S.; Wiench, J. W.; Yoo, J.-C.; Pruski, M.; Lin, V. S.-Y. *Chem. Mater.* **2003,** *15,* 4247–4256. doi:10.1021/cm0210041
46. Burkett, S. L.; Sims, S. D.; Mann, S. *Chem. Commun.* **1996,** 1367–1368. doi:10.1039/cc9960001367
47. Sims, S. D.; Burkett, S. L.; Mann, S. *MRS Online Proc. Libr.* **1996,** *431,* 77–82. doi:10.1557/proc-431-77
48. Macquarrie, D. J. *Chem. Commun.* **1996,** 1961–1962. doi:10.1039/cc9960001961
49. Huo, Q.; Margolese, D. I.; Stucky, G. D. *Chem. Mater.* **1996,** *8,* 1147–1160. doi:10.1021/cm960137h
50. Lim, M. H.; Blanford, C. F.; Stein, A. *J. Am. Chem. Soc.* **1997,** *119,* 4090–4091. doi:10.1021/ja9638824
51. Stein, A.; Melde, B. J.; Schroden, R. C. *Adv. Mater. (Weinheim, Ger.)* **2000,** *12,* 1403–1419. doi:10.1002/1521-4095(200010)12:19<1403::aid-adma1403>3.0.co;2-x
52. Yu, C.; Fan, J.; Tian, B.; Zhao, D.; Stucky, G. D. *Adv. Mater. (Weinheim, Ger.)* **2002,** *14,* 1742–1745. doi:10.1002/1521-4095(20021203)14:23<1742::aid-adma1742>3.0.co;2-3
53. Sayari, A.; Han, B.-H.; Yang, Y. *J. Am. Chem. Soc.* **2004,** *126,* 14348–14349. doi:10.1021/ja0478734
54. Bao, X. Y.; Zhao, X. S. *J. Phys. Chem. B* **2005,** *109,* 10727–10736. doi:10.1021/jp050449k
55. Jin, Z.; Wang, X.; Cui, X. *Colloids Surf., A* **2008,** *316,* 27–36. doi:10.1016/j.colsurfa.2007.08.013
56. Johansson, E. M.; Ballem, M. A.; Córdoba, J. M.; Odén, M. *Langmuir* **2011,** *27,* 4994–4999. doi:10.1021/la104864d
57. Björk, E. M.; Söderlind, F.; Odén, M. *Langmuir* **2013,** *29,* 13551–13561. doi:10.1021/la403201v
58. Schmidt-Winkel, P.; Yang, P.; Margolese, D. I.; Chmelka, B. F.; Stucky, G. D. *Adv. Mater. (Weinheim, Ger.)* **1999,** *11,* 303–307. doi:10.1002/(sici)1521-4095(199903)11:4<303::aid-adma303>3.3.co;2-d
59. Zhao, D.; Sun, J.; Li, Q.; Stucky, G. D. *Chem. Mater.* **2000,** *12,* 275–279. doi:10.1021/cm9911363
60. Björk, E. M.; Söderlind, F.; Odén, M. *J. Colloid Interface Sci.* **2014,** *413,* 1–7. doi:10.1016/j.jcis.2013.09.023
61. Jeenpadiphat, S.; Björk, E. M.; Odén, M.; Tungasmita, D. N. *J. Mol. Catal. A: Chem.* **2015,** *410,* 253–259. doi:10.1016/j.molcata.2015.10.002
62. Goettmann, F.; Sanchez, C. *J. Mater. Chem.* **2007,** *17,* 24–30. doi:10.1039/b608748p
63. Zhao, L.; Li, Y.; Yu, P.; Han, X.; He, J. *ACS Catal.* **2012,** *2,* 1118–1126. doi:10.1021/cs200588c
64. Franconetti, A.; de Gonzalo, G. *ChemCatChem* **2018,** *10,* 5554–5572. doi:10.1002/cctc.201801459
65. Zhou, Z.; Meng, Q.; Seifert, A.; Wagener, A.; Sun, Y.; Ernst, S.; Thiel, W. R. *Microporous Mesoporous Mater.* **2009,** *121,* 145–151. doi:10.1016/j.micromeso.2009.01.022
66. Padon, K. S.; Scranton, A. B. *J. Polym. Sci., Part A: Polym. Chem.* **2001,** *39,* 715–723. doi:10.1002/1099-0518(20010301)39:5<715::aid-pola1043>3.3.co;2-f

67. McMorn, P.; Hutchings, G. J. *Chem. Soc. Rev.* **2004,** *33,* 108–122. doi:10.1039/b200387m
68. Aprile, C.; Giacalone, F.; Gruttadauria, M.; Marculescu, A. M.; Noto, R.; Revell, J. D.; Wennemers, H. *Green Chem.* **2007,** *9,* 1328–1334. doi:10.1039/b709471j
69. Zhang, L.; Luo, S.; Cheng, J.-P. *Catal. Sci. Technol.* **2011,** *1,* 507–516. doi:10.1039/c1cy00029b
70. Aguilera, D. A.; Spinozzi Di Sante, L.; Pettignano, A.; Riccioli, R.; Roeske, J.; Albergati, L.; Corti, V.; Fochi, M.; Bernardi, L.; Quignard, F.; Tanchoux, N. *Eur. J. Org. Chem.* **2019,** 3842–3849. doi:10.1002/ejoc.201900247
71. Guisan, J. M., Ed. *Immobilization of Enzymes and Cells,* 3rd ed.; Methods in Molecular Biology; Humana Press: New York, NY, USA, 2013. doi:10.1007/978-1-62703-550-7
72. Zhao, X. S.; Bao, X. Y.; Guo, W.; Lee, F. Y. *Mater. Today* **2006,** *9,* 32–39. doi:10.1016/s1369-7021(06)71388-8
73. Wagner, H. H.; Hausmann, H.; Hölderich, W. F. *J. Catal.* **2001,** *203,* 150–156. doi:10.1006/jcat.2001.3296
74. Fonseca, D. P.; Amorim, A. C.; Carreiro, E. P.; Prates Ramalho, J. P.; Hermann, G. J.; Federsel, H.-J.; Duarte, A. R. C.; Burke, A. J. *SynOpen* **2023,** *07,* 374–380. doi:10.1055/a-2117-9971
75. Sadjadi, S., Ed. *Encapsulated Catalysts;* Academic Press: London, UK, 2017. doi:10.1016/c2014-0-04759-4
76. Rother, C.; Nidetzky, B. Enzyme Immobilization by Microencapsulation: Methods, Materials, and Technological Applications. *Encyclopedia of Industrial Biotechnology: Bioprocess, Bioseparation, and Cell Technology;* Wiley-VCH: Weinheim, Germany, 2014; pp 1–21. doi:10.1002/9780470054581.eib275
77. Gao, C.; Deng, X.; Zhang, J.; Ma, X. *Appl. Catal., A* **2023,** *650,* 119003. doi:10.1016/j.apcata.2022.119003
78. Shen, Q.; Yang, R.; Hua, X.; Ye, F.; Zhang, W.; Zhao, W. *Process Biochem. (Oxford, U. K.)* **2011,** *46,* 1565–1571. doi:10.1016/j.procbio.2011.04.010
79. Zaera, F. *Chem. Rev.* **2022,** *122,* 8594–8757. doi:10.1021/acs.chemrev.1c00905
80. Hoskins, B. F.; Robson, R. *J. Am. Chem. Soc.* **1990,** *112,* 1546–1554. doi:10.1021/ja00160a038
81. Lee, J.; Farha, O. K.; Roberts, J.; Scheidt, K. A.; Nguyen, S. T.; Hupp, J. T. *Chem. Soc. Rev.* **2009,** *38,* 1450–1459. doi:10.1039/b807080f
82. Corma, A.; García, H.; Llabrés i Xamena, F. X. *Chem. Rev.* **2010,** *110,* 4606–4655. doi:10.1021/cr9003924
83. Isaeva, V. I.; Kustov, L. M. *Pet. Chem.* **2010,** *50,* 167–180. doi:10.1134/s0965544110030011
84. Liu, J.; Chen, L.; Cui, H.; Zhang, J.; Zhang, L.; Su, C.-Y. *Chem. Soc. Rev.* **2014,** *43,* 6011–6061. doi:10.1039/c4cs00094c
85. Zhu, L.; Liu, X.-Q.; Jiang, H.-L.; Sun, L.-B. *Chem. Rev.* **2017,** *117,* 8129–8176. doi:10.1021/acs.chemrev.7b00091
86. Xu, W.; Thapa, K. B.; Ju, Q.; Fang, Z.; Huang, W. *Coord. Chem. Rev.* **2018,** *373,* 199–232. doi:10.1016/j.ccr.2017.10.014
87. Dhakshinamoorthy, A.; Li, Z.; Garcia, H. *Chem. Soc. Rev.* **2018,** *47,* 8134–8172. doi:10.1039/c8cs00256h
88. Yuan, S.; Feng, L.; Wang, K.; Pang, J.; Bosch, M.; Lollar, C.; Sun, Y.; Qin, J.; Yang, X.; Zhang, P.; Wang, Q.; Zou, L.; Zhang, Y.; Zhang, L.; Fang, Y.; Li, J.; Zhou, H.-C. *Adv. Mater. (Weinheim, Ger.)* **2018,** *30,* 1704303. doi:10.1002/adma.201704303
89. Chen, Y.-Z.; Zhang, R.; Jiao, L.; Jiang, H.-L. *Coord. Chem. Rev.* **2018,** *362,* 1–23. doi:10.1016/j.ccr.2018.02.008
90. Yang, D.; Gates, B. C. *ACS Catal.* **2019,** *9,* 1779–1798. doi:10.1021/acscatal.8b04515
91. Ma, L.; Falkowski, J. M.; Abney, C.; Lin, W. *Nat. Chem.* **2010,** *2,* 838–846. doi:10.1038/nchem.738
92. Mo, K.; Yang, Y.; Cui, Y. *J. Am. Chem. Soc.* **2014,** *136,* 1746–1749. doi:10.1021/ja411887c
93. Chen, X.; Qiao, Z.; Hou, B.; Jiang, H.; Gong, W.; Dong, J.; Li, H.-Y.; Cui, Y.; Liu, Y. *Nano Res.* **2021,** *14,* 466–472. doi:10.1007/s12274-020-2905-7
94. Banerjee, M.; Das, S.; Yoon, M.; Choi, H. J.; Hyun, M. H.; Park, S. M.; Seo, G.; Kim, K. *J. Am. Chem. Soc.* **2009,** *131,* 7524–7525. doi:10.1021/ja901440g
95. Zhang, Y.; Guo, J.; Shi, L.; Zhu, Y.; Hou, K.; Zheng, Y.; Tang, Z. *Sci. Adv.* **2017,** *3,* e1701162. doi:10.1126/sciadv.1701162
96. Côte, A. P.; Benin, A. I.; Ockwig, N. W.; O'Keeffe, M.; Matzger, A. J.; Yaghi, O. M. *Science* **2005,** *310,* 1166–1170. doi:10.1126/science.1120411
97. Rogge, S. M. J.; Bavykina, A.; Hajek, J.; Garcia, H.; Olivos-Suarez, A. I.; Sepúlveda-Escribano, A.; Vimont, A.; Clet, G.; Bazin, P.; Kapteijn, F.; Daturi, M.; Ramos-Fernandez, E. V.; Llabrés i Xamena, F. X.; Van Speybroeck, V.; Gascon, J. *Chem. Soc. Rev.* **2017,** *46,* 3134–3184. doi:10.1039/c7cs00033b
98. Zhang, J.; Han, X.; Wu, X.; Liu, Y.; Cui, Y. *ACS Sustainable Chem. Eng.* **2019,** *7,* 5065–5071. doi:10.1021/acssuschemeng.8b05887
99. Xu, H.; Chen, X.; Gao, J.; Lin, J.; Addicoat, M.; Irle, S.; Jiang, D. *Chem. Commun.* **2014,** *50,* 1292–1294. doi:10.1039/c3cc48813f
100. Xu, H.; Gao, J.; Jiang, D. *Nat. Chem.* **2015,** *7,* 905–912. doi:10.1038/nchem.2352
101. Xu, H.-S.; Ding, S.-Y.; An, W.-K.; Wu, H.; Wang, W. *J. Am. Chem. Soc.* **2016,** *138,* 11489–11492. doi:10.1021/jacs.6b07516
102. Debruyne, M.; Van Speybroeck, V.; Van Der Voort, P.; Stevens, C. V. *Green Chem.* **2021,** *23,* 7361–7434. doi:10.1039/d1gc02319e
103. Das, S.; Heasman, P.; Ben, T.; Qiu, S. *Chem. Rev.* **2017,** *117,* 1515–1563. doi:10.1021/acs.chemrev.6b00439
104. Irfan, M.; Seiler, M. *Ind. Eng. Chem. Res.* **2010,** *49,* 1169–1196. doi:10.1021/ie900216r
105. Wang, S.; Liu, P.; Wang, W.-J.; Zhang, Z.; Li, B.-G. *Catal. Sci. Technol.* **2015,** *5,* 3798–3805. doi:10.1039/c5cy00250h
106. Nabae, Y.; Kakimoto, M.-a. *Polymers (Basel, Switz.)* **2018,** *10,* 1344. doi:10.3390/polym10121344
107. Kofoed, J.; Darbre, T.; Reymond, J.-L. *Org. Biomol. Chem.* **2006,** *4,* 3268–3281. doi:10.1039/b607342e
108. Wu, Y.; Zhang, Y.; Yu, M.; Zhao, G.; Wang, S. *Org. Lett.* **2006,** *8,* 4417–4420. doi:10.1021/ol061418q
109. Kehat, T.; Portnoy, M. *Chem. Commun.* **2007,** 2823–2825. doi:10.1039/b703016a
110. Wang, D.; Astruc, D. *Coord. Chem. Rev.* **2013,** *257,* 2317–2334. doi:10.1016/j.ccr.2013.03.032
111. Kofoed, J.; Reymond, J.-L. *Curr. Opin. Chem. Biol.* **2005,** *9,* 656–664. doi:10.1016/j.cbpa.2005.10.013
112. Kirkorian, K.; Ellis, A.; Twyman, L. J. *Chem. Soc. Rev.* **2012,** *41,* 6138–6159. doi:10.1039/c2cs35238a
113. Chang, H.; Stamoulis, A. G.; Huber, G. W.; Dumesic, J. A. *Green Chem.* **2023,** *25,* 1809–1822. doi:10.1039/d2gc04243f
114. Kandel, K.; Althaus, S. M.; Peeraphatdit, C.; Kobayashi, T.; Trewyn, B. G.; Pruski, M.; Slowing, I. I. *J. Catal.* **2012,** *291,* 63–68. doi:10.1016/j.jcat.2012.04.005
115. Rodríguez-Escrich, C.; Pericàs, M. A. *Eur. J. Org. Chem.* **2015,** 1173–1188. doi:10.1002/ejoc.201403042

116. Di Carmine, G.; Ragno, D.; Massi, A.; D'Agostino, C. *Org. Lett.* **2020,** *22,* 4927–4931. doi:10.1021/acs.orglett.0c01188
117. Fotaras, S.; Kokotos, C. G.; Kokotos, G. *Org. Biomol. Chem.* **2012,** *10,* 5613–5619. doi:10.1039/c2ob25693b
118. Chen, T.; Qiu, M.; Peng, Y.; Yi, C.; Xu, Z. *Coord. Chem. Rev.* **2023,** *474,* 214863. doi:10.1016/j.ccr.2022.214863
119. Yolsal, U.; Horton, T. A. R.; Wang, M.; Shaver, M. P. *Prog. Polym. Sci.* **2020,** *111,* 101313. doi:10.1016/j.progpolymsci.2020.101313
120. Koros, R. M.; Nowak, E. J. *Chem. Eng. Sci.* **1967,** *22,* 470. doi:10.1016/0009-2509(67)80134-9
121. Ötvös, S. B.; Mándity, I. M.; Fülöp, F. *ChemSusChem* **2012,** *5,* 266–269. doi:10.1002/cssc.201100332
122. Zhang, F.; Yang, X.; Jiang, L.; Liang, C.; Zhu, R.; Li, H. *Green Chem.* **2013,** *15,* 1665–1672. doi:10.1039/c3gc40215k
123. Calderón, F.; Fernández, R.; Sánchez, F.; Fernández-Mayoralas, A. *Adv. Synth. Catal.* **2005,** *347,* 1395–1403. doi:10.1002/adsc.200505058
124. Prasetyanto, E. A.; Jeong, S.-M.; Park, S.-E. *Top. Catal.* **2010,** *53,* 192–199. doi:10.1007/s11244-009-9417-8
125. Shylesh, S.; Zhou, Z.; Meng, Q.; Wagener, A.; Seifert, A.; Ernst, S.; Thiel, W. R. *J. Mol. Catal. A: Chem.* **2010,** *332,* 65–69. doi:10.1016/j.molcata.2010.08.022
126. Inokuma, T.; Furukawa, M.; Uno, T.; Suzuki, Y.; Yoshida, K.; Yano, Y.; Matsuzaki, K.; Takemoto, Y. *Chem. – Eur. J.* **2011,** *17,* 10470–10477. doi:10.1002/chem.201101338
127. Nagy, S.; Fehér, Z.; Kárpáti, L.; Bagi, P.; Kisszékelyi, P.; Koczka, B.; Huszthy, P.; Pukánszky, B.; Kupai, J. *Chem. – Eur. J.* **2020,** *26,* 13513–13522. doi:10.1002/chem.202001993
128. Okino, T.; Hoashi, Y.; Furukawa, T.; Xu, X.; Takemoto, Y. *J. Am. Chem. Soc.* **2005,** *127,* 119–125. doi:10.1021/ja044370p
129. Hamza, A.; Schubert, G.; Soós, T.; Pápai, I. *J. Am. Chem. Soc.* **2006,** *128,* 13151–13160. doi:10.1021/ja063201x
130. Kótai, B.; Kardos, G.; Hamza, A.; Farkas, V.; Pápai, I.; Soós, T. *Chem. – Eur. J.* **2014,** *20,* 5631–5639. doi:10.1002/chem.201304553
131. Varga, E.; Mika, L. T.; Csámpai, A.; Holczbauer, T.; Kardos, G.; Soós, T. *RSC Adv.* **2015,** *5,* 95079–95086. doi:10.1039/c5ra19593d
132. Grayson, M. N. *J. Org. Chem.* **2017,** *82,* 4396–4401. doi:10.1021/acs.joc.7b00521

License and Terms